A KINETIC STUDY OF THERMAL DECOMPOSITION OF SOLIDS

T H E S I S

SUBMITTED FOR THE
DEGREE OF DOCTOR OF PHILOSOPHY
IN THE UNIVERSITY OF LONDON
BY

ABDUL RAHIM TARIQ KUREISHY, B.Sc.(Hons.), M.Sc.

Imperial College,
LONDON S.W.7.

May, 1960

ACKNOWLEDGMENTS

I wish to express my gratitude to my supervisor, Dr. P.F.M. Jacobs of Imperial College, for his constant advice and interest throughout this work, and his invaluable guidance during the preparation of this thesis. I also wish to thank Professor R.M. Barrer, F.R.S., for the provision of laboratory facilities. I would like to thank the Pakistan Petroleum Co. Ltd., for the award of a scholarship and the Overseas Staff Department of the Burmah Oil Co. Ltd., for their helpful co-operation throughout the period of this research.

ABSTRACT

A kinetic study of thermal decomposition of the nickel oxalate dihydrate and of the dehydrated salt have been made and the results have been interpreted in terms of the formation and growth of nuclei. A mathematical analysis of variable growth rates based on a physical model has been proposed to explain the induction period. The effects of cold working, the inclusion of metals (e.g. Ni, Au and Pt), and of different gases (e.g. O_2, H_2, N_2, He and CO_2) on the kinetics of the reaction have also been investigated.

The kinetics of the thermal decomposition and ignition of mixtures of ammonium perchlorate and cuprous oxide have been studied. There are three stages of the reaction: (i) a surface reaction catalysed by cuprous oxide, (ii) oxidation of Cu_2O to CuO and (iii) thermal decomposition of the salt catalysed by oxidised Cu_2O. Only (ii) and (iii) can lead to ignition of the reactants.

The temperature variation in samples undergoing thermal decomposition has been studied and

it has been shown that the ignition by either mechanism is due to self-heating. Theoretical expressions for the excess temperature as a function of time and for the induction periods have been obtained by integrating the heat balance equation. The agreement between the theory and experimental results has been shown to be very satisfactory.

C O N T E N T S.

PAGE.

PART I.

THERMAL DECOMPOSITION OF NICKEL OXALATE.

INTRODUCTION

1.1 THERMAL DECOMPOSITION OF SOLIDS

The usual practice in studying the thermal decomposition of solids is, first to find out the shape of the curve representing the plot of fraction decomposed, α, as a function of time, t. These plots are generally sigmoid, indicating an autocatalytic reaction. Chemically, the majority of such reactions can be represented by the equation:

$$A\ (solid) \rightarrow B\ (solid) + C\ (gas) \qquad (1)$$

in which the onset of the reaction involves the formation of new phase B at special points in the lattice of A. The new phase B first spreads slowly around these points known as 'germ nuclei'. After these germ nuclei have reached a critical size they grow freely in one, two or three dimensions, and are termed 'growth nuclei'. It is reasonable to believe that in reactions where there is a long induction period, these germ nuclei are being formed and are growing slowly during the period of induction, at the end of which most of them have attained the critical size and are growing freely. There are several theories describing nucleation and growth, according to which different reactions can be classified: these are fully

described by Jacobs and Tompkins (1).

The second stage of investigation is then to find out the effect of varying conditions on the course of reaction. The induction period, in general, may be reduced by cold working the crystals (2) or, if the substance undergoes photochemical decomposition (e.g. barium azide), by pre-irradiation with U.V. light (3, 4). An oxidising or reducing atmosphere may also effect the kinetics of reaction (e.g. silver oxalate (5)). The kinetics of reaction under different conditions may then be fitted by mathematical equations derived from different theories and a mechanism for the reaction under study proposed.

This method of investigation is by no means complete in itself and other physical measurements, such as crystallographic study and electron microscopy, are needed to obtain a complete picture. In some cases it is possible to see growth nuclei, using an electron microscope (6) and to find their shape on different faces of crystals. Such studies are valuable adjuncts but are not always possible, in which case the kinetic study of the reaction may have to be the sole guide to the nature of a solid state reaction.

1.2 THERMAL DECOMPOSITION OF OXALATES (CONTRAL)

1.21 Silver Oxalate: This was first studied by Macdonald and Hinshelwood (7). They found that it decomposes according to the equation:

$$Ag_2C_2O_4 \longrightarrow 2Ag + 2CO_2 \qquad (2)$$

and that the rate of decomposition is governed by the formation and growth of nuclei of Ag in the space lattice of the oxalate crystal. The rate of decomposition is sensitive to the presence of adsorbed ions (7, 8), that obtained when oxalate ions are in excess during precipitation being of the "unstable accelerating" type, whereas that prepared using an excess of silver ions is of the "stable, feebly accelerating type". Finch, Jacobs and Tompkins (9) have given an explanation for the effect of adsorbed ions in terms of lattice defects and have also measured the ionic and photoconductance and the effect of U.V. irradiation on the thermal decomposition of the salt. Fenton and Cunningham (10) and Tompkins (11) found that the pressure of carbon dioxide evolved varied as the third or fourth power of time, indicating three-dimensional growth of silver nuclei, whereas Macdonald (8) proposed two-dimensional growth from a fixed number of nuclei with a chain-branching mechanism to explain the predominently exponential character of the p-t curves.

Macdonald and Sandison (12) showed by measuring the ionic conductance that the concept of solid nuclei is favoured, although the p-t plots were again exponential. Finch, Jacobs and Tompkins (9) have developed Macdonald's branching-chain mechanism to account quantitatively for all the features of the thermal decomposition. Erofeev, Belkovich and Volkova (13) found that first 20-50% decomposition can be fitted by the equation:

$$-\log (1-\alpha) = kt^n \text{ with } n = 4 \text{ to } 5$$

Usubo and Biro-Sugar (5) have confirmed the poisoning effect of oxygen observed first by Macdonald and Hinshelwood (7) and also found that hydrogen and argon have a catalytic effect on the decomposition. Macdonald (15) has commented on this effect and proposed a three step mechanism for the decomposition.

Crystallographic studies (14, 16) have shown that silver oxalate has a layer lattice and that the thermal decomposition is accompanied by fragmentation of the crystal, the fragments produced being slightly disoriented with respect to the original crystal. The undecomposed $Ag_2C_2O_4$ maintains its structure until the reaction is complete. The silver formed by the decomposition exists in the form of f.c.c. crystals having a size of approximately 10^{-5} cm.

1.22 Mercuric Oxalate: The thermal decomposition of mercuric

oxalate has been studied by Prout and Tompkins (17). It is reported that the reaction is a surface one, unaffected by end products. The chemical nature of the reaction can be best represented by the equation:

$$2\ Hg_2C_2O_4 \longrightarrow 3Hg_g + H_gO + 3CO_2 + CO \qquad (3)$$

The reaction spreads rapidly over the surface from a number of initial centres of reactivity, after which the rate is controlled by the linear propagation of the interface inwards, the activation energies associated with these two processes being 25.6 and 37.1 kcal/mole respectively. The initial rate is accelerated by pretreatment with light and cathode rays, which produce mercurous oxalate by electron transfer. This decomposes rapidly on heating according to a first-order law. The authors state that because mercuric oxalate is expected to have a molecular lattice, the Mott theory (18) based on the Wagner-Schottky concept (19) of ionic conductivity, is not applicable in this case. The reaction is poisoned by the presence of water vapour in the initial stages, but the subsequent rate is unaffected.

1.23 Lead Oxalate: The thermal decomposition can best be represented by the equation (20):

$$3\ PbC_2O_4 \longrightarrow 2\ PbO + Pb + 4CO_2 + 2\ CO$$

The kinetics of the decomposition are fitted (21) by the

Prout-Tompkins' equation:

$$\log (\alpha/1-\alpha) = kt + c \qquad (4)$$

Grinding of the sample reduces the induction period and also slightly reduces the accelerator period. A chain-branching mechanism has been proposed. The activation energy for both the accelerator and decay period is found to be 36 kcal/mole. Boldyrev (22) has studied the effect of ageing and pre-irradiation. Freshly prepared lead oxalate decomposes at a higher rate than does an aged sample because there are more dislocations in a freshly prepared sample. Irradiation with U.V. light or heating at temperatures below the decomposition point also decreases the rate of thermal decomposition. Possibly, these treatments result in a more ordered crystal. When the salt is treated with hydrazine hydrate, the rate of decomposition is increased owing to the catalytic effect of the particles of metallic lead.

1.24 Rare-earth and other oxalates: The work on these oxalates has been mainly qualitative in nature. Becket and Winfield (23) have studied the thermal decomposition of thorium oxalate by determining the weight loss and have measured the electrical conductivity of the sample as the decomposition proceeds. The latter was found to increase as the weight of the sample decreases. Electron

microscopy shows that there is little difference in outward appearance of the crystal as its composition is varied in stages from Th $(C_2O_4)_2$ H_2O to ThO_2. A minor change was detected in the fine structure which may be due to contraction in wall thickness of the sponge, of which the crystal is composed.

Americium oxalate has been studied by Markin (24) and different hydrate stages found as the decomposition proceeds. The final product of decomposition in air is AmO_2 whereas, in vacuum it is Am_2O_3.

With Neodymium oxalate (25), a mixture of CO and CO_2 is evolved on heating the salt in vacuum. When the amounts of these gases are plotted as a function of time the curves are never identical.

Clasher and Steinberg (26) have studied the thermal decomposition of oxalates of the lanthanon series. The solid residues were: mixed oxalate-carbonates, carbonates, oxycarbonates and oxides. The residues were tinted brown, owing to the presence of finely divided C, and the gases contained a high percentage of CO_2, together with CO, even if decomposition only to the stage of carbonate had taken place. The extent of the disproportionation: $2CO \rightarrow CO_2 + C$, is dependent on the rare-earth ion. The pressure-time curves were sigmoid showing the autocatalytic nature of the reaction.

presence of adsorbed moisture in the sample had a pronounced poisoning effect on the reaction.

1.3 THERMAL DECOMPOSITION OF NICKEL OXALATE

The thermal decomposition of nickel oxalate has been studied previously by Allen and Conlfe (27). They studied the reaction under an atmosphere of H_2 with large amounts of the sample (200 mg). They have observed two stages of the reaction:

(i) the initial fast decay reaction which can be fitted by the equation:

$$V = k_1 (t - t_o)^{\frac{1}{2}} \qquad (5)$$

where V is the volume of gas evolved; and (ii) an initially linear reaction at the end of this first decay period. The activation energies associated with these two processes are reported to be 47.6 and 36.4 kcal/mole respectively. A mechanism based on the formation of anion vacancies at the surface and diffusion of anions to the surface is the rate determining process, a square root law can be derived assuming that under these conditions the concentration gradient controlling the diffusion of anions to the free surface is inversely proportional to the extent of reaction, i.e.:

$$\frac{dV}{dt} \propto \frac{1}{V} \qquad (6)$$

It is suggested that at the end of initial reaction the lattice in the upper surface layers becomes so defective that it collapses to form metallic nuclei and an initially

linear process results.

A more recent study of the thermal decomposition of this salt has been made by Dančs and Ponec (28). They have studied the reaction under a high pressure of CO_2 (100-800mm of Hg.) in the temperature range 270°- 300°C. and with large sample weights (100 mg) by measuring the volume of gas evolved, keeping the pressure constant. They find that the Prout-Tompkins equation holds in the beginning of the reaction, but does not hold very well after the maximum rate is attained. The Avrami-Erofeyev equation:

$$-\ln (1 - \alpha) = kt^n \qquad (7)$$

holds for between 4 and 40% with $n = 2.4 \pm 0.1$ and after 40% with $n = 1$. The activation energies calculated by using different equations are within the range 32 ± 3 kcal/mole, but those calculated by using Avrami-Erofeyev equation and power law are reported to be 79.5 and 93.5 kcal/mole respectively. No initial reaction was observed by these authors; this is probably due to high pressure of CO_2 in the system. The dehydration of $Ni(C_2O_4 \cdot 2H_2O$ was also studied by Dancs and Ponec (28) by measuring the loss in weight with time. The value of the activation energy associated with dehydration was found to be 10 kcal/mole.

Allen and Scaife (27) report that x-ray analyses of samples taken during the initial reaction yields identical

patterns with those obtained for undecomposed nickel oxalate, whereas, samples taken during the second part of the reaction show patterns of metallic nickel. It was estimated from synthetic mixtures that 1% Ni would be observable. There was no sign of the presence of NiO or $NiCO_3$ in any of the samples, although in the case of latter, as much as 10% might escape detection.

2. EXPERIMENTAL

2.1 APPARATUS A FOR THE STUDY OF LOW TEMPERATURE THERMAL DECOMPOSITION

The usual high-vacuum constant-volume system was used to study the thermal decomposition of nickel oxalate in the lower temperature range. The apparatus is shown diagrammatically in Diagram 1.

A vacuum of better than 10^{-6} mm of mercury was obtained by using a two-stage mercury diffusion pump, backed by a rotary oil pump. The apparatus could be isolated from the pumps by means of the tap T; but a mercury cut-off between McLeod gauges and the tap was used to isolate the system as it maintained a better vacuum in the system. The apparatus could hold a vacuum of the order of 10^{-5} mm of mercury for the period of a run 1-6 hours). All samples were outgassed for more than 5 and usually 16 hours before a run.

The sample to be decomposed was contained in a small pyrex boat, hooked to a thin platinum wire which was attached to an iron slug sealed in glass. The sample could be pulled into the required position by means of a magnet. A small pyrex tube (2 cm long; 0.4 cm dia.) was used in order to minimise the time required to attain the furnace temperature.

An electric furnace was used to heat the reaction zone. Its heating elements were so adjusted as to give a uniform temperature (within $\pm$ 0.5°C.) zone about 4 cm long, and the temperature was maintained constant ($\pm$ 0.5°C.) with the aid of an electronic controller (29). Two chromel/Alumel thermocouples, calibrated at the ice, steam, tin, lead and antimony points, were used to measure the temperature of the reaction zone. One thermocouple was placed outside the reaction tube and inside the furnace tube immediately below the position of the sample, the other was placed immediately above the sample in a narrow glass tube, sealed to the standard ground glass joint used to introduce the sample boat. The cold junctions of the thermocouples were kept at 0°C in melting ice. The corrected readings of both thermocouples agreed within $\pm$ 0.5°C in every run.

Two McLeod gauges covering the ranges 10^{-5} - 10^{-1} and 10^{-2} - 5 mm of mercury were used to measure the pressure in the system.

A U-tube trap was used between the reaction tube and McLeod gauges to remove water vapour. Cardice mixed with CCl_4 to make a slurry was used as a coolant for this trap. The level of cardice was kept constant during a run.

DIAGRAM 1

APPARATUS A. USED FOR LOW TEMPERATURE THERMAL DECOMPOSITION STUDIES.

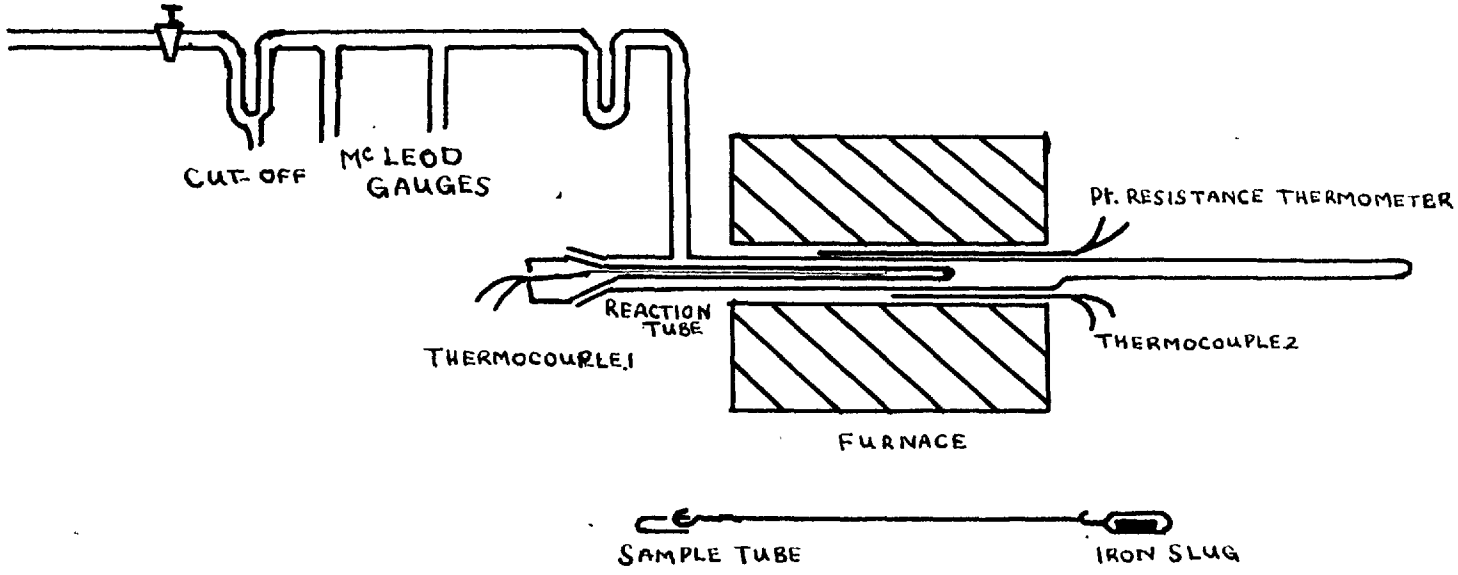

2.2 APPARATUS B FOR THE STUDY OF HIGH TEMPERATURE THERMAL DECOMPOSITIONS.

The apparatus described in section 2.1 (Apparatus A) was not suitable for the study of faster reactions at high temperatures because:

(i) The time required for sample to reach in equilibrium with the hot zone was long compared with the duration of the reaction (it took 3-4 min to reach equilibrium).

(ii) The Mcleod gauge readings cannot be taken quickly enough to follow the fast reactions accurately.

(iii) The effect of different gases could not be studied in Apparatus A because larger pressures (10-400 mm) of these gases were used to find the effect.

These drawbacks were overcome in a second apparatus shown in Diagram 2. A conical reaction tube was used, which projected inside a furnace similar to that described in section 2.1. The thin part of the reaction tube was in the constant temperature zone of the furnace. A calibrated thermocouple in contact with this end was used to record the temperature. The temperature of furnace was controlled with a variac. The reaction tube was connected to the rest of

the system by a ground-glass joint, sealed either with picein wax or high vacuum silicone grease to facilitate its removal from the rest of the system.

The sample, in the form of a pellet fragment was kept in a spoon directly above the reaction tube, and could be dropped into the reaction zone by rotating the ground-glass joint to which the spoon was connected.

The pressure changes in the system were followed by means of a glass spiral deflection gauge, the deflection caused by the pressure difference across the spiral being measured by a lamp and scale. The gauge was calibrated against a mercury manometer, the deflection ϕ being directly proportional to the pressure difference, P. This is shown in Diagram 3. The sensitivity of the gauge is 2.24 mm of Hg per cm deflection on the scale. The initial pressure of gas present in the system does not affect the sensitivity which also did not change with time.

The system was connected to the same pumping system described in section 2.1 through tap T. A trap (using cardice as coolant) could be used to condense water vapour.

The required pressure of a gas could be introduced through tap T_2 and two sides of the gauge then isolated by tap T_4. Tap T_3 was used to isolate the mercury manometer when it was not required.

The sample was kept in the spoon during the outgassing; the system was isolated from the pumps before doing a run by closing the tap T_1, and gas (if required) introduced via T_2, with taps T_3 and T_4 open, and its pressure measured on the manometer. T_3 and T_4 were then closed and the sample was dropped into the reaction vessel by rotating the spoon and simultaneously starting a stop-watch. The readings of the deflection were taken on the scale at suitable intervals of time which could be as small as 10 sec. As no container was used for the sample in this apparatus, the time taken for sample to reach equilibrium with the reaction vessel was greatly reduced and was probably about (20-30 secs). The only disadvantage in this system was that the initial decomposition of NiC_2O_4 could not be followed because the gas pressure produced during this reaction was too small to be followed accurately using a spiral gauge.

DIAGRAM 2

APPARATUS B. USED FOR HIGH TEMPERATURE THERMAL DECOMPOSITION STUDIES

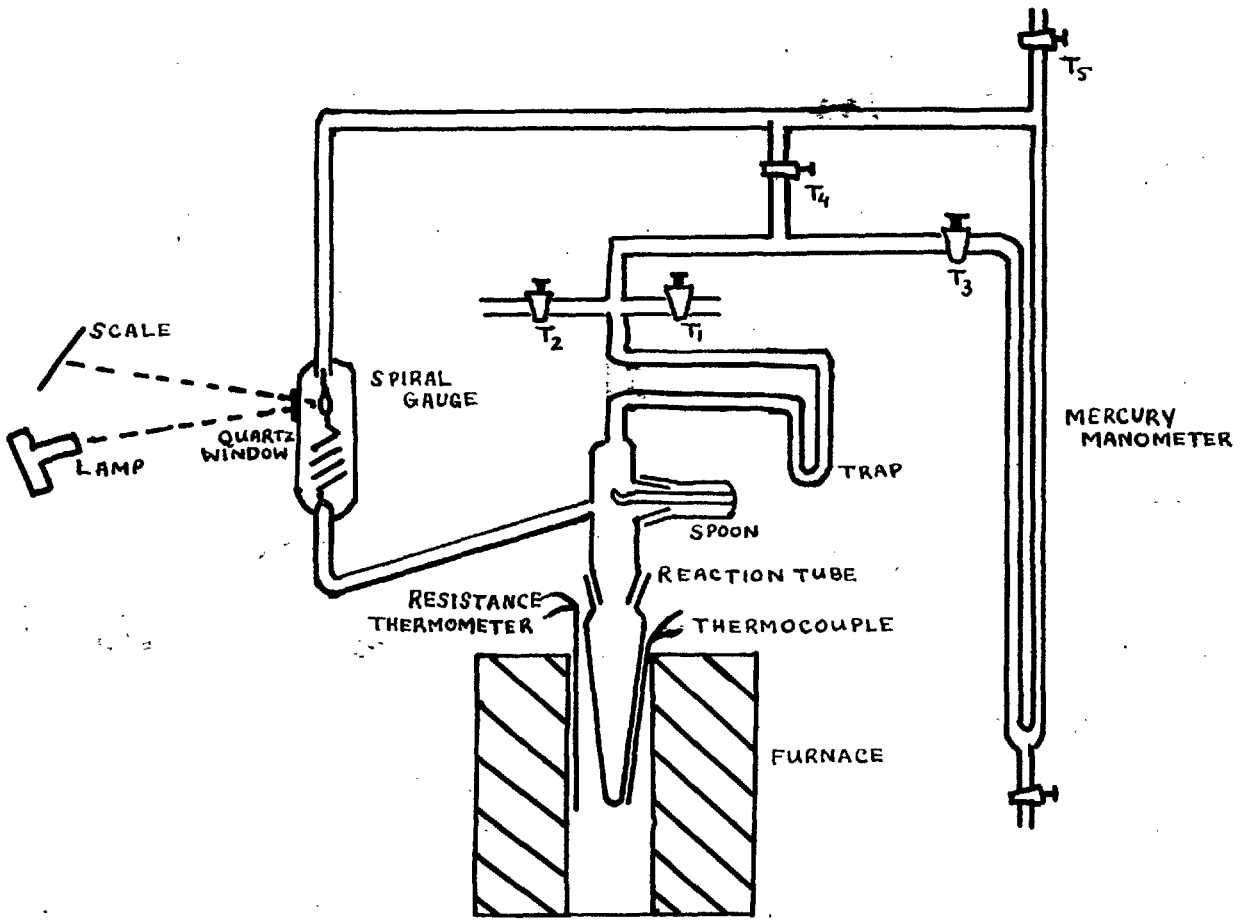

DIAGRAM 3

CALIBRATION OF GLASS SPIRAL GAUGE

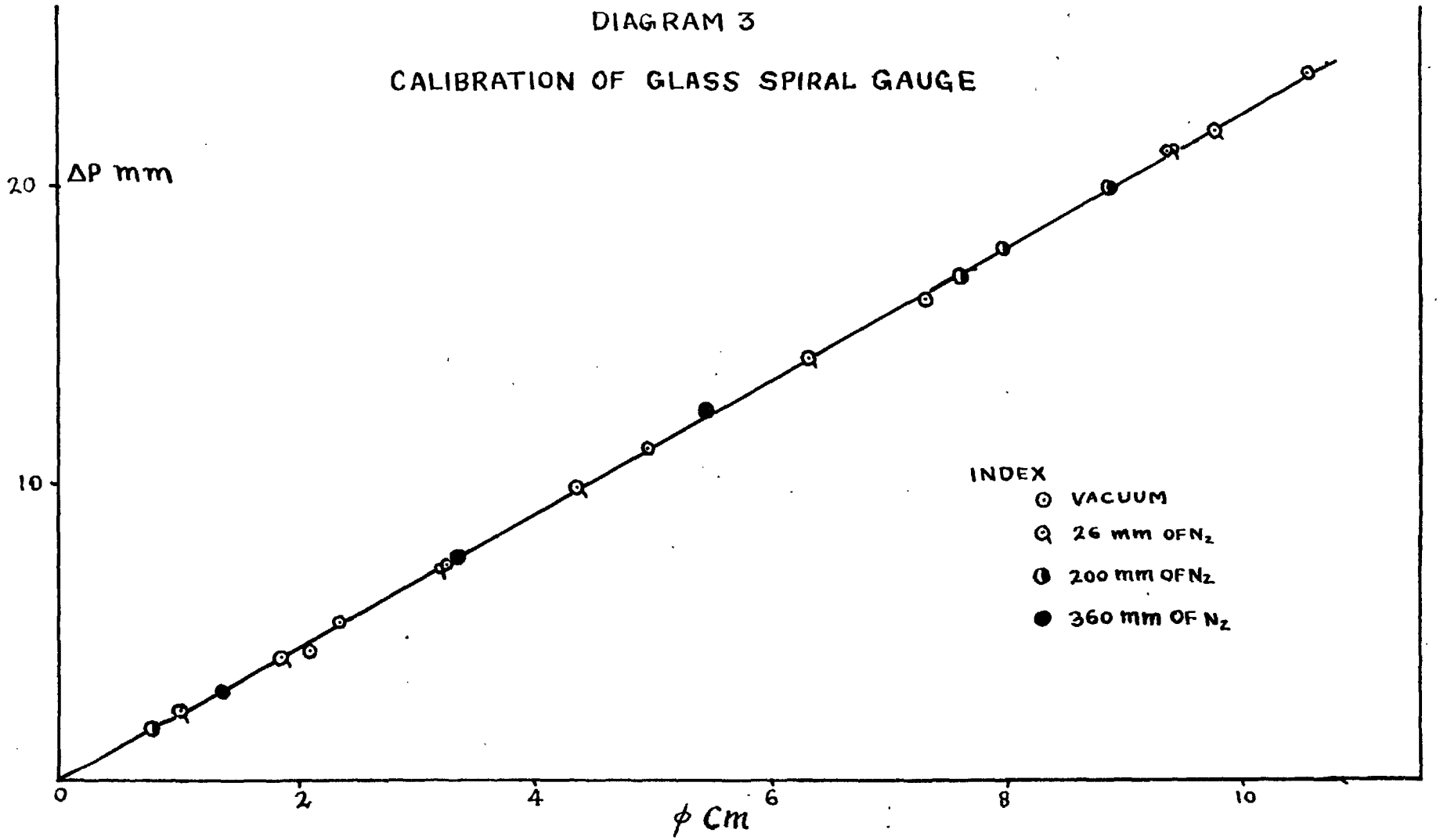

2.3 PREPARATION OF THE SAMPLE

Nickel oxalate di-hydrate was prepared by running slowly, ½ litre of hot (60°C) potassium oxalate solution (M/5) from a burette into ½ litre of hot (60°C) nickel nitrate solution (M/5), contained in a two-litre beaker, with vigorous stirring. Both potassium oxalate and nickel nitrate used in the preparation were Analar reagents. The precipitate of nickel oxalate was allowed to stand for two hours; it was then washed thoroughly (about 15 times) with hot distilled water by decantation and finally washed twice in the funnel. The salt was dried over P_2O_5 for two days and then heated at 100°C in vacuum before use. It was stored over P_2O_5 for the entire period of this work.

The dehydrated salt was prepared from the di-hydrate by heating it at 150°C in vacuum for more than 8 hours. It was stored over P_2O_5 in a separate desiccator.

Pellets were made by compressing the salt in a small stainless steel pellet press using a hand vice to apply pressure. The pellets thus obtained were broken into small fragments of suitable size (6-8 mg).

3. RESULTS

3.1 DEHYDRATED SALT

3.11 Powder and pellets; accumulatory runs: The thermal decomposition of dehydrated nickel oxalate in the form of powder and compressed pellets was studied in the temperature range 240° - 280°C. The products of decomposition are Ni and CO_2 only, the reaction being represented by the equation (27):

$$NiC_2O_4 \rightarrow Ni \text{ (solid)} + 2CO_2 \text{ (gas)}$$

Using Apparatus A, 6 mg samples of the salt were decomposed isothermally and the gas produced allowed to accumulate. The kinetics were followed by measuring the pressure of CO_2 at regular intervals of time. Fig. 1a shows α-t plots for Run 23 and Run 29 at the same temperature (250°C) to check the reproducibility. In Run 23 powder was used and in Run 29, a pellet fragment. The results are reproducible and apart from a slight variation in the induction period pelleting is seen to have no effect.

There is an initial fast reaction which decays rapidly, the total amount of salt decomposed during this process being 1% of the total decomposition. Fig. 1b shows the -t plot for this reaction on an enlarged scale. The extrapolated curves do not pass through the origin. This

is due to the time required for the sample to attain the furnace temperature. Fig. 2 shows the α-t plots for the whole series of runs at different temperatures. Runs up to 260°C were carried out in apparatus A with powder and above 260°C up to 280°C in apparatus B with pellets. It was not possible to follow the initial fast reaction in apparatus B, therefore, Fig. 3 shows α-t plots for the initial period up to 260°C only.

If we denote the total fractional decomposition by α and the total amount decomposed in the initial process by α_0(=0.010), the fraction decomposed in this initial process is $\alpha' = \frac{\alpha}{\alpha_0}$. The initial reaction then obeys the "Contracting Area" formula.

$$1 - (1 - \alpha')^{\frac{1}{2}} = k't \qquad (8)$$

Fig. 4a shows a typical plot of $1 - (1 - \alpha')^{\frac{1}{2}}$ vs.t, the slope of this straight line being k'. Values of k' and the range of α over which equation (8) holds are given in Table 1. Fig. 5a is a plot of log k' vs.1/T for these runs. The activation energy found from this plot is 32.9 kcal/mole.

Denoting the fractional decomposition in the second reaction by α'', then:

$$\alpha'' = \frac{\alpha - \alpha_0}{1 - \alpha_0}$$

where α and α_0 have the same meaning as before. This second reaction then obeys an Avrami-Erofeyev type of

equation:

$$[-\log(1-\alpha'')]^{1/n} = k''t \qquad (9)$$

with n = 2. The range over which this equation holds is α = 0.04 to 0.85. Fig. 4b shows a plot of the function $[-\log(1-\alpha'')]^{\frac{1}{2}}$ vs.t for Run 23, the slope of this line being the Avrami-Erofeyev rate constant, k''. In Table 2, the values of k'' and the range of α over which the equation holds, are given for all the runs in this series. Fig. 5b is a plot of log k'' vs 1/T from which an activation energy of 32.0 kcal/mole may be calculated.

The decay period is also fitted by the unimolecular decay law:

$$-\log(1-\alpha'') = k'''t \qquad (10)$$

Fig. 6 shows a plot of $-\log(1-\alpha')$ vs.t for Run 23 and Fig. 7a that of log k''' vs.1/T for the whole series. The values of the decay law rate constant, k''', are given in Table 3, together with the range of α over which this equation holds.

The plot of log t_o vs.1/T, where t_o is the time at which the second reaction starts, is also a straight line. The activation energy calculated from this plot, Fig. 8a, is 39.8 kcal/mole. Numerical values of t_o are given in Table 4.

Four runs were done after the dehydrated powder

had been stored for 2-3 months. There is no appreciable ageing effect and the rate constants calculated for these runs lie on the same activation energy plot as those for the fresh sample (Fig. 5b). Numerical values of rate constants are given in Table 5.

5.12 Differential Runs: The kinetics of the decomposition of aged dehydrated salt were also studied by a differential method, i.e. by measuring the rate of evolution of CO_2 at regular intervals of time. The system remained connected to the pumps throughout the reaction except while measuring the rate, when it was isolated and the gas allowed to accumulate for 2-3 min. The pressure divided by the time interval gave the rate of decomposition. Fig. 9a shows a plot of this rate against time. The α (t) curve is then determined by numerical integration (Fig. 9b). The reaction is again found to obey the Avrami-Erofeyev equation with n=2, but the range of α over which this equation holds is now 4 -95% (Fig. 9c). The AE rate constants at various temperatures are also lower than those obtained for the respective accumulatory runs. This effect is shown in the Arrhenius plot in Fig. 5c. Values of k″ are given in Table 6.

TABLE 1

THERMAL DECOMPOSITION OF NiC_2O_4. RATE CONSTANT OBTAINED FROM 'CONTRACTING AREA' EQUATION FOR SURFACE REACTION.

Run	Temp °C	$10^3/T°K$	$k'(min^{-1})$	Range of α	log k'
25	240°	1.9485	0.00920	0.000 - .0093	$\bar{3}$.9638
24	245°	1.9295	0.01220	0.000 - .0093	$\bar{2}$.0864
23	250°	1.9115	0.01891	0.000 - .0050	$\bar{2}$.2765
26	255°	1.8932	0.02228	0.000 - .0086	$\bar{2}$.3479
27	260°	1.8754	0.03250	0.000 - .0092	$\bar{2}$.5159

TABLE 2

THERMAL DECOMPOSITION OF DEHYDRATED NICKEL OXALATE. RATE CONSTANTS DETERMINED FROM THE AVRAMI-EROFEYEV EQUATION

APPARATUS A

Run	θ_{comp} °C	$10^3/T$ °K	$k''(min^{-1})$	$\log k''$	α-range
25	240.0	1.9485	0.009305	$\bar{3}$.9687	.05 - .77
24	245.0	1.9295	0.01153	$\bar{2}$.0618	.04 - .82
23	250.0	1.9115	0.01518	$\bar{2}$.1813	.06 - .84
26	255.0	1.8932	0.02015	$\bar{2}$.3043	.05 - .88
27	260.0	1.8754	0.03095	$\bar{2}$.4905	.04 - .77

APPARATUS B

137	264.4	1.8601	0.04250	$\bar{2}$.6284	.03 - .62
138	269.2	1.8463	0.06100	$\bar{2}$.7853	.04 - .84
139	277.4	1.8162	0.07530	$\bar{2}$.8768	.03 - .76
141	282.8	1.7986	0.1080	$\bar{1}$.0334	.03 - .80

TABLE 3

THERMAL DECOMPOSITION OF DEHYDRATED NICKEL OXALATE.
RATE CONSTANTS DETERMINED FROM UNIMOLECULAR DECAY LAW.

Run	Temp °C	$10^3/T°K$	$k''(min^{-1})$	log k''	α-range
25	240.0	1.9485	0.01349	$\bar{2}$.1301	.64 - .98
24	245.0	1.9295	0.01664	$\bar{2}$.2211	.59 - .97
23	250.0	1.9115	0.02343	$\bar{2}$.3696	.56 - .97
26	255.0	1.8932	0.03126	$\bar{2}$.4950	.56 - .96
27	260.0	1.8754	0.04055	$\bar{2}$.6080	.50 - .97
137	264.4	1.8601	0.05130	$\bar{2}$.7101	.61 - .95
138	269.2	1.8463	0.06808	$\bar{2}$.8331	.58 - .98
139	277.4	1.8162	0.09888	$\bar{2}$.9951	.61 - .97
141	282.8	1.7986	0.1262	$\bar{1}$.1011	.63 - .98

TABLE 4

THERMAL DECOMPOSITION OF DEHYDRATED NICKEL OXALATE: INDUCTION PERIODS.

Run	Temp°C	$10^3/T°K$	t_o min
25	240.0	1.9485	151
24	245.0	1.9295	89
23	250.0	1.9115	75
26	255.0	1.8932	41
27	260.0	1.8754	30
137	264.4	1.8601	23.5
138	269.2	1.8463	20.0
139	277.4	1.8162	8.5
141	282.8	1.7986	7.0

TABLE 5

THERMAL DECOMPOSITION OF AGED NiC_2O_4. RATE CONSTANTS DETERMINED FROM TWO AS ORIGINATORS

Run	Temp°C	$10^3/T°K$	$k''(min^{-1})$	log k''	α - range
92	245.0	1.9295	0.00966	3.9850	.026 - .65
110	247.5	1.9190	0.01000	2.0000	.026 - .71
91	250.0	1.9115	0.01440	2.1584	.040 - .58
93	255.5	1.8914	0.02205	2.3434	.040 - .60

TABLE 6

THERMAL DECOMPOSITION OF AGED NiC_2O_4: DIFFERENTIAL RUNS.
RATE CONSTANTS DETERMINED FROM AVRAMI-EROFEYEV EQUATION.

Run	Temp °C	$10^3/T°K$	$k''(min^{-1})$	α-range	log k''
107	245.0	1.9295	.00730	.06 -.95	$\bar{3}$.8633
109	247.4	1.9309	.00850	.06 -.95	$\bar{3}$.9294
108	249.2	1.9142	.00950	.03 -.95	$\bar{3}$.9777
106	255.5	1.8914	.01490	.04 -.97	$\bar{2}$.1732

FIGURE 1

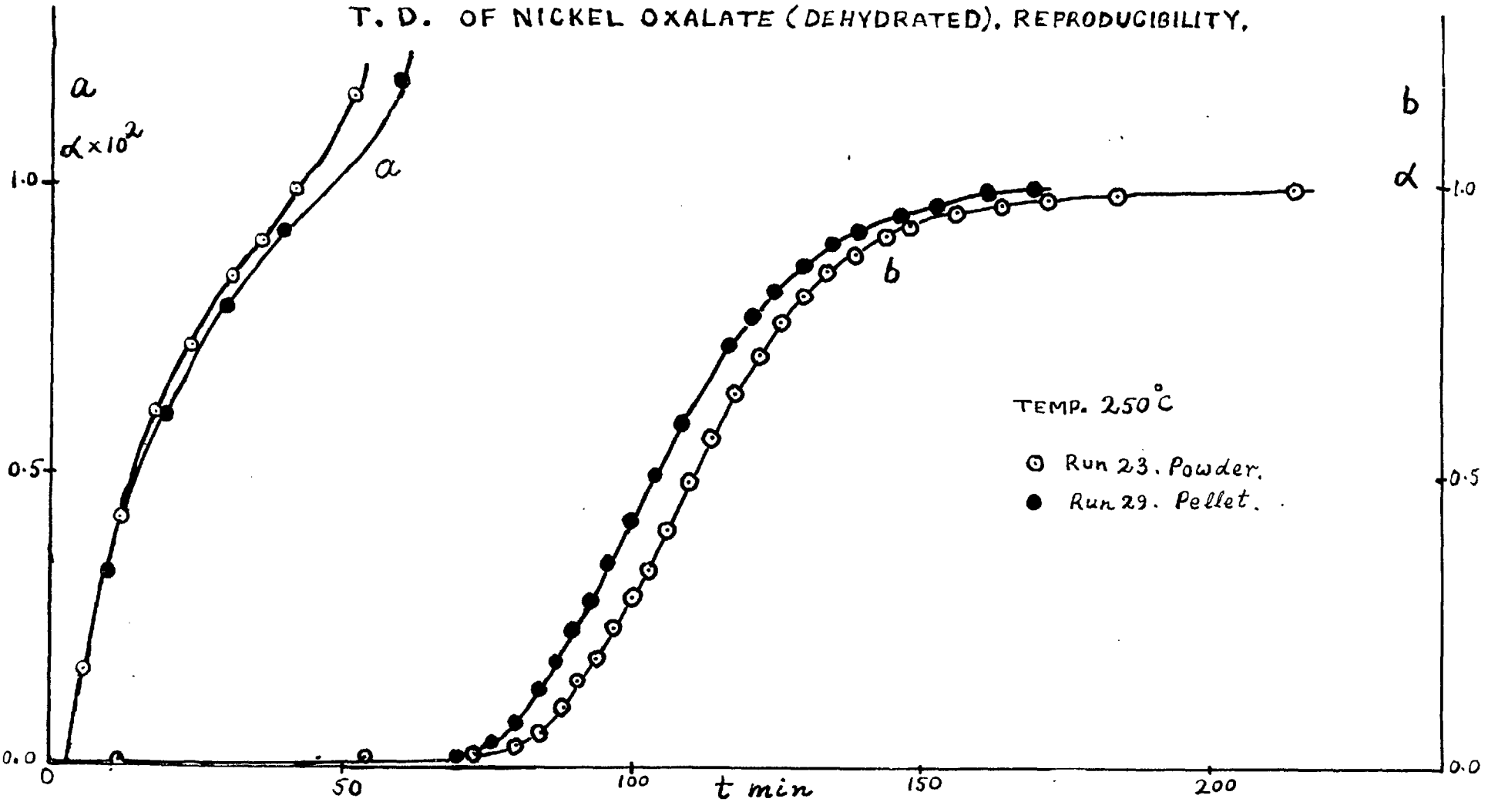
T. D. OF NICKEL OXALATE (DEHYDRATED). REPRODUCIBILITY.
a
$\alpha \times 10^2$
1.0
0.5
0.0
a
b
α
1.0
0.5
0.0
b
TEMP. 250°C
Run 23. Powder.
Run 29. Pellet.
0
50
100
150
200
t min

FIGURE 2

T.D. OF NiC_2O_4 (DEHYDRATED). α-t PLOTS

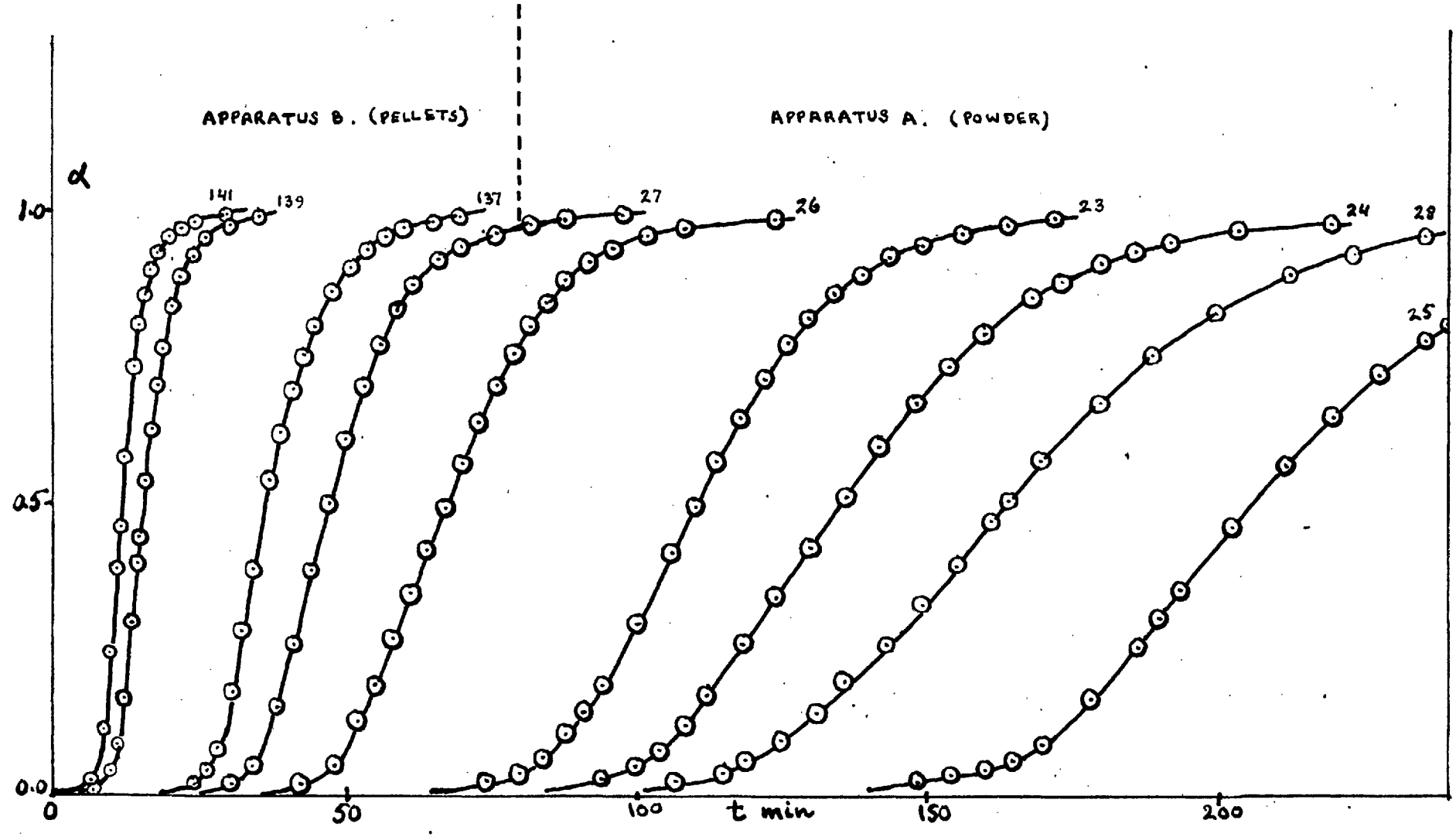

FIGURE 3

T. D. OF NiC_2O_4 . SURFACE REACTION

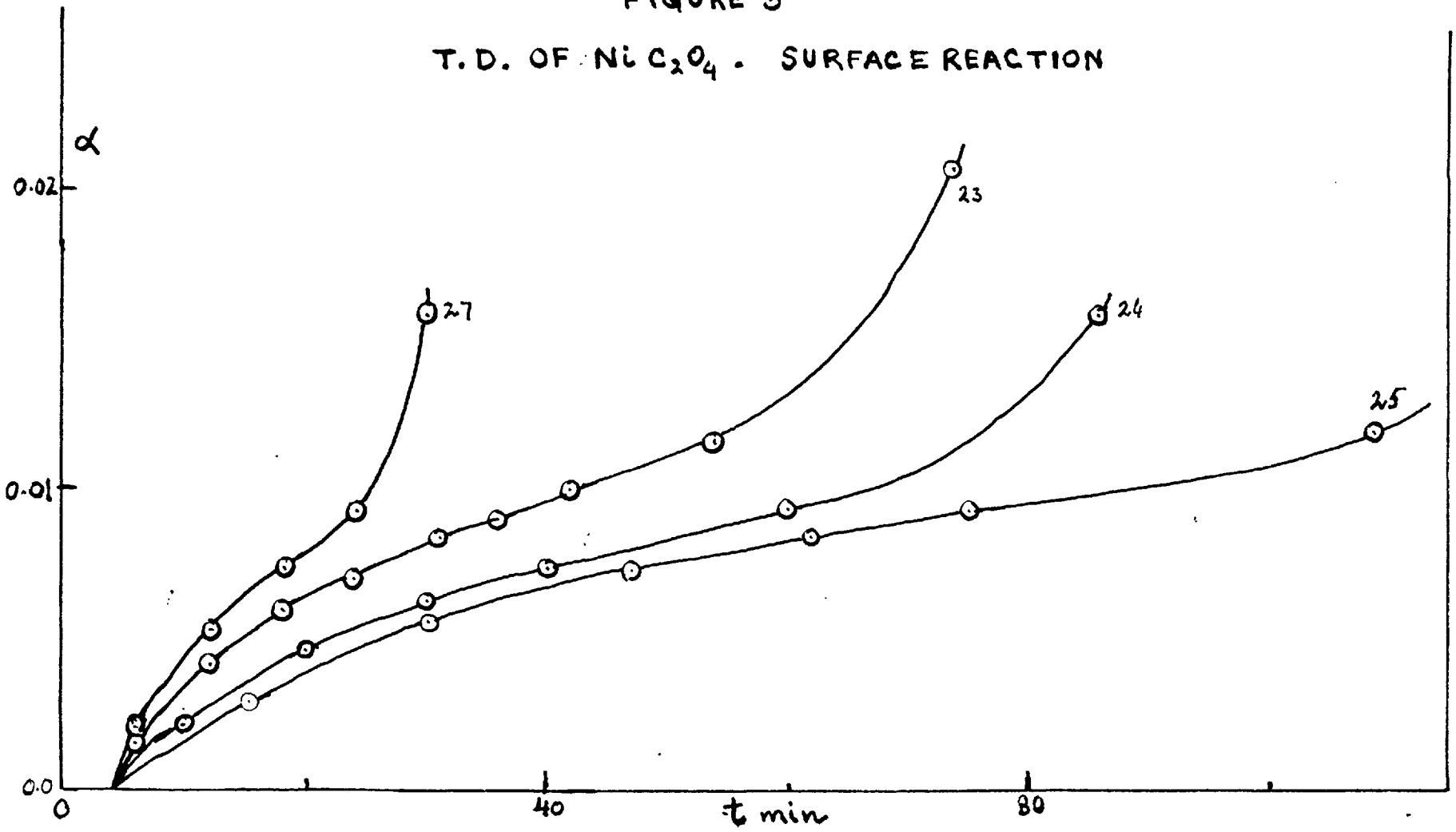

FIGURE . 4

T. D. OF NiC_2O_4 · (C.A. AND A.E. PLOTS)

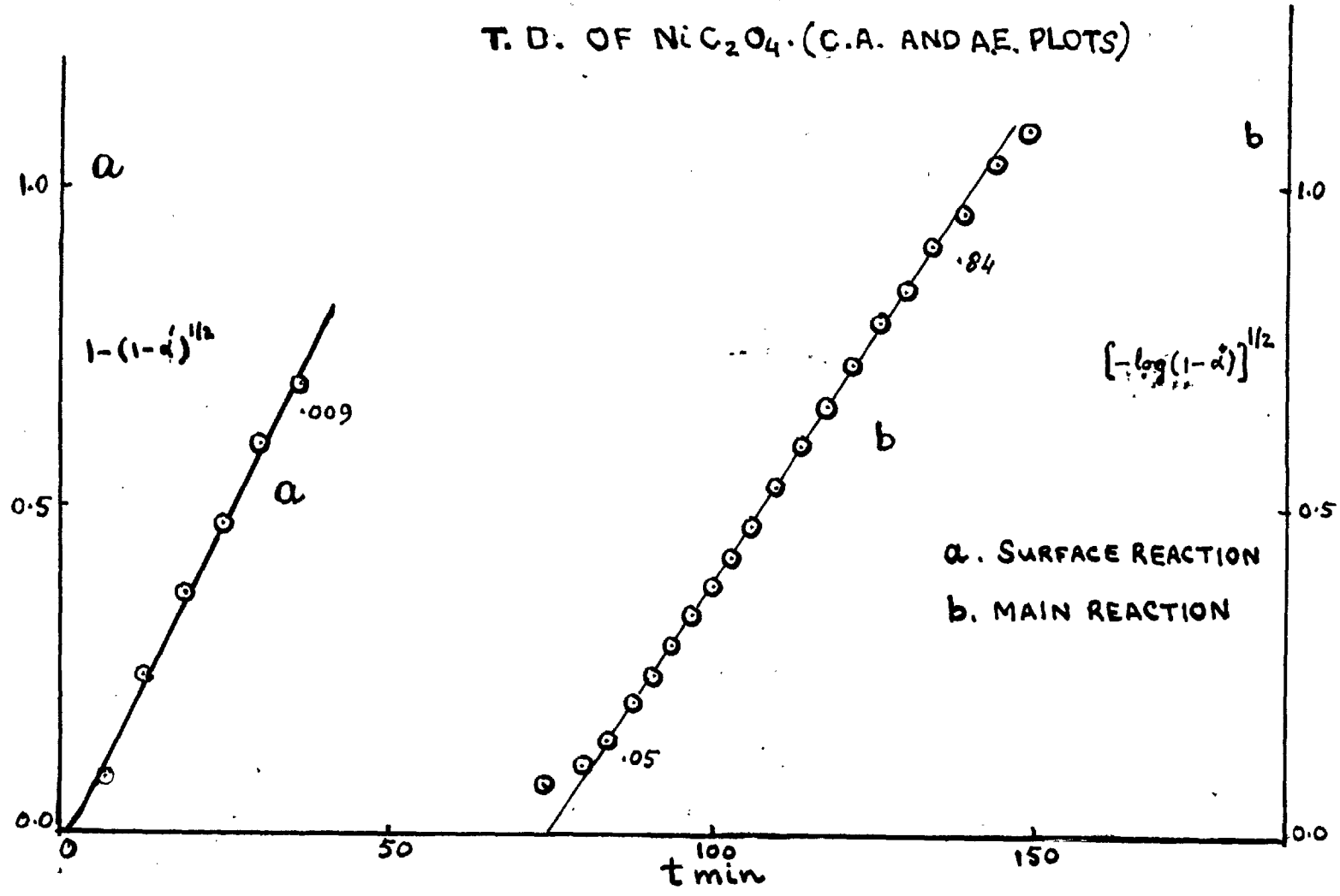

FIGURE 5

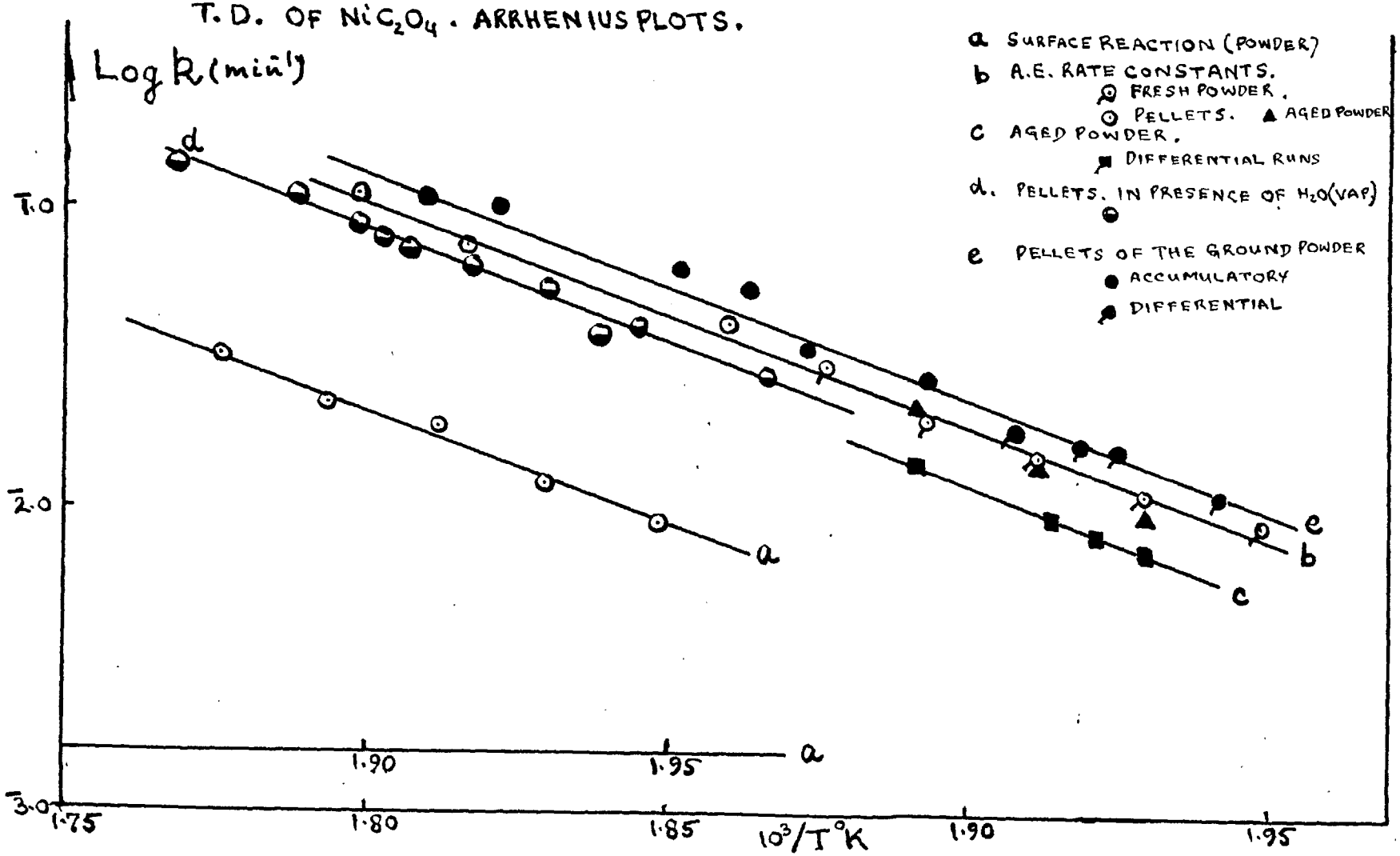
T. D. OF NiC_2O_4 . ARRHENIUS PLOTS.
Log k (min⁻¹)
a SURFACE REACTION (POWDER)
b A.E. RATE CONSTANTS.
FRESH POWDER.
PELLETS. AGED POWDER
c AGED POWDER.
DIFFERENTIAL RUNS
d. PELLETS. IN PRESENCE OF H_2O(VAP)
e PELLETS OF THE GROUND POWDER
ACCUMULATORY
DIFFERENTIAL
T.0
$\bar{2}.0$
$\bar{3}.0$
1·75
1·80
1·85
1·90
1·95
$10^3/T°K$
a
b
c
d
e

FIGURE 6

T. D. OF NiC_2O_4. UMD LAW PLOT.

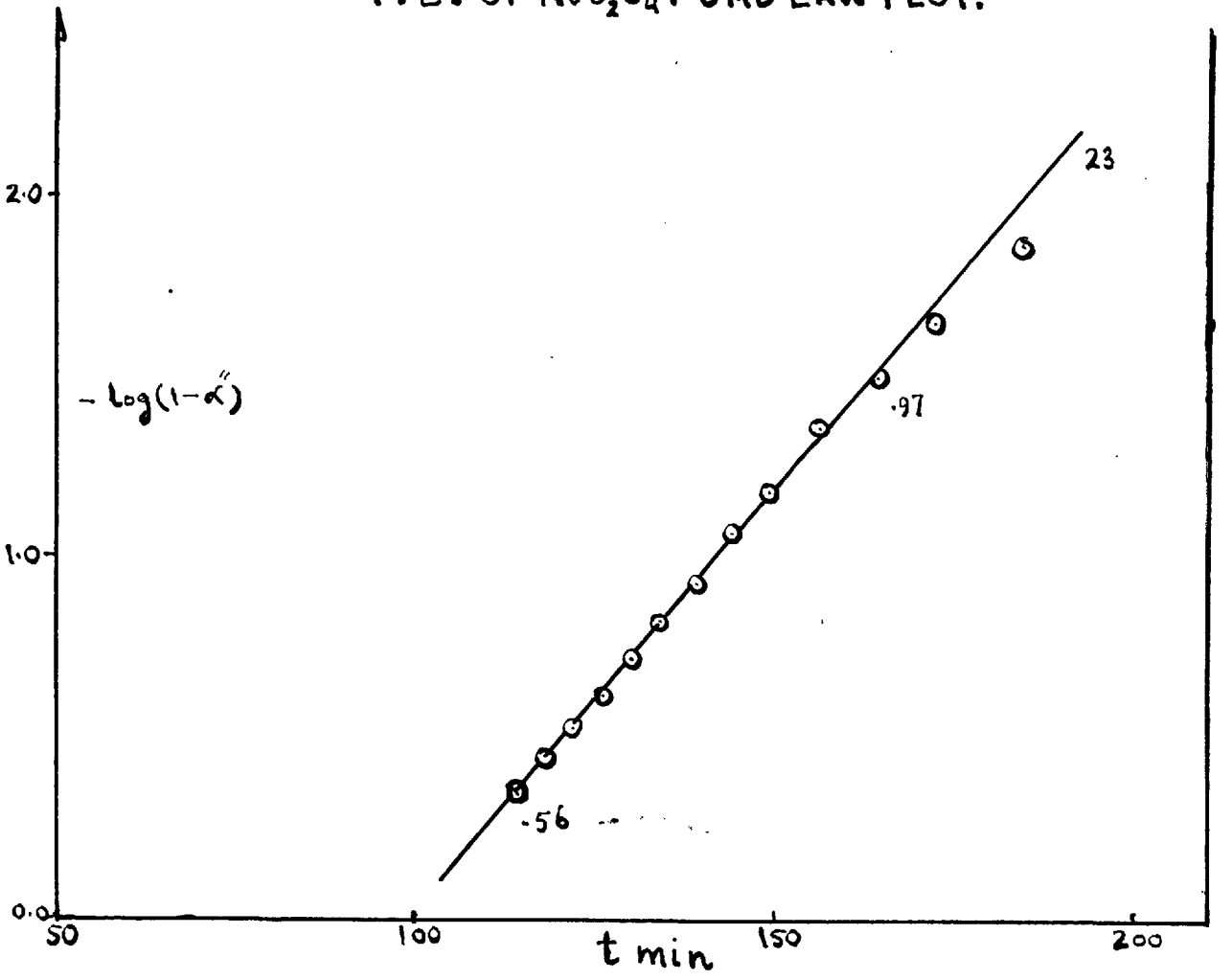

FIGURE 7

T.D. OF NiC_2O_4. ARRHENIUS PLOT (UMD LAW k)

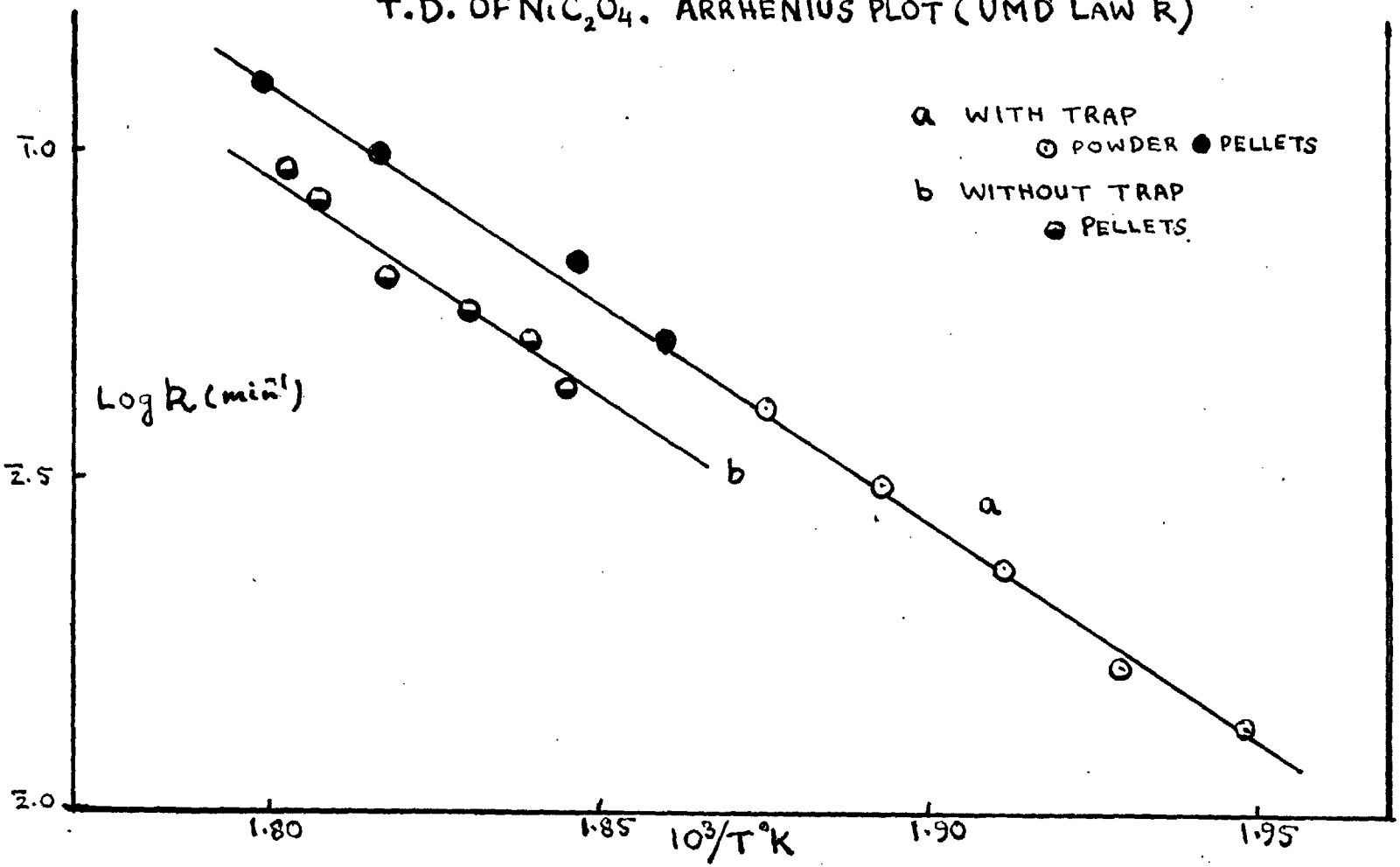

FIGURE 8

T.D. OF NiC_2O_4. ARRHENIUS PLOT (INDUCTION PERIODS)

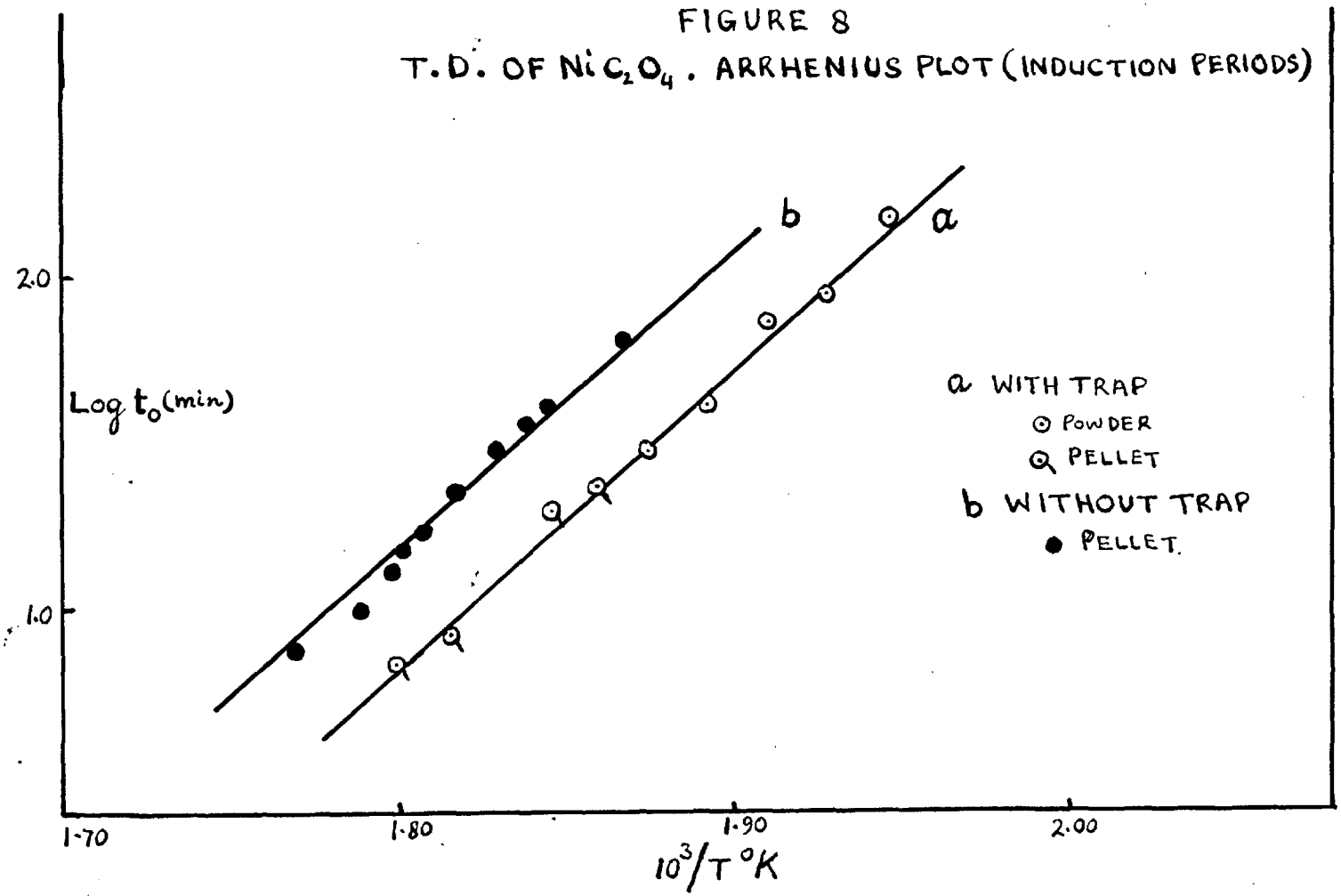

FIGURE 9

T. D. OF NiC_2O_4 . DIFFERENTIAL METHOD.

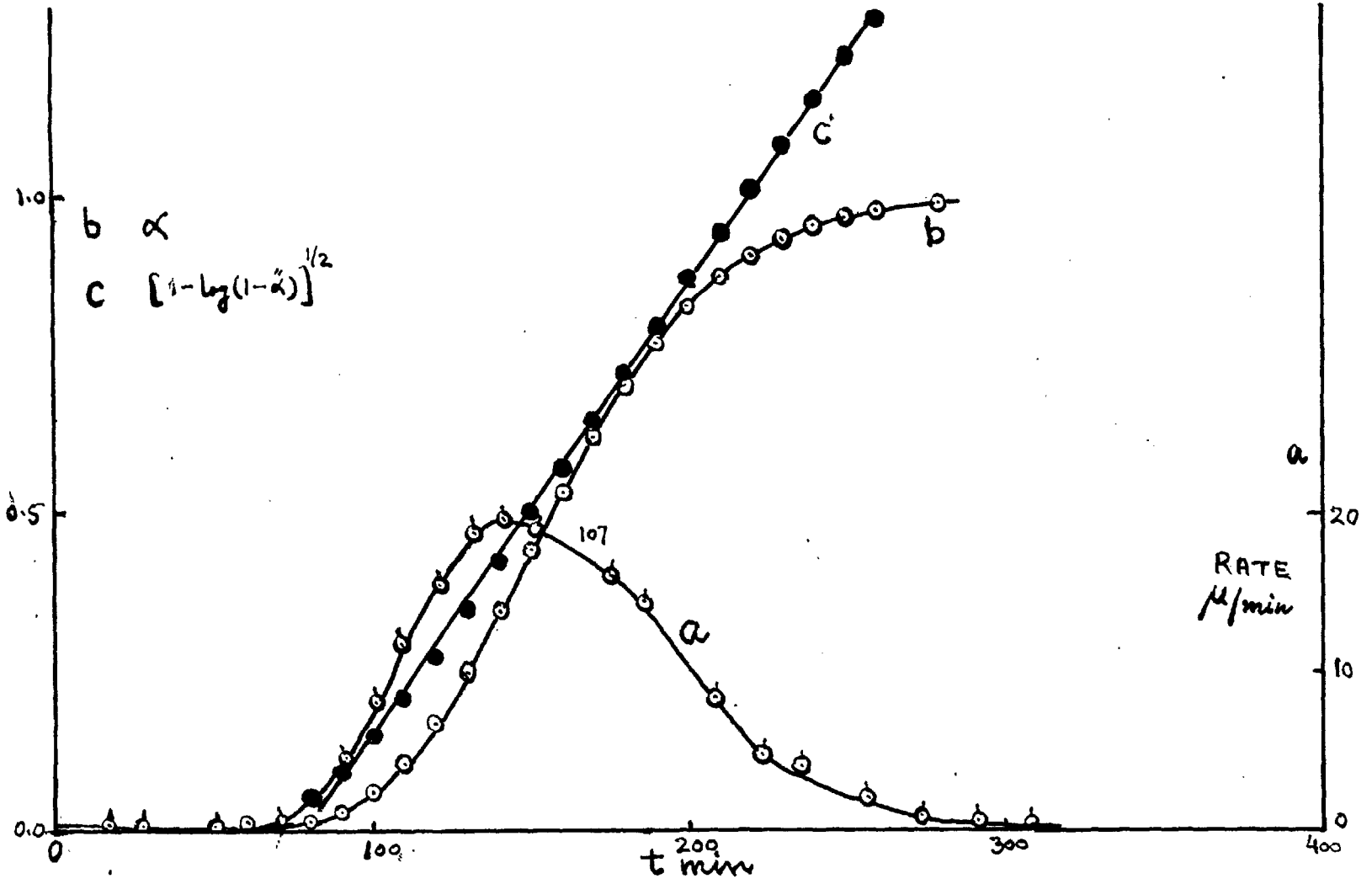

3.13 Effect of Water Vapour: Dehydrated nickel oxalate absorbs moisture from the atmosphere readily, which it does not lose over P_2O_5 in a desiccator; hence there is always a certain amount of water present (15-20% of the original) in the sample being decomposed. As this absorbed water is more readily given up during heating than the original water of crystallisation, it does not affect the kinetics of decomposition of dehydrated salt when a cold trap is present in the system. If, however, there is no trap in the system and water vapour at a pressure of (2.0 ± 0.2 mm) is allowed to remain in contact with the sample throughout the run, the kinetics of thermal decomposition is affected as follows:

(i) The induction period, t_o, becomes considerably longer (Fig. 8b). Numerical values of t_o are given in Table 7.

(ii) The rate constants, $k_{AE}^{\wedge}$, are lower and the range of α over which this equation holds is shorter at the lower temperature, varying from 0.04 - 0.40 to 0.02 - 0.94 as T increases. Fig.10 shows the fit of this equation at the two extreme temperatures. Table 7 gives the values of rate constants for all runs in this series and the range of over which the equation is obeyed.

The Arrhenius plot is shown in Fig. 5d, the activation energy being unaltered by the presence of water vapour.

(iii) The decay part of the reaction is fitted by the unimolecular decay law, but the rate constants are lower than the corresponding values when a trap is used. Arrhenius plot for these runs is shown in Fig. 7b. Numerical values of rate constants are given in Table 9.

3.14 Effect of other gases: When a relatively high pressure of gas is present in the system, there are two factors which make it difficult to retain the cold trap used for condensing water vapour given up by the sample. Firstly, due to evaporation of cardice coolant the effective volume of the system changes, causing fluctuations in the pressure recorded; these fluctuations are quite considerable compared with the pressure of the reaction product. Secondly, water vapour evolved from the sample takes considerable time to reach the cold trap (in 250 mm N_2, the time taken for complete removal of water vapour was 50 min). This produces a variable pressure of water vapour during the reaction. These two factors made it essential to study the effect of different gases on the kinetics of decomposition of nickel oxalate in the presence of water vapour evolved from the sample and to

compare these results with those obtained in section 3.13. All experiments described in this section and 3.13 were done in apparatus B with pellets.

Hydrogen and Oxygen: Both these gases react with one or the other of the reaction products and hence their effect on the kinetics of the decomposition reaction could not be studied. Oxygen slowed down the reaction quite considerably and the final pressure of CO_2 recorded was nearly 3/4 of the original value for the same mass of NiC_2O_4. This is probably due to the reaction of O_2 with the finely divided Ni residue, thus poisoning the nuclei. Further, as O_2 is being removed from the system by reaction, the measured rate is the difference of the rate of decomposition of NiC_2O_4 and the rate of oxidation of Ni. The value for the final pressure suggests that nearly all Ni has been oxidised by O_2 according to equation:

$$2\,Ni + O_2 \longrightarrow 2NiO$$

With H_2, the pressure in the system starts to decrease after a certain amount of decomposition has taken place, indicating a gas-phase reaction between H_2 and the reaction products. Fig. 11 shows a comparison of p-t curves in presence of O_2 + H_2O (vapour), H_2 + H_2O (vapour alone.

Nitrogen, Helium and Carbon dioxide: The effect of these gases at different pressure has been studied. The kinetics still obey the Avrami-Erofeyev equation from α = 0.05 to α = 0.75 and the decay period is fitted by the unimolecular decay law. Fig. 12 shows the comparison of some α-t curves under different pressures of these gases and Figs. 13 and 14 show the fit of the two equations. Both AE and UMD rate constants decrease with increasing pressure of the gas, whereas the induction period increases with increasing pressure. The AE rate constant falls sharply with pressure becoming constant at high pressures (Fig. 15a). The variable $\sqrt{PM}$ has been used instead of P for comparison. The UMD rate constant falls linearly with $\sqrt{PM}$ where P is the pressure of gas and M its molecular weight (Fig. 15b). The induction period rises linearly with $\sqrt{PM}$ for He and N_2 but the effect of CO_2 is more pronounced at high pressures (Fig. 15c). Table 10 shows numerical values of t_o and the rate constants for these runs.

3.15. Effect of grinding: Before studying the decomposition of pellets made from oxalate - metal mixtures, it was necessary to find out if there was any effect due to grinding the dehydrated nickel oxalate, because it was intended to make a uniform intimate mixture of salt and metal by grinding them together. Therefore, nickel oxalate

was ground in an agate mortar for five minutes and a pellet was made. Runs at lower temperatures were done in Apparatus A by the differential method while those at high temperatures (above 260°C) were done in Apparatus B by the accumulatory method. All these runs form a uniform continuous series showing that there is no real difference between differential and accumulatory runs for this series. The reaction is again found to obey AE equation from α = 0.05 - 0.80 for accumulatory runs and α = 0.13 - 0.80 for differential runs. Fig. 16 shows the α -t plots for the whole series and Fig. 17 shows the AE plot for one differential and one accumulatory run. The decay period is also fitted by the unimolecular decay law and a representative plot for both accumulatory and differential runs is shown in Fig. 18. The values of rate constants are given in Tables 11 and 12. The Arrhenius plot of AE rate constants is shown in Fig. 5e for comparison with the powder and pellets made from unground powder. These lines show that there is a slight increase in rate constants on grinding, the activation energy remaining the same.

3.16 Effect of Ni (residue), Au and Pt: Pellets were made containing 4.4% Ni (residue left after the decomposition of NiC_2O_4 from previous runs), 9.1% Au and 19.8% Pt. Runs on fragments of these pellets were carried out both by differential and accumulatory methods in Apparatus A and B

respectively in the same way as in section 3.14. None of these metals were found to have any appreciable catalytic effect on the decomposition of NiC_2O_4. The AS plots for one accumulatory run with each metal are shown in Fig. 19. Tables 13 and 14 give the values for the AS and UNB rate constants and the ranges of over which these equations hold. Fig. 20 shows the Arrhenius plot of all these runs with those in section 3.15 using AS and UNB law rate constants. There is some scatter but it can be seen that addition of these metals exerts no appreciable effect. Fig. 21 is a plot of log t_o vs.1/T for all these runs with those in section 3.15, showing again that there is no effect of mixing metals on the reaction. The values of t_o are given in Tables 13 and 14. The activation energy found from this plot is 30.7 kcal/mole.

TABLE 7

THERMAL DECOMPOSITION OF DEHYDRATED NICKEL OXALATE IN PRESENCE OF WATER VAPOUR. INDUCTION PERIODS.

Run	Temp ^{o}C	$10^{3}/T^{o}$K	t_{o} (min)
158	262.6	1.8664	65.0
156	268.9	1.8447	41.0
150	270.5	1.8392	36.6
148	273.3	1.8293	30.4
142	277.0	1.8175	23.0
149	280.2	1.8070	17.0
157	281.6	1.8024	15.2
153	282.6	1.7986	13.8
154	285.9	1.7886	10.0
155	292.2	1.7657	7.6

TABLE 8

THERMAL DECOMPOSITION OF DEHYDRATED NICKEL OXALATE IN PRESENCE OF WATER VAPOUR. RATE CONSTANTS DETERMINED FROM AVRAMI-EROFEYEV EQUATION.

Run	Temp°C	$10^3/T°K$	$k''(min^{-1})$	α-range	log k''
158	262.6	1.8664	.02800	.05-.44	$\bar{2}$.4472
156	268.9	1.8447	.04160	.04-.43	$\bar{2}$.6191
150	270.5	1.8392	.05137	.04-.60	$\bar{2}$.7107
148	273.3	1.8298	.05535	.03-.40	$\bar{2}$.7431
142	277.0	1.8175	.06571	.03-.62	$\bar{2}$.8177
149	280.2	1.8070	.07109	.01-.66	$\bar{2}$.8518
157	281.6	1.8024	.07917	.01-.72	$\bar{2}$.8986
153	282.8	1.7986	.09127	.02-.75	$\bar{2}$.9603
154	285.9	1.7886	.1120	.04-.69	$\bar{1}$.0492
155	292.2	1.7687	.1333	.01-.94	$\bar{1}$.1249

TABLE 9

THERMAL DECOMPOSITION OF NiC_2O_4 IN PRESENCE OF WATER VAPOUR. RATE CONSTANTS DETERMINED FROM UMD LAW

Run	Temp °C	$10^3/T°K$	$k'''(min^{-1})$	α-range	log k'''
156	268.9	1.8447	.04338	0.51 - 0.93	2.6373
150	270.5	1.8392	.05158	0.53 - .94	2.7125
148	273.3	1.8298	.05714	0.48 - .96	2.7569
142	277.0	1.8175	.06383	0.49 - .90	2.8050
149	280.2	1.8070	.08451	0.52 - .96	2.9270
157	281.6	1.8024	.09424	0.56 - .93	2.9743

TABLE 10

THERMAL DECOMPOSITION OF NiC_2O_4. EFFECT OF GASES ON INDUCTION PERIODS AND RATE CONSTANTS.

Temp. 276° ± 0.5°C.
Pressure of H_2O 1.8 ± 0.3mm.

Gas	Run	P.mm	$\sqrt{PM}$	t_o	$k''(min^{-1})$ AR	$k'(min^{-1})$ UMD
	178	0	0	23	.0875	.07563
	181	20	23.71	21	.0520	.06382
N_2	180	53	38.5	30	.9545	.06250
	177	102	53.4	30	.0370	.05000
	182	250	83.7	34	.0350	.0458
	183	500	118.3	38	.0435	.03696
	208	100	20.0	25	.0510	.07060
	207	335	36.6	29	.0540	.06476
He	206	484	44.0	32	.0510	.04801
	202	52	47.8	32	.0635	.06040
	203	106	68.3	38	.0504	.04946
CO_2	204	244	103.6	50	.0351	.03805
	205	387	130.5	60	.0353	.03214

TABLE 11

THERMAL DECOMPOSITION OF NiC_2O_4: PELLET OF GROUND POWDER. RATE CONSTANTS DETERMINED FROM AE EQUATION.

DIFFERENTIAL:

Run	Temp°C	$10^3/T°K$	$k''(min^{-1})$	α-range	log k''	t_o(min)
121	241.9	1.9414	.01110	.16-.86	2.0453	150
120	246.3	1.9249	.0168	.13-.71	2.2253	100
122	248.0	1.9186	.0171	.15-.76	2.330	93
113	251.1	1.9073	.01830	.17-.82	2.2625	62
119	251.9	1.9043	.0190	.11-.67	2.2788	60

ACCUMULATORY:

172	255.2	1.8925	.02675	.09-.63	2.4273	58
171	260.7	1.8730	.03343	.06-.79	2.5241	48
166	263.4	1.8636	.05675	.08-.77	2.7540	30
165	266.8	1.8516	.06360	.05-.84	2.8035	20
164	276.0	1.8205	.1056	.03-.83	1.0212	11
163	279.5	1.8093	.1100	.04-.83	1.0414	9

TABLE 12

THERMAL DECOMPOSITION OF NiC_2O_4. PELLET OF GROUND POWDER. RATE CONSTANTS DETERMINED FROM UMD LAW.

DIFFERENTIAL:

Run	Temp°C	$10^3/T°K$	$k'''(min^{-1})$	α-range	log k'''
121	241.9	1.9414	.01590	.58-.95	$\bar{2}$.2014
120	246.3	.19249	.02000	.53-.95	$\bar{2}$.3010
122	248.0	1.9186	.02093	.57-.94	$\bar{2}$.3208
113	251.1	1.9073	.02550	.51-.95	$\bar{2}$.4065

ACCUMULATORY:

172	255.2	1.8925	.03129	.50-.95	$\bar{2}$.4954
171	260.7	1.8730	.04128	.59-.93	$\bar{2}$.6157
166	263.4	1.8636	.06317	.55-.93	$\bar{2}$.8005
164	276.0	1.8205	.1278	.60-.97	$\bar{1}$.1065
163	279.5	1.8093	.1484	.60-.96	$\bar{1}$.1714

TABLE 13

THERMAL DECOMPOSITION OF NiC_2O_4. IN PRESENCE OF METALS. RATE CONSTANTS DETERMINED FROM AE EQUATION.

D = differential run; A = accumulatory run.

Run	Temp°C	$10^3/T°K$	t_o(min)	$k''(min^{-1})$	α-range	log k''	Method.
4.4% Ni.							
118	241.6	1.9425	150	.00890	.14-.82	$\bar{3}$.9494	
116	245.2	1.9290	105	.01190	.05-.69	$\bar{2}$.0755	D
114	251.3	1.9066	65	.01804	.01-.82	$\bar{2}$.2562	
117	254.0	1.8968	50	.01940	.07-.71	$\bar{2}$.2878	
161	264.8	1.8587	20	.04050	.04-.73	$\bar{2}$.6075	
160	275.6	1.8222	13	.07270	.02-.71	$\bar{2}$.8615	A
162	280.6	1.8057	7	.0965	.07-.80	$\bar{2}$.9845	
9.1% Au.							
124	242.2	1.9402	140	.01212	.16-.83	$\bar{2}$.0835	
130	247.7	1.9197	95	.01566	.09-.83	$\bar{2}$.1947	
123	248.6	1.9165	70	.01830	.14-.82	$\bar{2}$.2625	D
125	254.0	1.8968	55	.02180	.13-.83	$\bar{2}$.3385	
170	265.0	1.8580	30	.05970	.04-.54	$\bar{2}$.7760	
167	269.0	1.8443	24	.06820	.05-.65	$\bar{2}$.8338	A
168	282.3	1.8002	9	.1215	.04-.77	$\bar{1}$.0846	
19.8% Pt.							
127	240.6	1.9463	135	.01015	.14-.87	$\bar{2}$.0064	
129	247.8	1.9194	80	.01330	.15-.80	$\bar{2}$.1239	D
126	249.5	1.9131	70	.91680	.12-.82	$\bar{2}$.2253	
128	255.4	1.8918	45	.02026	.10-.85	$\bar{2}$.3067	
175	263.1	1.8646	30	.04135	.05-.92	$\bar{2}$.6165	
173	272.8	1.8315	15	.06565	.04-.88	$\bar{2}$.8172	A
174	280.1	1.8073	10	.1030	.05-.86	$\bar{1}$.0128	

TABLE 14

THERMAL DECOMPOSITION OF NiC_2O_4 IN PRESENCE OF METALS.

RATE CONSTANTS DETERMINED FROM UMD LAW.

Run	Temp°C	$10^3/T°K$	K''' (min^{-1})	α-range	log K'''	Method.
4.4% Ni.						
118	241.6	1.9425	.01349	.56-.95	$\bar{2}$.1300	
116	245.2	1.9290	.01396	.58-.97	$\bar{2}$.1449	D
114	251.3	1.9066	.02284	.57-.93	$\bar{2}$.3587	
117	254.0	1.8968	.02208	.52-.94	$\bar{2}$.3440	
161	264.8	1.8587	.05769	.57-.97	$\bar{2}$.7611	
160	275.6	1.8222	.09279	.53-.96	$\bar{2}$.9675	A
162	280.6	1.8057	.1295	.50-.96	$\bar{1}$.1123	
9.1% Au.						
124	242.2	1.9402	.01717	.60-.96	$\bar{2}$.2348	
130	247.7	1.9197	.02098	.53-.97	$\bar{2}$.3218	D
123	248.6	1.9165	.02308	.58-.91	$\bar{2}$.3632	
125	254.0	1.8968	.02761	.53-.91	$\bar{2}$.4411	
170	265.0	1.8580	.05714	.48-.88	$\bar{2}$.7569	
167	269.0	1.8443	.09000	.59-.99	$\bar{2}$.9542	A
168	282.3	1.8002	.1513	.53-.96	$\bar{1}$.1799	
19.8% Pt.						
127	240.6	1.9463	.01648	.60-.96	$\bar{2}$.2170	
129	247.8	1.9194	.01846	.46-.96	$\bar{2}$.2662	D
126	249.5	1.9131	.02407	.48-.93	$\bar{2}$.3814	
128	255.4	1.8918	.02728	.58-.94	$\bar{2}$.4358	
175	263.1	1.8646	.06667	.54-.96	$\bar{2}$.8240	
173	272.8	1.8315	.09730	.43-.95	$\bar{2}$.9881	A
174	280.1	1.8073	.1552	.56-.99	$\bar{1}$.1909	

FIGURE 10

T.D. OF NiC_2O_4 IN PRESENCE OF WATER VAPOUR. AE PLOT.

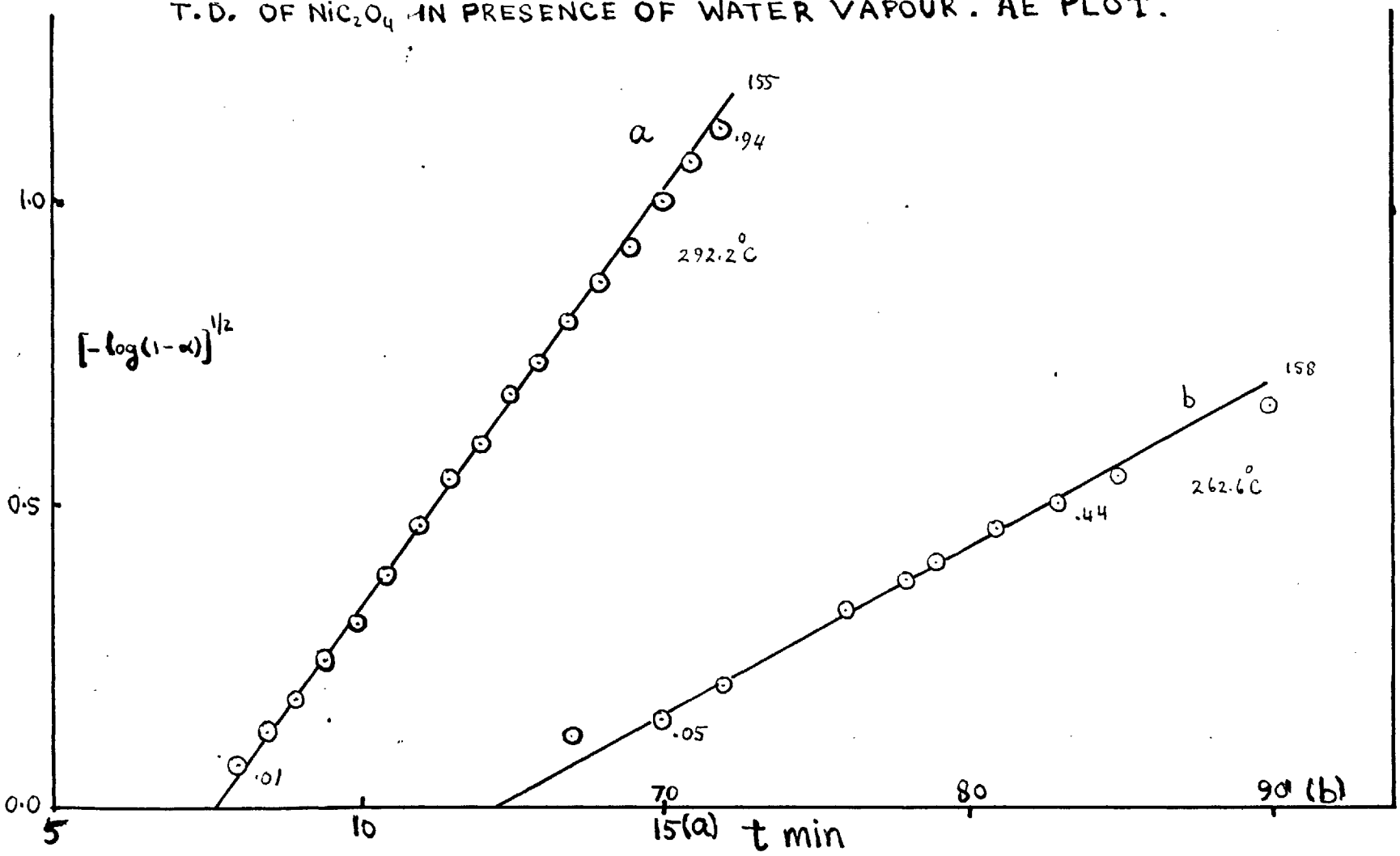

FIGURE II

T. D. OF NiC_2O_4 . EFFECT OF H_2 AND O_2 .

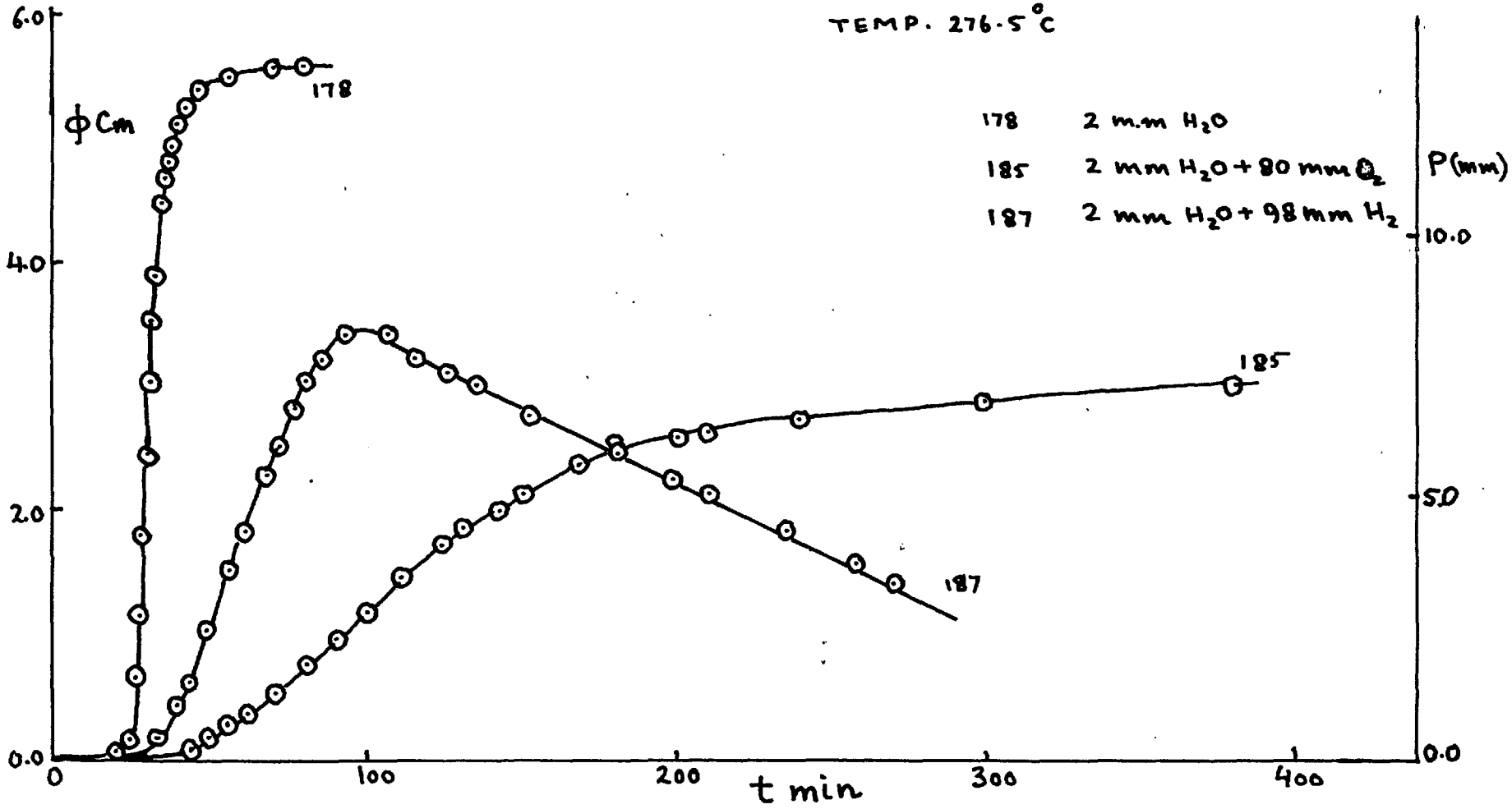

FIGURE 12

T.D. OF NiC_2O_4. EFFECT OF GASES. α-t PLOTS.

TEMP. 276.5°C.

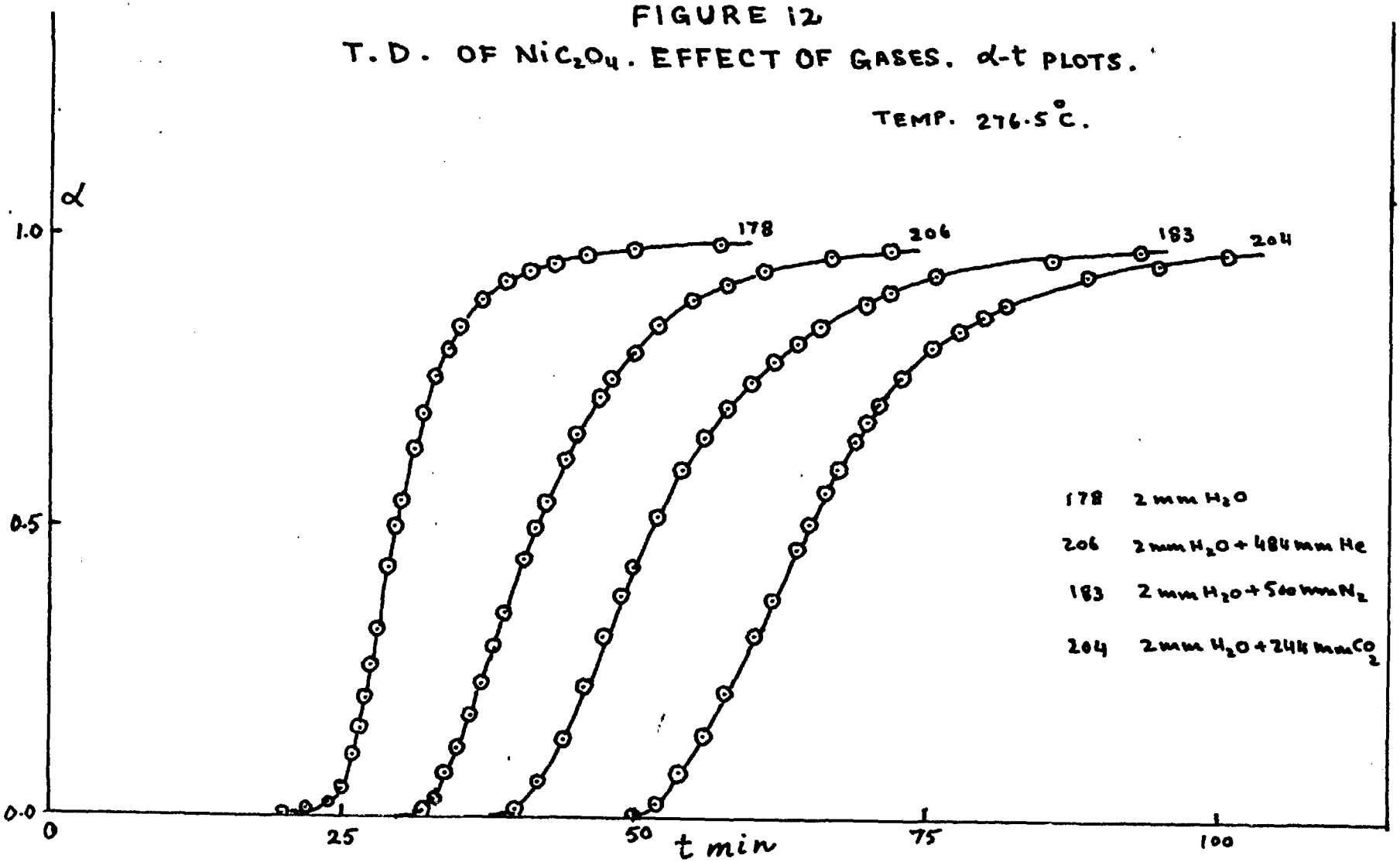

FIGURE 13

T.D. OF NiC_2O_4 · EFFECT OF GASES. AE PLOTS.

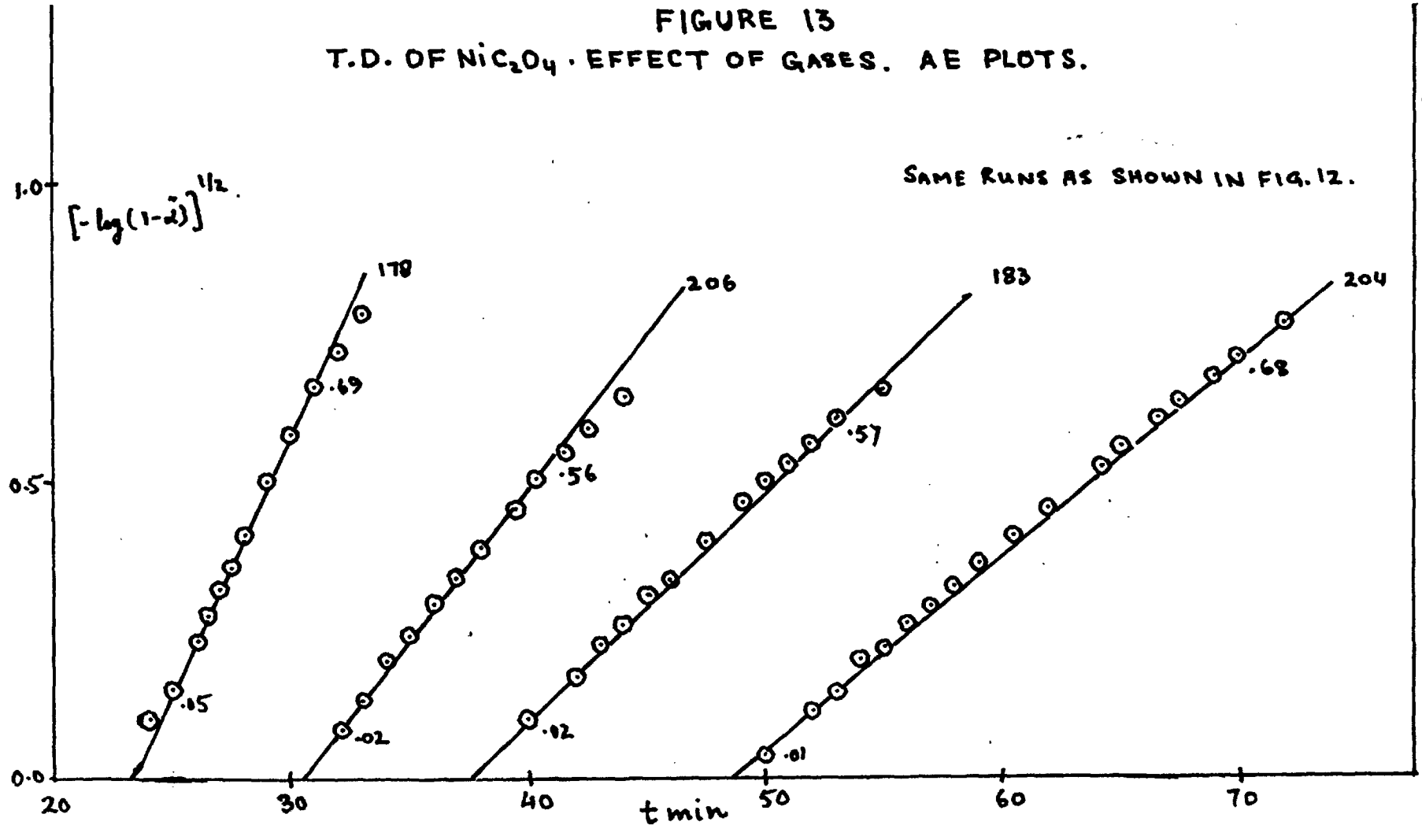

FIGURE 14

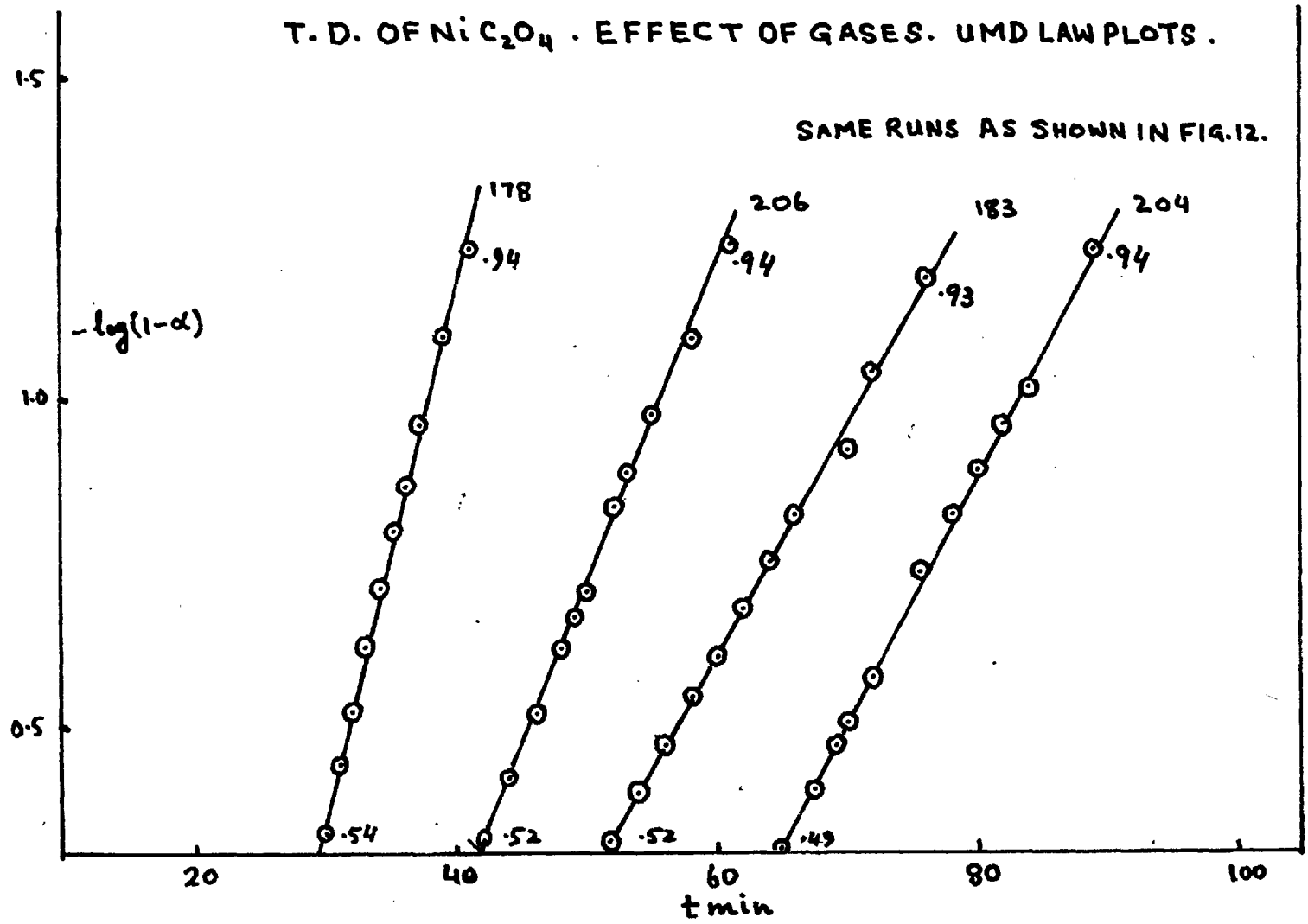
T. D. OF Ni C2O4 . EFFECT OF GASES. UMD LAW PLOTS .
SAME RUNS AS SHOWN IN FIG. 12.
-log(1-α)
1.5
1.0
0.5
178
.94
.54
206
.94
.52
183
.93
.52
204
.94
.49
20
40
60
80
100
t min

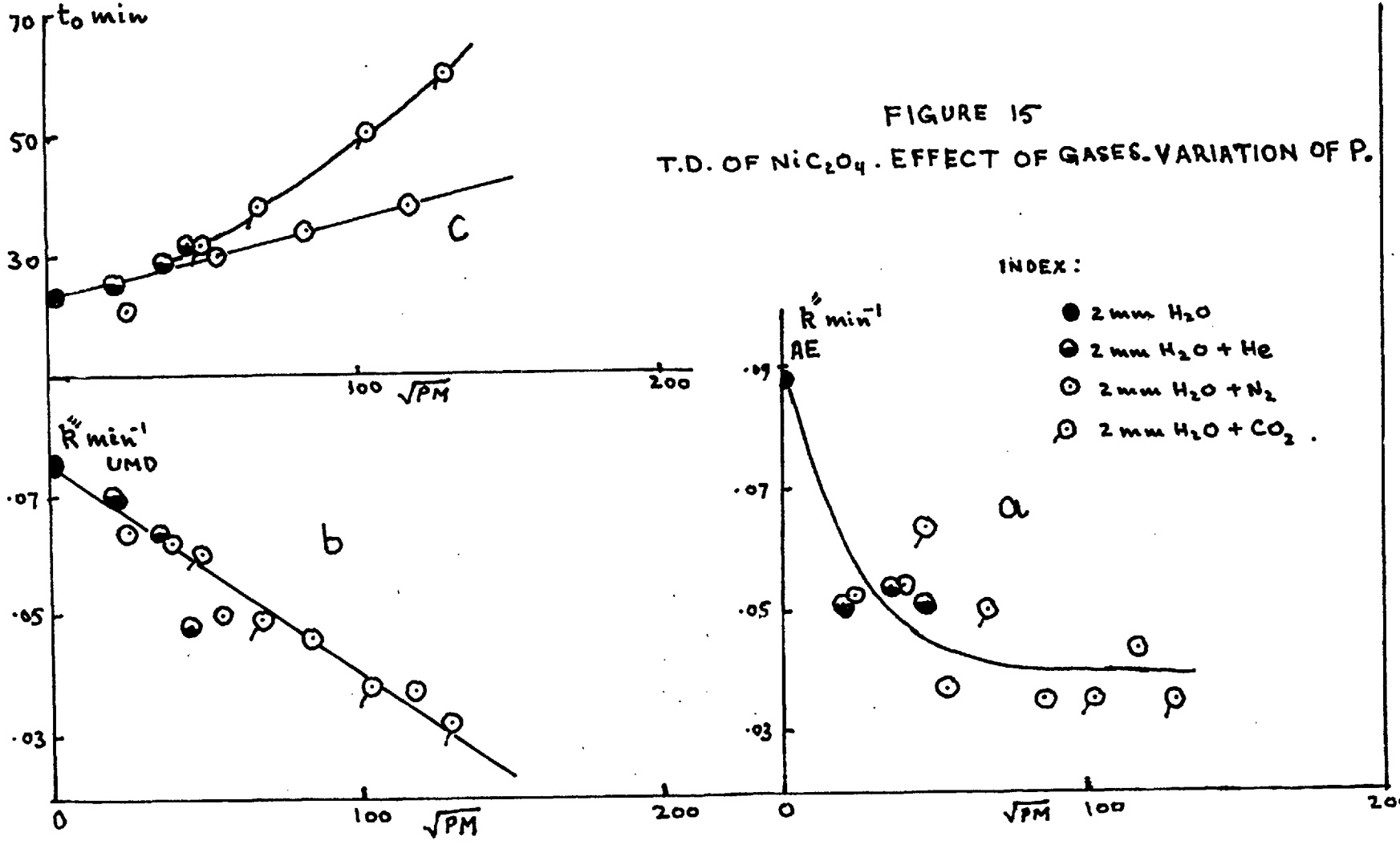

FIGURE 15

T.D. OF NiC_2O_4 . EFFECT OF GASES. VARIATION OF P.

FIGURE 16

T. D. OF NiC_2O_4 . PELLET OF GROUND POWDER . α-t PLOTS.

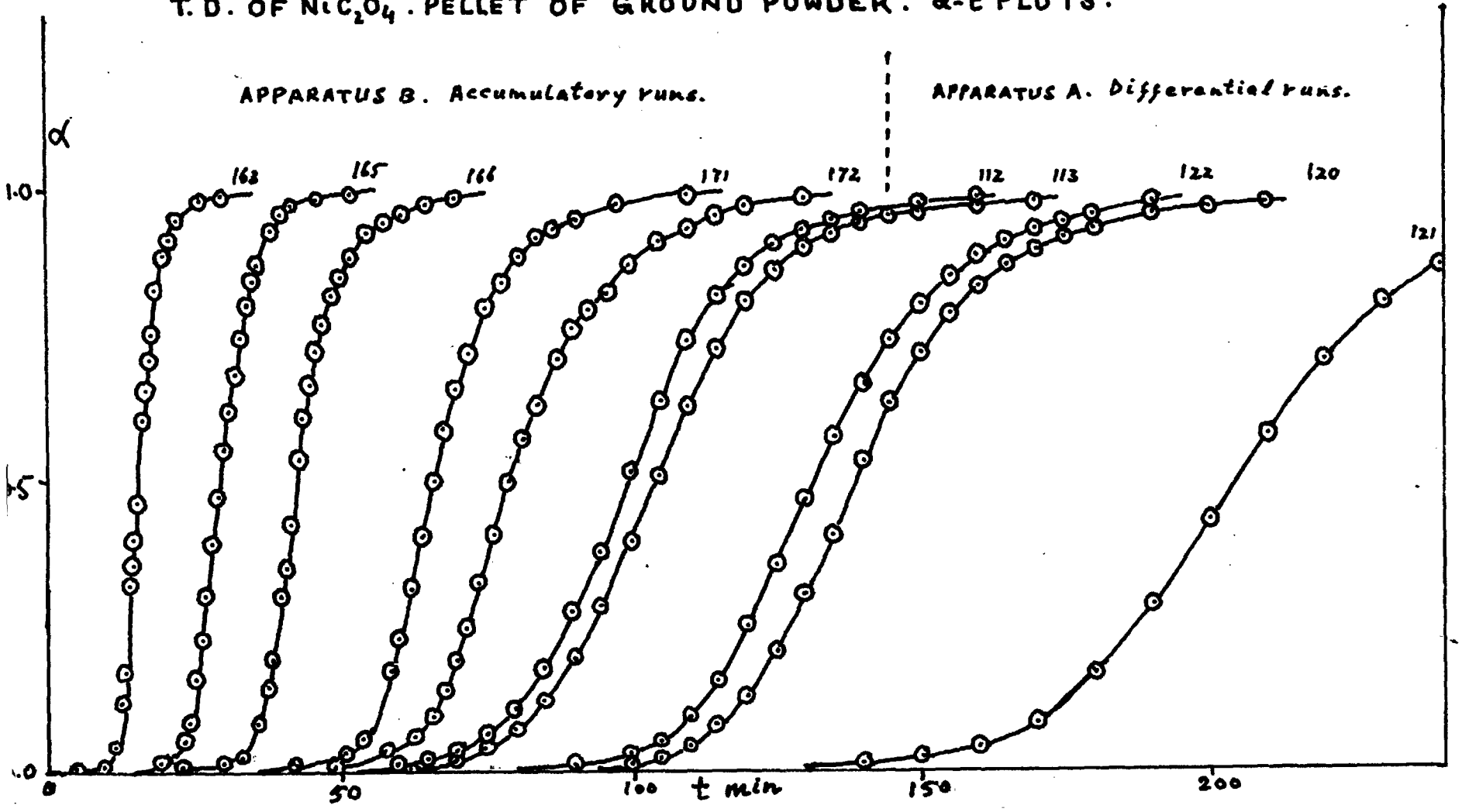

FIGURE 17

T.D. OF NiC_2O_4. PELLET OF GROUND POWDER. AE PLOTS.

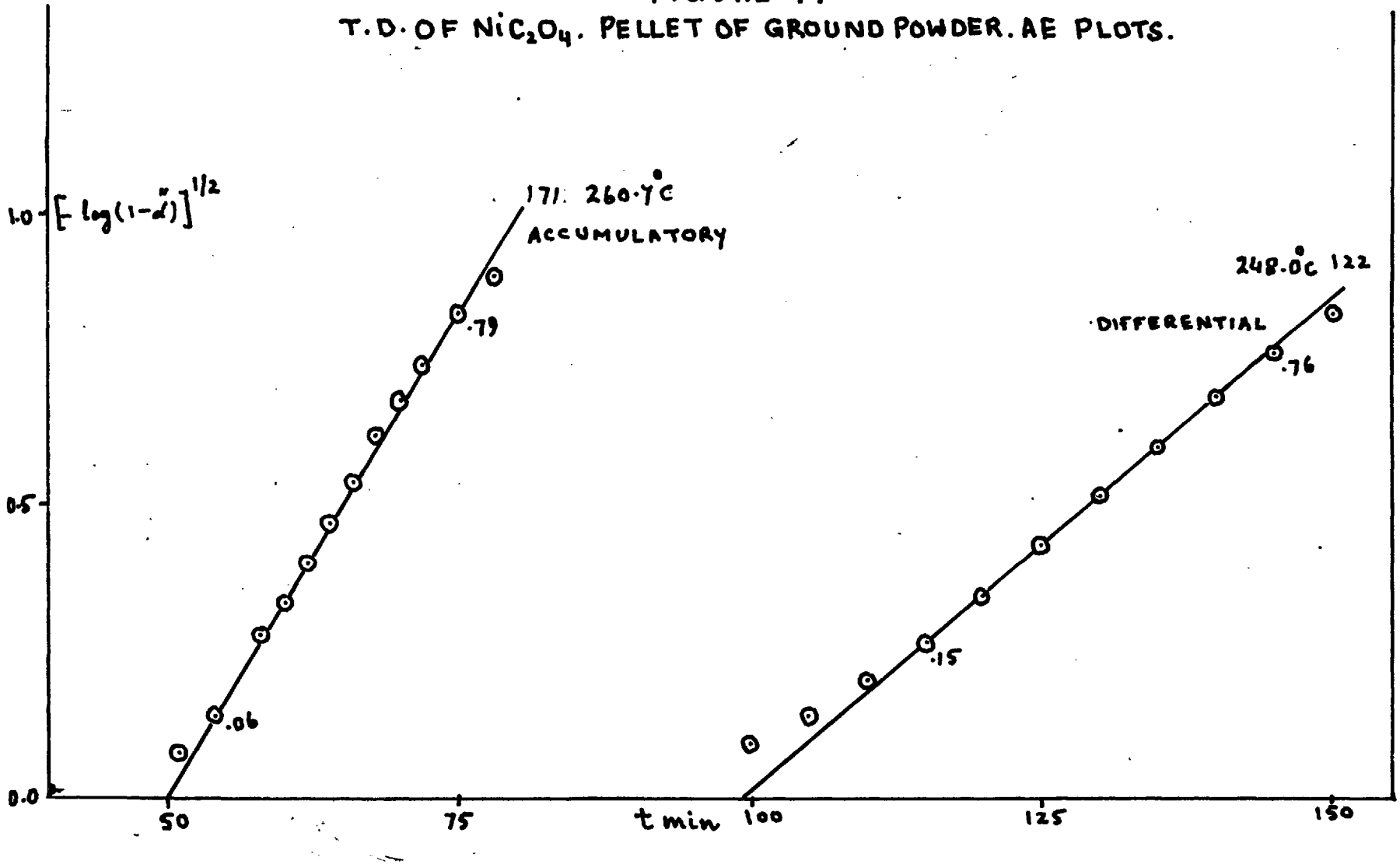

FIGURE 18

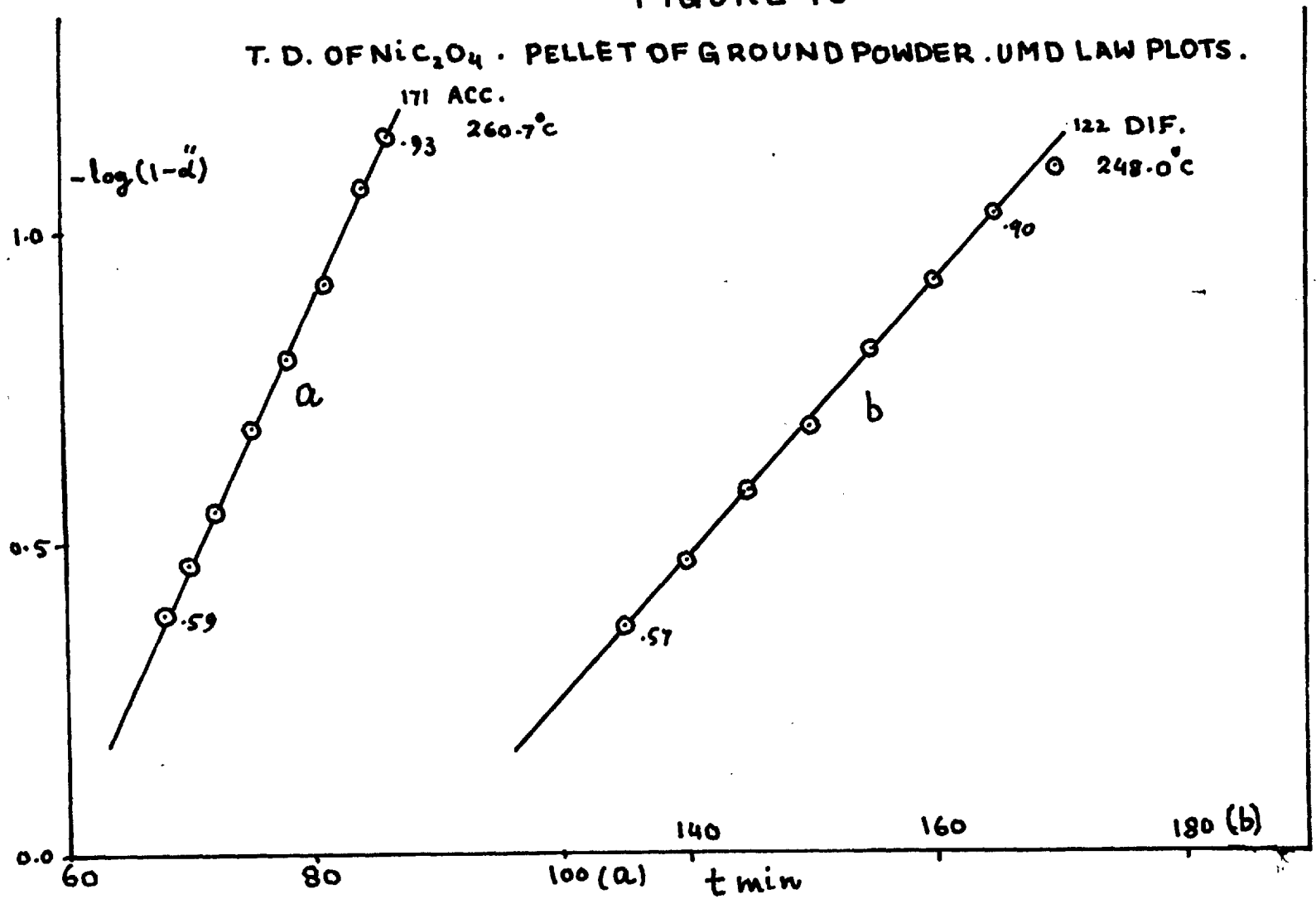
T. D. OF NiC_2O_4 . PELLET OF GROUND POWDER . UMD LAW PLOTS.
171 ACC.
260.7°C
.93
122 DIF.
248.0°C
.90
$-\log(1-\alpha)$
1.0
0.5
0.0
.59
.57
a
b
60
80
100 (a)
140
160
180 (b)
t min

FIGURE 19.

T. D. OF NiC_2O_4 IN PRESENCE OF METELS. AE PLOTS.

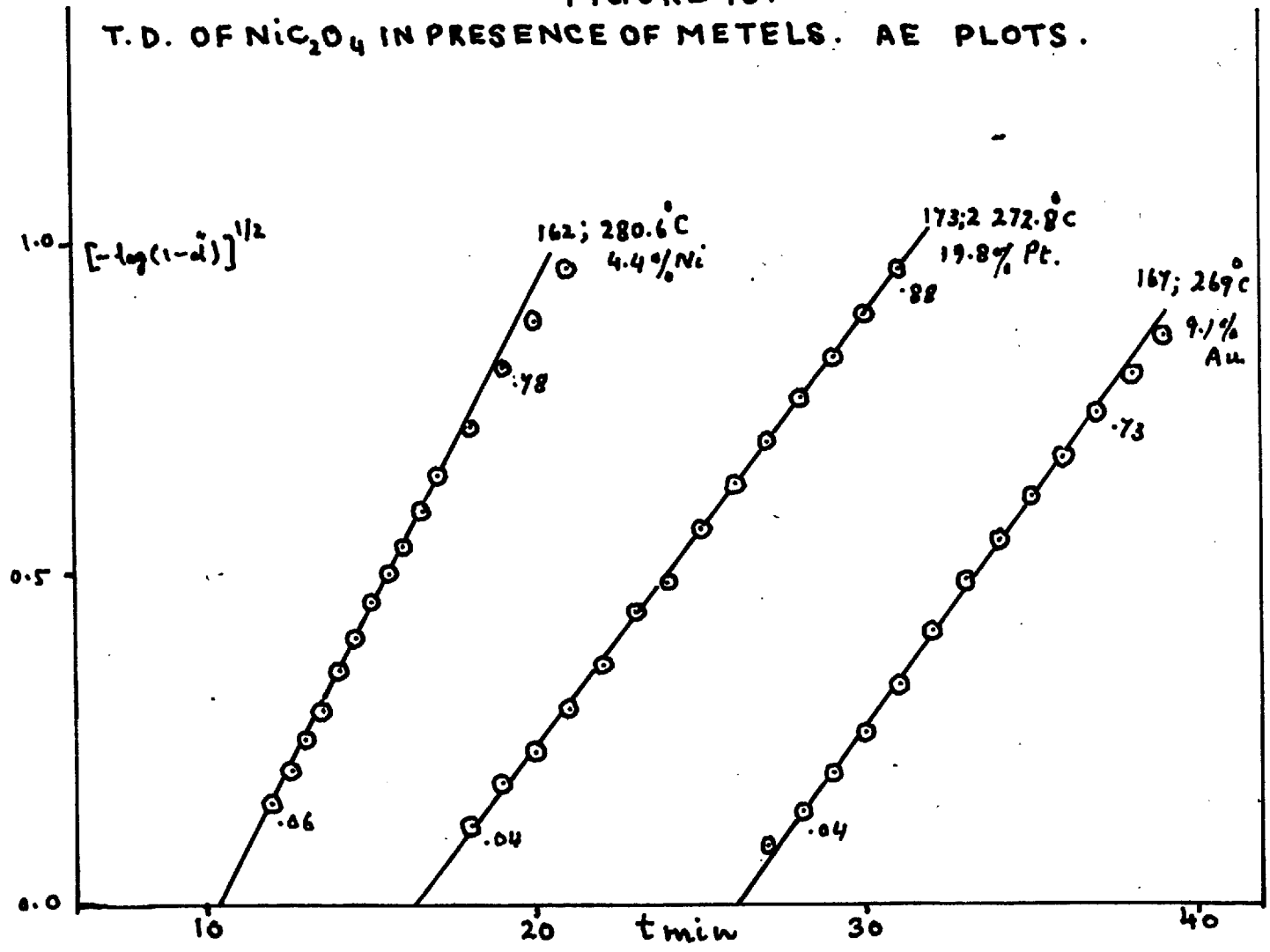

FIGURE 20

T. D. OF NiC_2O_4 INPRESENCE OF METELS. ARRHENIUS PLOTS.

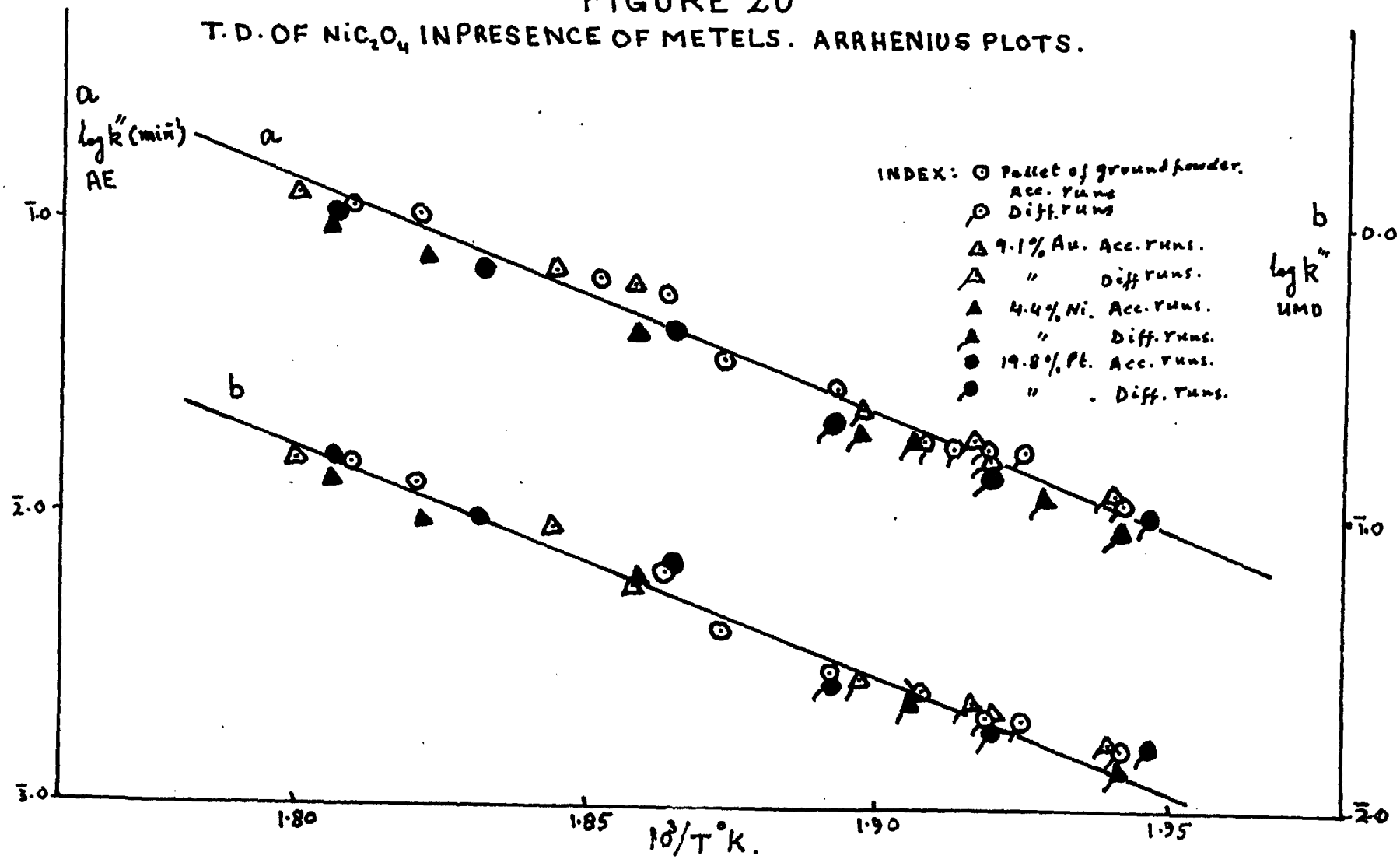

FIGURE 21.

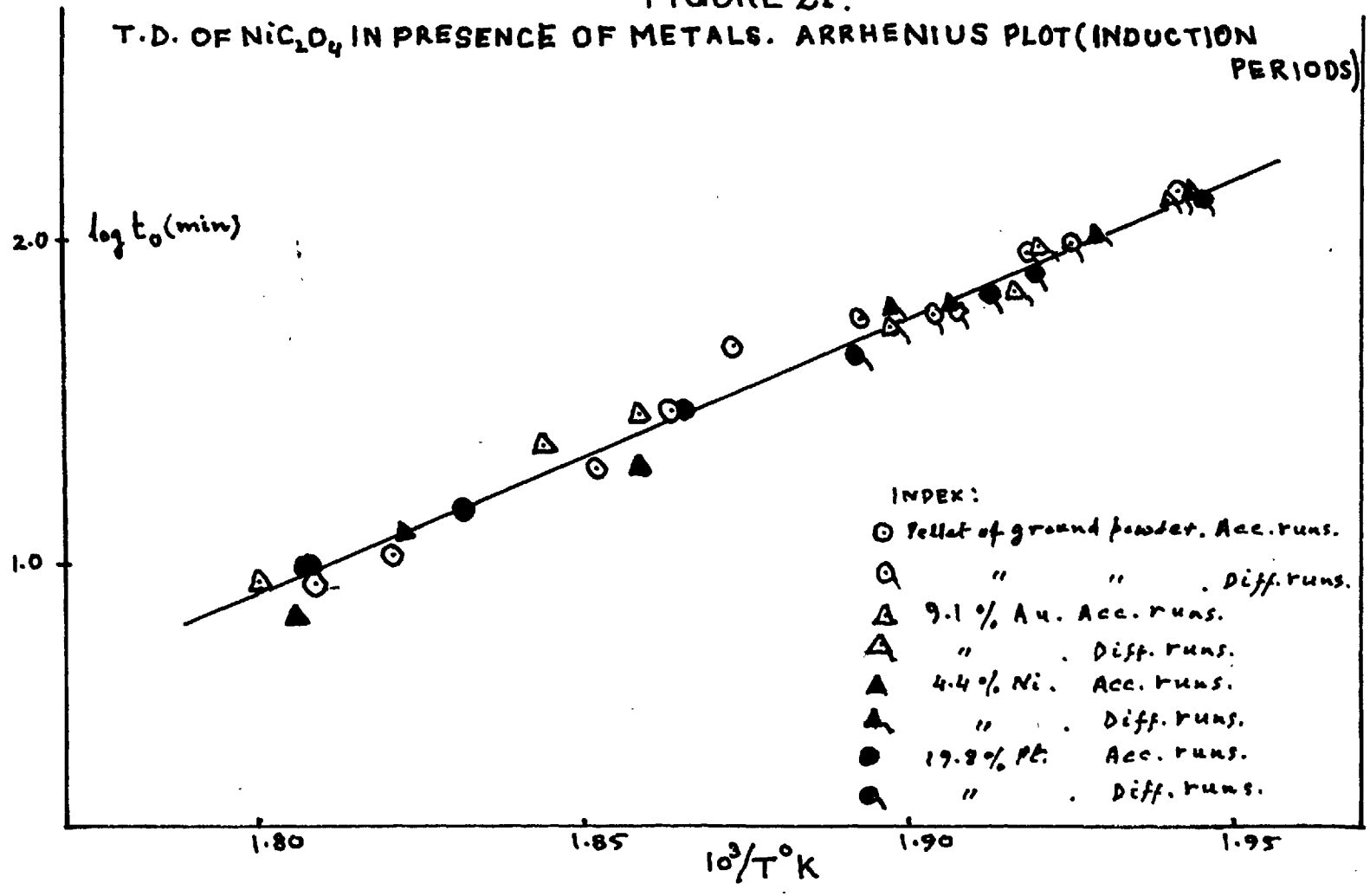
T.D. OF NiC_2O_4 IN PRESENCE OF METALS. ARRHENIUS PLOT (INDUCTION PERIODS)
2.0
1.0
log t_0 (min)
1.80
1.85
1.90
1.95
$10^3/T°K$
INDEX:
Pellet of ground powder. Acc. runs.
" " . Diff. runs.
9.1 % Au. Acc. runs.
" . Diff. runs.
4.4 % Ni. Acc. runs.
" . Diff. runs.
19.8 % Pt. Acc. runs.
" . Diff. runs.

3.2 NICKEL OXALATE DI-HYDRATE

3.21 $NiC_2O_4.2H_2O$ powder and pellets ; accumulatory runs:

Using Apparatus A, 6 mg samples of the salt were decomposed isothermally. Results obtained on compressed pellets of this salt were very irreproducible; hence all the work on hydrated salt was done on powder. Only Apparatus A could be used which limited the temperature range to between 245°C and 260°C, above which the reaction becomes too fast to be followed accurately with a Mcleod gauge. The shape of the α-t curves is sigmoid, as shown in Fig. 22a. Runs 9 and 10 were done at the same temperature to check reproducibility. There is also an initial decay reaction as in dehydrated salt; this is shown in Fig. 22b on an enlarged scale. This corresponds, as in the dehydrated salt, to 1% of the total decomposition. Defining α' in the same way as in section 3.11, this initial reaction again obeys the contracting area law, $1-(1-\alpha')^{\frac{1}{2}} = kt$. Fig. 23a shows two characteristic plots of $1-(1-\alpha')^{\frac{1}{2}}$ vs.t. The values of these rate constants for all runs of this series are given in Table 15 together with the range of α over which the equation holds. The Arrhenius plot is shown in Fig. 24a. The value of activation energy calculated from this plot is 33.8 kcal/mole. The rest of the reaction from α = 0.10 to 0.85 is fitted by the AE equation with n = 2. Two

typical AB plots are shown in Fig. 23b and values of rate constants given in Table 16. Fig. 24b shows the Arrhenius plot; the activation energy is 50.3 kcal/mole.

3.22 Differential runs: The α-t plots were determined from rate curves by numerical integration as before. Fig. 25a shows a typical rate curve and 25b the integrated α-t curve. The latter could not be fitted by the Avrami-Erofeyev equation below α = 0.20 but between α=0.20 and α= 0.68 the equation holds well; one such plot is shown in Fig. 25c. Values of the rate constants are given in Table 17 and the Arrhenius plot is shown in Fig. 24c. The activation energy found from this plot is 31.1 kcal/mole. Log t_o vs. 1/T plots for both accumulatory and differential runs are shown in Fig. 26. The activation energies calculated from this plot is 39.3 kcal/mole. The numerical values of t_o are given in Tables 16 and 17. Lines b and c, shown for comparison in Fig. 26, are for dehydrated salt with and without the trap, respectively.

3.23 Dehydration of $NiC_2O_4.2H_2O$: The dehydration of the salt was studied in the temperature range of 172° - 223°C using Apparatus B. The salt was made into a pellet which was broken into fragments of suitable size (12 - 18 mg). The dehydration of these fragments was followed by measuring the

deflection of spiral gauge. The plots of ϕ/m (where ϕ is deflection in cm and m the mass of the sample in g) vs.t are shown in Fig. 27 for three runs. The initial part of these plots can be fitted by unimolecular decay law if the fraction dehydrated is calculated from $\alpha = \phi/\phi_{max}$, where ϕ is the observed deflection and ϕ max. is the total deflection calculated from the mass of the sample and the volume of the system (194 ml). The range of α over which UMD law holds is rather small and increases steadily with temperature. This is due to the complicating effects of the rehydration process. UMD law plots at three different temperatures are shown in Fig. 28. An Arrhenius plot for these rate constants is shown in Fig. 29 from which a value of 18.4 kcal/mole is obtained for the activation energy associated with the dehydration process.

TABLE 15

SURFACE REACTION IN THERMAL DECOMPOSITION OF $NiC_2O_4.2H_2O$.

RATE CONSTANTS DETERMINED FROM CONTRACTING AREA EQUATION.

Run	Temp °C	$10^3/T°_K$	$k(min^{-1})$	α-range	$\log k$
12	245.0	1.9295	.01280	.00-.0090	$\bar{2}.1072$
14	247.5	1.9205	.01632	.00-.0095	$\bar{2}.2127$
10	250.0	1.9115	.02045	.00-.0095	$\bar{2}.3120$
11	250.0	1.9115	.01870	.00-.0092	$\bar{2}.2718$
15	252.5	1.9022	.02267	.00-.0074	$\bar{2}.3555$
17	255.0	1.8932	.02525	.00-.0081	$\bar{2}.4022$
20	260.0	1.8754	.03250	.00-.0066	$\bar{2}.5119$

TABLE 16

THERMAL DECOMPOSITION OF NiC_2O_4: ACCUMULATORY RUNS. RATE CONSTANTS DETERMINED FROM THE AVRAMI-EROFEYEV EQUATION

Run	Temp°C	$10^3/T°K$	$k''(min^{-1})$	α-range	log k''	t_o(min)
12	245.0	1.9295	.02000	.06-.82	2.3010	142
14	247.5	1.9205	.02456	.07-.82	2.3900	118
10	250.0	1.9115	.02900	.06-.96	2.4620	101
11	250.0	1.9115	.02900	.08-.87	2.4620	100
15	252.5	1.9022	.03750	.10-.79	2.5740	72.5
17	255.0	1.8932	.05075	.11-.81	2.7050	76.0
21	257.5	1.8843	.05925	.11-.85	2.7730	58.2
20	260.0	1.8754	.08100	.05-.96	2.9080	54.7

TABLE 17

THERMAL DECOMPOSITION OF NiC_2O_4. DIFFERENTIAL RUNS. RATE CONSTANTS DETERMINED FROM THE AVRAMI-EROFEYEV EQUATION.

Run	Temp°C	$10^3/T°K$	$k''(min^{-1})$	α-range	log k''	t_o(min)
103	235.3	1.9666	.01250	.25-.88	$\bar{2}$.0969	320
98	238.0	1.9562	.01400	.29-.87	$\bar{2}$.1461	232
97	240.6	1.9470	.01640	.19-.87	$\bar{2}$.2148	202
99	243.9	1.9339	.02040	.18-.84	$\bar{2}$.3096	152
100	247.8	1.9194	.02420	.27-.88	$\bar{2}$.3838	100
102	251.9	1.9044	.02810	.25-.85	$\bar{2}$.4487	94

TABLE 18

DEHYDRATION OF $NiC_2O_4.2H_2O$: UNIMOLECULAR DECAY LAW RATE CONSTANTS.

Run	Temp °C	$10^3/T°K$	$k(min^{-1})$	log k	α-range
192	172.4	2.2442	0.01316	2.1193	.00-.16
199	178.6	2.2134	0.01773	2.2487	.00-.16
193	185.5	2.1801	0.02174	2.3373	.00-.23
196	192.6	2.1468	0.02760	2.4409	.00-.25
197	200.1	2.1128	0.04100	2.6128	.00-.36
198	207.9	2.0786	0.05750	2.5797	.00-.45
200	215.7	2.0454	.08257	2.9169	.00-.51
201	222.8	2.0161	0.1085	1.0354	.00-.61

FIGURE 22

T.D. OF $NiC_2O_4 \cdot 2H_2O$. α-t PLOTS TO SHOW REPRODUCIBILITY.

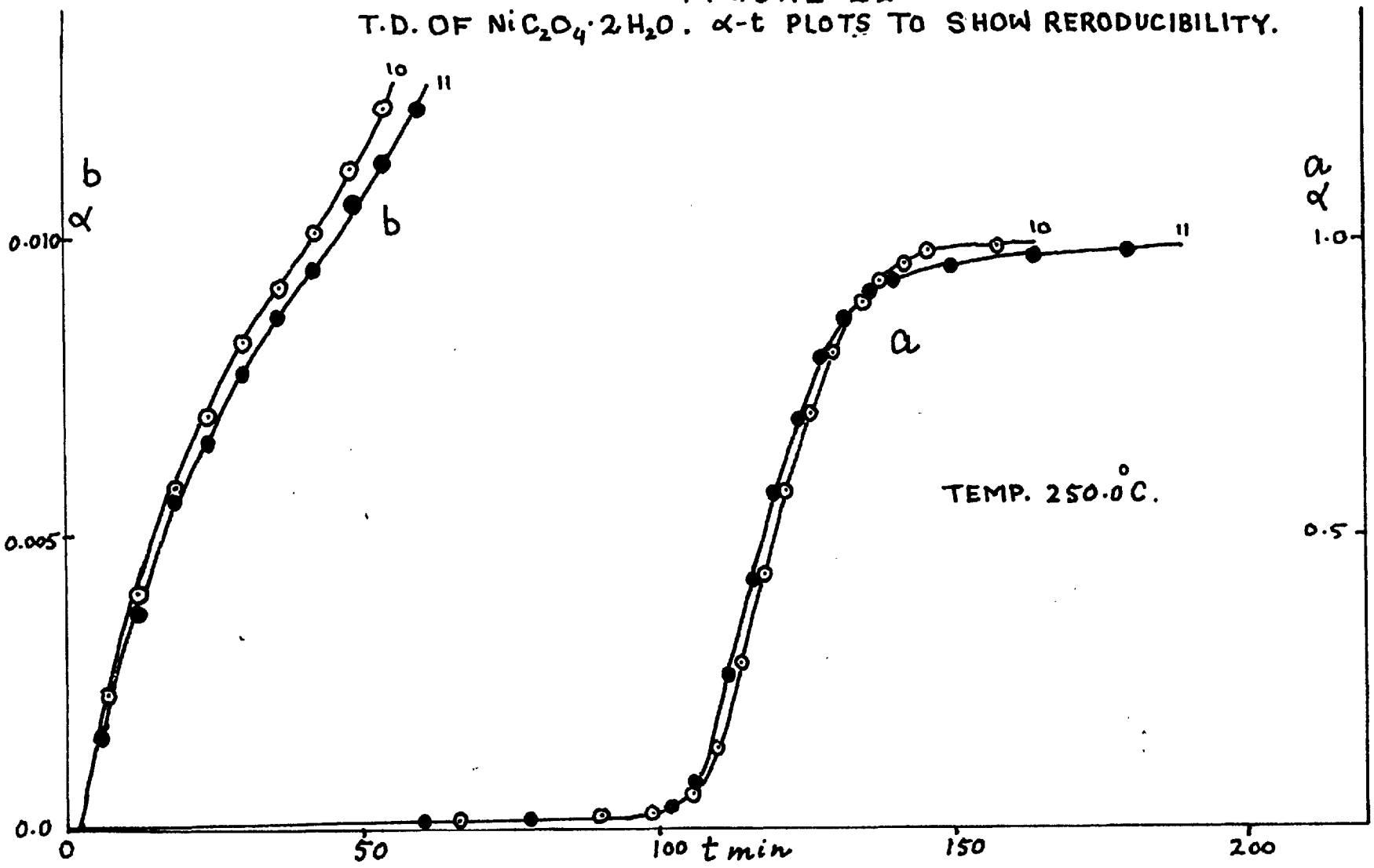

FIGURE 23

T.D. OF $NiC_2O_4 \cdot 2H_2O$. (a) C.A. PLOTS (b) AE PLOTS. TEMP. 250°C.

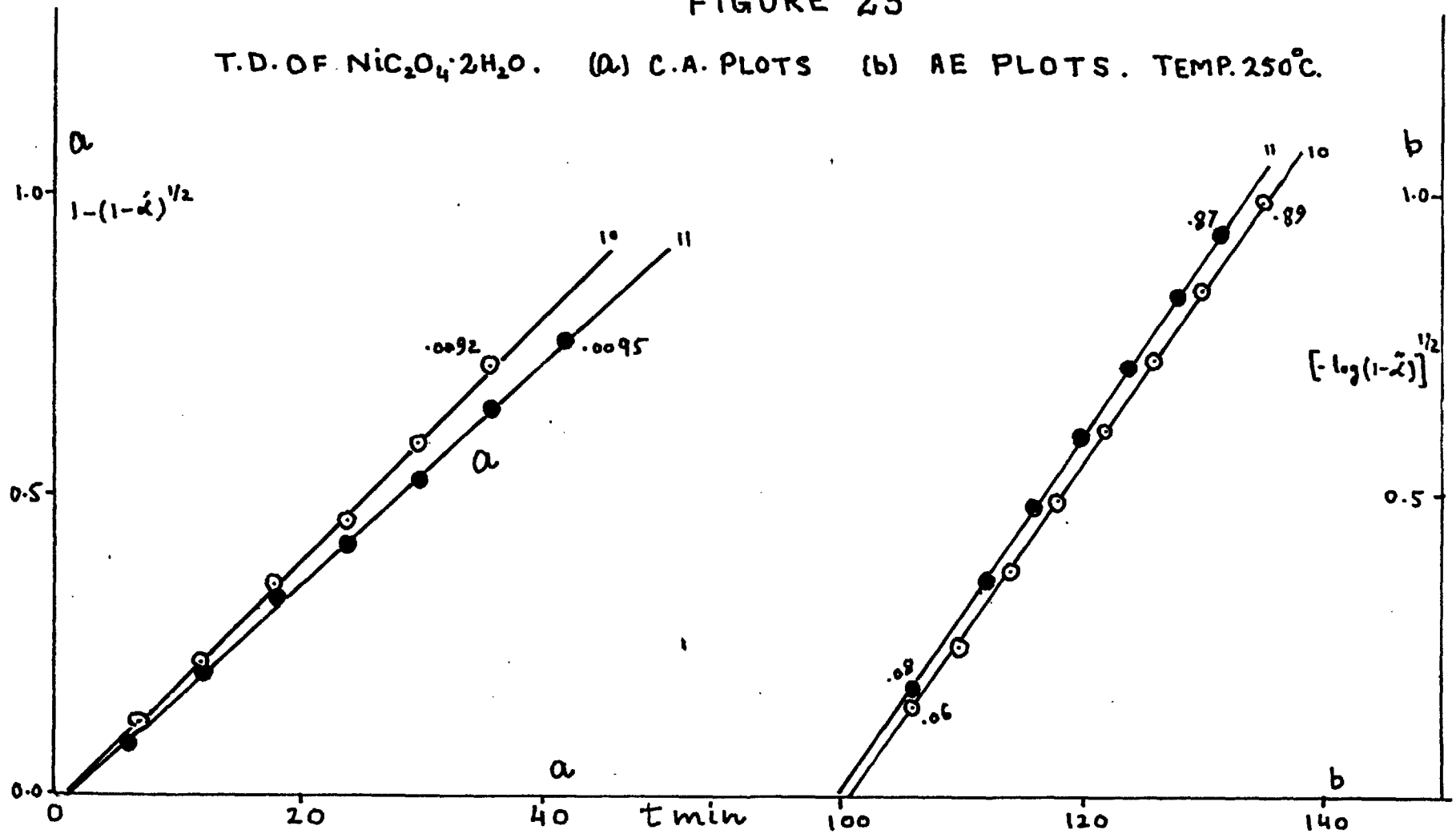

FIGURE 24.

T.D. OF $NiC_2O_4 \cdot 2H_2O$. ARRHENIUS PLOTS.

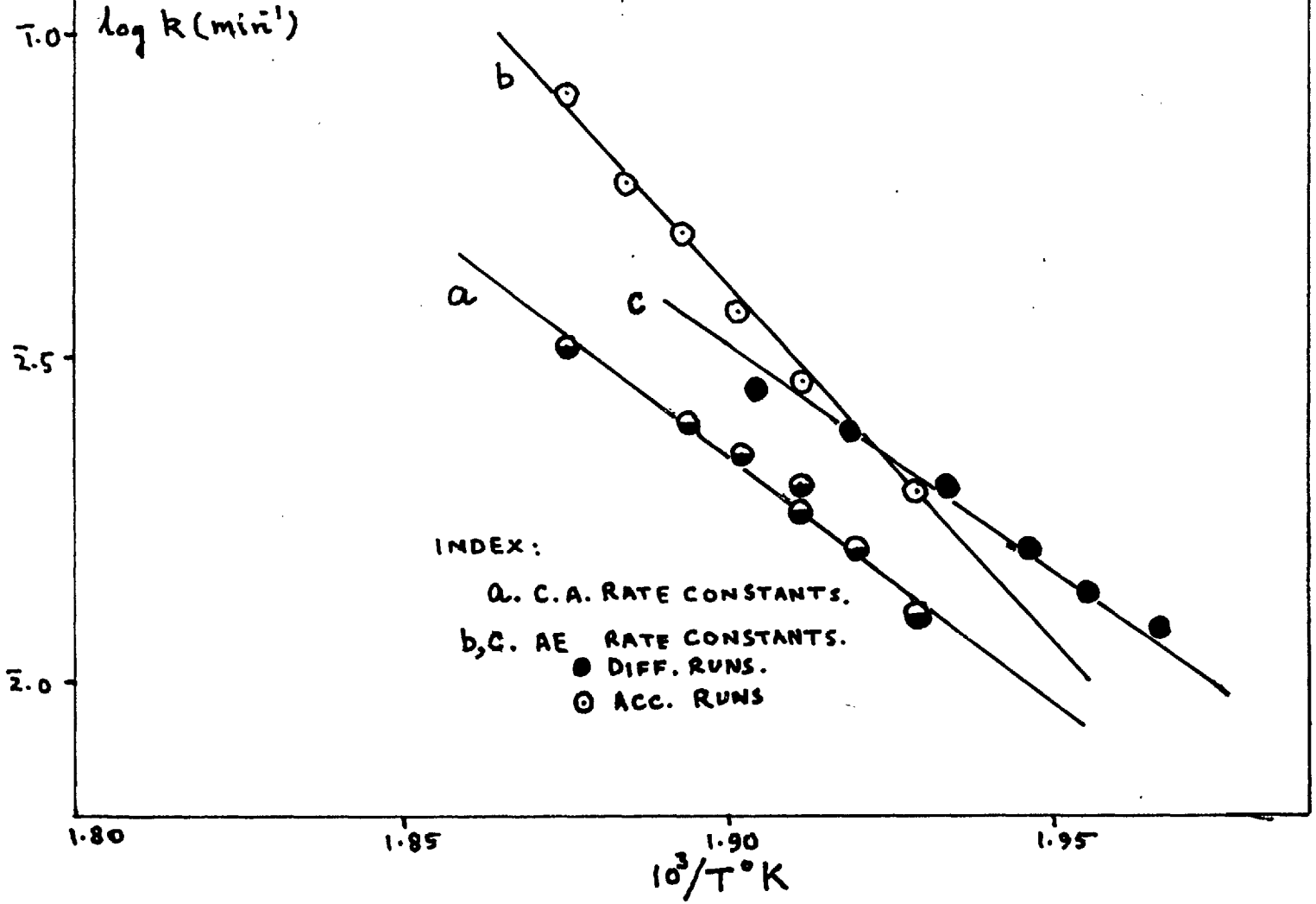

FIGURE 25

T.D. OF $NiC_2O_4 \cdot 2H_2O$ BY DIFFERENTIAL METHOD.

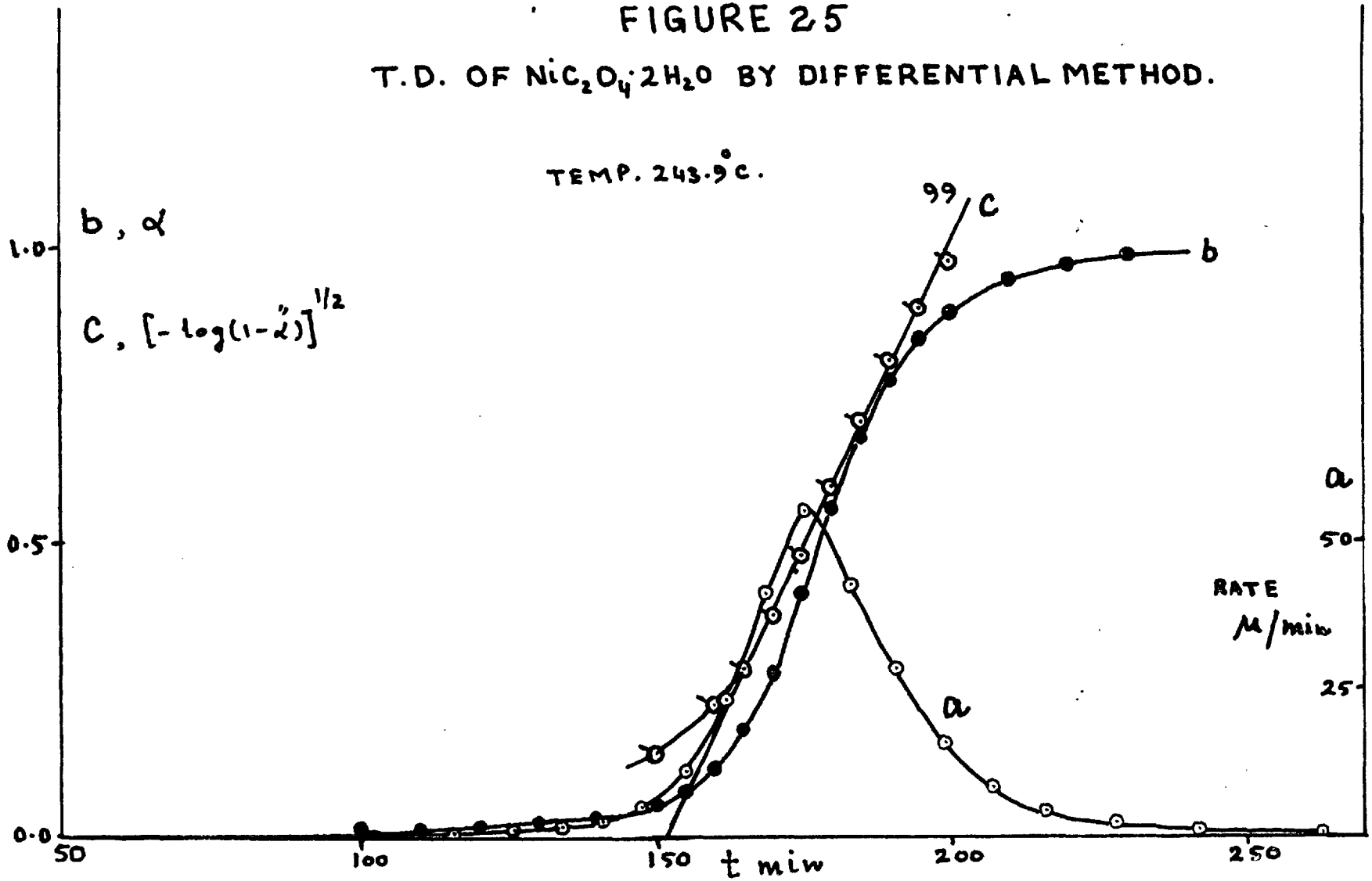

FIGURE 26

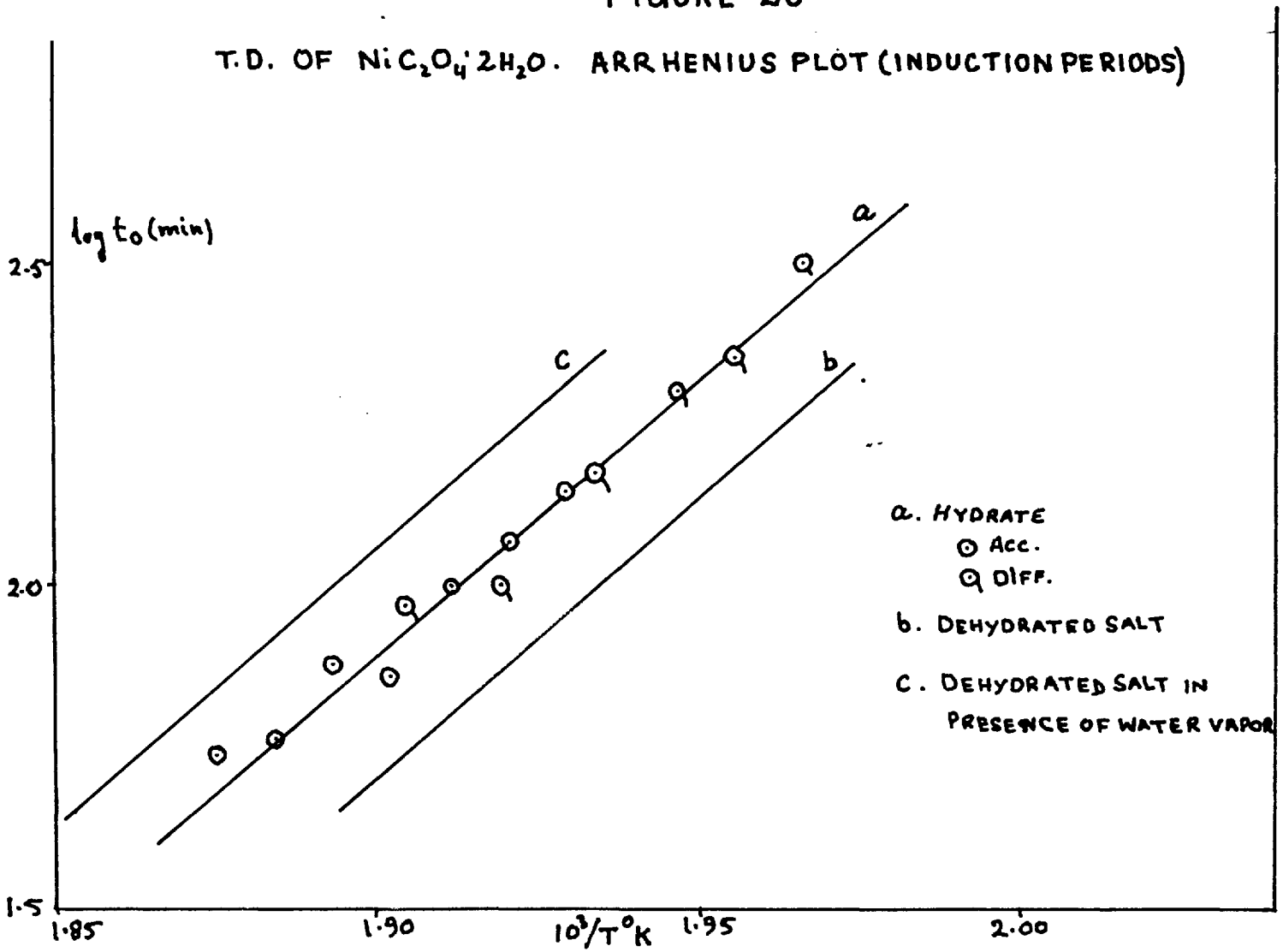
T.D. OF $NiC_2O_4 \cdot 2H_2O$. ARRHENIUS PLOT (INDUCTION PERIODS)
log t_0 (min)
2.5
2.0
1.5
1.85
1.90
$10^3/T^\circ K$
1.95
2.00
a
b
c
a. HYDRATE
⊙ Acc.
Q Diff.
b. DEHYDRATED SALT
C. DEHYDRATED SALT IN PRESENCE OF WATER VAPOR

FIGURE 27

DEHYDRATION OF $NiC_2O_4 \cdot 2H_2O$. PRESSURE-TIME PLOTS.

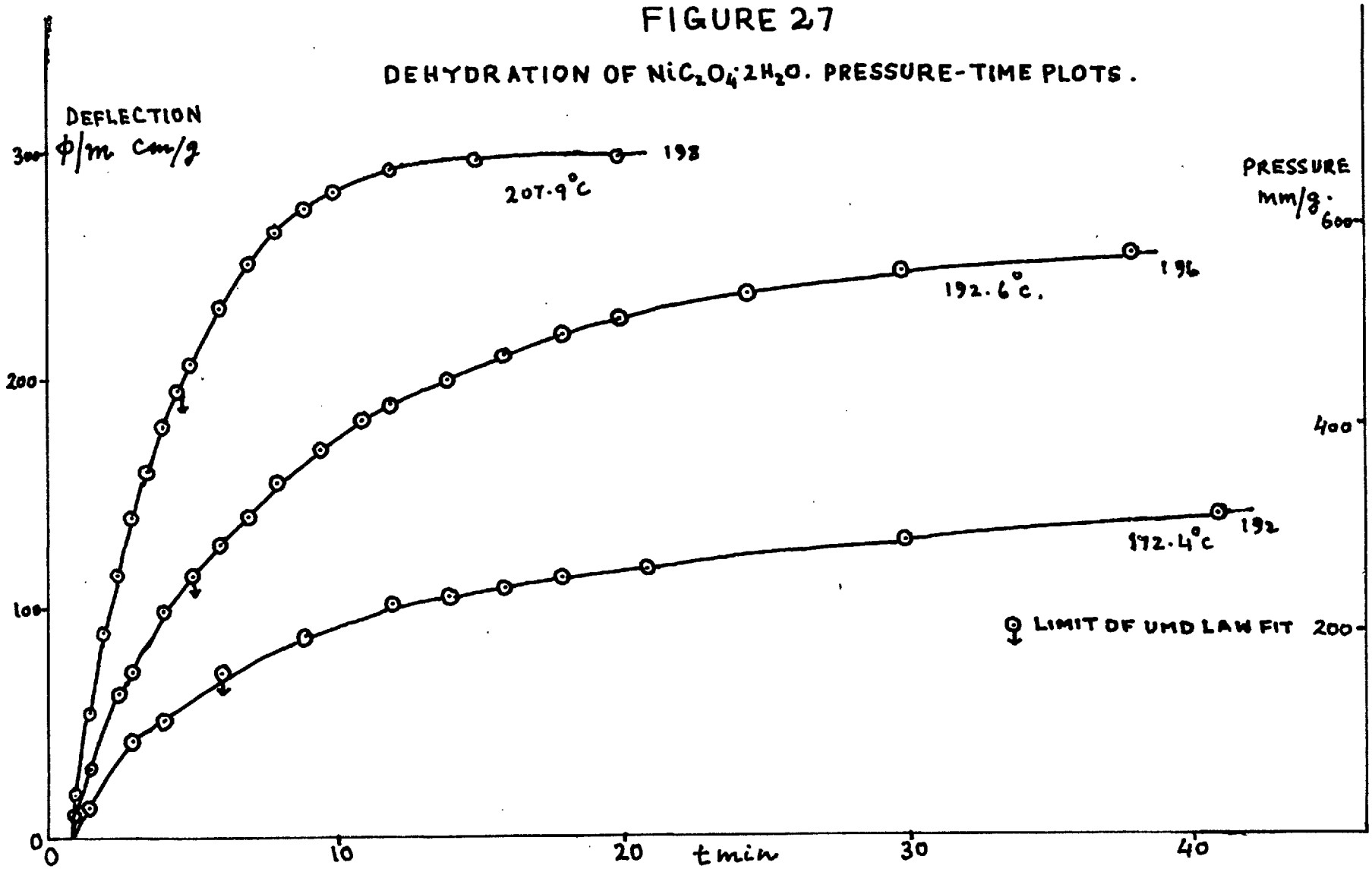

FIGURE 28

DEHYDRATION OF $NiC_2O_4 2H_2O$. UMD LAW PLOTS.

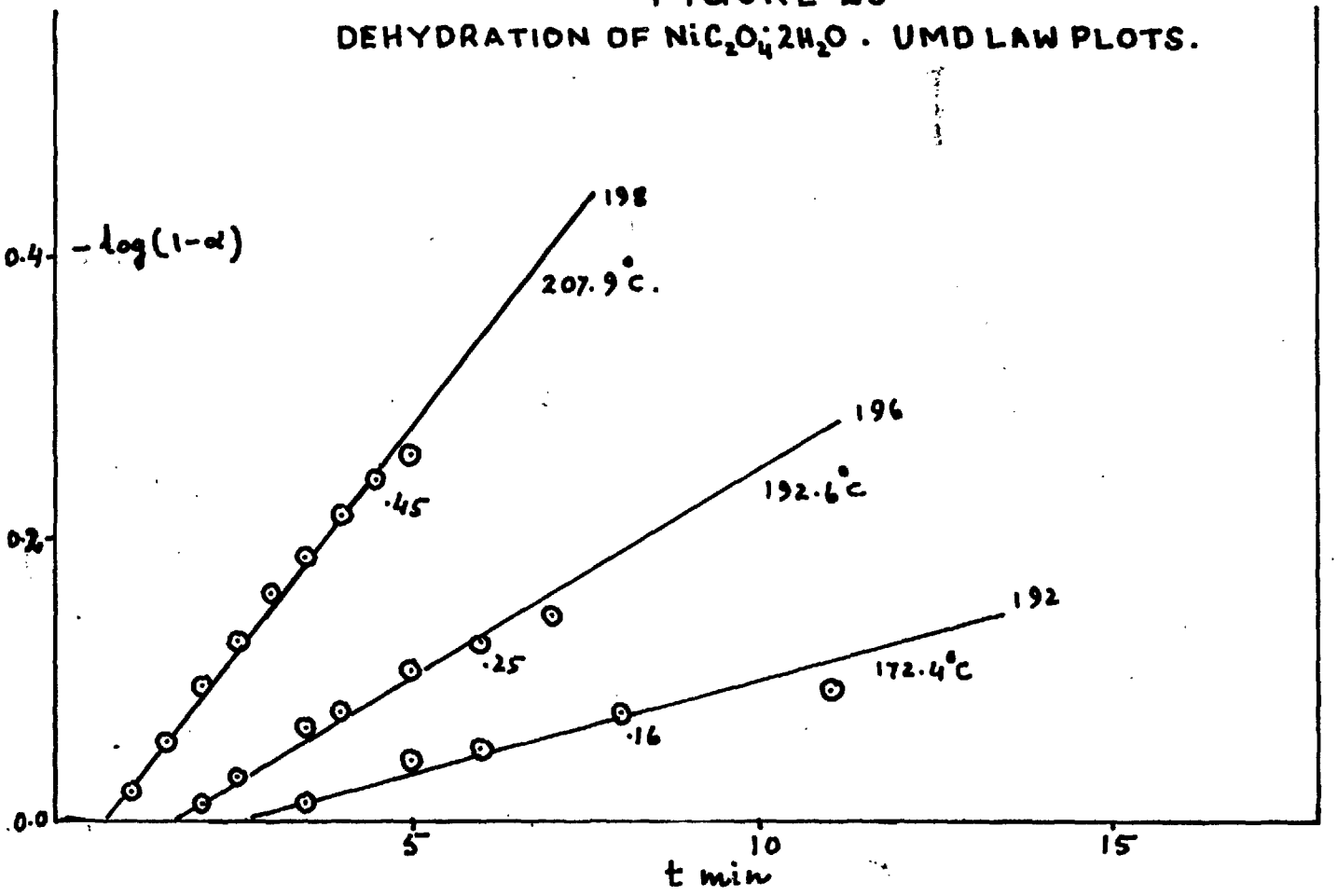

FIGURE 29.

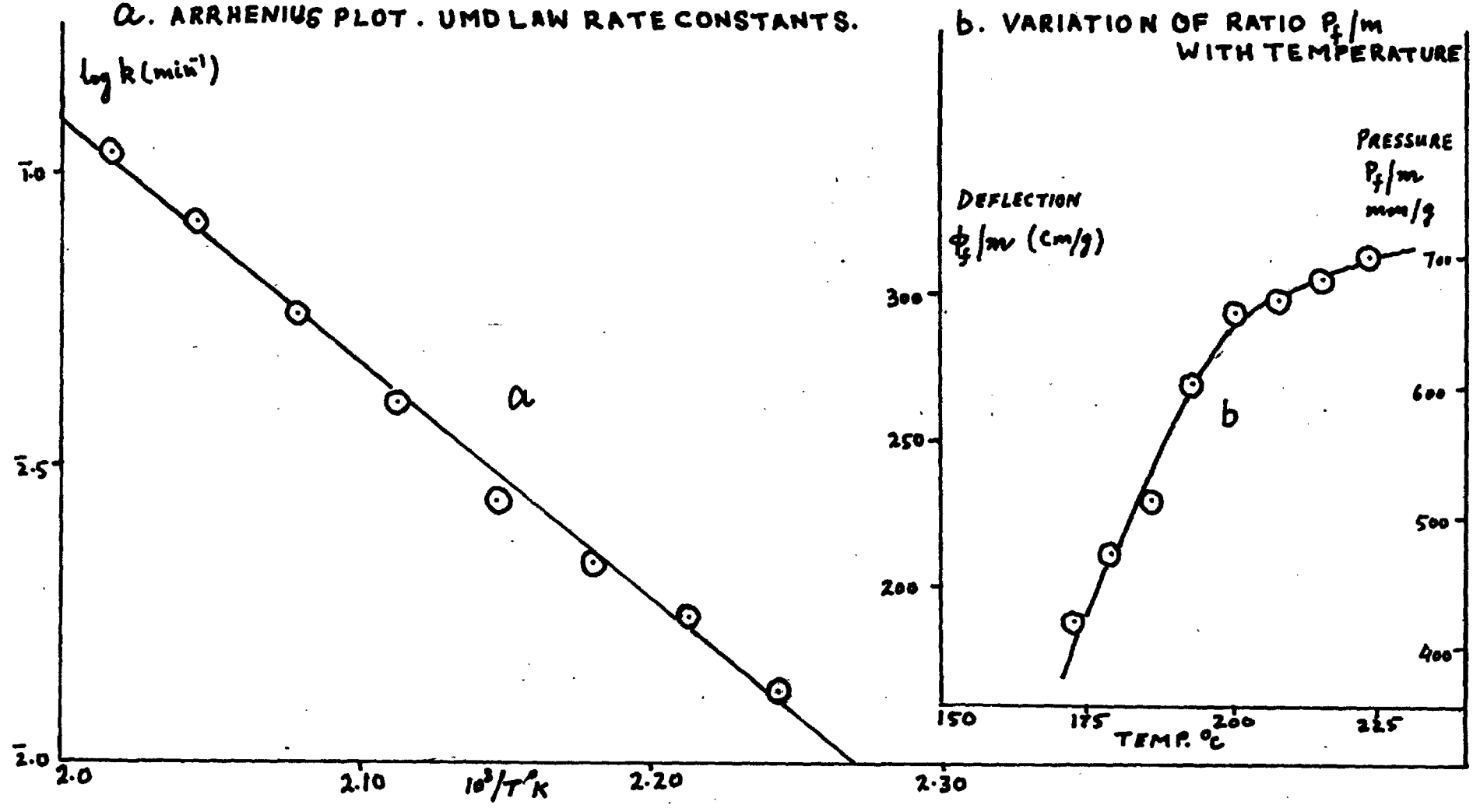
a. ARRHENIUS PLOT. UMD LAW RATE CONSTANTS.
log k (min⁻¹)
1·0
2·5
2·0
2.0
2.10
10³/T°K
2·20
2·30
a
b. VARIATION OF RATIO Pf/m WITH TEMPERATURE
DEFLECTION
Φf/m (cm/g)
PRESSURE
Pf/m
mm/g
300
250
200
700
600
500
400
150
175
200
225
TEMP. °C
b

4. DISCUSSION

4.1 THERMAL DECOMPOSITION OF NICKEL OXALATE AND NICKEL OXALATE DI-HYDRATE: ACCUMULATORY RUNS.

All the results discussed in this section were obtained by the accumulatory method, using powder of the di-hydrate and both powder and pellets of the dehydrated salt.

4.11 Initial surface reaction: As described in sections 3.11 and 3.21, there is an initial reaction in the thermal decomposition of both the hydrate and the dehydrated salt. This reaction commences without an induction period and decays rapidly. As the second reaction also starts at t = o, there is no absolute method of determining the total extent of this reaction, but from careful extrapolation of the decay part of α-t plots (Fig.3) it can be estimated fairly accurately. The extent of the initial reaction in both cases (viz. hydrate and dehydrated salt) has been estimated in this way to be 1% of the total decomposition. The fractional decomposition for this initial reaction is therefore:

$$\alpha' = \alpha / \alpha_o \qquad (11)$$

where α' is the total fractional decomposition and α_o, the extent of this initial reaction ($\alpha_o = 0.01$).

Allan and Scaife (27) fitted their results by the equation:

$$V = k_1 (t-t_o)^{\frac{1}{2}} \qquad (12)$$

where V is volume of product gases. They have put forward a mechanism based on the diffusion of anions to the surface as the rate determining process for this reaction. They assumed that the rate of diffusion of anions to the surface is inversely proportional to the extent of reaction, V, i.e. $dV/dt \propto 1/V$, from which equation (12) is derived.

However, the ionic conductivities of metallic oxalates so far studied, are very low. The extra-polated values of specific conductivities obtained from Finch's (30) work for lead and mercury oxalates are of the order of 10^{-11} ohm^{-1} cm^{-1} at 250°C, whereas those for silver and barium oxalates are of the order of 10^{-9} ohm^{-1} at the same temperature. It seems likely that the ionic conductivity of nickel oxalate will also be of the same order of magnitude and that a mechanism for the thermal decomposition of this salt based on ionic mobility as the rate determining process is unlikely (38). The temperature coefficient of ionic conductance is also low and for the oxalates mentioned above, lies between 10 and 15 kcal/mole. Allan and Scaife have found the activation energy associated with this initial process to be 47.6 kcal/mole which is considerably higher

than the probable diffusion value, which will be equal to that for conductance. Allen and Scaife's mechanism being untenable, the results were examined in terms of the model of a contracting area of surface decomposition. It seems probable that the reaction starts on the corners and edges of the particles which are nucleated within a very short time (probably within the time in which the sample is heating up to the furnace temperature). The produce phase then spreads over the surface at a constant rate. Hume and Colvin (31) found that in the decomposition of potassium hydrogen oxalate hemihydrate, nucleation of the transparent plates occurred preferentially at corners and edges. The rate of advance of the interface was measured directly and found to be constant. On this model considering the available area as a square surface of side, a, the fraction decomposed after time, t, is given by:

$$\alpha = \left[a^2 - (a-2k't)^2\right]/a^2 \qquad (13)$$

where k' is the constant rate of advance of interface. This equation can be written in the form:

$$1 - (1-\alpha)^{\frac{1}{2}} = k'(t-t_o) \qquad (14)$$

where $k' = 2k'/a$, and t_o is the nucleation time. The initial reaction is fitted satisfactorily by this equation as shown in Figs. 4a and 23a. The values of t_o are of the order of 3 min, a reasonable value for the heat up time in Apparatus A.

The activation energies for hydrate and dehydrated salt are 33.8 and 32.9 kcal/mole respectively and the pre-exponential factors $10^{12.59}$ and $10^{12.00}$. The agreement between these values shows that the surface of the hydrate has been dehydrated during evacuation and the heat-up time.

The thickness of this surface layer can be calculated from the surface area of the salt. The approximate particle size determined by electron microscopy is of the order of 6000 A^{o}. For the fraction decomposed we can write the relation:

$$\alpha_{o} = v/V = \sigma l^{2} b/l^{3}$$

$$\text{or} \qquad \alpha_{o} = \sigma b/l \qquad (15)$$

where l is the size of the particle, σ the shape factor (= 6 for a cube), b the thickness of surface layer, v the volume decomposed and V the total volume. All the quantities in equation (15) are known except b, which can therefore be calculated. The thickness of the surface layer comes out to be of the order of 10 A^{o}, that is a few (perhaps even one) atomic layers.

The overall mechanism for the decomposition of nickel oxalate must be that of electron transfer from an oxalate ion to a nickel ion followed by the decomposition of positive holes:

$$C_2O_4 \longrightarrow 2e + C_2O_4 \longrightarrow 2CO_2$$

$$Ni^{++} + 2e \longrightarrow Ni \qquad (16)$$

Because the decomposition occurs at the interface between product and salt, the overall process may consist of intermediate ones in which the electrons are transferred first to metal specks or to vacancies present at the interface. However, because of the virtual two-dimensional character of the reaction, it seems more probable that the mechanism of catalysis is one of an effect of the interface on the energy of positive hole formation (via strain) rather than the provision of acceptor energy levels by the metal product. The possible role of vacancies created in situ cannot, however, be excluded. The activation energies quoted above are for the rate determining step which are therefore associated with the creation of positive holes.

The kinetic equations can be written as:

$$\log k' = -\frac{33,800}{2.303RT} + 12.59 \qquad (17)$$

for the hydrate, and

$$\log k' = -\frac{32,900}{2.303RT} + 12.00 \qquad (18)$$

for the dehydrated salt, where k' is in the units min^{-1}.

4.12 Second Reaction: This reaction starts inside the crystal after a long induction period. The fraction decomposed during this reaction can be calculated as described in section 3.11. The main part of this reaction (α = 0.05 - 0.80 for the dehydrated salt and α = 0.10 - 0.87 for the hydrate) is

fitted by an Avrami-Erofeyev type of equation with n = 2:

$$\left[-\log (1-\alpha'') \right]^{\frac{1}{2}} = k(t-t_o) \qquad (19)$$

The fit of this equation has been shown in Figs. 4b and 23b; t_o is the point where the straight lines intersect the time axis. The use of a t_o term is conventionally justified (35) by assuming that the nuclei are formed all at the same time t_o; equation (19) then follows if these nuclei then grow two-dimensionally at a constant rate, overlap being allowed for in the manner of Avrami. This seems most unlikely on general grounds for what is happening during t_o. It could, in principle, represent the time in which nuclei are being formed slowly, but then (because n = 2) growth would have to be one-dimensional. It has often been suggested that only after attaining a certain size do nuclei grow at a constant rate and that the rate of growth of small nuclei is much smaller than this. The reaction below α = 0.05 for the dehydrated salt and below α = 0.10 for the hydrate is discussed in section 4.13 in terms of this hypothesis.

The activation energy associated with the decomposition of the dehydrated salt is again 32.9 kcal/mole and the pre-exponential factor = $10^{11.96}$. The kinetic equation for the dehydrated salt can therefore be written as:

$$\log k'' = \frac{32,900}{2.303RT} + 11.96 \qquad (20)$$

These values are in good agreement with those obtained for the initial surface reaction (section 4.11). Therefore, the mechanism of this reaction is the same as given for the surface reaction, i.e. the rate determining step is the creation of positive holes.

The decay part of the reaction from $\alpha = 0.60$ to 0.97 can also be fitted by the unimolecular decay law. The fall in the power n from 2 to 1 (unimolecular decay law) is most probably due to the retarding effect of CO_2 the pressure of which has risen to about 2-3 mm near the end of the reaction. In differential runs with the dehydrated salt, where the CO_2 is continually pumped away, the Avrami-Erofeyev equation with n = 2 holds up to $\alpha \rightarrow 0.95$ (Fig. 9c). The activation energy obtained by using the UMD law is 30.2 kcal/mole, and the pre-exponential factor $10^{10.98}$ (Fig. 7a). The small differences in these values from those calculated from the AE equation can be due to the sensitivity of UMD plots to the values of final pressure, which are subject to slight errors from run to run.

The activation energy and pre-exponential factor associated with the decomposition of the hydrate are, however, higher than for the dehydrated salt, the kinetic equation for the AE rate constants being:

$$\log k'' = \frac{50,300}{2.303RT} + 19.90 \qquad (21)$$

The higher values of E and A are to be expected if the dehydration of the salt is also one of the rate determining factors. In accumulatory runs the rate of dehydration is likely to be slow because of the slower diffusion through the lattice and through the gas phase to the trap. The dehydration reaction, as described in section 3.23, can be fitted by the UND law in the early stages. As the dehydration was studied under reversible conditions, it is expected that the true law of dehydration will not hold throughout the reaction because of rehydration becoming considerable as the pressure of water vapour increases. However, it is reasonable to assume that in the early stages, rehydration is not important and the true law (UND) holds. It was observed that ϕ max (the gauge deflection corresponding to total dehydration) was not reached even after long intervals of time at temperatures as high as 222.8°C. The value of ϕ_f (final deflection on the spiral gauge) was much smaller than max; hence, ϕ max was used in the calculations of fraction dehydrated, α, rather than ϕ_f. The comparison of ϕ_f values with the values corresponding to true equilibrium of water vapour with this salt (32) showed that ϕ_f was also much smaller than these. This indicates that the attainment of true equilibrium is a much slower process and that a pseudo-equilibrium is set

up, such that further dehydration is very slow. It is also apparent (Fig. 29b) that this pseudo-equilibrium vapour pressure becomes fairly independent of temperature at higher temperatures. This evidence has been used in postulating a mechanism for the thermal decomposition of the hydrate.

We assume that the reactant matrix retains sufficient water for it to be fully hydrated at the reaction interface. The reason for this preferential hydration is that it is just the sort of disordered region at which re-hydration will occur most readily. Thus, although the salt as a whole has lost a good deal of its water, it is essentially hydrate which is undergoing decomposition, apart from the surface reaction already referred to. The nature of the bonding in the hydrate is unknown, but it is quite conceivable that it utilises Ni^{++} orbitals which are required to receive electrons from the oxalate ion and so dehydration must precede decomposition. The activation energy for the whole process is thus, that for dehydration + that for electron transfer. Water liberated in the decomposition is not lost from the salt, but rather serves to re-hydrate fresh material at the advancing interface.

To summarise, because the equilibrium vapour

pressure of water above the hydrate is never attained, the salt retains a considerable fraction of its original water. Such water is in a state of pseudo-equilibrium, in that it is not necessarily bound to the same fraction of oxalate but participates in a continuous process of dehydration and re-hydration. Such re-hydration occurs preferentially at the decomposition interface, as that dehydration is a necessary pre-requisite for and part of decomposition.

The activation energy for dehydration is found to be 18.4 kcal/mole (section 3.12) and that for the decomposition of dehydrated salt is 32.9 kcal/mole (section 4.12). The sum of these two values, 51.3 kcal/mole, agrees very well with that obtained for the decomposition of the hydrate, 50.3 kcal/mole. Tompkins and Young (36) have also shown that in the decomposition of barium styphnate mono-hydrate the presence of water vapour at the interface plays an important role.

4.13 Slow growth: In section 4.12 it was mentioned that the Avrami-Erofeyev equation holds only after $\alpha = 0.05$ for dehydrated salt and $\alpha = 0.15$ for the hydrate. These values correspond to $\alpha'' = 0.04$ and $\alpha'' = 0.14$ respectively. The departure from Avrami-Erofeyev plot in this range is shown in Fig. 30 for dehydrated salt (a) and the hydrate (b).

The values of t and α , above which Avrami-Erofeyev equation holds! will be called t^* and α^* .

! Footnote: Values of at which the AE equation starts to fit may show slight differences to those values given in the Results. The reason is that those given earlier refer to the first point actually on the curve on the scale used to find k', while those given now are more precise values found during the slow-growth analysis.

Now if the model on which AE equation is based, i.e. two-dimensional growth of nuclei at a constant rate k'' is true, then the linear plots of $[-\log (1-\alpha)]^{\frac{1}{2}}$ vs.t should pass through the origin which is not so, for in practice they intersect the time axis at $t=t_o$. It has been customary to explain this departure from the law by saying that t_o is the so-called incubation period in which the nuclei are forming and that they all start growing at a constant rate at $t=t_o$, the pressure built up during this time being due to nucleation. Use of t_o has been made in several cases where the power law holds in the solid-state decompositions (33, 34, 35). Thomas and Tompkins (33) have suggested a period of slow-growth at a smaller rate changing over to normal growth with a higher rate constant, but no detailed mathematical treatment of slow-growth has yet been given. It is proposed

that during the period of slow-growth, the same growth law holds at any instant but that the rate constant is varying because it is some function of α'' up to $\alpha'' = \alpha^*$, when the interface undergoes some radical change after which the rate constant does not vary any further. An analysis of the slow-growth period will now be attempted on this basis.

There are two main possibilities for the variation of k'' during slow growth:

(a) that it is proportional to the linear size (perimeter) of the nucleus, and,

(b) that it is proportional to the surface area of the nucleus, which for two-dimensional growth also means proportional to the volume.

Mathematically, these two possibilities can be written down as:

$$k''(\alpha'') = K\alpha''^{\frac{1}{2}} + k_o \qquad (22)$$

and

$$k''(\alpha'') = K\alpha'' + k_o \qquad (23)$$

where k_o is the rate of growth of freshly formed nuclei. The results (Fig. 33) show that this is so small that it may be neglected in further analysis, so that (22) becomes:

$$k''(\alpha'') = K\alpha''^{\frac{1}{2}} \qquad (24)$$

Now the basic assumption is that the relation:

$$dF(\alpha'')/dt = k''(\alpha'') \qquad (25)$$

is true for all values of , where $F(\alpha'')$ has been written for - $\left[-\log(1-\alpha'')\right]^{\frac{1}{2}}$. It is shown by the data in Table 19 that to a high degree of approximation,

$$F(\alpha'') = a\alpha''^{\frac{1}{2}} \qquad (26)$$

for small values of α'', where a is a constant, the value of which is 0.663 below $\alpha'' = 0.05$ and 0.666 below $\alpha'' = 0.10$. Substituting $F(\alpha'')$ by $a\alpha''^{\frac{1}{2}}$ in equation (25).

$$ad\alpha''^{\frac{1}{2}}/dt = k''(\alpha'') \qquad (27)$$

combining (24) and (27)

$$ad\alpha''^{\frac{1}{2}}/dt = K\alpha''^{\frac{1}{2}}$$

or $\frac{1}{2}a\alpha''^{-\frac{1}{2}}\, d\alpha''/dt = K\alpha''^{\frac{1}{2}}$ (28)

which on rearrangement and integration gives:

$$\log \alpha'' = (2/2.303a)\, Kt + \log \alpha(o) \qquad (29)$$

where $\alpha(o)$ is the finite value of α'' at t=o due to instantaneous nucleation. The fit of this equation was examined, but as shown in Fig. 31a it does not hold right up to $\alpha'' = \alpha^*$, the rate increasing faster than required by this law as α^* is approached. The gap between the fit of the exponential law (eqn. 29) and where the AE law begins to hold is small in time but quite considerable in α'' because of the rapid acceleration of the reaction.

If, however, we consider the second possibility (b) and start from equation (25), then equation (28) becomes

$$(\tfrac{1}{2}a\,\alpha''^{-\frac{1}{2}})\, d\alpha''/dt = K\alpha'' \qquad (30)$$

which on rearrangement and integration gives:

$$\alpha(o)^{-\frac{1}{2}} - \alpha''^{-\frac{1}{2}} = (K/a)t \qquad (31)$$

where $\alpha(o)$ is the value of α'' at t=o due to instantaneous nucleation. The fit of equation (31) is shown in Fig. 31b: this is satisfactory right up to $\alpha'' = \alpha^*$. The experimental evidence is therefore, that- $k(\alpha')$ is proportional to α'' rather than to $\frac{1}{2}$. If the variation of $k(\alpha'')$ is due to the development of more and more strain in the lattice it seems likely that the lattice will be distorted all along the surface of the decomposed material (a sectional representation of this strain is shown in the inset figure) and not merely at the perimeter. In two-dimensional growth the surface area is proportional to the amount decomposed, α''.

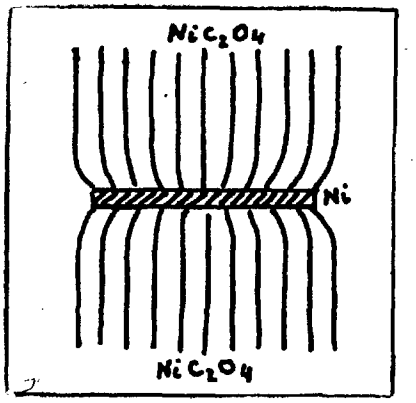

From the slopes of the plots of $-\alpha''^{-\frac{1}{2}}$ vs.t, the values of K/a, and hence of K, can be obtained. The theoretical plots of $k(\alpha')$ as a function of α'' are shown in Fig. 32 a and b for hydrate and the dehydrated salt respectively. Fig. 33 a and b shows a comparison of calculated values of $k(\alpha'')$ with values obtained experimentally by graphical differentiation of plots of $F(\alpha'')$ against t. The

agreement is as good as can be expected considering the practical difficulties in measuring small values of α''. The values of α^* show a scatter in both cases for the average value for the dehydrated salt is 0.04 and for the hydrate, 0.15. This would imply that the lattice of hydrate can withstand more strain than that of dehydrated salt.

From equation (23) it is seen that the activation energy calculated from E will be the same as that obtained from $k(\alpha'')$ at any particular value of α''. The value thus found for slow-growth is 37.5 kcal/mole for the hydrate and 38.0 kcal/mole for the dehydrated salt (Fig. 34). The Arrhenius plots show some scatter due to the experimental difficulties referred to. The same value of E for both the hydrate and dehydrated salt for slow-growth period is possibly due to the fact that nucleation occurs at defect sites which, like the surface (section 4.11), will also tend to dehydrate quickly before any decomposition takes place. This conclusion is supported by the fact that the activation energies calculated from values of t_o are also the same for both the salts, viz., 39.3 and 39.8 kcal/mole for hydrate and the dehydrated salts respectively (sections 3.22 and 3.11). The values of pre-exponential factors also

agree very well, being $10^{15.01}$ and $10^{15.44}$ min^{-1}.

4.14 Theoretical $\alpha(t)$ plot: It has been shown in sections 4.11, 4.12 and 4.13 that the whole course of thermal decomposition of nickel oxalate consists of three stages - namely, a surface reaction, a period of slow growth and finally the main reaction. These stages, as has been shown, are fitted by the following equations:

$$1 - (1-\alpha')^{\frac{1}{2}} = k'(t-t_o') \qquad (14)$$

$$\alpha(o)^{-\frac{1}{2}} - \alpha''^{-\frac{1}{2}} = (K/a)t \qquad (31)$$

and $$\left[-\log(1-\alpha'')\right]^{\frac{1}{2}} = k''(t-t_o'') \qquad (19)$$

The values of k', K, k'', t_o' and t_o'' can all be found graphically. From these values a theoretical $\alpha(t)$ curve can be plotted utilising the definitions of α' and α''. This has been done for one run to show the agreement between the experimental results and the theoretical curve (Fig. 35). This agreement is excellent apart from the last stages of the decay period where the reaction is retarded by CO_2.

TABLE 19

THE RATIO $F(\alpha'')/\alpha''^{\frac{1}{2}}$ FOR SMALL α''.

α''	$F(\alpha'')$	$\alpha''^{\frac{1}{2}}$	a
0.005	0.0469	0.0707	0.663
0.010	0.0663	0.1000	0.663
0.020	0.0938	0.1414	0.663
0.030	0.1149	0.1732	0.663
0.050	0.1493	0.2236	0.668
0.071	0.1775	0.2646	0.671
0.100	0.2140	0.3162	0.677

FIGURE 30

T. D. OF NiC_2O_4 AND $NiC_2O_4 \cdot 2H_2O$. DEVIATION FROM AE EQUATION.

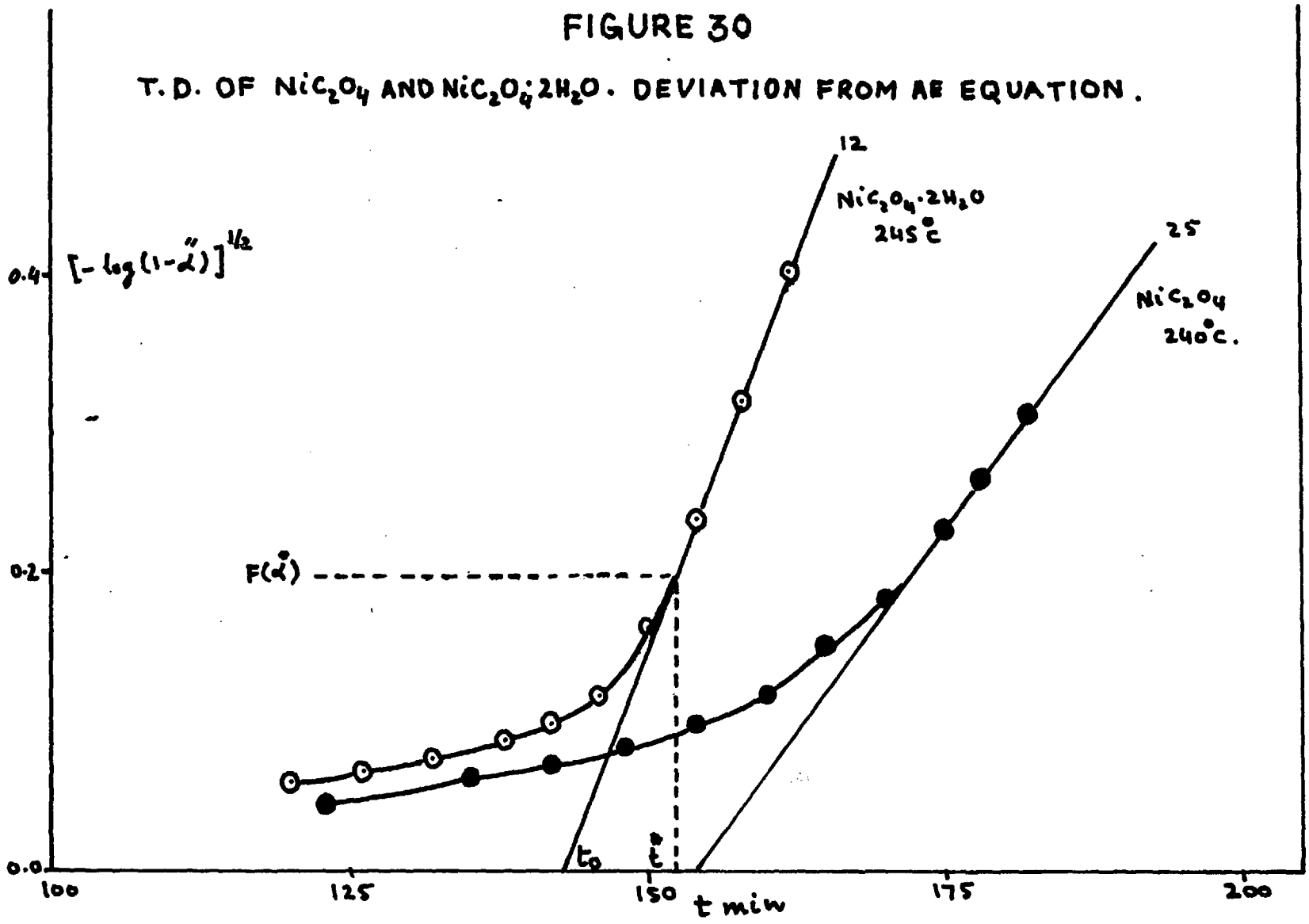

FIGURE 31

T.D. OF NiC_2O_4 AND $NiC_2O_4 \cdot 2H_2O$. SLOW GROWTH.

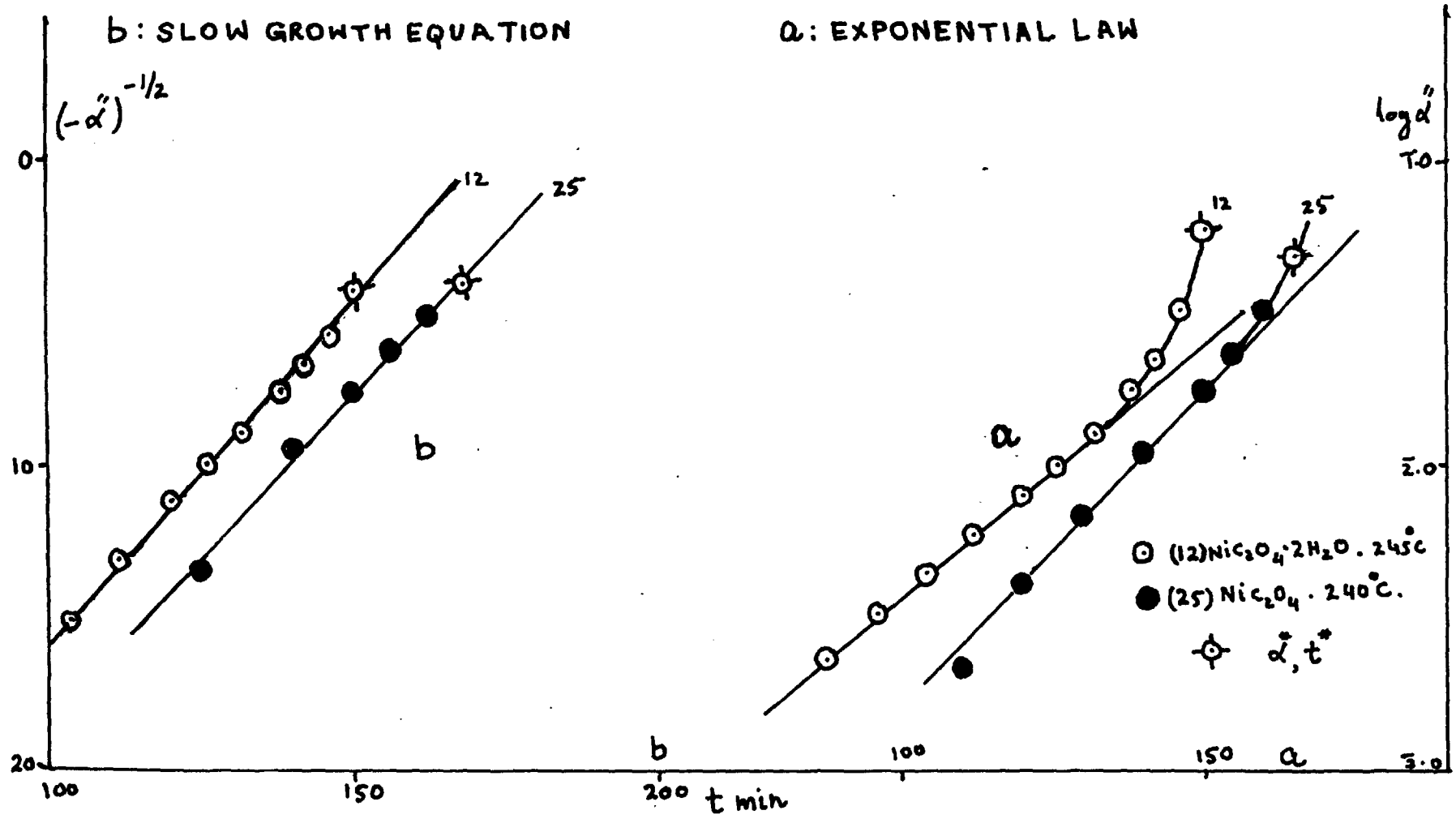

FIGURE 32

SLOW GROWTH PERIOD. VARIATION OF $k(\alpha'')$ WITH α''

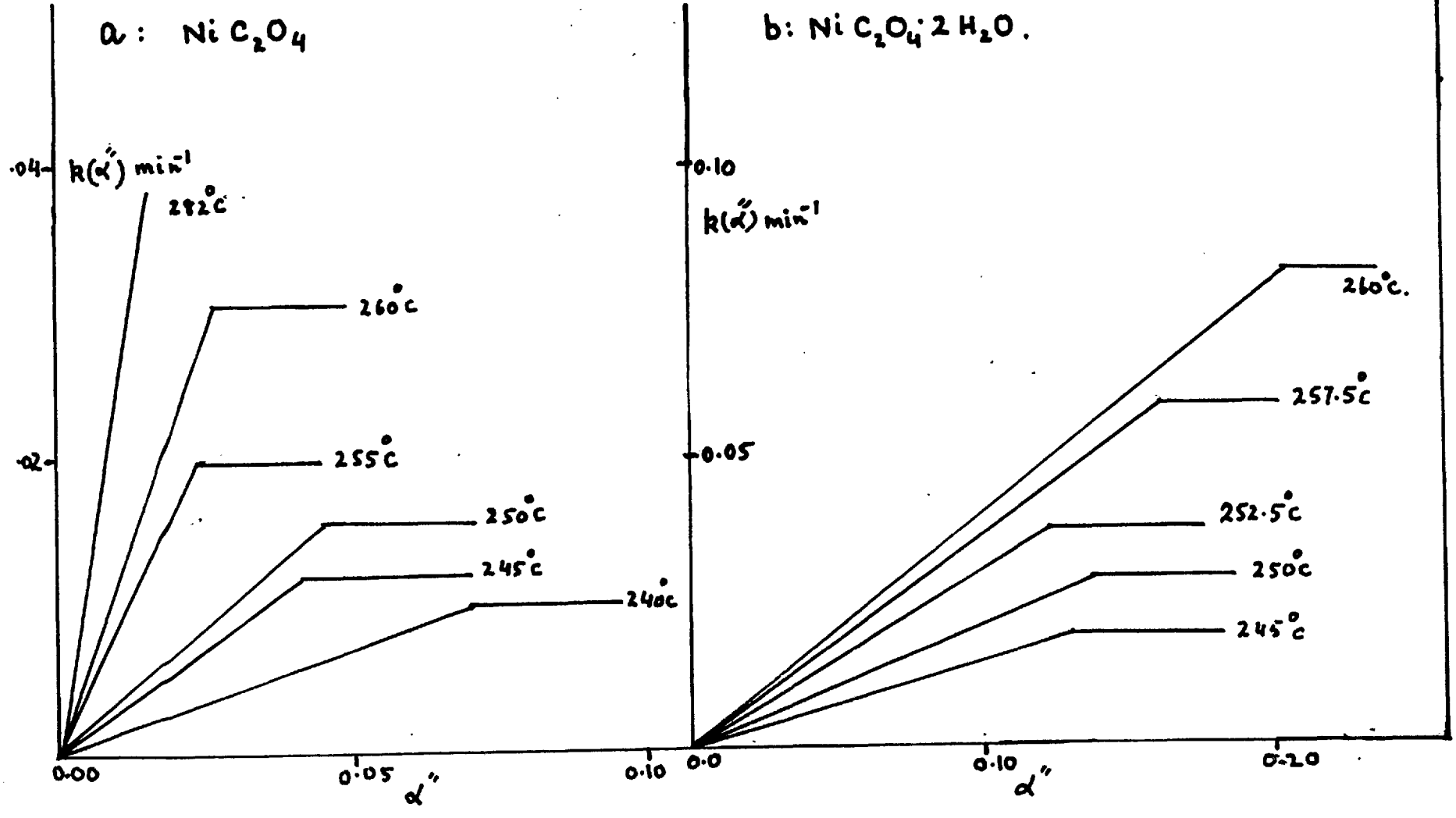

FIGURE 33.

SLOW GROWTH PERIOD. VARIATION OF $R(\alpha'')$ WITH α''

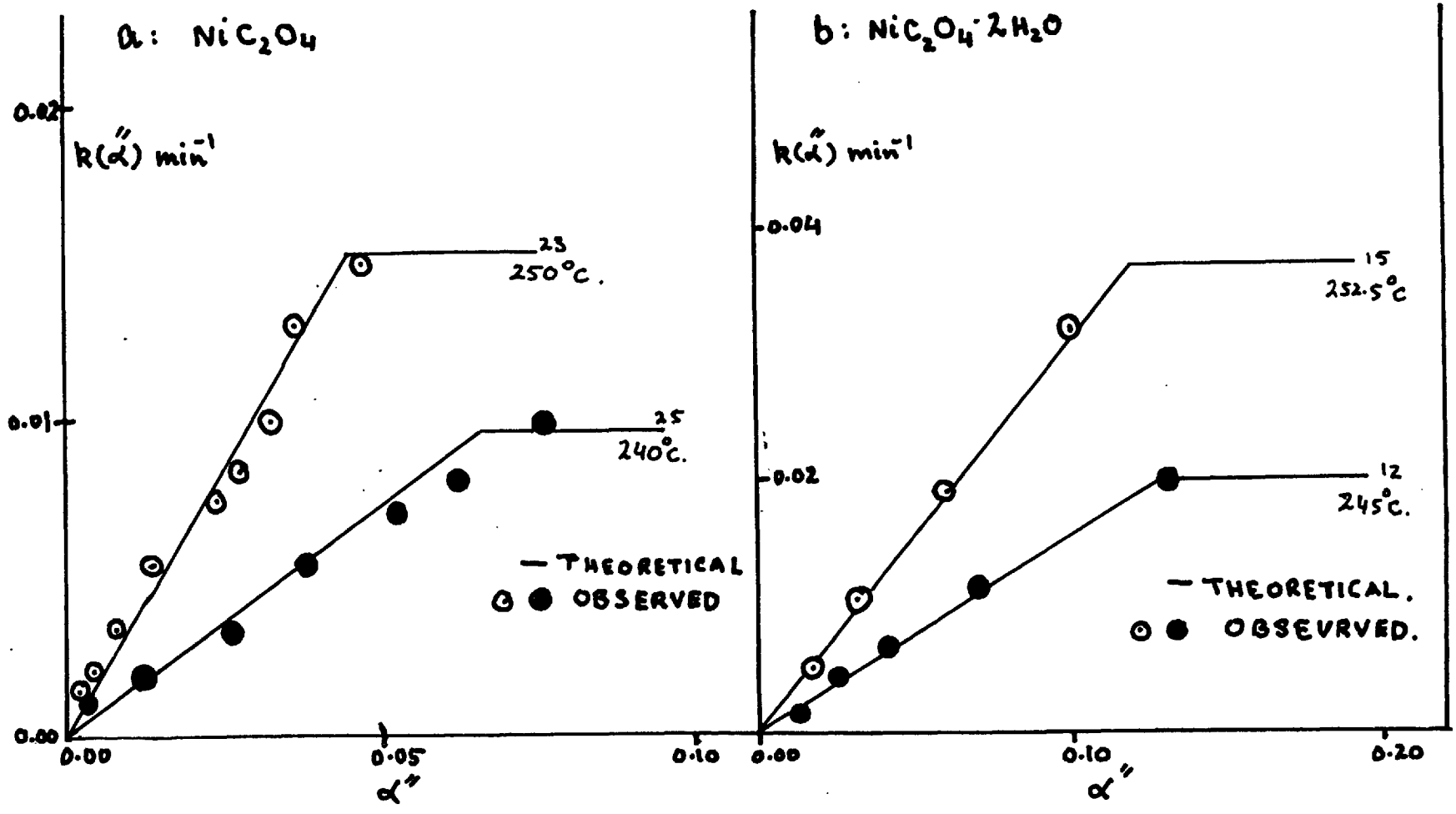

FIGURE 34

SLOW GROWTH PERIOD. ARRHENIUS PLOTS.

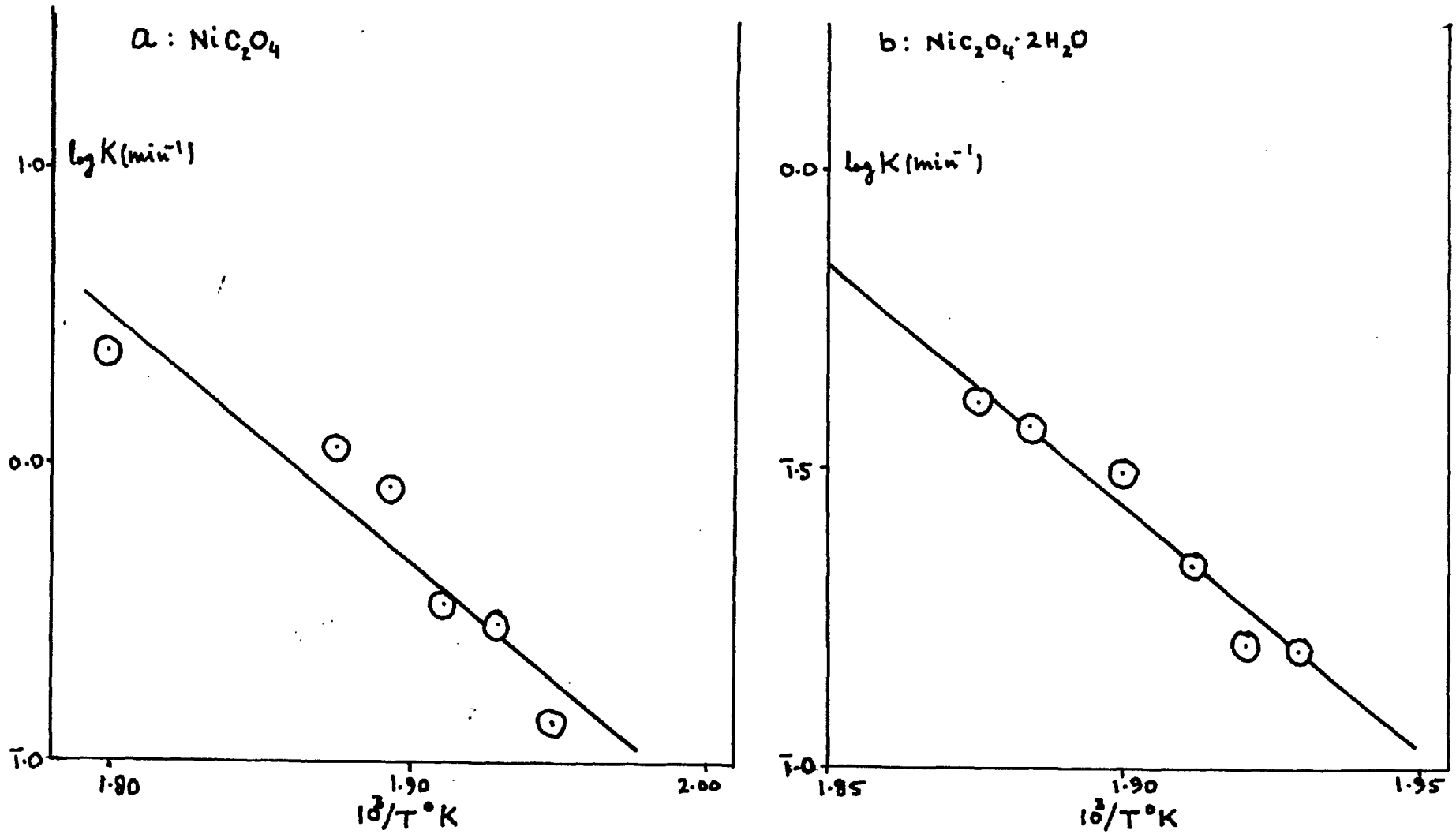

FIGURE 35.

T.D. OF $NiC_2O_4 \cdot 2H_2O$. THEORETICAL α-t PLOT.

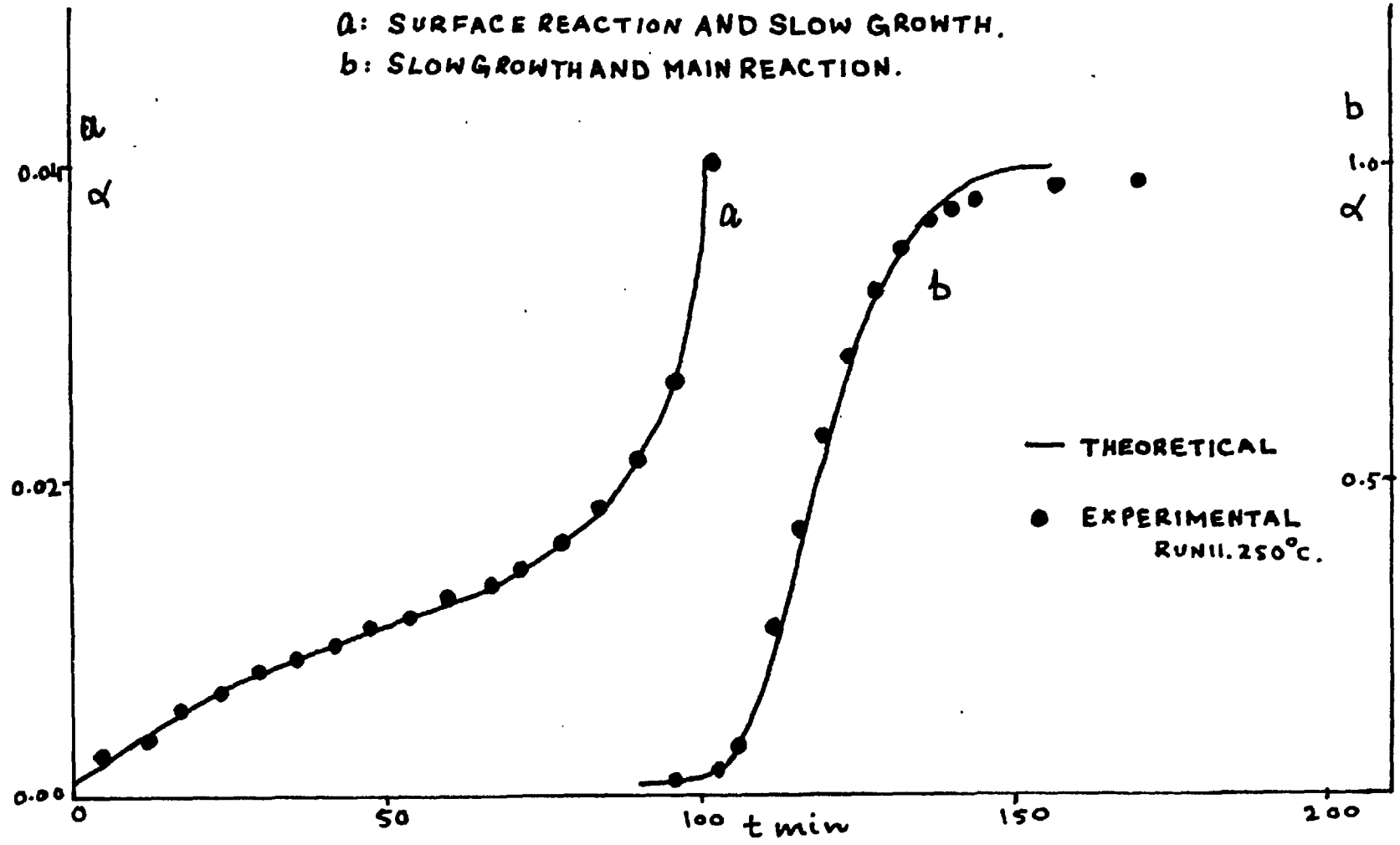

4.2 DIFFERENTIAL RUNS

These runs were done to find out if this technique offered any definite advantages over the more usual accumulatory one. Using the same mass of sample, neither the surface reaction nor the slow growth period could be followed accurately enough for the results to be analysed; the sample mass was not, however, increased because of the possibility that the time taken by the sample to reach thermal equilibrium would also increase.

For dehydrated salt, the kinetics of the reaction were the same except that the rate constants measured by this method were slightly lower than the corresponding values obtained from accumulatory runs; the activation energy was unaltered (Fig. 5c). The lower values of rate constants found are probably due to the difference in experimental technique since this method is far less accurate than the accumulatory one. The fit of the AE equation is very good (Fig. 9c) and the equation is obeyed from α = 0.03 to 0.97. The range of temperature over which the decomposition could be studied was also limited because when the reaction becomes fast it cannot be followed accurately due to short pumping time allowed between the readings; also Apparatus B could not be used to do differential runs.

For hydrate, the kinetics still obeyed the AE equation from $\alpha = 0.20$ to 0.88 (cf $\alpha = 0.15 - 0.85$ for the accumulatory method). The most significant difference, however, is in the value of the activation energy, which is found to be 31.1 kcal/mole (Fig. 24c) for the second reaction. By the accumulatory method, the value obtained was 50.3 kcal/mole (section 4.12). It seems that in differential runs, because the water is being continually removed by pumping, it is no longer retained in the reacting interface (described in section 4.12), so that the only rate determining step is the decomposition of NiC_2O_4. The value of 31.1 kcal/mole agrees well with that for the decomposition of dehydrated salt, i.e. 32.9 kcal/mole. The pre-exponential factor $10^{11.44}$ is also in good agreement with the value of $10^{11.96}$ associated with the decomposition of dehydrated salt.

4.3 EFFECT OF METALS ON THE DECOMPOSITION OF DEHYDRATED SALT.

These effects could not be studied using the hydrate as the pelleting gave irreproducible results.

4.31 Effect of grinding: Grinding the dehydrated salt in an agate mortar for five minutes before making a pellet has very slight effect on the decomposition of the salt. It does not alter the activation energy but increases the pre-exponential factor slightly - $10^{12.04}$ as compared to $10^{11.96}$ - which is hardly significant but is in the right direction, for grinding would be expected to increase N_o, the number of nucleus forming sites, and therefrom k'', as the measured rate constant, k'', includes a factor N_o for two-dimensional growth. The Arrhenius plot (Fig. 5e) includes points obtained from both the differential and accumulatory runs, showing again that there is no essential difference in results obtained by these different techniques.

4.32 Effect of metals: 4.4% Ni, 9.1% Au or 19.8% Pt had no appreciable catalytic effect on the decomposition of nickel oxalate. The Arrhenius plot of AE rate constants and UMD law rate constants scatter about the same straight line as those for pellet made from ground powder (Fig. 20). Previously Prout (37) had found that for $KMnO_4$ the addition of end products had no catalytic effect on the decomposition

of this salt; Prout and Tompkins (17) have also reported that there was no effect of end products in the decomposition of HgC_2O_4. It seems likely that only the metal formed in the lattice of the salt can have a catalytic effect, whereas mixing it mechanically with the salt does not have the same effect. This supports the view expressed earlier that the catalytic effect of the product is due rather to strain than to the participation of metal in the reaction. There may be a further reason in NiC_2O_4 because the growth is two-dimensional and the nuclei formed on the surface do not grow into the crystal (Section 4.11). As the surface already contains a large number of potential nucleus forming sites the inclusion of metal particles will have no appreciable effect.

4.4 EFFECT OF DIFFERENT GASES

4.41 Effect of water vapour: Water vapour has a strong poisoning effect on the decomposition of NiC_2O_4. As dehydrated salt absorbs moisture from the air during handling, the effect of water vapour can be studied simply by omitting the cold trap in the system. In Apparatus B the water evolved could easily be measured on the spiral gauge and by keeping the mass of the sample constant, the pressure of water vapour could be kept constant at 1.8 ± 0.2 mm of Mercury. At lower temperatures the AE equation only fits in the range $\alpha = 0.05 - 0.40$, the decay period being fitted by the UMD law, whereas at higher temperatures nearly the whole course of reaction is fitted by the AE equation with n=2 (Fig. 10a). The rate constants are always lower, however, than the corresponding values when water vapour is removed by condensation in a trap. It has already been shown that dehydration is only partial even at decomposition temperatures and that a certain amount of water remains in the salt particularly at the reaction interface. With fully hydrated salt, this is sufficient to keep the nickel oxalate at the reaction interface hydrated, but with this partially de-hydrated salt, without a trap, there is sufficient water to hydrate only some of the nickel oxalate.

The result is a reduction in k'' but no change in E, as only the unhydrated oxalate decomposes. The break-down in the n=2 law at relatively early stages is connected with this inhibition by water. Thus at higher temperatures as the dehydration becomes more and more complete the range of applicability of AE equation increases. The inhibiting effect of water vapour is most pronounced on the length of the induction period; nevertheless the value of the activation energy, whether determined from t_o, or from either rate law remains unchanged (Figs. 5d, 7 and 8) in keeping with the above hypothesis.

The poisoning effect of water has also been observed in mercuric oxalate (17) and oxalates of the lanthanon series (26).

It was found in a further experiment that water vapour does not react chemically with Ni nuclei, by condensing all the gaseous products of decomposition at the end of a run in a cold trap using liquid N_2 as coolant, whence no residual gas pressure was observed showing that no H_2 had been produced during the reaction.

As the water vapour diffused very slowly to the trap in presence of a high pressure of gas, the subsequent study of effect of other gases on the decomposition was made without attempting to condense the water vapour.

4.42 Effect of O_2 and H_2: Both these gases react with the products of decomposition and hence their physical effect (if any) could not be studied.

O_2 presumably reacts with Ni nuclei, oxidising the metal to NiO. Since the reaction is followed by pressure changes the net rate is the difference between the reduced rate of decomposition of NiC_2O_4 and the rate of oxidation of Ni. This view is supported by the values of ϕ_f/W (where ϕ_f= final deflection and W=weight of the sample) in two cases. In run 178, 12.0 mg of NiC_2O_4 produced a final deflection of 5.6 cm on the spiral gauge when the decomposition was carried out in vacuum and without a trap, whereas in the presence of O_2 (pressure = 80 mm of Hg) 9.5 mg of NiC_2O_4 produced 2.95 cm deflection. The two values of the ratio ϕ_f/W are 0.467 and 0.310 cm/mg respectively. If all the Ni produced is oxidised to NiO the pressure decrease due to it should be 1/4 of the pressure of CO_2 produced provided the reaction goes to completion. Hence the ϕ_f/W values should be in the ratio 4:3 and the observed values are in good agreement with this conclusion.

For H_2, the pressure in the system first rises due to decomposition of NiC_2O_4 and then starts to decrease (Fig. 11) showing that a gas phase reaction is occurring. The precise nature of this reaction was not investigated

but it seems probable that the reaction is the reduction of CO_2 by H_2, for which the nickel nuclei act as a catalyst.

4.43 Effect of He, N_2 and CO_2: The effect of a variation of pressure of these gases has been studied keeping the temperature constant (276.0 ± 0.5°C) and the mass of the sample within the limit 15 ± 3 mg; the pressure of water vapour was 2 ± 0.2 mm of Hg. The induction period, t_o, increases with increasing pressure. If t_o is plotted against PM (where P is the pressure of the gas and M its molecular weight) a straight line is obtained for N_2 and He, but the effect of CO_2 is more pronounced at higher pressures of this gas (Fig. 15a). The second reaction is again fitted by the AE equation with n=2 but the range of α over which this equation fits is less, i.e. α = 0.05 to 0.58. The decay part from α = 0.55 to 0.95 is fitted by UMD law. The plot of the AE rate constant against $\sqrt{PM}$ shows a sharp decrease up to $\sqrt{PM}$ = 40, above which it remains appreciably constant although there is a considerable scatter (Fig. 15c). UMD law rate constants change more reproducibly with the pressure of the gas and the plot of UMD rate constant against $\sqrt{PM}$ is linear (Fig. 15b).

It has been shown in section 4.11 that the presence of water vapour retards the decomposition of nickel oxalate.

The further retarding effect due to these gases seems simply due to the slower diffusion of water vapour from the reaction zone except that the effect of CO_2 on the induction period (Fig. 15c) which is more pronounced. This shows that the higher pressure of CO_2 react with Ni nuclei, thus prolonging the induction period more than do the other gases, He and N_2. After the slow growth period, the specific retardation by CO_2 is not observed owing to the inhibition of the reaction by the water. Clearly any back-reaction during the induction period is more apparent because of the markedly auto-catalytic nature of the kinetics.

For the same reason, there is a sharp drop in the AE rate constants.

REFERENCES

1) Jacobs and Tompkins: "Chemistry of Solid State." Chap. 7. Butterworths (1955).

2) Garner and Tanner: J.C.S. (1930). 47.

3) Garner and Maggs: Proc. Roy. Soc. A. (1939) 172. 299.

4) Thomas and Tompkins: ibid. (1951) 209. 550; 210. 111.

5) Szabo' and Biro' - Sugar: Z electrochem. (1956) 60. 869.

6) Acock, Garner, Milsted and Willavoys: Proc. Roy. Soc.A. (1946). 189. 508.

7) Macdonald and Hinshelwood: J.C.S. (1925) 127. 2764.

8) Macdonald: ibid. (1936) 832, 839.

9) Finch, Jacobs and Tompkins: ibid. (1954). 2053.

10) Benton and Cunningham: J.A.C.S. (1935). 57. 2227.

11) Tompkins: Trans. Farad. Soc. (1948). 44. 206.

12) Macdonald and Sandison: ibid. (1938). 34. 589.

13) Erofeev, Belkovich and Volkova: J. Phys. Chem. U.S.S.R. (1946) 20. 1103.

14) Griffith: J. Chem. Phys. (1943). 11. 499.

15) Macdonald: Farad. Disc. (1957). 230.

16) Griffith: J. Chem. Phys. (1946). 14. 408.

17) Prout and Tompkins: Trans. Farad. Soc. (1947). 43. 148.

18) Mott: Proc. Roy. Soc. (1939). 172. 325.

19) Wagner and Schottky: Z. Phys. Chem. (1930). 11. 163.

20) Bircumshaw and Harris: J.C.S. (1939). 1637.

21) Bircumshaw and Harris: ibid. (1948). 1898.

22) Boldyrev: Sbornik. Nauch. Rabot. Akad. Nauk. Beloruss (S.S.R.) Inst. Khim. (1956) 5. 100.

23) Becket and Winfield: Austral. J. Sci. Res. (1951). 4. 644

24) Markin: J. Inorg. Nuc. Chem. (1958). 7. 290

25) Gunther and Rehaag: Ber. (1938) 71B. 1771

26) Glasner and Steinberg: Paper read at XVIIth. Int.Cong. of Pure and Applied Chem.(1959).

27) Allen and Scaife: J. Phys. Chem. (1954) 58. 667

28) Daněs and Ponec: Collection. Czechoslov. Chem. Commun. (1958) 23. 848

29) Roberts: Electronic Engineering. Feb. 1951. 51.

30) Finch: Ph.D. Thesis. London University (1953).

31) Hume and Colvin: Proc. Roy. Soc.A (1929). 125. 635

32) Allen and Scaife: J. Phys. Chem. (1953) 57. 864

33) Thomas and Tompkins: Proc. Roy. Soc.A. (1951) 209. 550.

34) Young: Ph.D. Thesis. London University (1955).

35) Garner and Haycock: Proc. Roy. Soc. A. (1952) 211. 335

36) Tompkins and Young: Trans. Farad. Soc. (1956) 52. 1245

37) Prout: M.Sc. Thesis. Natal University College (1943).

38) Thomas and Tompkins: J. Chem. Phys. (1952) 20. 662.

PART II.

THERMAL DECOMPOSITION OF AMMONIUM PERCHLORATE.

1. INTRODUCTION

1.1 THERMAL DECOMPOSITION OF AMMONIUM PERCHLORATE

The thermal decomposition of ammonium perchlorate was first studied by Naoum and Aufschlager (1) and Dodé (2), who both investigated the products of decomposition. Dodé found them to be N_2, O_2, Cl_2, H_2O, NO, and N_2O. Later Bircumshaw and Newman (3) undertook a detailed kinetic study of the thermal decomposition of this salt. They found in addition to the above: ClO_2, $HClO_4$ and N_2O_4 in the products of decomposition below 300°C. Bircumshaw and Newman agree with Dodé that the equation representing the bulk of the decomposition products below 300°C is:

$$4\ NH_4ClO_4 \longrightarrow 2Cl_2 + 3O_2 + 8H_2O + 2N_2O$$

For the reaction they propose the following equation as being more representative above 350°C, though not completely quantitative:

$$2\ NH_4ClO_4 \longrightarrow Cl_2 + O_2 + 4H_2O + 2NO$$

The low temperature decomposition (215°- 300°C) did not go to completion, but ceased after $\alpha = 0.3$, leaving a residue of NH_4ClO_4 chemically identical with the salt and showing identical x-ray patterns. Galway

and Jacobs (4) have confirmed this and showed that the residue had much greater surface area than the original salt and corresponded to blocks of material of size of the same order as that of mosaic blocks in the crystal. They have concluded that the low-temperature reaction represents the decomposition of strained material in the inter-mosaic grain boundaries, whereas the high-temperature reaction (5) represents the decomposition of unstrained material forming the core of the mosaic blocks.

Oxides of the transition metals (such as MnO_2 or Fe_2O_3) showed a strong catalytic effect, more than 30% decomposition occurring and the induction period of the reaction being reduced (3). Gaseous ammonia, on the other hand, increased the induction period and reduced the reaction rate. Addition of NH_4NO_3 or $HClO_4$ reduced the induction period. Bircumshaw and Newman (3) fitted their results for the low-temperature reaction to the Prout-Tompkins (6) equation:

$$\ln (\alpha/1-\alpha) = kt + c$$

whereas Galway and Jacobs (4) found that the fit of this equation was not uniformly satisfactory. Visual observations of whole crystals (3) show that the nuclei are formed on the surface and grow three-dimensionally

until a coherent interface is built up which then penetrates into the crystal. This model leads to the kinetic equation which approximates to:

$$-\ln(1-\alpha) = (kt)^n$$

This is known as the Avrami-Erofeyev equation (7,8).

The results are fitted satisfactorily by this equation with n=3 in the orthorhombic region and n=2 in the cubic region. This model is consistent with the observed facts. Schultz and Dekker (9) have calculated the rate of linear progression of the reaction interface through an ammonium perchlorate crystal on the basis of an assumed model for the transition complex, and compared their results with those found experimentally by Bircumshaw and Newman (3). The high-temperature reaction is fitted by a contracting-cube formula (5):

$$1 - (1-\alpha)^{\frac{1}{3}} = kt$$

which can be justified theoretically in contrast to the empirical power law:

$$p = kt^n$$

used by Bircumshaw and Newman (3) (with n=0.5).

The basic steps in the thermal decomposition of NH_4ClO_4 are proposed to be an electron transfer process for the low-temperature decomposition, and a proton-transfer process for the high-temperature reaction.

Galway and Jacobs (10) have also studied the effect of MnO_2 on the thermal decomposition of NH_4ClO_4. There is an initial fast reaction which, after an induction period is decelerator; when this reaction ceases, the rest of the salt decomposes according to the unimolecular decay law. The initial reaction is believed to be catalysed by Mn^{+4} ions which act as traps for electrons. This ends when the contact between the salt and oxide surfaces is lost and the remaining salt decomposes as isolated blocks.

Carbon can catalyse the high-temperature reaction (11). The kinetics in the presence of carbon are fitted by a power law but the value of the exponent n varies with temperature. At higher temperatures, ignition of the sample due to self-heating occurs.

1.2 THEORY OF SELF-HEATING.

The general heat conduction equation for an exothermic reaction in an isotropic medium at constant pressure can be written as:

$$C_p \rho (dT/dt) = \lambda \nabla^2 T + Q\left(-\frac{dC}{dt}\right) \qquad (1)$$

where C_p is the specific heat at constant pressure (cal.deg^{-1} mole^{-1}), C the concentration (mole cm^{-3}), T the absolute temperature, t the time (sec), λ the thermal conductivity (cal cm^{-1} deg^{-1} sec^{-1}), ∇^2 the Laplacian operator, Q the heat of reaction (cal mole^{-1}) and $(-dC/dt)$ the rate of reaction (mole cm^{-3} sec^{-1}) at temperature T°A. Most of the important self-heating theories have been concerned with gaseous systems. However, they can be easily applied to solids. In this text the equations are written in the form directly applicable to solids. Therefore, equation (1) will be re-written as:

$$C_p m(dT/dt) = V\lambda \nabla^2 T + Q m_o (d\alpha/dt) \qquad (2)$$

where m is the mass of the solid at time t, m_o the initial mass and $d\alpha/dt$ the fractional rate of decomposition. C_p and Q are now in cal g^{-1}. Here three basic assumptions are usually made: (i) a linear law of decomposition, i.e. $d\alpha/dt = k = Ae^{-E/RT}$; (ii) the consumption of reactants to be negligible, i.e. $m = m_o$ and (iii) replacement of the conduction term $V\lambda\nabla^2 T$ by a heat-loss term $\chi S(T-T_o)$; it may be noted that

this was Semenov's (12) assumption of a uniform temperature $T > T_o$ (but see later). Equation (2) may then be written as:

$$Cp\ m_o\ (dT/dt) = -\chi S(T-T_o) + Q m_o A e^{-E/RT} \qquad (3)$$

where T is now the mean temperature, S the surface area of the solid, and χ the effective heat transfer coefficient. The first two assumptions may be justified in many cases but may prove to be serious approximations in others. The third assumption of uniform temperature has been made by Semenov (12), Rice et al (13) and Todes (14). Gray and Harper (15) have shown that such an assumption is justifiable. The assumption of uniform temperature with an abrupt step at the surface corresponds physically to a reactant of infinite conductivity and low emmisivity, whereas Frank-Kamenetskii's postulate (16) that the surface temperature T_s is equal to that of the surroundings T_o, corresponds to the other extreme, i.e. low conductivity with high emmisivity. Real cases will, however, lie in between these two extremes. Thomas (17) following Chambré (18) has shown that the equation for such an intermediate case may be solved under critical conditions. The heat transfer to the boundary is according to Frank-Kamenetskii, $\lambda (dT/dx)_s$ and from the boundary, according to Semenov, is $\chi(T_s - T_o)$. The heat

conduction equation is thus subject to the general boundary condition:

$$\chi(T_s - T_o) + \lambda (dT/dx)_s = 0 \qquad (4)$$

or in terms of dimensionless temperature $\theta = \frac{E}{RT_o^2}(T-T_o)$ and dimensionless distance $\zeta = x/r_o$, where r_o is a characteristic parameter (radius of sphere or infinite cylinder of half-width of infinite slab):

$$(\chi r_o/\lambda)\theta_s + (d\theta/d\zeta)_s = 0 \qquad (5)$$

When $(\chi r_o/\lambda)$ is large, θ_s is small and the distribution approaches that of Frank-Kamenetskii. When $(\chi r_o/\lambda)$ is small, Semenov's solution is obtained with T independent of position. Frank-Kamenetskii's assumption makes a uniform temperature impossible: the temperature variation is approximately parabolic (19) with a maximum at the centre of the reactant. Critical steady-state conditions, in terms of the temperature of surroundings, T_o, are given by the equation:

$$(E/RT_o^2)\, Q m_o A e^{-E/RT} = V \delta_k \lambda / r_o \qquad (6)$$

where k is the geometric factor, viz., $k = 0$ for an infinite slab and $\delta_0 = 0.88$, $k=1$ for an infinite cylinder and $\delta_1 = 2$ and $k = 2$ for a sphere and $\delta_2 = 3.32$. The analogous expression derived from the average-temperature treatment is:

$$(E/RT_o^2)\, Q m_o A e^{-E/RT} = \chi S/e = V(k+1)\chi/r_o e \qquad (7)$$

Because (6) and (7) are of the same form and (6) is always true, it is clear that the uniform temperature approximation can always be used with an effective heat transfer coefficient given by:

$$\chi' = (e\delta_\chi/k+1)(\lambda/r_o) = h\lambda/r_o \qquad (8)$$

Furthermore, Thomas (20) has also shown that just as χ' can replace $h\lambda/r_o$, when thermal conduction alone is important, similarly an overall heat transfer coefficient χ'' corresponds to the intermediate case: this is given by:

$$1/\chi'' = 1/\chi' + 1/\chi \qquad (9)$$

Thus the use of an effective uniform temperature is in keeping with the spatial distribution of the temperature and not merely a crude approximation.

Equation (3) can now be integrated on the lines of Gray and Harper (15). This treatment is essentially the same as that of Semenov (12) with the addition of the quadratic approximation to be discussed in this section.

The term $e^{-E/RT}$ can be written as $e^{-E/RT_o}\, e^{\theta}$, where $\theta = (T-T_o)E/RT_o^2$. This is obtained by expanding the argument of the exponential term, $-E/RT$, by a Taylor series in $(T-T_o)/T_o$ and omitting all but the first two terms, i.e.:

$$E/RT \simeq E/RT_o - (T-T_o)E/RT_o^2 \qquad (10)$$

In the quadratic approximation if e^{θ} is replaced by

$$1 + (e-2)\theta + \theta^2$$

good agreement with the exponential approximation is obtained for the range $\theta = 0\text{-}1$ (19). Equation (3) may now be written in terms of θ as:

$$(C_p m_0 R T_0^2/E)(d\theta/dt) = -(\chi S R T_0^2/E)\theta + Q m_0 \{1 + (e-2)\theta + \theta^2\} A e^{-E/RT_0}$$

or
$$\tau_\infty (d\theta/dt) = 1 + (e - 2 - \tau_r)\theta + \theta^2 \qquad (11)$$

where
$$\tau_\infty = (C_p R T_0^2/QAE)\, e^{E/RT_0} \qquad (12)$$

and
$$\tau_r = (\chi S/C_p m_0)\, \tau_\infty \qquad (13)$$

Equation (11) may now be integrated:

$$t/\tau_\infty = \int_0^\theta \frac{d\theta}{1 + (e-2-\tau_r)\theta + \theta^2} = \int_0^\theta \frac{d\theta}{(\theta+b)^2 + 1 - b^2} \qquad (14)$$

where
$$b = \frac{e - \tau_r}{2} - 1 \qquad (15)$$

Only negative values of b are physically significant.

Three cases may be distinguished here: (i) No real roots. Physically this corresponds to explosion. Mathematically:

$$(e - 2 - \tau_r)^2 < 4$$

or
$$|e - 2 - \tau_r| < \pm 2$$

$$0 > b > -1 \qquad (16)$$

(ii) Two real roots. Physically this corresponds to no

explosion. Mathematically:

$$b < \pm 1 \qquad (17)$$

and (iii) Two identical roots. Physically this is the limiting case and defines the explosion limit. Mathematically

$$b = \pm 1 \qquad (18)$$

combining (18) and (14):

$$t/\tau_\infty = \int_0^\theta \frac{d\theta}{(\theta \pm 1)^2} = -\frac{1}{\theta \pm 1}$$

or $$\theta \pm 1 = -\tau_\infty / t$$

when $$b = -1, \quad \theta = 1 - \tau_\infty / t \qquad (19)$$

In the limiting condition when b = -1, from equation (15):

$$\tau_i = e$$

or using (13),

or $$m_0 = (\chi S / QAe)(RT_0^2/E)\, e^{E/RT_0} \qquad (20)$$

Similarly, equation (11) is readily integrated when satisfies either (17) or (18) to yield $\theta(t)$ and hence the induction period; the solutions are in Gray and Harper's paper (15).

1.3 PREVIOUS WORK ON THERMAL EXPLOSION OF SOLIDS

Most of the work in this field has been connected with initiation of explosions by friction and impact. A full and critical account of this work is given by Bowden and Yoffe (22) and will not be discussed here. Only the thermal explosions are discussed in this section.

The thermal decomposition and explosion of mercury fulminate was studied by Garner and Hailes (23). The plot of log τ against $1/T$ (where τ is the induction period and T the absolute temperature) is linear. The mean value for activation energy obtained from such plots is 30 kcal/mole. The effect of cold working was also studied. Hydrogen and helium were found to increase the induction period - hydrogen more than helium. The maximum rise in temperature was calculated to be 2° - 8°C. Vaughan and Philips (24) have measured the temperature of loose mercury fulminate undergoing decomposition. They have concluded that the theories based on "self-heating" extending only over a few molecules (hot-spots) are not consistent with their observations. A theory based on chain-branching mechanism and extensive self-heating of the salt has been proposed. A microscopic study of this salt has been carried out by Singh (25). He has reported

that the minimum size of the crystal which undergoes explosion is of the same order of magnitude ($22 \pm 3\mu$) as the values derived from theoretical considerations (1, 5).

The burning and explosions of single crystals of a number of solids (e.g. mercury fulminate, lead styphnate, silver azide, etc.) have been studied by Evans and Yoffe (27). Using a high speed cine camera they have observed the cracking of single crystals along crystal defects before explosion took place. A comparison of burning rates in single crystals and in a thin film of these substances is given. The thermal explosions of various azides (e.g. AgN_3, TlN_3, trinitro-triazido benzene and cyanuric triazide), which melt below the ignition temperature, have been made by Yoffe (28). The induction periods and limiting pressures of an inert gas for the explosion of trinitro-triazido benzene have been given. Groocock (29) has studied the thermal explosion of α-lead azide. He has measured the rates of decomposition prior to explosion and has interpreted his results on the basis of a self-heating theory.

2. EXPERIMENTAL.

Two apparatus, namely Apparatus B and Apparatus C have been used to study the thermal decomposition of NH_4ClO_4 and its mixtures with Cu_2O. Apparatus B has been described in Part I (Section 2.2) of this thesis; only Apparatus C is described here.

2.1 APPARATUS TO MEASURE SELF-HEATING IN NH_4ClO_4 - Cu_2O MIXTURES.

(Apparatus C):

This apparatus is shown diagrammatically in Diagram 4a. The reaction tube R was connected to Apparatus B via two standard ground glass joints J_1 and J_2 which were connected together by a length of pressure tubing D; the joints J_1 and J_2 and rubber tubing connections were made vacuum tight by picein wax. The use of rubber tubing was necessary to allow the reaction tube to be lowered into the heating bath when required; as all the runs were done under 250 mm

pressure of H_2, this system proved to be quite satisfactory. A cylindrical steel vessel containing molten woods metal was used as a heating bath B. To make the heat transfer efficient, the space between the bath and the walls of the furnace was filled by copper foil C and the upper end of the heating bath, which projected outside the furnace, was insulated with asbestos wool A to minimise the heat losses. The sample S was in the form of a pellet with one junction of thermocouple T_2 embedded in it; it was made in the pellet press shown in Diagram 4b. Very fine chromel-Alumel wires (40 s.w.g.) were used for thermocouples T_2 and T_3. During pelleting the thermocouple junction was kept approximately in the same position inside the pellet each time, the wires coming out through the holes in the head H of the press; these were led through the open grooves on top to avoid breaking them during pressing.

The sample with thermocouple T_2 was kept in reaction tube R and the two thermocouple wires were insulated from each other by passing one of them through a fine glass capillary. The wires were taken

out through the vacuum tight piecin joint J_1. The junction of thermocouple T_3 was kept in the heating bath. T_2 and T_3 were connected in opposition and the difference in e.m.f. applied across a previously calibrated galvanometer G through a variable series resistance. The difference in temperatures between the pellet and the bath, ΔT, could thus be measured. The sensitivity of galvanometer could be varied by varying the resistance in series; with no resistance ΔT could be measured to $\pm$ 0.005°C, with R=10^3 ohms to $\pm$ 0.025°C, with R=10^4 ohms to $\pm$ 0.1°C and with R=10^5 ohms to $\pm$ 1.0°C. As the values of ΔT were reasonably large (of the order of 15° - 50°C) 10^4 ohms resistance was normally used; only in the beginning of each run when ΔT was very large (the sample being initially at room temperature) was 10^5 ohms used. This was decreased to 10^4 ohms as the sample heated up to furnace temperature, and all subsequent readings taken with this resistance in series with galvanometer.

The temperature of the heating bath T_0 was recorded by a calibrated chromel-Alumel thermocouple T_1.

The system was evacuated for 2 - 3 hours before each run. The temperature of the heating bath was maintained at 8 - 10°C higher than the temperature at which

the run was to be carried out. The system was isolated from the pumps and dry N_2 introduced to give 250 mm of Hg pressure. The two sides of spiral gauge were isolated and the reaction tube introduced quickly into the heating bath up to a fixed mark so that the sample, T_1 and T_3 were at the same level in the bath. It was found that the heating bath came to thermal equilibrium 8 - 10°C below the original temperature within 1-2 min. during which period the sample also attained the temperature of the bath. Readings of ΔT_Λ and ΔP were taken at regular intervals by recording the deflection of the galvanometer and of the spiral gauge. The temperature of the heating bath was also checked during the run and with a little manipulation could be kept constant to within $\pm$ 1.0°C during a run.

DIAGRAM 4

APPARATUS C. USED FOR MEASURING SELF-HEATING.

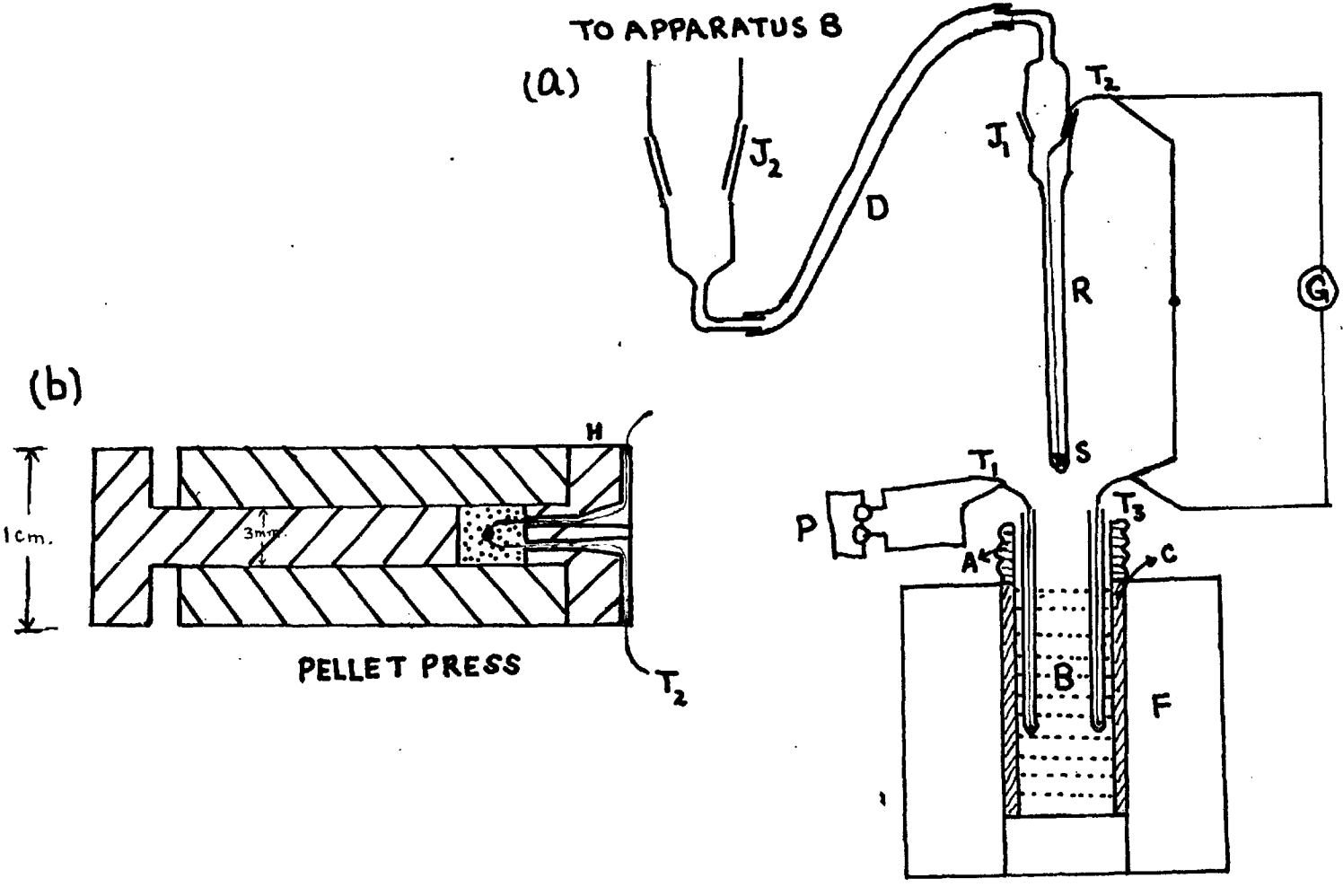

2.2 MATERIALS

The ammonium perchlorate used was B.D.H. reagent grade. It was used as such without further purification. It was, however, ground in an agate mortar and sieved to obtain fractions of known particle size. The fraction mostly used in this work was that below 240 mesh B.S.S. (particle size $< 66\mu$).

The cuprous oxide used was Hopkins and Williams general purpose reagent of specification: Cl^- 1.5% max., alkalis (Na) 0.3% max., and Cu_2O 88% minimum.

The mixtures were made by weighing the required amounts of two salts and shaking them together, in a sample tube, vigorously for 10-20 min. till the mixture appeared uniform.

3. RESULTS

3.1 THERMAL DECOMPOSITION OF "PURE" AMMONIUM PERCHLORATE.

3.11 Reproducibility and Effect of N_2 Pressure: The reproducibility of the results was checked at 265.1 ± 0.2°C under 400 mm N_2 pressure. The α-t plots of three runs on fragments of two different pellets are shown in Fig. 1; the results are fairly reproducible. The effect of varying N_2 pressure in the system was also studied at the same temperature. The particle size of the salt used was < 66 μ and this material is called "fine" powder in the future text.

The percentage decomposition increased with increasing pressure of N_2 and became constant at pressures above 250 mm of Hg. The numerical values of percentage decomposition as a function of nitrogen pressure are given in Table 1.

3.12 Thermal Decomposition of Cubic NH_4ClO_4: The thermal decomposition of "pure" NH_4ClO_4 in the cubic region (> 240°C) was studied for pellets made from material of two different particle sizes, namely, "fine" (< 66μ size) and "coarse" (152 - 175 μ particle size). The results for pellets of "fine" powder could be fitted by the AB equation with n = 2 from α = 0.03 to α = 0.83 (Fig. 2);

but for pellets of "coarse" powder AE equation fitted the results with n = 2 in the range of α = 0.03 to 0.30 and with n = 1 from α = 0.25 - 0.85. The activation energies obtained are 27.2 kcal/mole for both "fine" and "coarse" powder from AE rate constants with n = 2, and 24.0 kcal/mole for "coarse" powder from AE rate constants with n = 1. The Arrhenius plot is shown in Fig. 3, and the numerical values of rate constants with the range of α over which the equation holds are given in Table 2.

3.13 Thermal decomposition of NH_4ClO_4 in orthorhombic region: The thermal decomposition of both the "coarse" and the "fine" material was studied in the orthorhombic region (below 240°C). The results could be fitted by the AE equation with n = 3. The range of α over which this equation held was from α = 0.02 to 0.80 on an average for both the materials. The Arrhenius plot is shown in Fig. 3; the points for both the materials lie on the same straight line. The activation energy obtained from this plot is 32.6 kcal/mole. The numerical values of AE rate constants are given in Table 3.

TABLE 1

THERMAL DECOMPOSITION OF "PURE" AMMONIUM PERCHLORATE. EFFECT OF N_2 PRESSURE OF t_o AE RATE CONSTANT AND % DECOMPOSITION.

Temp. 265.1 ± 0.2°C.

Run	P_{N_2}, mm	t_o, min	k, min^{-1}	% decomp.
R 14	0	4.8	0.1810	17.1
R 13	23	3.0	0.1160	16.9
R 11	102	2.9	0.0780	20.9
R 16	250	4.5	0.0910	22.5
R 10	400	4.9	0.0830	21.8
R 15	400	5.0	-	23.2
R 12	760	5.9	0.0910	21.9

TABLE 2

THERMAL DECOMPOSITION OF "PURE" AMMONIUM PERCHLORATE.
CUBIC REGION. RATE CONSTANTS DETERMINED FROM AE EQUATION.

Material: "Coarse"

Run	Temp.°C	$10^3/T°K$	n=2 $k.min^{-1}$	α-range	n=1 $k.min^{-1}$	α-range
R 21	247.5	1.9205	0.02864	0.03-0.25	0.02350	0.25-0.85
R 20	257.2	1.8854	0.04136	0.02-0.30	0.03040	0.26-0.82
R 18	272.3	1.8332	0.09265	0.01-0.35	0.0623	0.25-0.82
R 19	280.0	1.8077	0.1259	0.03-0.37	0.0840	0.15-0.82
Material: "Fine"						
R 32	245.0	1.9295	0.03051	0.01-0.92	-	-
R 16	265.3	1.8570	0.07573	0.06-0.72	-	-
R 30	256.4	1.8880	0.05202	0.03-0.95	-	-
R 31	271.0	1.8376	0.1098	0.03-0.71	-	-

TABLE 3

THERMAL DECOMPOSITION OF "PURE" AMMONIUM PERCHLORATE. ORTHORHOMBIC REGION. RATE CONSTANTS DETERMINED FROM AE EQUATION

Material	Run	Temp. °C	$10^5/T^\circ K$	$n = 3$ k, min^{-1}	α-range.
	R 25	223.4	2.0137	0.00936	0.06-0.96
	R 24	227.8	1.9955	0.01390	0.05-0.97
"Coarse"	R 23	230.4	1.9857	0.01720	0.04-0.57
	R 22	235.4	1.9662	0.02410	0.01-0.58
	R 29	220.7	2.0247	0.00714	0.16-0.80
"Fine"	R 26	227.8	1.9955	0.01200	0.05-0.97
	R 27	231.6	1.9810	0.01630	0.05-0.78
	R 28	237.1	1.9596	0.02090	0.03-0.74

FIGURE 1

T·D. OF NH_4ClO_4. REPRODUCIBILITY. α-t PLOTS.

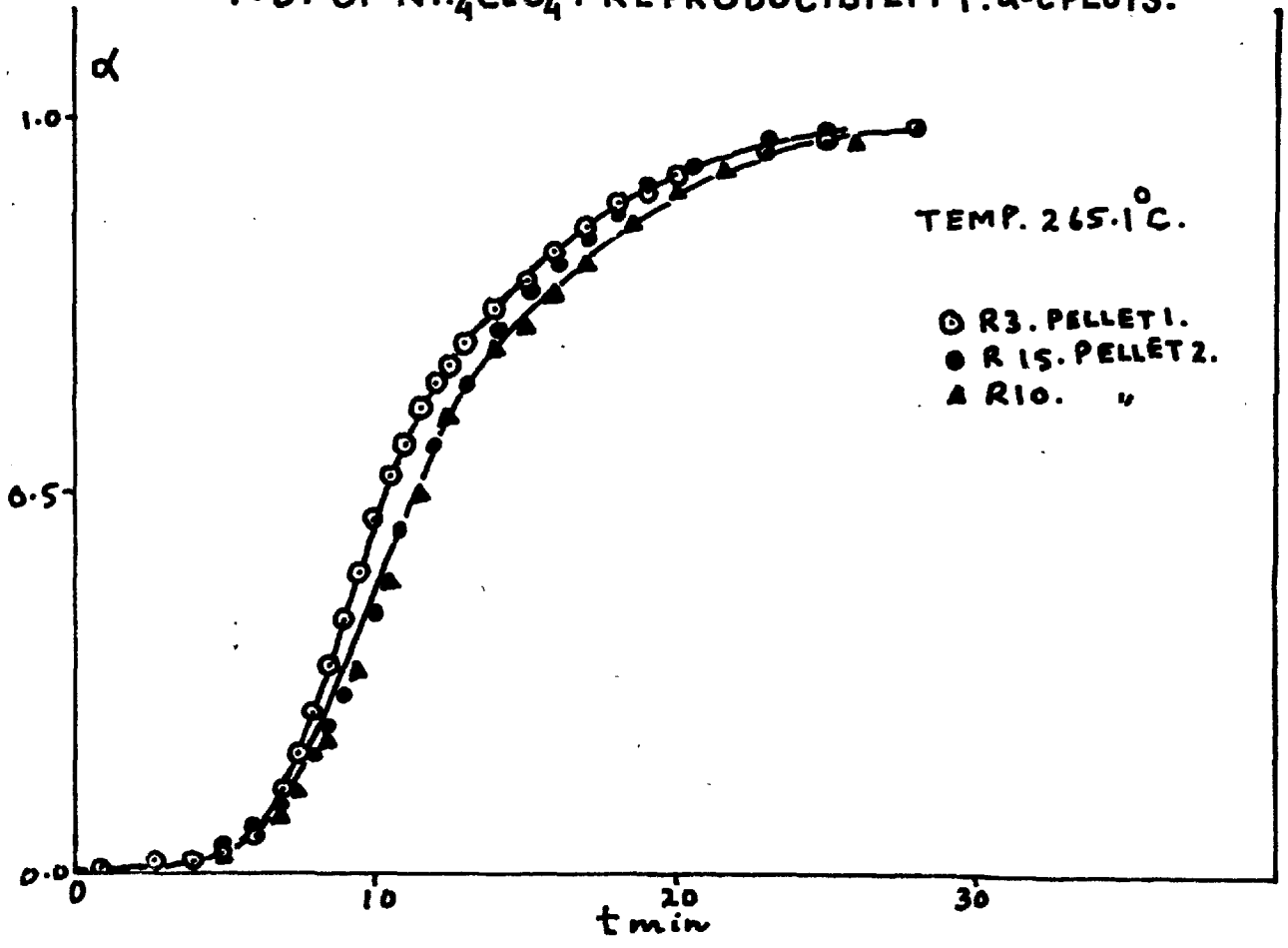

FIGURE 2

T.D. OF NH_4ClO_4. AE AND α-t PLOTS.

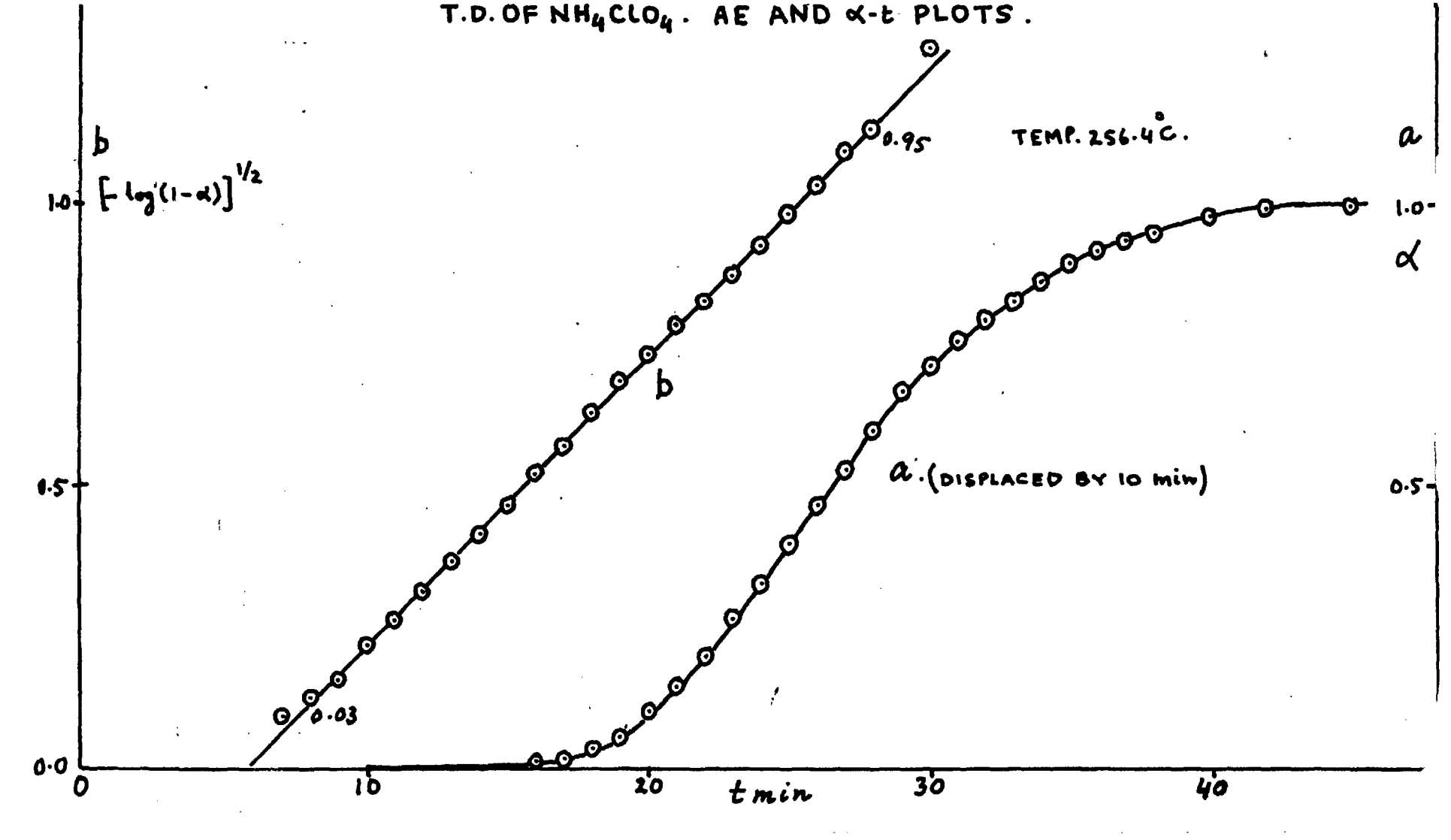

FIGURE 3

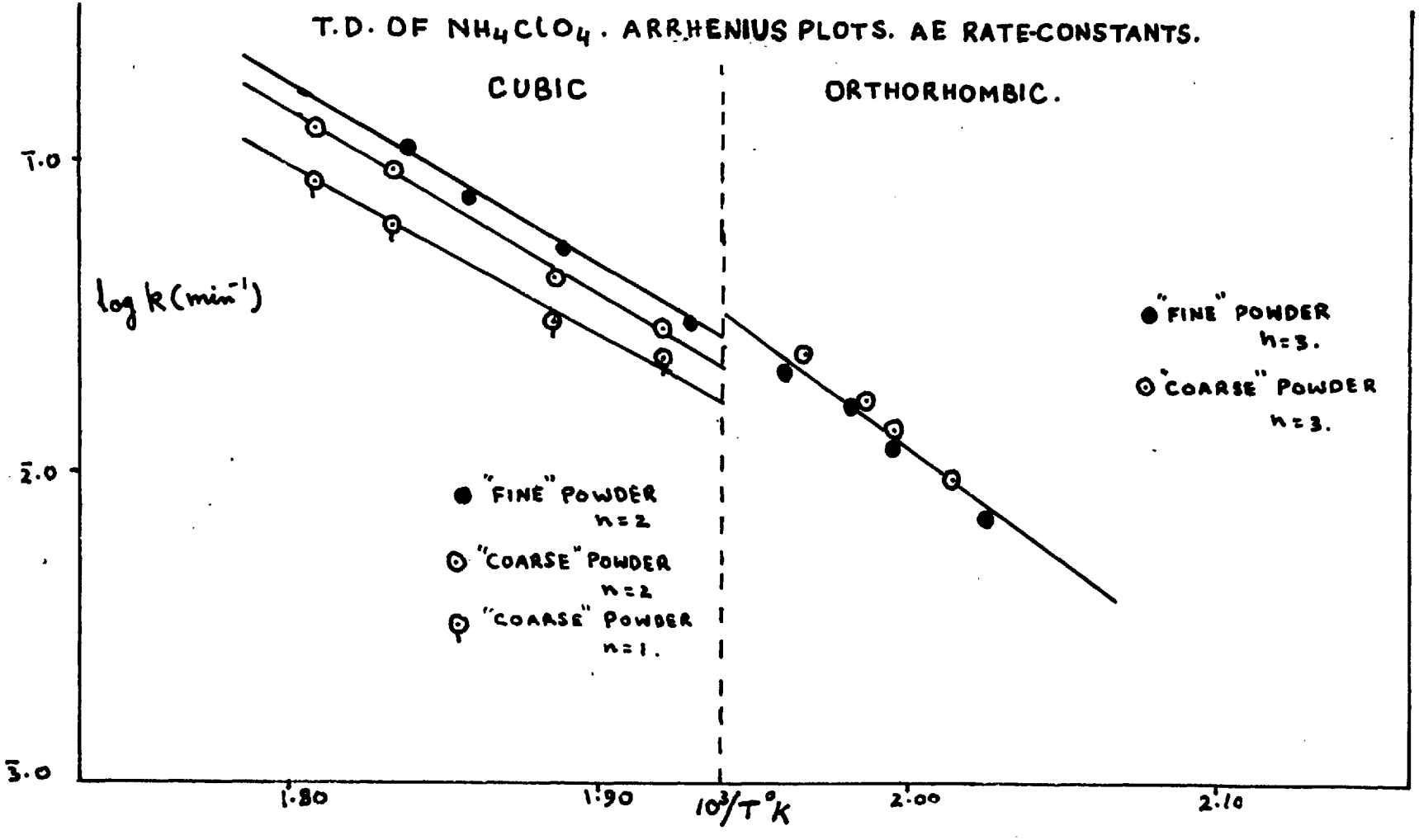
T.D. OF NH_4ClO_4. ARRHENIUS PLOTS. AE RATE-CONSTANTS.
CUBIC
ORTHORHOMBIC.
log k(min⁻¹)
-1.0
-2.0
-3.0
"FINE" POWDER n=2
"COARSE" POWDER n=2
"COARSE" POWDER n=1.
"FINE" POWDER n=3.
"COARSE" POWDER n=3.
1·80
1·90
$10^3/T°K$
2·00
2·10

3.2 THERMAL DECOMPOSITION OF NH_4ClO_4:Cu_2O MIXTURES

All work on NH_4ClO_4:Cu_2O mixtures described in this section and subsequent sections was done by using "fine" powder to make the mixtures of desired compositions and under a pressure of 250 mm N_2, unless otherwise stated. All percentages are expressed as mole percent of Cu_2O in the mixture.

3.21 The variation of composition: The effect of varying the composition of mixture was studied at 270.3° ± 0.2°C. The ϕ-t (where ϕ is deflection of spiral gauge) plots for different compositions are shown in Fig. 4. The mass of the sample for each composition was chosen to keep the amount of NH_4ClO_4 constant at about 25 ± 3 mg. The ϕ-t plots show that there are two types of reaction which lead to explosion. The variation of τ , the time for explosion, with composition of the mixture is shown in Fig. 5. The time for explosion increases with increasing percentage of Cu_2O up to about 10% above which it remains appreciably constant; above 20% Cu_2O, τ decreases sharply, indicating another mechanism for explosion, and decreases linearly with further increase in amount of Cu_2O. The numerical data is given in Table 4. The mechanism by which the explosion

occure at above 20% Cu_2O mixtures has been called the "first mechanism" and the other the "second mechanism". The critical composition of the mixture which divides the range of these mechanisms depends on mass of the sample and the temperature of the reaction.

3.22 The explosion limits: The critical mass for both types of explosion was found for different compositions at a constant temperature of 257°C. The plot of critical mass, m*, against mole % of Cu_2O in the mixture is shown in Fig. 6. There are two distinct boundaries dividing the zones of explosion by the two mechanisms and the zone where no explosion can occur. The two types of explosions can be easily distinguished from their p-t plots, as explosions by the second mechanism occur after a relatively long time during which the pressure in the system decreases.

TABLE 4

THE TIMES FOR EXPLOSION FOR MIXTURES OF NH_4ClO_4 AND Cu_2O AT 270.3° ± 0.2°C.

Run	mass, mg.	Cu_2O, mole %	τ, secs
R 178	25.5	0.43	No explosion
R 180	25.7	0.99	259
R 181	22.7	0.99	250
R 176	27.5	2.01	267
R 177	25.4	2.01	275
R 129	29.5	4.56	315
R 133	25.4	4.56	290
R 169	30.1	8.44	350
R 170	32.8	8.44	352
R 172	28.2	17.76	364
R 173	25.2	17.76	345
R 184	33.8	20.4	355
R 185	33.5	20.4	165
R 182	34.4	23.92	147
R 183	30.5	23.92	149
R 175	40.6	29.04	140
R 175A	41.6	29.04	145
R 83	47.4	45.39	102
R 84	39.7	45.39	101

FIGURE 4.

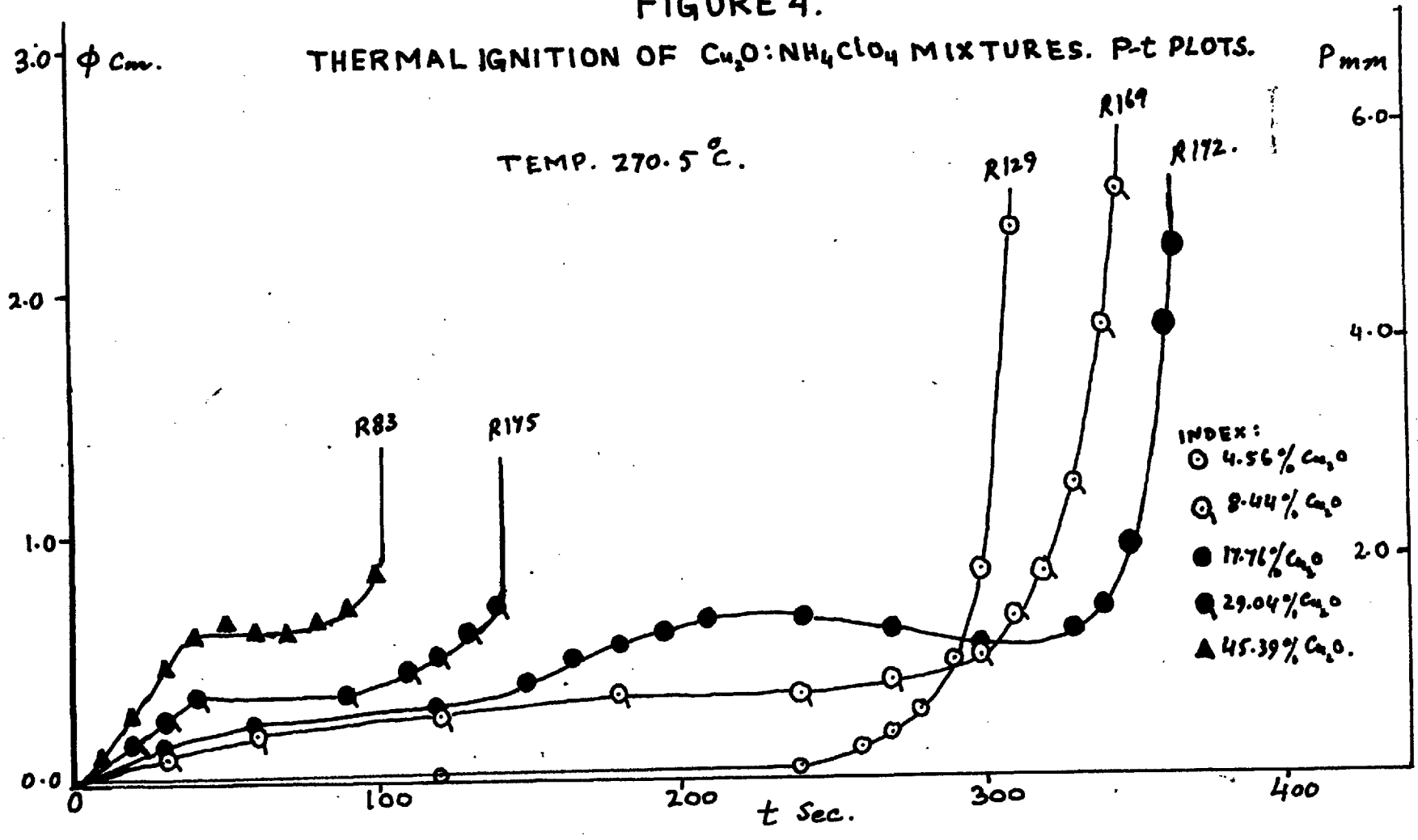
THERMAL IGNITION OF Cu_2O:NH_4ClO_4 MIXTURES. P-t PLOTS.
TEMP. 270.5 °C.
3.0 φ cm.
2.0
1.0
0.0
P mm
6.0
4.0
2.0
0
100
200
300
400
t Sec.
R83
R175
R129
R169
R172.
INDEX:
4.56% Cu_2O
8.44% Cu_2O
17.76% Cu_2O
29.04% Cu_2O
45.39% Cu_2O.

FIGURE 5

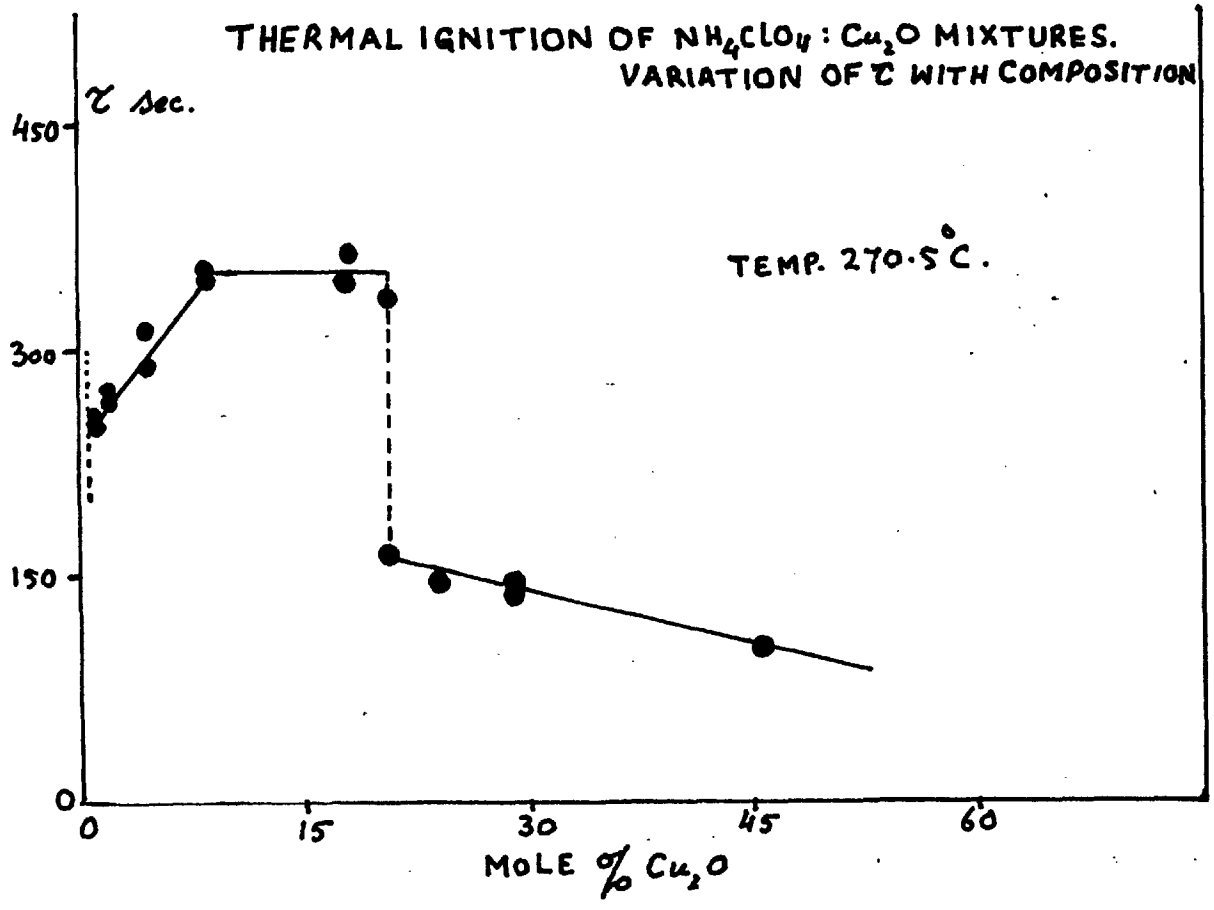
THERMAL IGNITION OF NH_4ClO_4 : Cu_2O MIXTURES.
VARIATION OF τ WITH COMPOSITION
τ sec.
450
300
150
0
TEMP. 270·5°C.
0
15
30
45
60
MOLE % Cu_2O

FIGURE 6

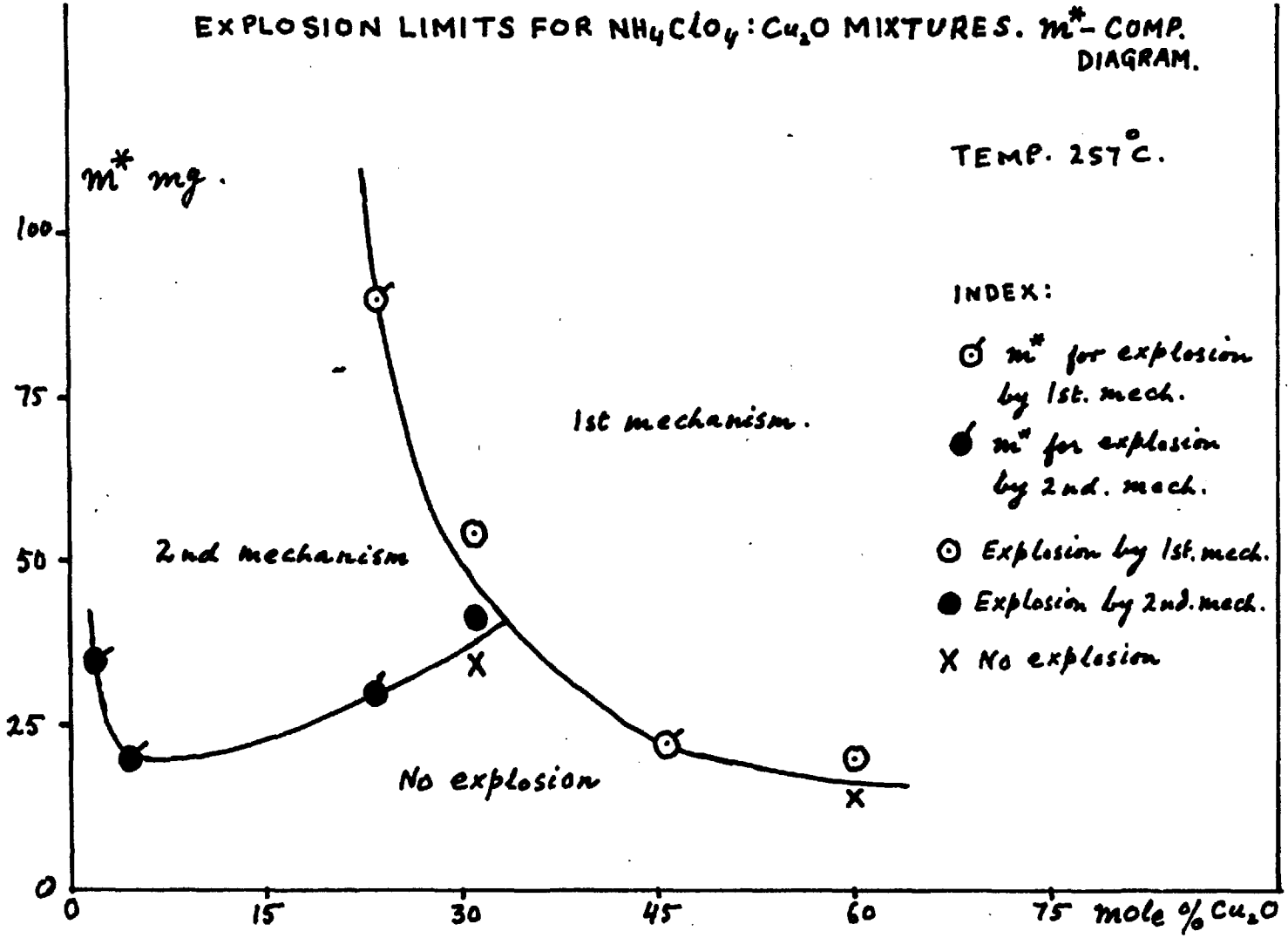
EXPLOSION LIMITS FOR $NH_4ClO_4 : Cu_2O$ MIXTURES. m^* - COMP. DIAGRAM.
TEMP. 257°C.
m^* mg.
100
75
50
25
0
0
15
30
45
60
75 mole % Cu_2O
1st mechanism.
2nd mechanism
No explosion
INDEX:
m^* for explosion by 1st. mech.
m'' for explosion by 2nd. mech.
Explosion by 1st. mech.
Explosion by 2nd. mech.
X No explosion

3.3 THERMAL DECOMPOSITION 45.4% Cu_2O:NH_4ClO_4 MIXTURE.

3.31 The reproducibility of results: The reproducibility was checked by making several pellets and decomposing fragments of approximately same mass at 260.6 ± 0.2°C. The reproducibility of τ, time for explosion, from pellet to pellet was good and the variation in were of the same order as for fragments of same pellet. The maximum variation in the values of τ was ± 10%. These values are plotted in Fig. 7 and variation in τ, for the samples of 45 ± 5 mg mass, is from 147 sec to 160 sec for fragments of different pellets. The dependence of τ on mass was also studied. The time for explosion increases with increasing mass; this increase is linear although the results for samples of mass below 30 mg show a considerable scatter (Fig. 7a). This was also studied in vacuum at 260.6 ± 0.2°C and under 250 mm N_2 pressure at 270.5 ± 0.2°C; the same effect was found (Fig. 7b and 7c); the numerical values are given in Tables 5 and 6. The increase in τ with mass is of the order of 1 sec/mg.

3.32 Activation energy for explosion: As the pressure of gas evolved prior to an explosion was very small for this composition (Fig. 8), pre-explosion kinetics could

could not be analysed. However, if log ($\tau_m - \tau_o$) is plotted against $1/T$ (where τ_m is the mean time taken for explosion, and τ_o , the heat-up time was found empirically to be 45 sec), a straight line is obtained. Fig. 9 shows this plot. The value of τ_m at each temperature was obtained by taking the mean of three runs at that temperature; τ_o was found by trial to be the time necessary to bring the points at high temperatures on the same straight line as those at low temperatures as it only becomes important when τ is small. The activation energy obtained from this plot is 33.4 kcal/mole. The numerical values of induction periods are given in Table 7.

3.33 Explosion limits: Explosion limits for explosion were found by gradually decreasing the mass of the sample at a particular temperature until it failed to explode. The boundary dividing the explosion and non-explosion region was found in this way by repeating the procedure at various temperatures. Such a plot is shown in Fig. 10 and the numerical data is given in Table 8. The curve which separates explosion and non-explosion region in this plot shows the variation of critical mass with temperature. The samples of mass very near to the critical mass, did not explode but showed a considerable acceleration; these are marked by ~~crosses inside~~ filled circles in Fig. 10 and

are almost on the boundary line.

TABLE 5

THE INDUCTION PERIODS FOR EXPLOSION, REPRODUCIBILITY AND VARIATION WITH MASS AT 260.6 ± 0.2°C for 45.39% Cu_2O:NH_4ClO_4 MIXTURE.

Swp = Single whole pellets made in the small pellet press.

Run	Pellet	mass.mg	τ.sec
R 41	6	20.0	133
R 42	"	21.5	138
R 43	"	24.0	127
R 44	"	29.0	142
R 45	"	31.5	136
R 47	Swp	39.2	158
R 48	"	42.7	158
R 49	"	43.7	155
R 50	"	40.7	152
R 51	7	62.5	169
R 52	"	40.3	147
R 53	"	48.8	160
R 54	"	42.4	149
R 56	"	27.0	133
R 57	"	31.6	138
R 60	8	43.5	155
R 64	"	20.1	124
R 65	"	23.1	126
R 66	"	38.0	138

TABLE 6

THE INDUCTION PERIODS FOR EXPLOSION. VARIATION WITH MASS AT 270.5 ± 0.2°C FOR 45.39% Cu_2O:NH_4ClO_4 MIXTURE.

Run	Pellet	mass.mg	τ_{sec}
R 35	5	28.8	78
R 82	11	45.0	95
R 83	"	47.4	102
R 84	"	39.7	101
R114	12	13.0	68
R115	"	10.1	60
R116	"	5.8	53

TABLE 7

THE INDUCTION PERIODS FOR EXPLOSION, 45.39% MIXTURE. VARIATION WITH TEMPERATURE. MASS OF THE SAMPLES 45± 5 mg.

τ_0 = 45 sec.

Run	Temp°C	$10^3/T°K$	τ, sec	τ_m, sec	$(\tau_m - \tau_0)$, sec
R 105	251.4	1.9062	250		
R 106	251.2	1.9069	264	259	214
R 107	251.0	1.9076	263		
R 100	256.2	1.8889	186		
R 102	256.2	1.8889	195	190	145
R 103	256.2	1.8889	188		
R 52	260.6	1.8734	147		
R 53	260.5	1.8737	160	152	107
R 54	260.5	1.8737	149		
R 60	260.8	1.8726	155		
R 61	260.6	1.8734	153	153	108
R 62	260.8	1.8726	150		
R 97	266.0	1.8546	109		
R 98	266.0	1.8546	121	114	69
R 99	266.0	1.8546	113		
R 82	270.2	1.8403	95		
R 83	270.5	1.8392	102	99	54
R 84	270.2	1.8403	101		
R 85	275.2	1.8235	83		
R 86	276.2	1.8202	93	87	42
R 87	275.4	1.8228	84		
R 88	279.8	1.8083	83		
R 89	280.0	1.8077	78	81	36
R 90	280.0	1.8077	83		
R 91	286.9	1.7854	69		
R 92	287.3	1.7841	67	69	24
R 93	287.1	1.7848	70		
R 94	293.4	1.7649	61		
R 95	293.4	1.7649	59	62	17
R 96	293.2	1.7655	66		

TABLE 8

THE EXPLOSION LIMITS FOR 45.39% Cu_2O:NH_4ClO_4 MIXTURE.

E = explosion; NE = no explosion; NEA = no explosion but acceleration.

Run	T_o °K	m,mg	Remarks.
R 108	518.4	55.6	NE
R 109	521.0	35.4	NE
R 110	522.4	48.0	NEA
R 34	521.4	23.5	NE
R 122	523.2	50.3	NEA
R 105	524.4	46.0	E
R 106	524.4	38.6	E
R 107	524.4	48.3	E
R 112	525.5	32.9	NE
R 113	528.6	28.4	E
R 111	526.6	22.9	NE
R 121	531.6	22.2	E
R 43	533.6	24.0	E
R 42	533.8	21.5	E
R 41	533.6	20.0	E
R 63	533.8	15.6	NEA
R 40	533.6	14.6	NEA
R 46	533.8	14.0	NEA
R 57	533.8	12.2	NE
R 120	536.8	13.6	E
R 117	538.4	8.8	NEA
R 118	540.0	5.5	NE
R 115	543.2	10.1	E
R 114	543.2	5.8	E
R 119	542.0	5.8	E

FIGURE 7

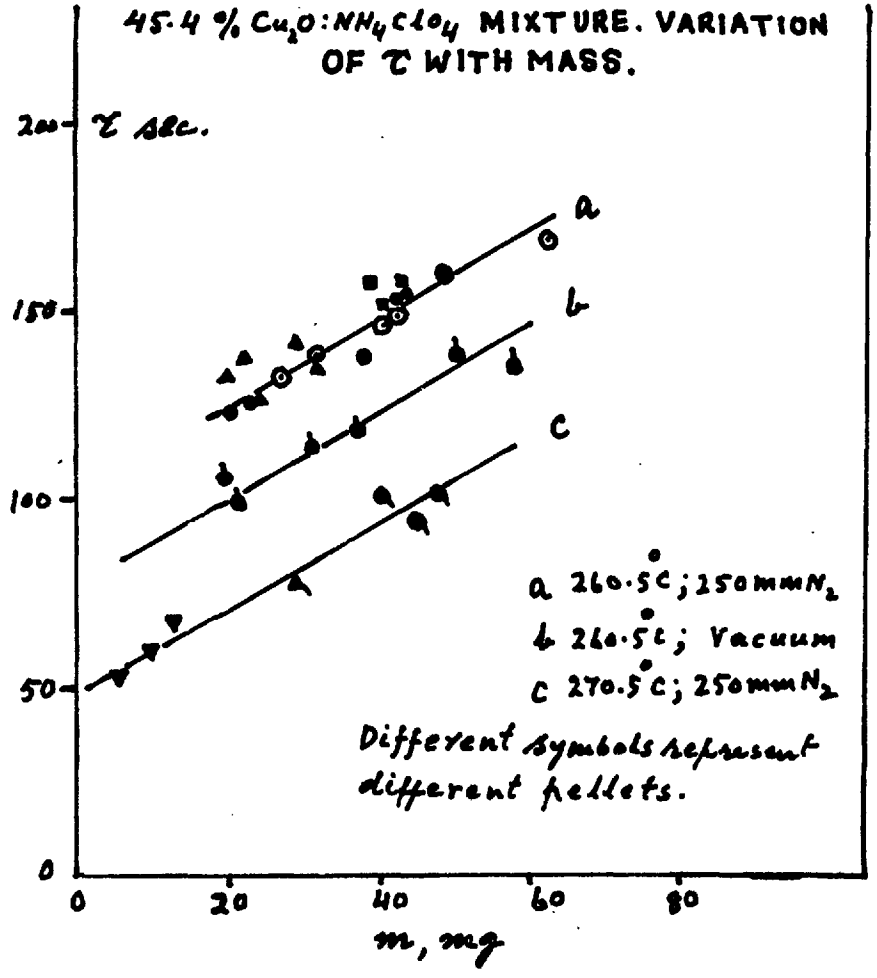

FIGURE 8

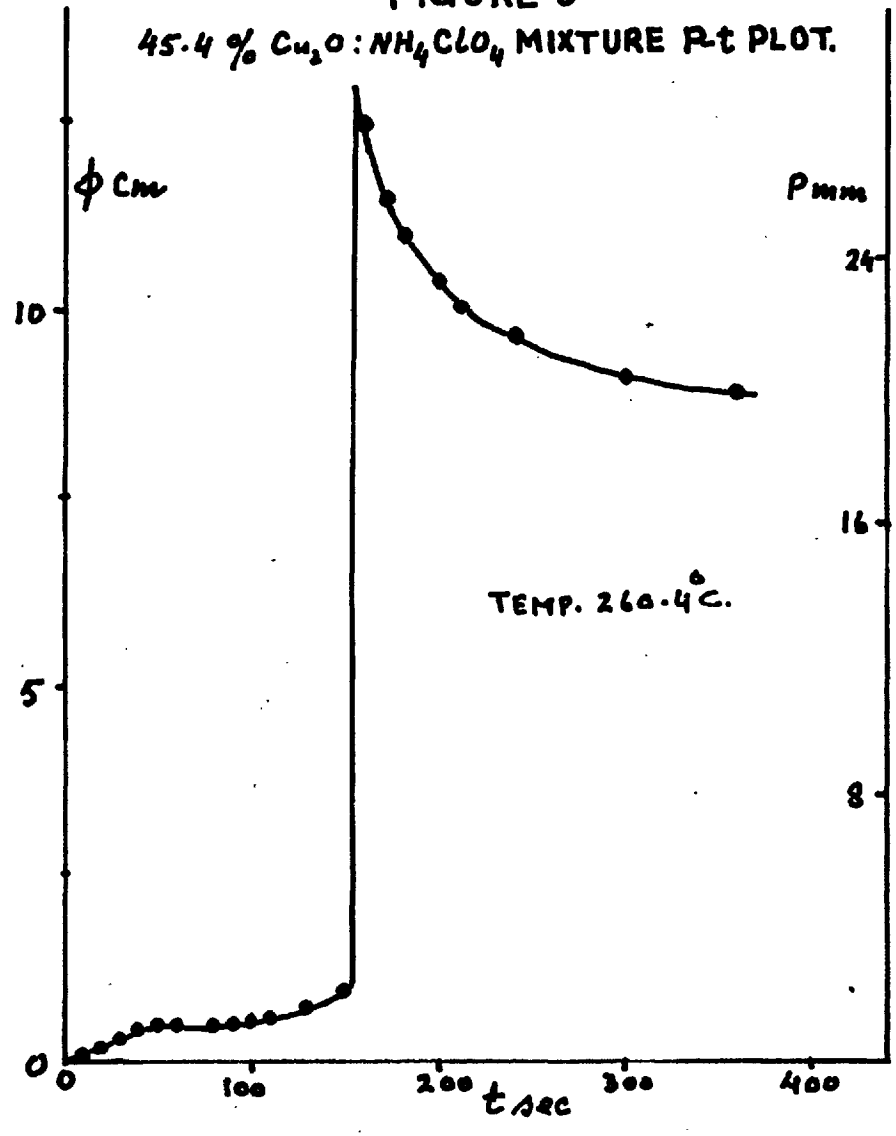

FIGURE 9

45·4 % Cu_2O : NH_4ClO_4 MIXTURE. INDUCTION PERIODS TO EXPLOSION. ARRHENIUS PLOT.

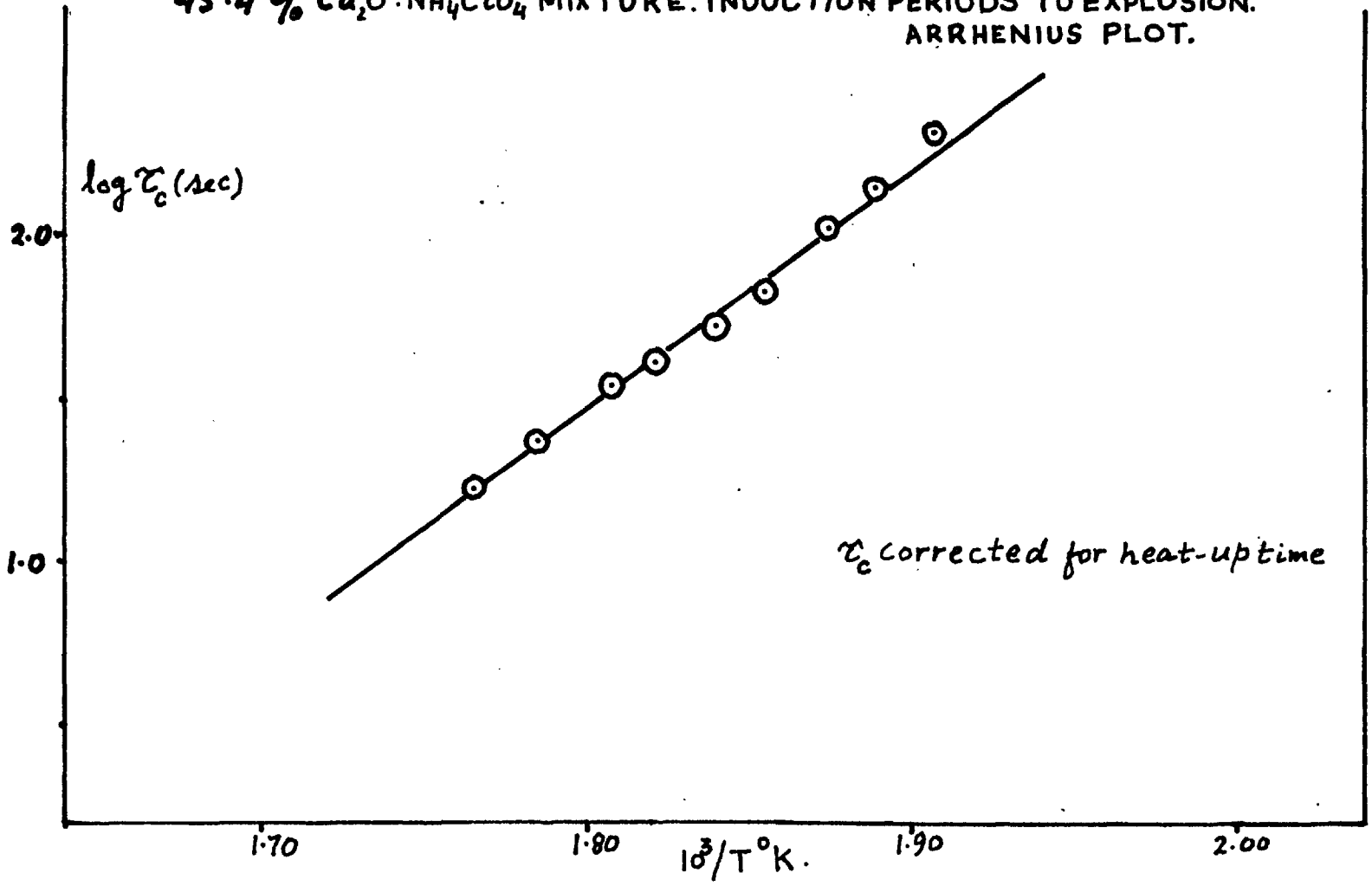

FIGURE 10

EXPLOSION LIMITS FOR 45·4 % Cu_2O:NH_4ClO_4 MIXTURE.

m^n – TEMP. DIAGRAM.

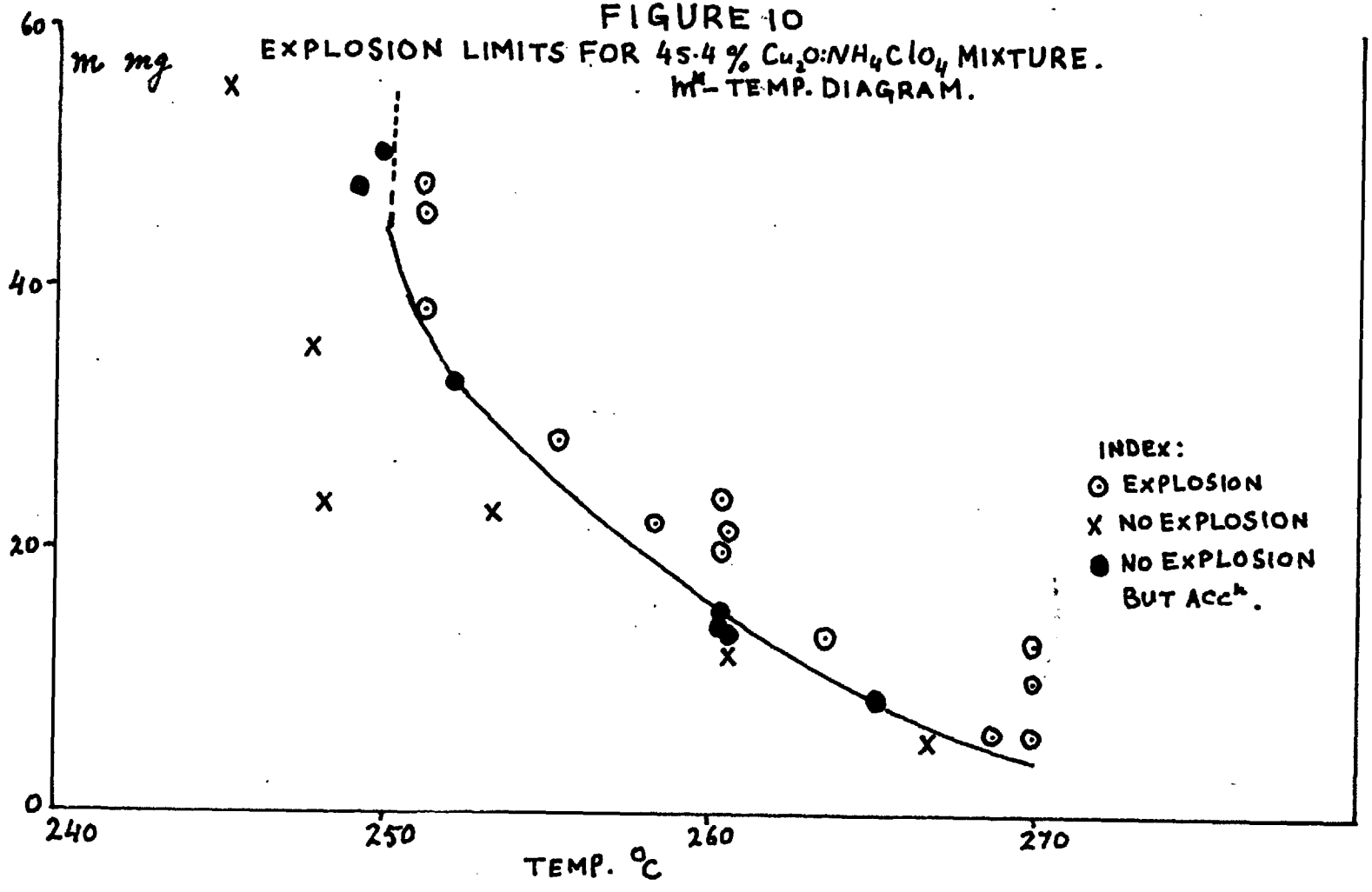

3.4 THERMAL DECOMPOSITION OF 4.56% Cu_2O:NH_4ClO_4 MIXTURE.

3.41 The reproducibility of the results: The reproducibility of the results for this mixture was checked at 270.5°C in the same way as for 45.39% mixture. The variation of k' (an exponential law rate constant for pre-explosion reaction) and τ (the induction period for explosion) with the mass of the sample is shown in Fig. 11a and 11b. τ shows a general increase with mass whereas the values of k' are scattered. However, for masses between 25 - 35 mg the values of k' vary only by ± 10% and those of τ by ± 8%. Therefore, masses between these limits were used in further study. The numerical data from these observations is given in Table 9.

3.42 Induction periods to explosion and pre-explosion kinetics: The pre-explosion reaction could be fitted by an exponential law for this mixture. The extent of fit, however, depended on the conditions of reaction, i.e. whether the sample exploded, or did not explode but was close to the explosion limit, or failed to explode and was well below the explosion limit ϕ-t and $(\log \phi)$-t (exponential law) plots for these three cases are shown in Figs. 12, 13 and 14. Fig. 12 is a plot for one that exploded; the exponential law holds in the beginning

but near the explosion time the reaction becomes much faster than required by the exponential law (Fig. 12b). For samples very near the explosion limit the exponential law holds all the way until the material is exhausted and the product gases start to react with reactants causing a decrease in pressure (Fig. 13b). The third case is that of samples much below the explosion limit when the exponential law only holds during the accelerator period (Fig. 14b) and there is a decay period which is of course not fitted by this law. The Arrhenius plot of the exponential law rate constants for 30 ± 5 mg samples, is shown in Fig. 15 and the activation energy obtained from this plot is 29.01 kcal/mole. The plot of log $(\tau_m - \tau_o)$ against $1/T$ was also a straight line (where τ_m is the mean induction period to explosion determined by taking the mean of two or three values of τ at the same temperature and τ_o is a heat-up time found empirically to be 30 sec). The activation energy obtained from this plot is 28.1 kcal/mole (Fig. 16). The numerical data for these observations is given in Table 10.

3.43 Explosion limits: The explosion limits for this composition were determined in the same way as for 45.39% mixture (section 3.33). The data is given in Table 11 and the plot is shown in Fig. 17. There are again three types -

those which explode and become faster than exponential near the explosion time; those which do not explode but show a very fast acceleration (near the boundary line); and those which have a decay period (much below the boundary line). These types are represented by different symbols in Fig. 17.

TABLE 9

THE INDUCTION PERIODS TO EXPLOSION AND THE RATE CONSTANTS DETERMINED FROM THE EXPONENTIAL LAW FOR PRE-EXPLOSION REACTION IN THERMAL DECOMPOSITION OF 4.56% $Cu_2O:NH_4ClO_4$ MIXTURE. REPRODUCIBILITY AND VARIATION WITH THE MASS OF THE SAMPLE. TEMP. 270.5°C.

Run	Pellet	m.mg	k'.sec^{-1}	τ.sec
R 123	18	30.2	0.0182	325
R 124	"	29.5	0.0198	328
R 125	"	32.7	0.0216	307
R 126	"	20.5	0.0172	294
R 127	"	16.9	0.0105	337
R 128	"	8.1	NE	NE
R 129	19	29.5	0.0204	315
R 130	"	41.5	0.0224	335
R 131	"	16.0	0.0194	269
R 132	"	13.5	0.0252	242
R 133	"	25.4	0.0212	290

THE INDUCTION PERIODS TO EXPLOSION AND RATE CONSTANTS DETERMINED FROM THE EXPONENTIAL LAW FOR THE PRE-EXPLOSION REACTION IN THE THERMAL DECOMPOSITION OF 4.56% $Cu_2O:NH_4ClO_4$ MIXTURE. MASS OF THE SAMPLES 30 ± mg. τ_0 = 30 sec.

Run	Pellet	temp°C	$10^3/T°K$	τ sec	τ_m sec	$(\tau_m-\tau_0)$ sec	$k'.sec^{-1}$
R 156	22A	248.0	1.9186	901	901	871	0.00665
R 155	"	252.0	1.9040	771	771	741	0.01030
R 154	"	255.2	1.8925	660			0.0112
R 153	"	255.0	1.8932	702	681	651	0.00970
R 152	21	259.7	1.8765	518			0.0121
R 151	"	259.9	1.8758	539	529	498	0.0125
R 150	"	264.8	1.8587	390			0.0201
R 149	"	264.8	1.8587	359	374	344	0.0184
R 133	19	270.0	1.8410	290			0.0212
R 130	"	270.2	1.8403	335			0.0224
R 129	"	270.2	1.8403	315	313	283	0.0204
R 125	18	270.2	1.8403	307			0.0216
R 124	"	270.2	1.8403	328			0.0198
R 123	"	270.5	1.8394	325	320	290	0.0182
R 147	21	276.0	1.8208	226			0.0356
R 148	"	276.0	1.8208	233	229	199	0.0332
R 135	19	282.0	1.8011	185			0.0384
R 134	"	282.2	1.8004	185	185	155	
R 136	18	293.4	1.7649	120			0.0444
R 137	19	293.4	1.7649	131	125	95	-
R 138	"	302.6	1.7367	84			-
R 139	"	302.4	1.7373	99			-
R 140	"	302.6	1.7367	86	90	60	-
R 141	20	312.4	1.7076	73			-
R 142	"	312.4	1.7076	78	75	45	-
R 143	"	319.6	1.6869	59			-
R 144	"	319.6	1.6869	66	62	32	-
R 145	"	333.8	1.6474	53			-
R 146	"	333.8	1.6474	47	50	20	-

TABLE 11

THE EXPLOSION LIMITS FOR 4.56% Cu_2O:NH_4ClO_4 MIXTURE.

E = explosion; NE = no explosion; NEA = no explosion but acceleration

Run	T_o °K	m, mg	Remarks
R 157	515.7	28.7	NEA
R 158	518.7	27.4	E
R 159	516.8	36.6	NEA
R 160	520.2	20.2	NE
R 161	523.6	23.3	E
R 162	527.3	18.4	NEA
R 163	533.9	15.3	E
R 164	535.4	12.5	NEA
R 165	539.5	11.9	NEA
R 128	543.4	8.1	NE
R 166	557.6	6.4	E
R 167	547.4	7.8	NE
R 132	543.4	13.5	E

FIGURE II

THERMAL IGNITION OF 4.56 % Cu_2O: NH_4ClO_4 MIXTURE.

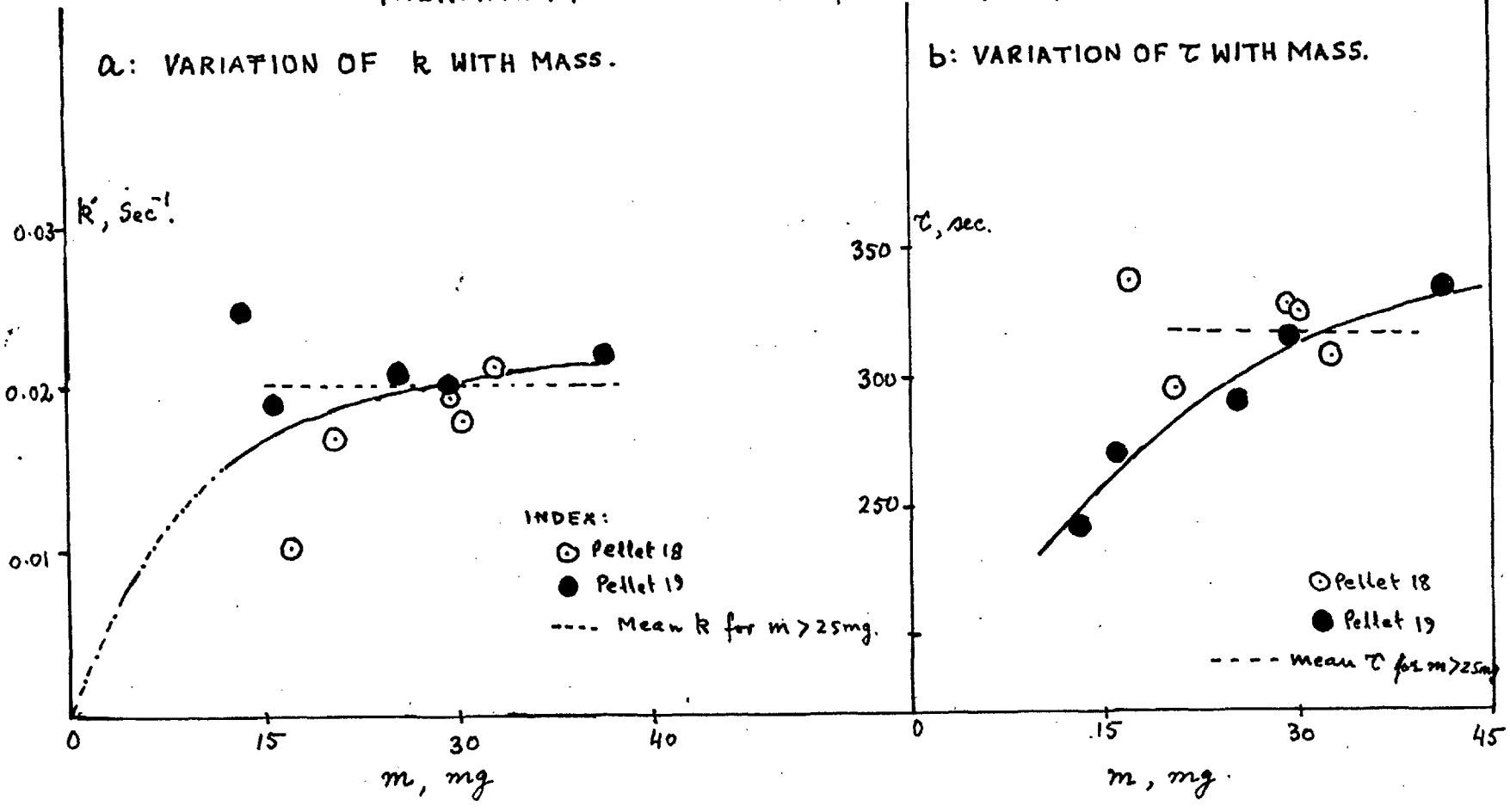

FIGURE 12

T.D. OF 4.56% Cu_2O : NH_4ClO_4 MIXTURE

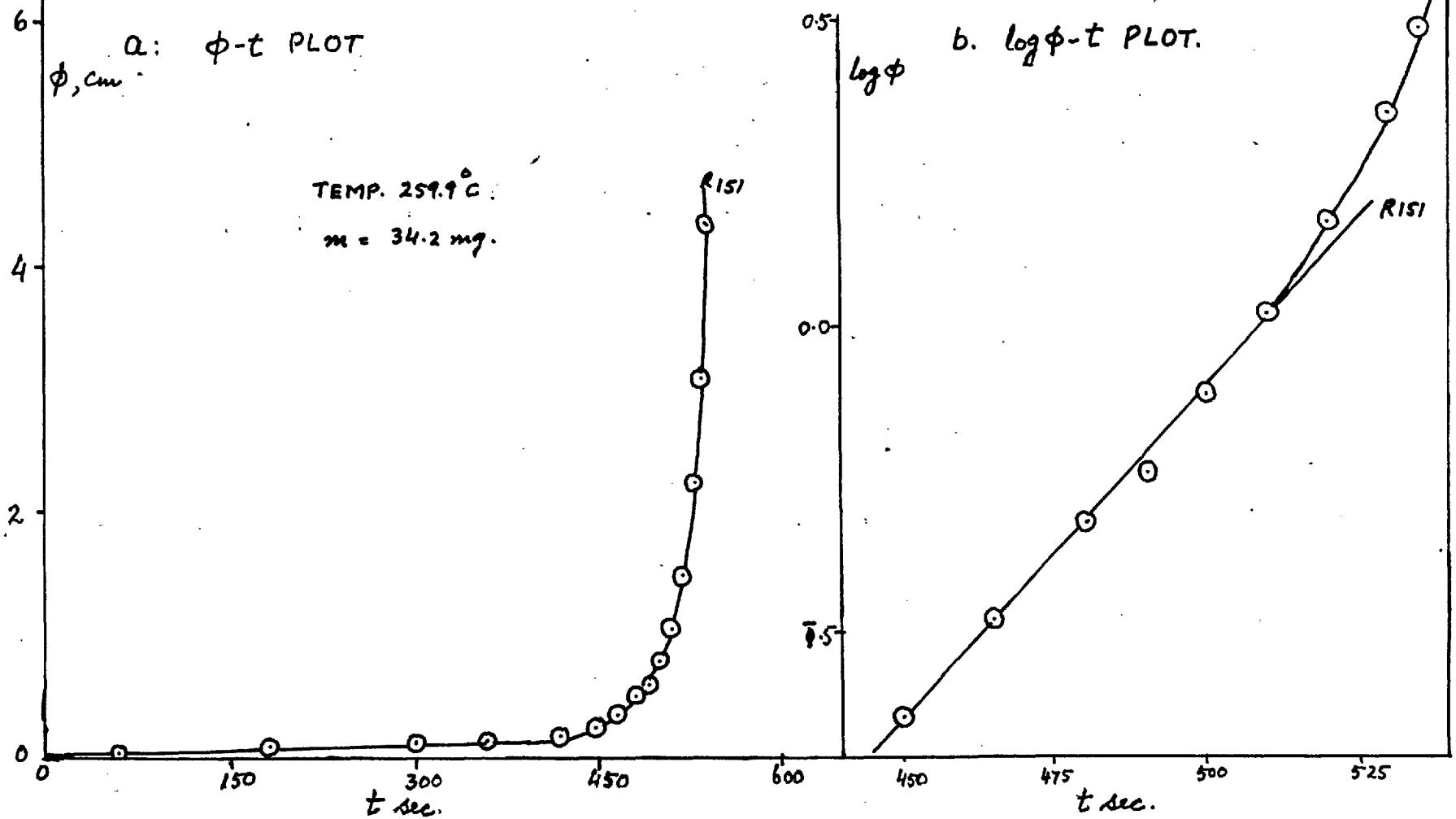

FIGURE 13.

T.D. OF 4.56 % Cu_2O:NH_4ClO_4 MIXTURE. (a). ϕ-t PLOT (b) $\log\phi$-t PLOT.

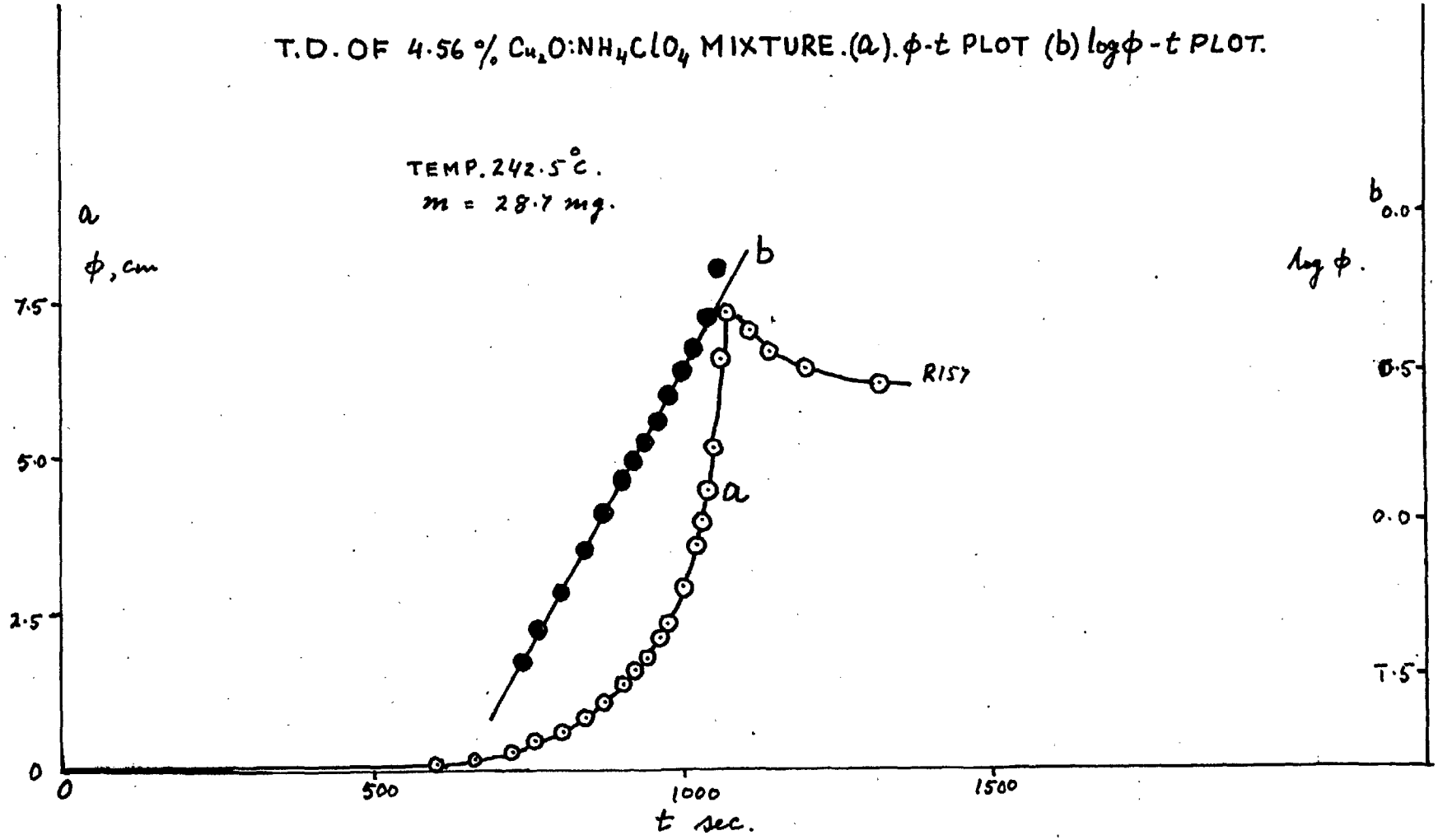

FIGURE 14

T.D. OF 4.56 % Cu_2O : NH_4ClO_4 MIXTURE. (a) ϕ-t PLOT. (b) logϕ-t PLOT.

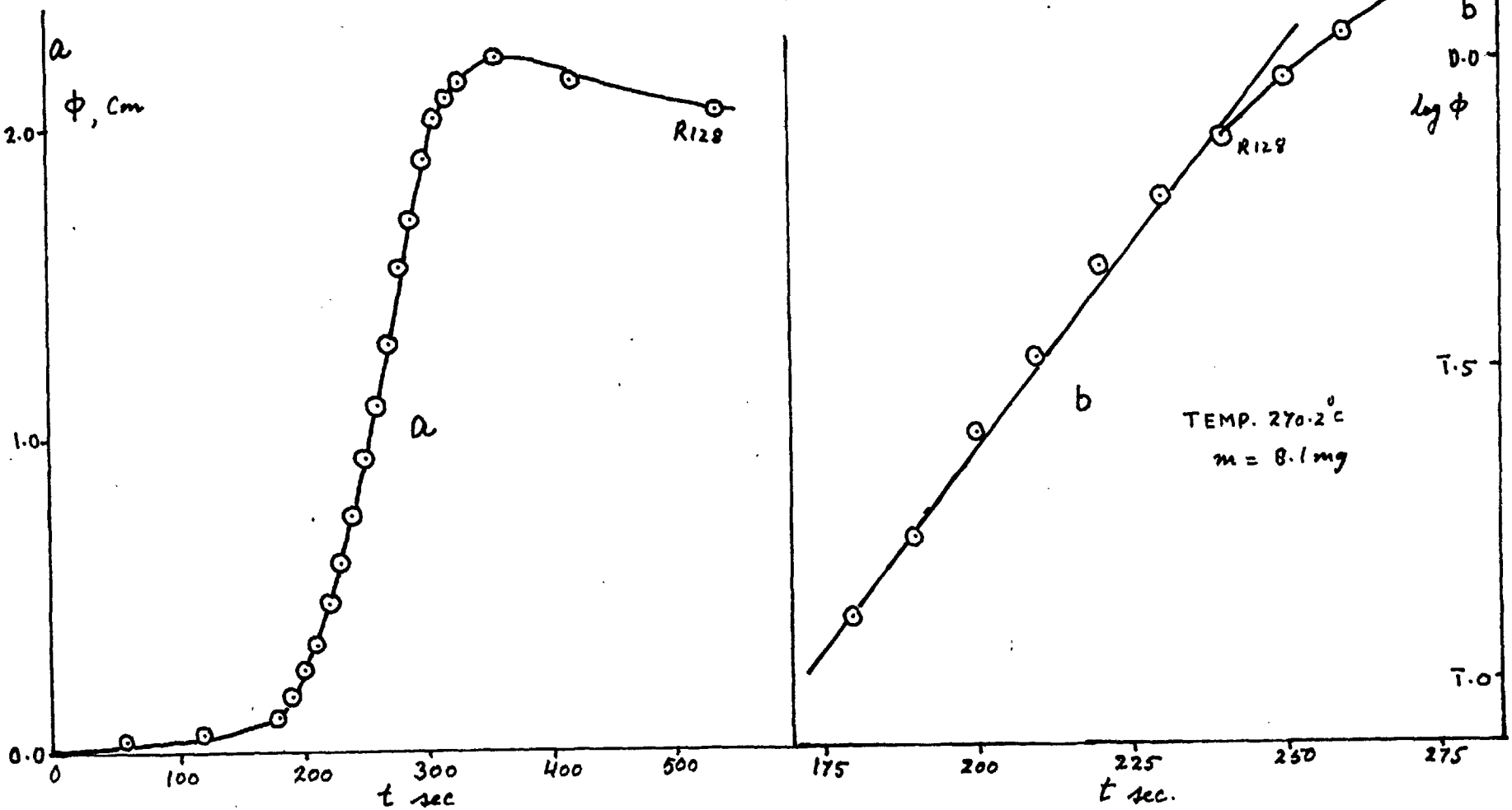

FIGURE 15

4.56 % Cu_2O : NH_4ClO_4. ARRHENIUS PLOT. EXP. LAW RATE CONSTANTS.

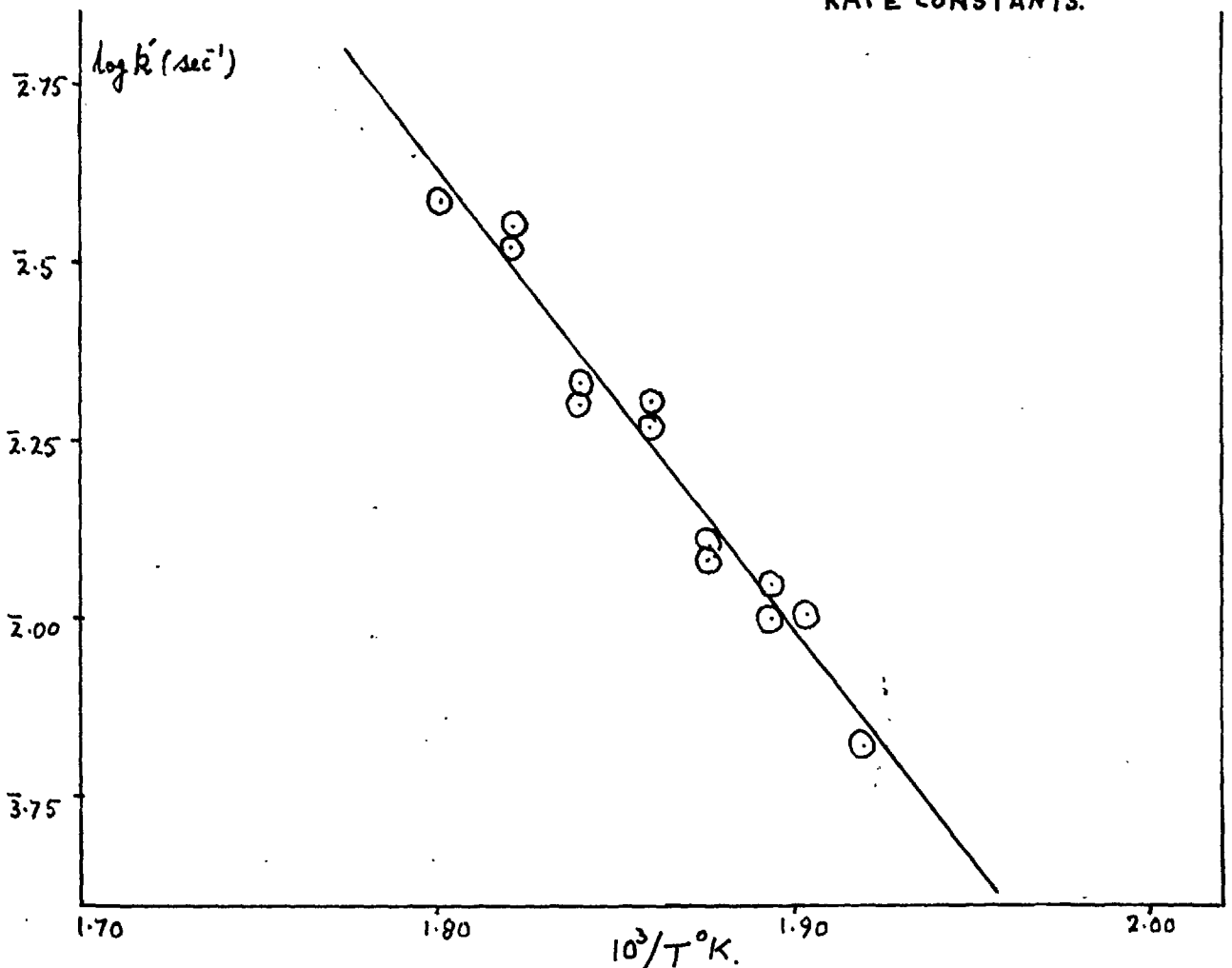

FIGURE 16

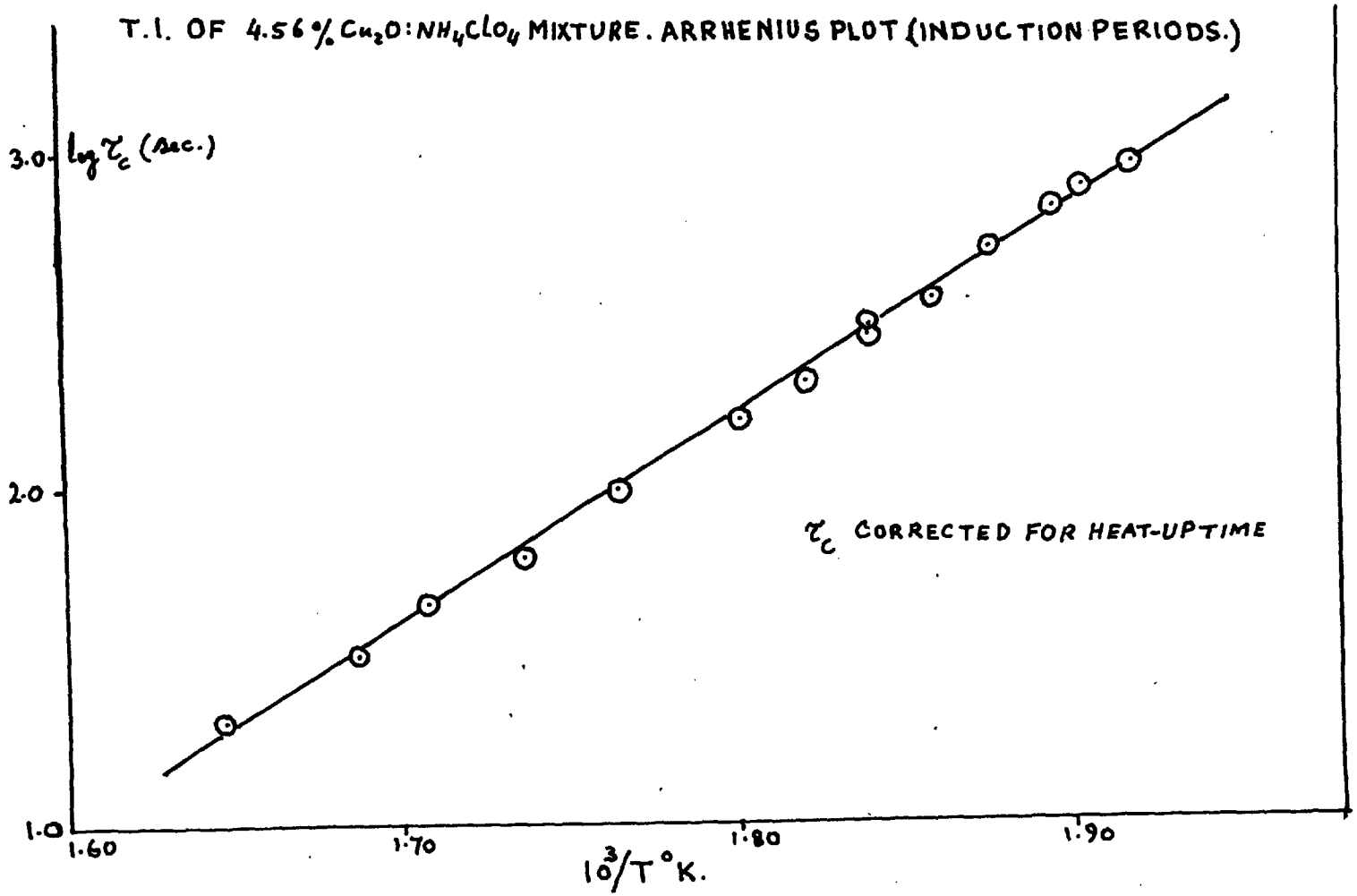
T.I. OF 4.56 % Cu_2O : NH_4ClO_4 MIXTURE. ARRHENIUS PLOT (INDUCTION PERIODS.)
3.0
$\log \tau_c$ (sec.)
2.0
1.0
τ_c CORRECTED FOR HEAT-UP TIME
1.60
1.70
1.80
1.90
$10^3/T$ °K.

FIGURE 17

EXPLOSION LIMITS FOR 4.56% $Cu_2O : NH_4ClO_4$ MIXT. m^*-TEMP. DIAGRAM.

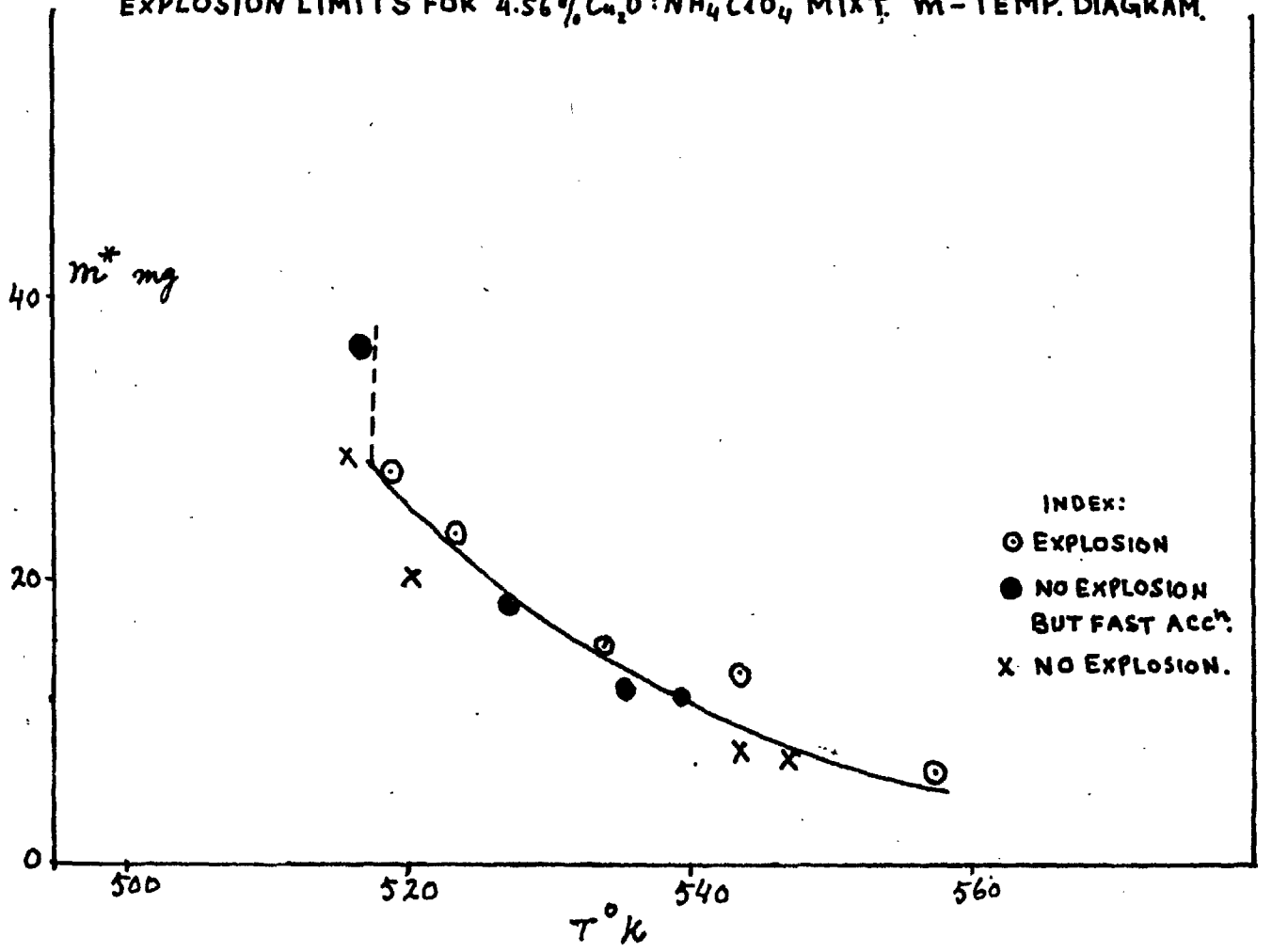

3.5 THERMAL DECOMPOSITION OF 23.9% Cu_2O:NH_4ClO_4 MIXTURE.

3.51 Explosion limits: A variation of temperature and the mass of the sample for this composition showed that the explosion could occur by both the mechanisms depending upon the choice of these two variable. Fig. 18 shows p-t plot for three runs - R 216 at 267.5°C with a 16.4 mg sample which did not explode, R 199 at 268.5°C with 18.2 mg sample which exploded by the second mechanism and R 200 at 269.2°C with a 30.6 mg sample exploded by the first mechanism. Hence, explosion limits were found between these three regions. The method was essentially the same as described previously (Section 3.33). A plot of the explosion limits is shown in Fig. 19 and the data is given in Table 12. The two boundaries describe the variation of critical mass, m^*, with temperature, T_o, for the two types of explosion.

TABLE 12

THE EXPLOSION LIMITS FOR 23.9% $Cu_2O:NH_4ClO_4$ MIXTURE.

E_I = explosion by first mechanism; E_{II} = explosion by second mechanism.
NE = no explosion

Run	m,mg	T_o °K	Remarks
R 192	25.5	531.9	NE
R 195	37.6	535.7	E_{II}
R 196	42.0	537.7	E_I
R 197	28.1	540.7	E_{II}
R 198	20.0	543.2	E_{II}
R 199	18.2	541.7	E_{II}
R 200	30.6	542.4	E_I
R 201	12.0	550.7	E_I
R 202	11.6	548.2	NE
R 203	8.7	553.2	E_I
R 204	7.0	553.2	E_{II}
R 205	23.3	551.2	NE
R 206	31.3	550.2	NE
R 207	21.1	538.2	E_{II}
R 208	23.5	534.4	NE
R 209	43.2	523.7	NE
R 210	36.3	529.2	E_{II}
R 211	17.5	546.2	E_{II}
R 212	15.0	548.2	E_I
R 213	7.9	550.2	NE
R 214	8.8	551.7	E_{II}
R 215	6.2	553.2	E_{II}
R 216	16.4	540.7	NE
R 217	14.3	546.4	E_{II}

FIGURE 18

T.D. OF 23.9 % Cu_2O : NH_4ClO_4 MIXTURE. ϕ - t PLOTS TO SHOW TWO MECHANISMS.

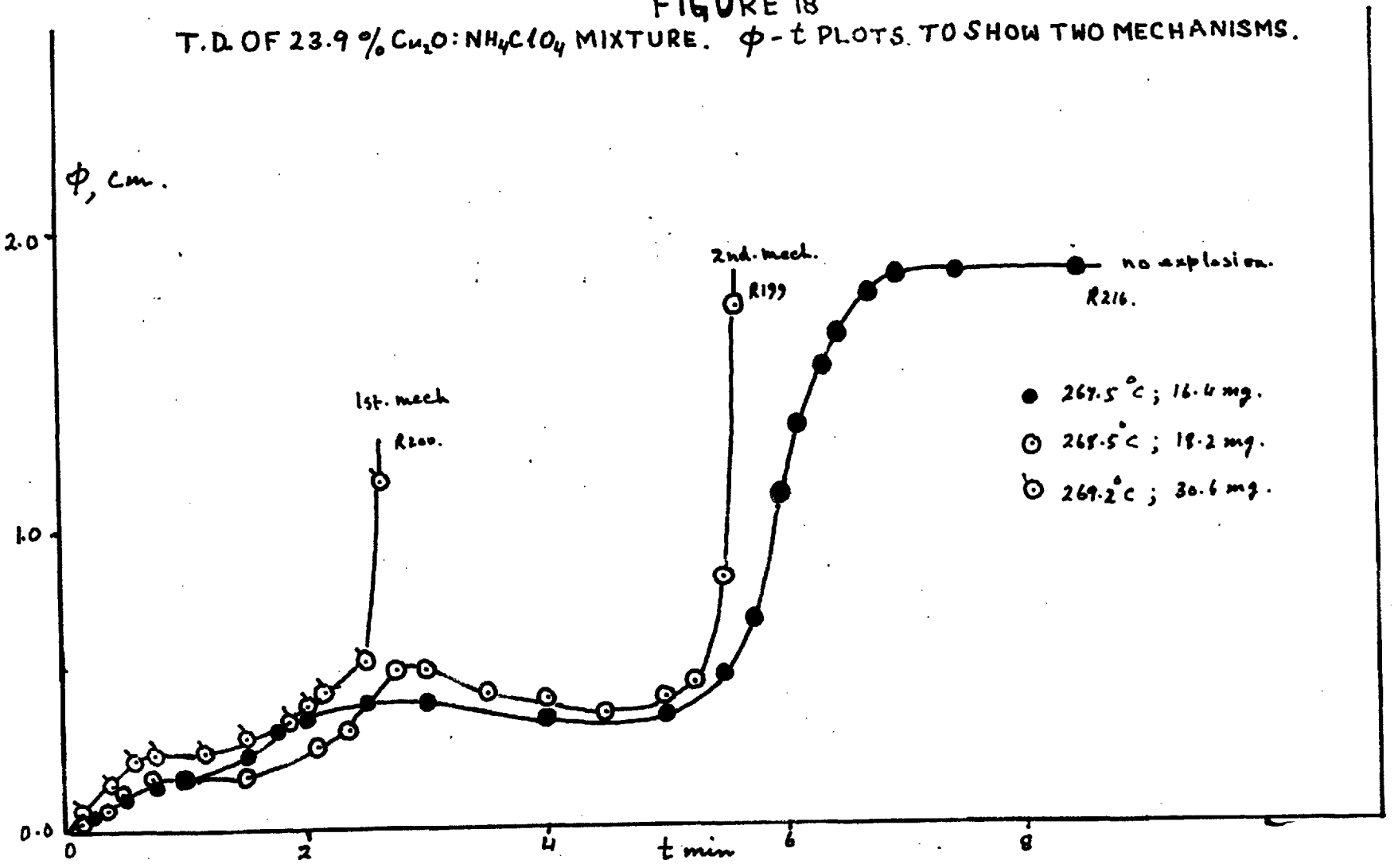

FIGURE 19

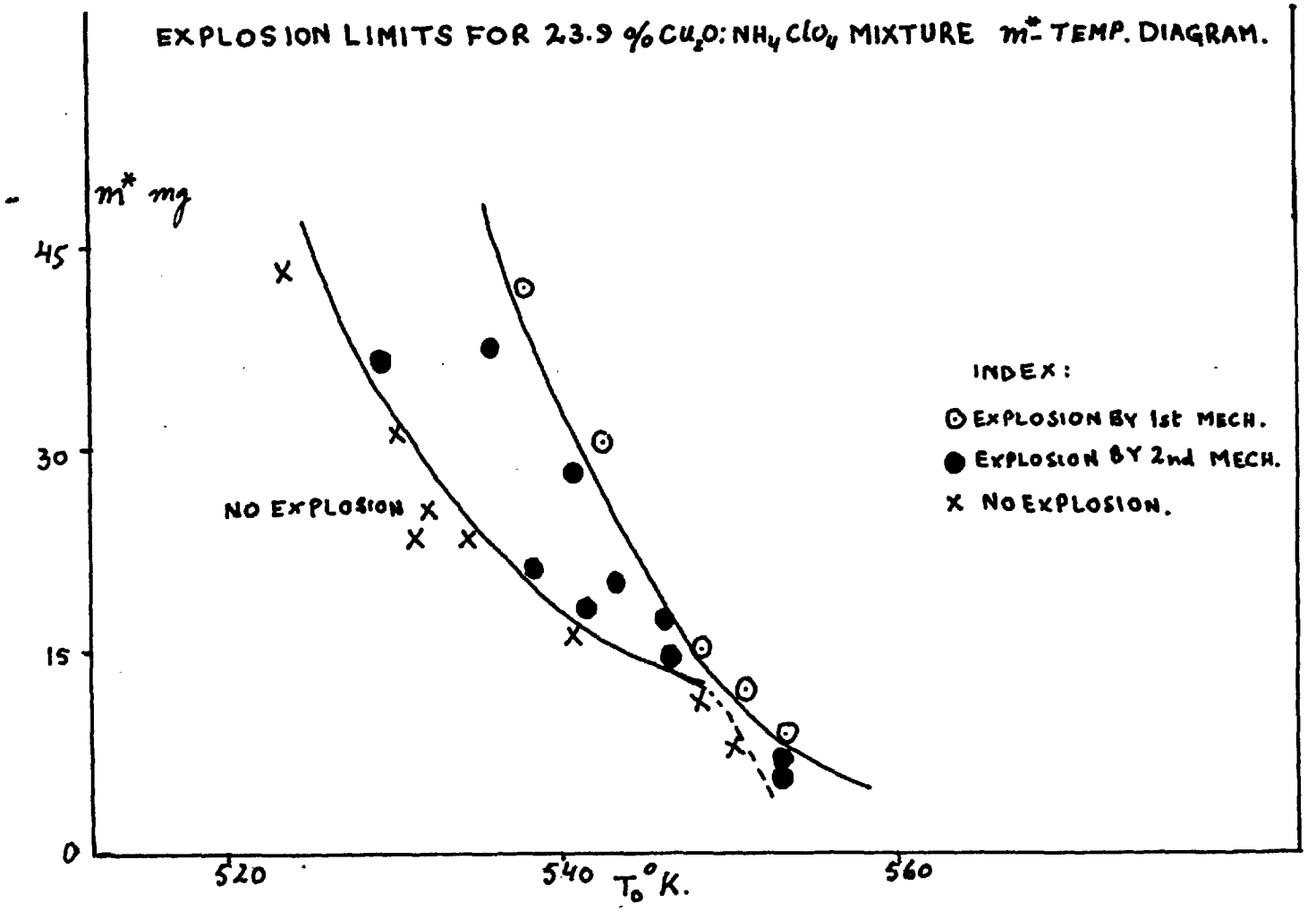
EXPLOSION LIMITS FOR 23.9 % Cu_2O: NH_4ClO_4 MIXTURE m^*- TEMP. DIAGRAM.
m^* mg
45
30
15
0
520
540
560
T_0°K.
NO EXPLOSION
INDEX:
EXPLOSION BY 1st MECH.
EXPLOSION BY 2nd MECH.
NO EXPLOSION.

3.6 MEASUREMENT OF SELF-HEATING IN THE THERMAL DECOMPOSITION OF Cu_2O:NH_4ClO_4 MIXTURES.

All the work described in this section was done in Apparatus C under a pressure of 250 mm of N_2.

3.61 Variation of Composition: It was found that "pure" ammonium perchlorate at 255°C shows very little self-heating. Fig. 20 shows plots of ϕ-t and ΔT-t for a 45 mg sample of "pure" NH_4ClO_4 at 255°C. There is a very small maxima (= 1.2°C) in ΔT corresponding to the maximum rate of reaction. Hence, the decomposition of "pure" NH_4ClO_4 can reasonably be regarded as isothermal. The variation of composition of cuprous oxide-ammonium perchlorate mixture showed that there are two maxima in the ΔT-t plot; these correspond to the two reaction mechanisms (section 3.21). Both of these maxima increase with increasing percentage of Cu_2O in the mixture. Fig. 21 shows plots for various compositions from 0.5% Cu_2O to 45.5% Cu_2O mixtures at 255 ± 2°C. The mass of the sample was taken such as to keep the amount of NH_4ClO_4 in it constant at 45 ± 3 mg. The induction period for the first reaction is masked by the heat-up time but the induction period for the second reaction increases with increasing amount of Cu_2O; this is in agreement with the results described in section 3.21. The variation of ΔT_{max} (for both first and second reactions)

with mole percent of Cu_2O is shown in Fig. 22. These values have been obtained from Fig. 21. 17.8% Cu_2O mixture explodes by the second mechanism but 20.4% Cu_2O mixture does not and the self-heating due to second reaction is also small because a considerable amount of the salt has been decomposed by the first reaction. 30% Cu_2O mixture shows considerable self-heating due to the first reaction (15°C) and 45.5% Cu_2O mixture explodes by the first mechanism.

The step in ΔT-t plot during the heat-up period is due to phase transition (orthorhombic to cubic) which occurs in NH_4ClO_4 at 240°C.

3.62 Self-heating in 29.04% Cu_2O:NH_4ClO_4 mixture: This mixture can only explode by the first mechanism and if it does not explode by this mechanism the self-heating due to the second reaction is very small and irreproducible. As the induction periods to explosions by the first mechanism are small, the temperature range in which self-heating could be studied for this mixture was very limited due to the unavoidably long heat-up time ($\simeq$2 min) in Apparatus C. Three runs at different temperatures with samples of 65 $\pm$ 2 mg mass are shown in Fig. 23. R 21 at 250.5°C shows small self-heating (ΔT_{max} = 3°C) due to first reaction and there is another small peak of 4°C at

43 min due to second reaction (not shown in Fig. 23); R 24 at 257°C shows a peak of 18°C due to first reaction and another of 11.2°C at 23.5 min (not shown) due to second reaction; R 25 at 262°C exploded (= 2.5 min) by the first mechanism.

3.63 Self-heating in 17.76% Cu_2O:NH_4ClO_4 mixture: This mixture can explode by either mechanism depending upon the mass of the sample and the temperature at which the reaction took place. Keeping the mass constant within 55 ± 2 mg and varying the temperature of the reaction it was observed that self-heating due to the first reaction became more and more pronounced as the temperature increased until at 279°C (R 33) the sample exploded by the first mechanism (Fig. 24). The value of activation energy obtained from log t_o vs 1/T plot (where t_o is the induction period corrected for heat-up time) is 37.9 kcal/mole (Fig. 25).

3.64 Self-heating in 4.56% Cu_2O:NH_4ClO_4 mixture: This mixture can be made to explode only by the second mechanism. The ΔT-t plots for this composition in the temperature range 235°C to 285°C are shown in Fig. 26. There is practically no self-heating due to first reaction up to temperatures as high as 271°C (R 5 at 271°C shows a maximum of only 1°C for first reaction). Whereas, R 4 at 285°C (Fig. 26) shows an observable self-heating due

to first reaction but explosion still occurs by the second mechanism. This composition was very suitable for studying self-heating as it allows a wide range of temperature to work in and the mechanism for explosion is the same throughout. The induction period, t_o, at which the temperature of pellet begins to rise can also be determined accurately. A plot of log t_o (where t_o is the induction period from which the heat-up time has been subtracted) against $1/T$ is linear (Fig. 27). The activation energy for the pre-explosion reaction obtained from this plot is 30.97 kcal/mole.

FIGURE 20.

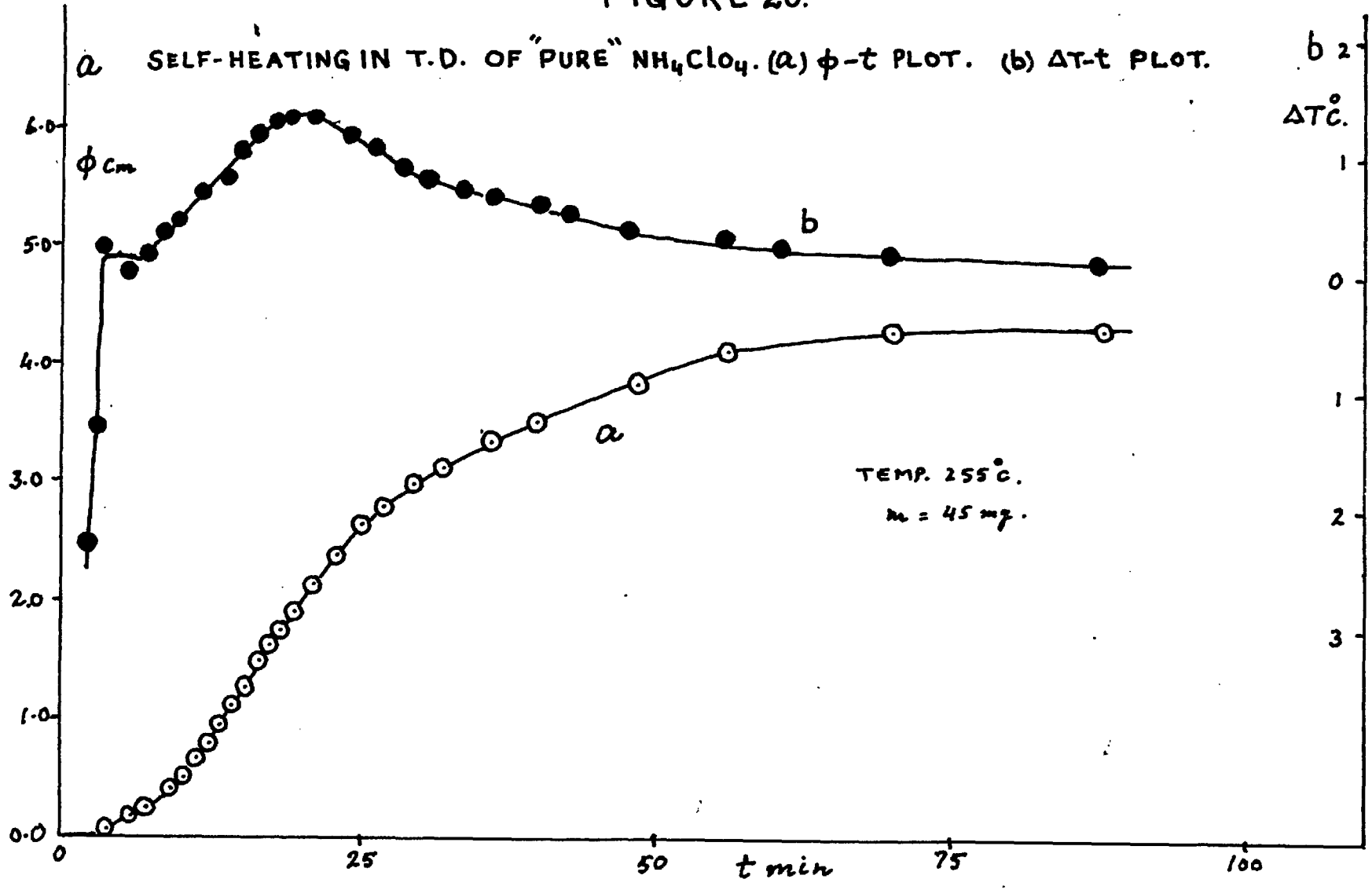
a SELF-HEATING IN T.D. OF "PURE" NH_4ClO_4. (a) ϕ-t PLOT. (b) ΔT-t PLOT.
b
$\Delta T^{\circ}C.$
ϕ cm
6.0
5.0
4.0
3.0
2.0
1.0
0.0
2
1
0
1
2
3
b
a
TEMP. 255°C.
m = 45 mg.
0
25
50
75
100
t min

FIGURE 21

SELF-HEATING IN T.D. OF Cu_2O : NH_4ClO_4 MIXTURES. ΔT-t PLOTS.

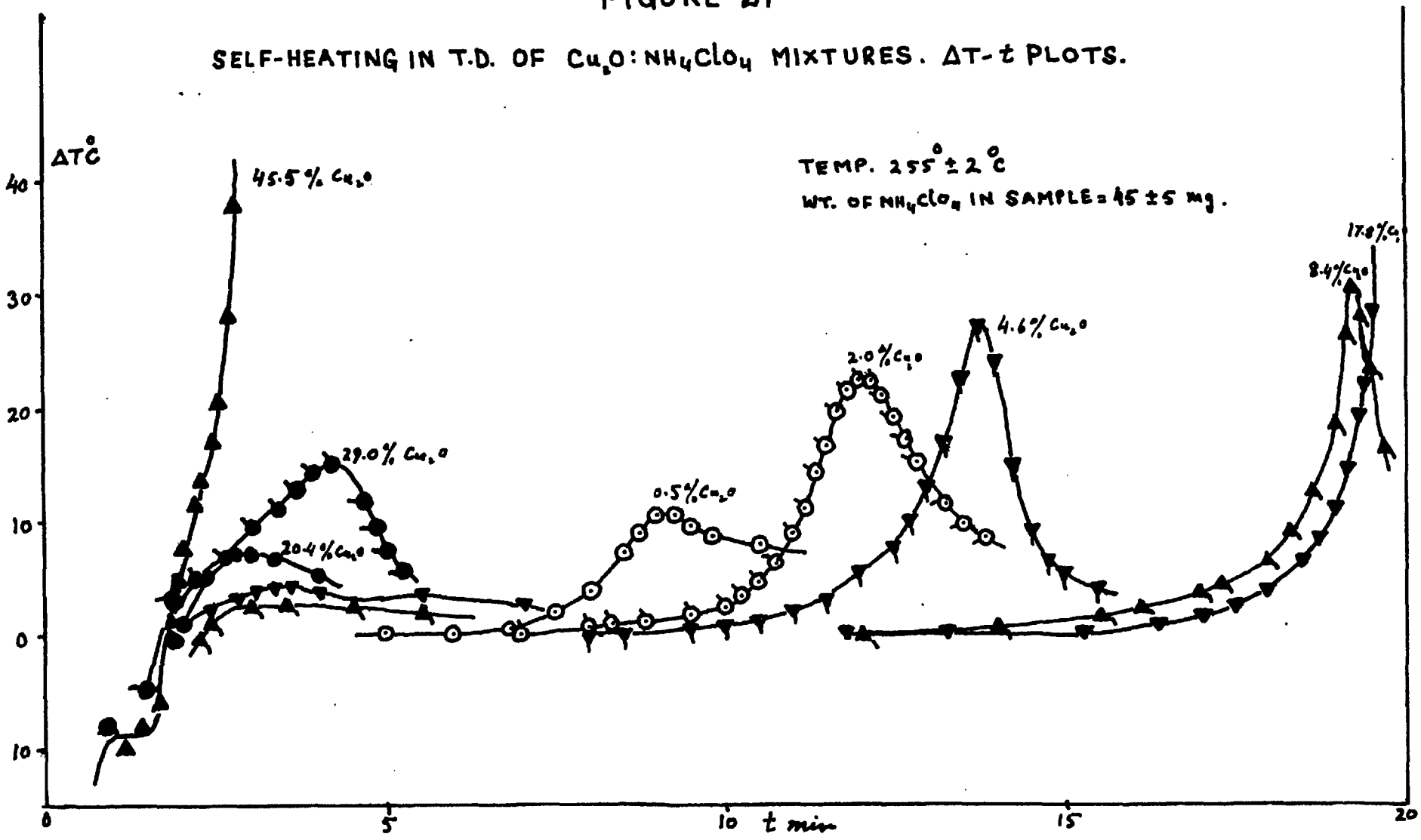

FIGURE 22

SELF-HEATING IN T.D. OF Cu_2O: NH_4ClO_4 MIXTURES. VARIATION OF ΔT_{max} WITH COMP.

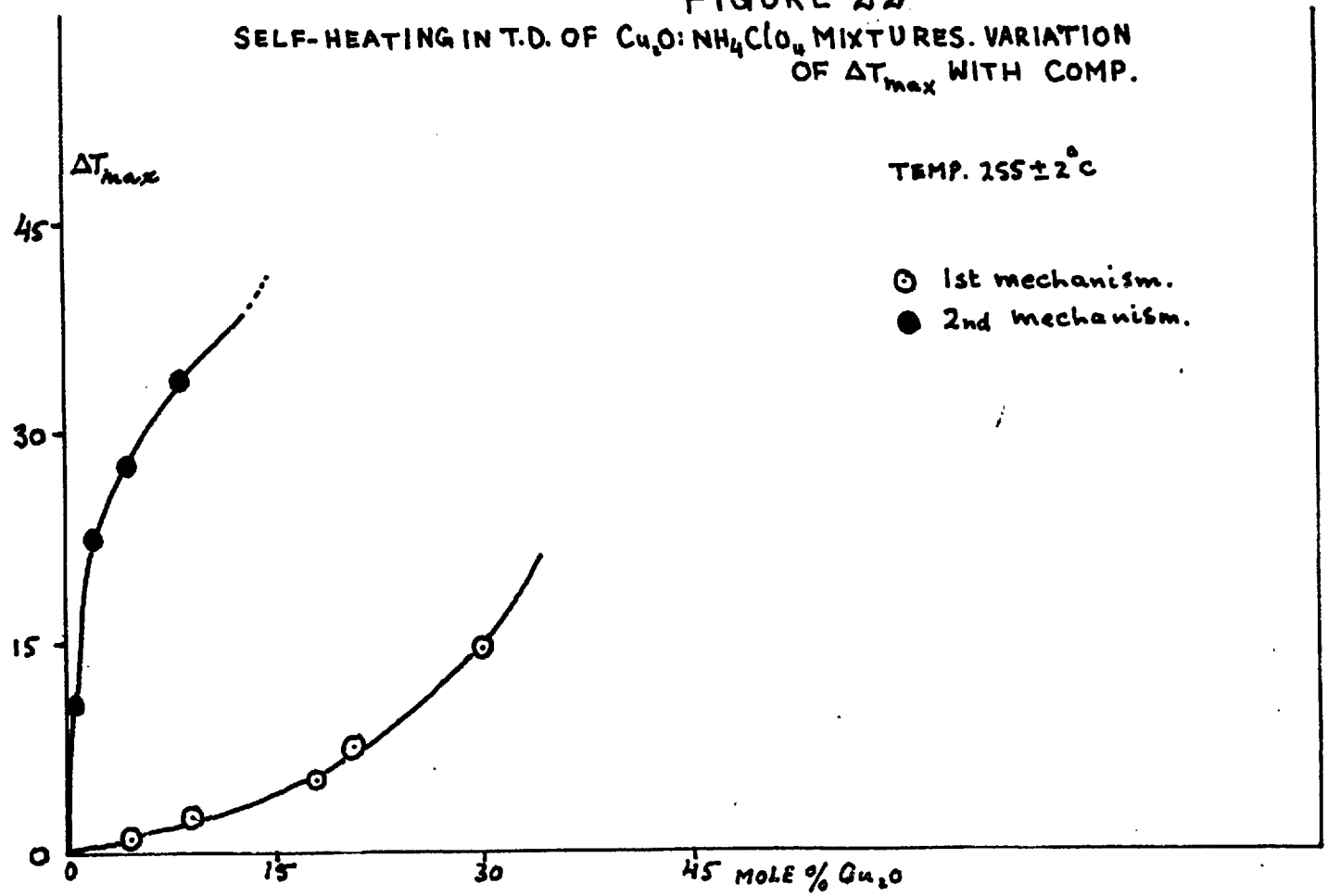

FIGURE 23.

SELF-HEATING IN T.D. OF 29.0 %Cu_2O : NH_4ClO_4 MIXTURE ΔT-t PLOTS.

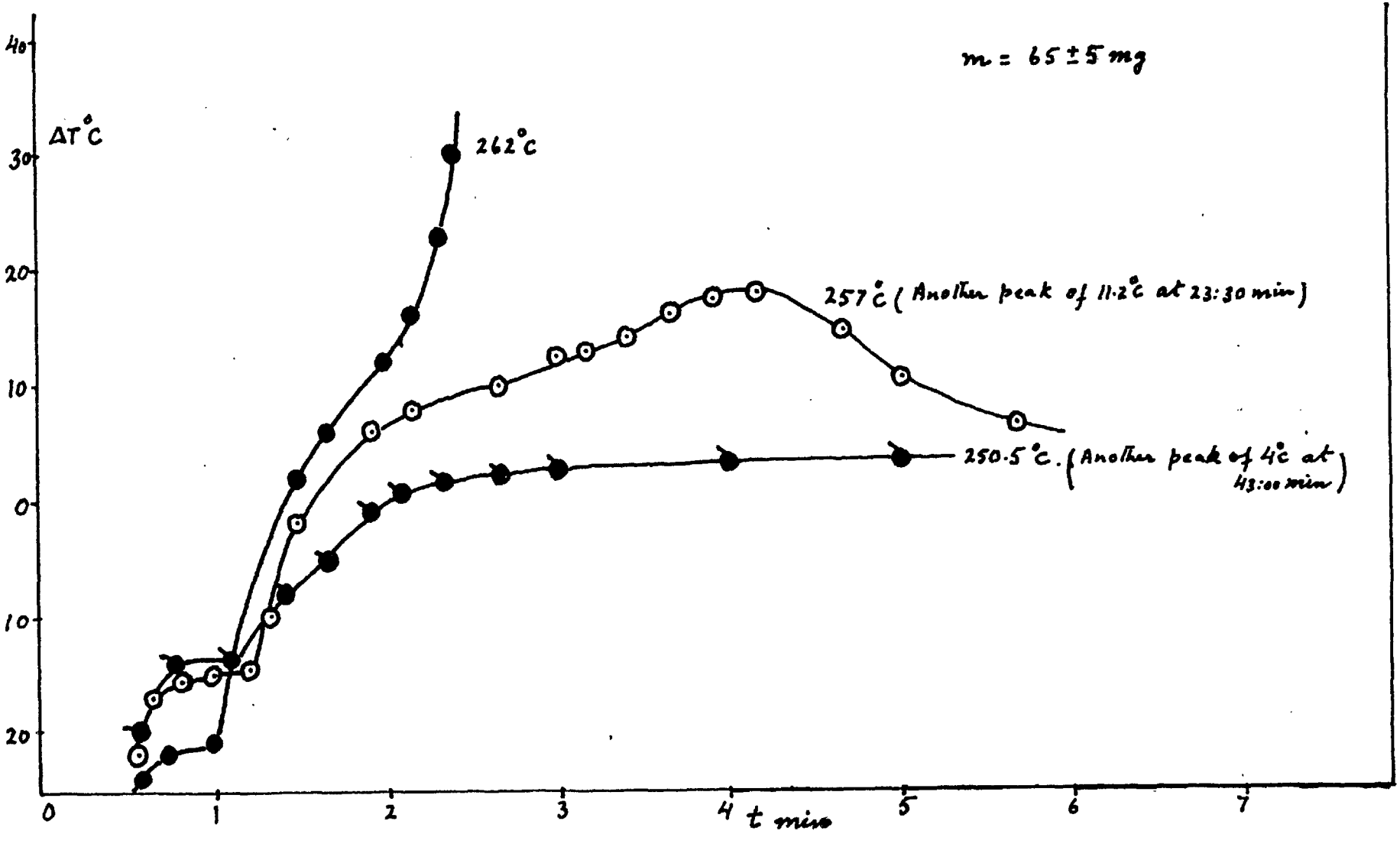

FIGURE 24.

SELF-HEATING IN T.D. OF 17.8% $Cu_2O : NH_4ClO_4$ MIXTURE ΔT-t PLOTS.

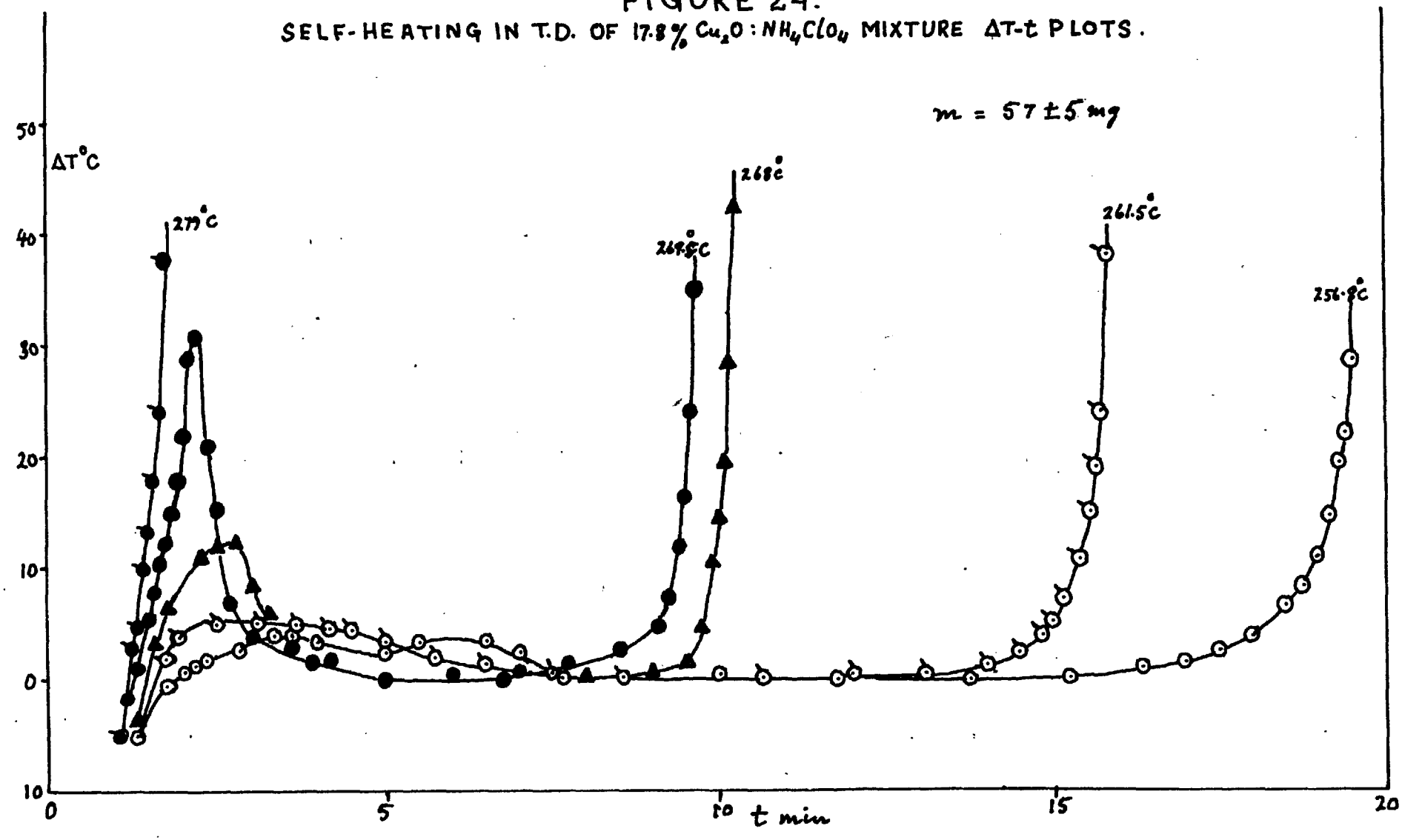

FIGURE 25.

17.8 % Cu_2O : NH_4ClO_4 MIXTURE. ARRHENIUS PLOT. (INDUCTION PERIODS.)

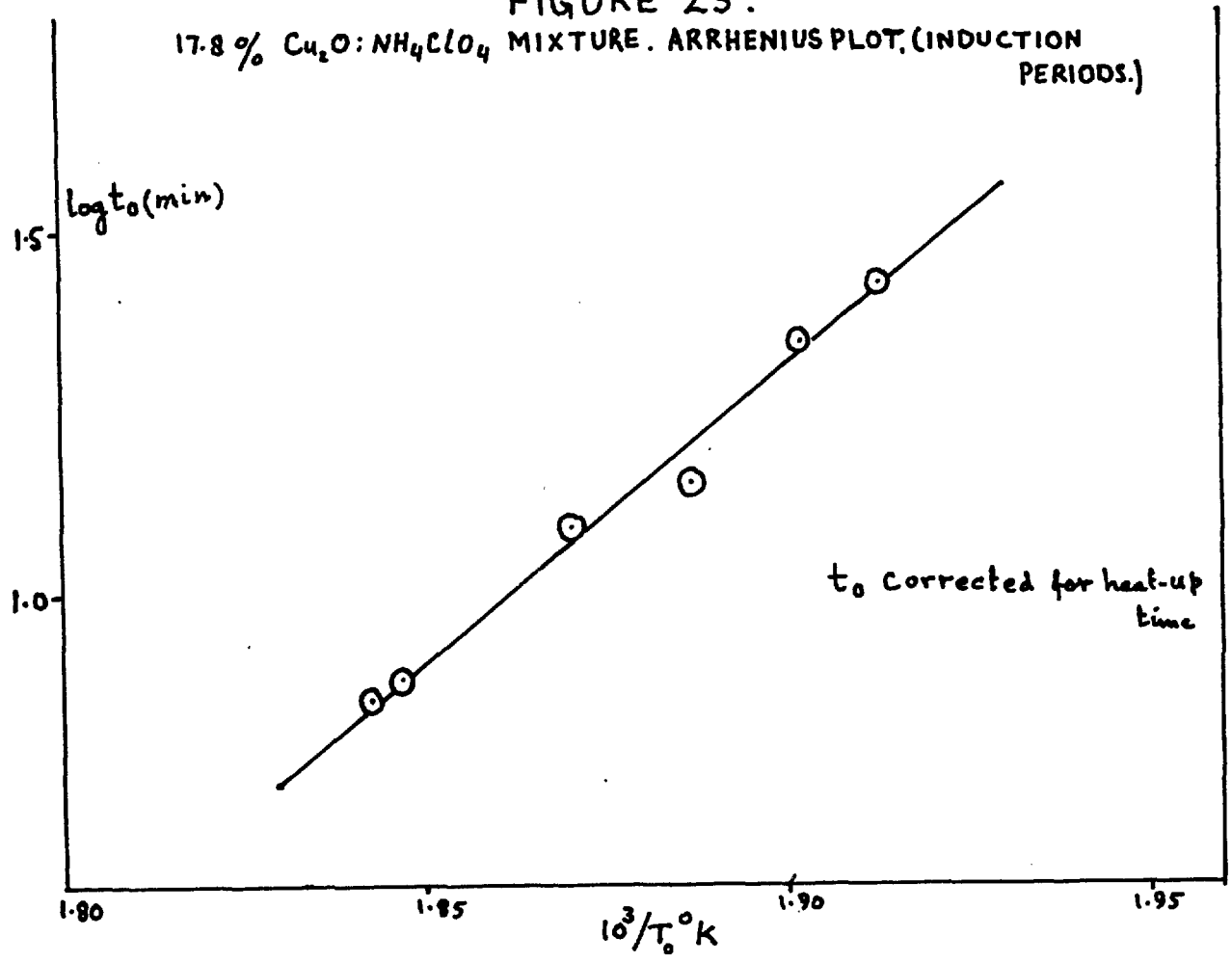

FIGURE 26.

SELF-HEATING IN T.D. OF 4.6% Cu_2O : NH_4ClO_4 MIXTURE. ΔT - t PLOTS.

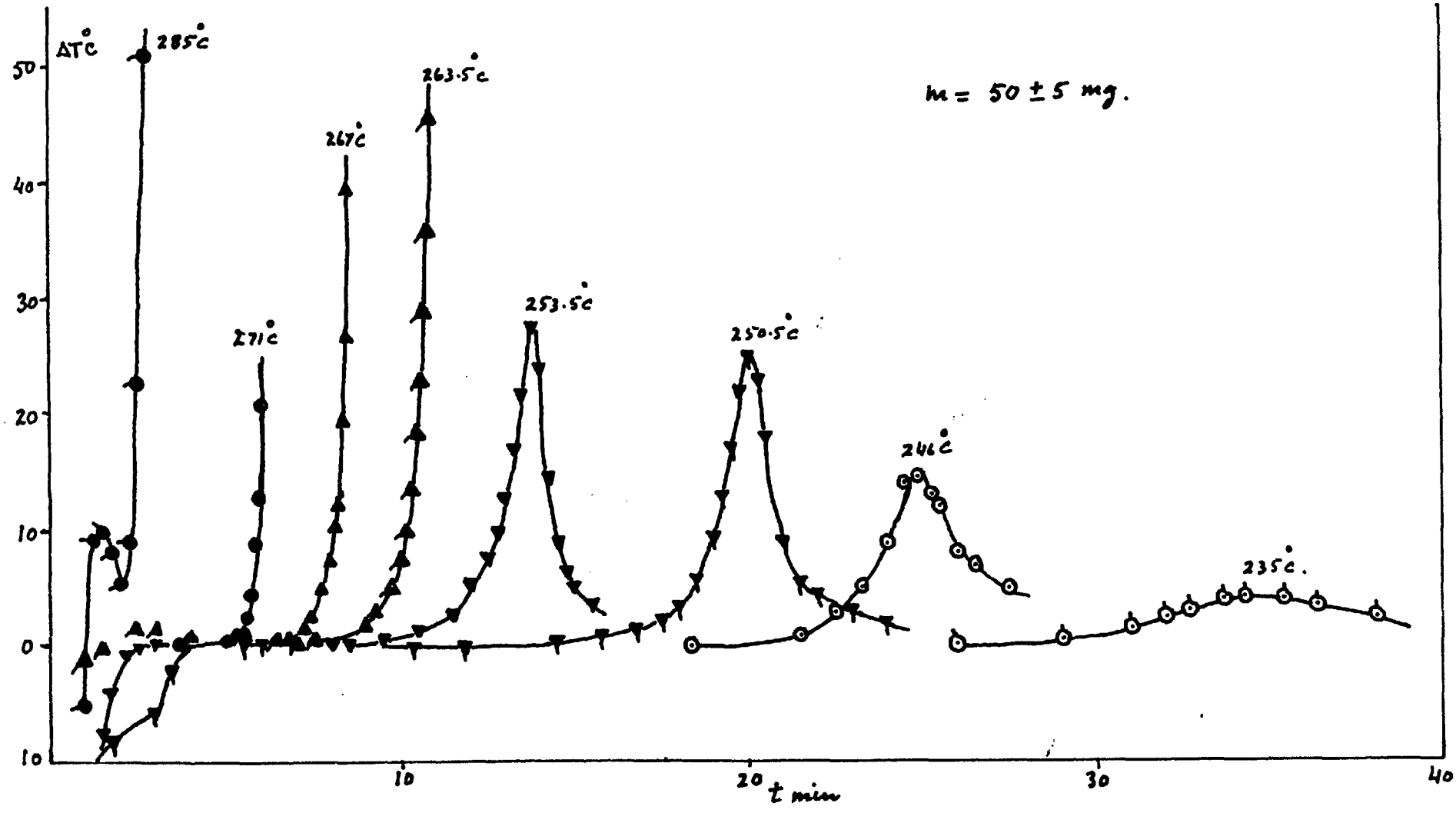

FIGURE 27.

4.6 % Cu_2O : NH_4ClO_4 MIXTURE. ARRHENIUS PLOT (INDUCTION PERIODS.)

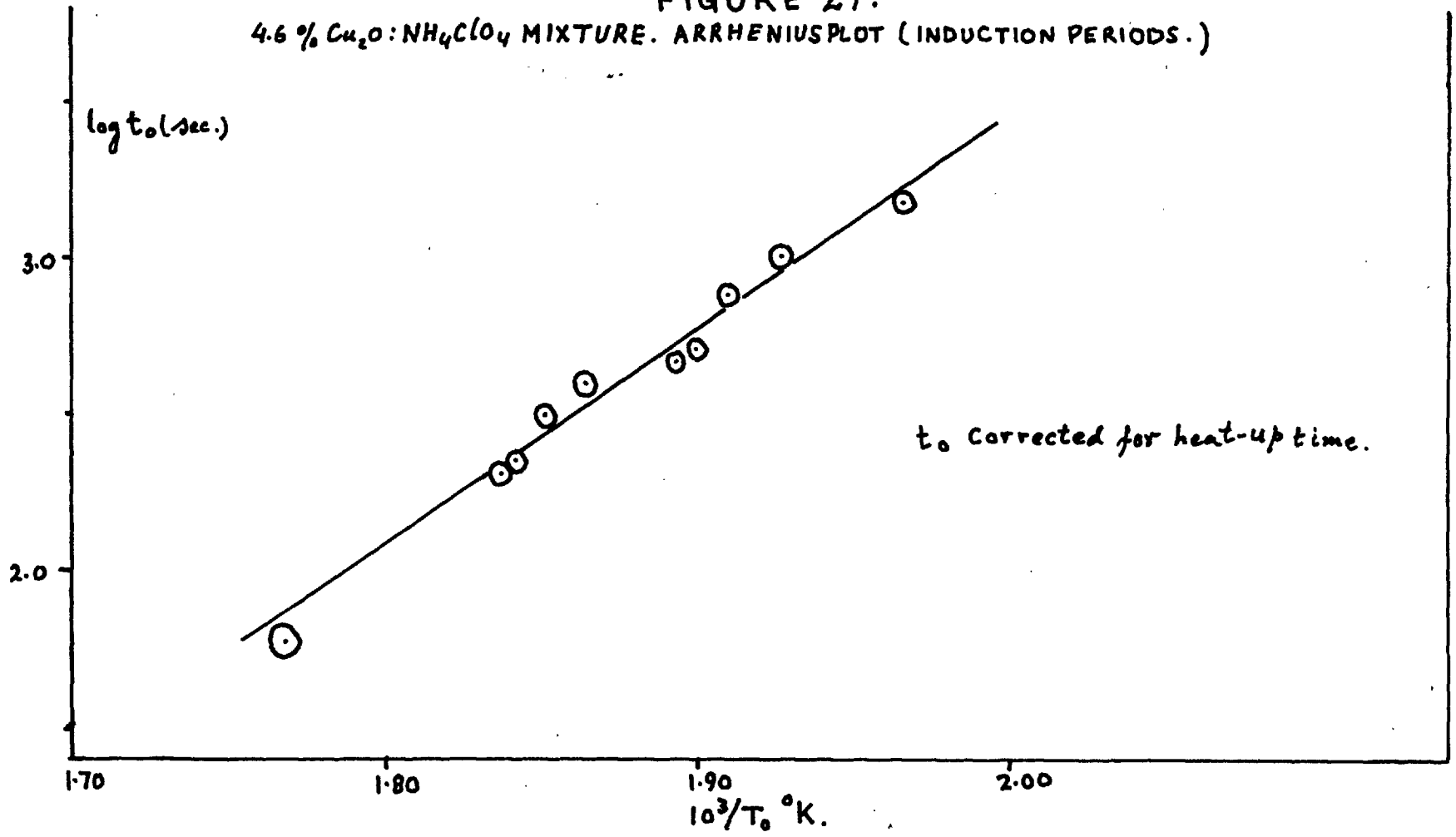

4. DISCUSSION

4.1 THERMAL DECOMPOSITION OF "PURE" AMMONIUM PERCHLORATE

The kinetics of the thermal decomposition of "Pure" salt are essentially the same as reported by Galway and Jacobs (4), and the activation energies for the orthorhombic and cubic regions (32.6 and 27.2 Kcal/mole respectively) are in good agreement with the values reported by these authors. The mechanism of the reaction can, therefore, be concluded to be the same as described in Section 1.1. However, as the salt used in this study was not recrystallised (whereas previous authors used twice recrystallised salt) some differences in the values of rate constants were to be expected. The values of rate constants obtained in this study were considerably higher than those reported by Galway and Jacobs (4). This is reasonable because the unrecrystallised salt would contain small amounts of impurities which could catalyse the reaction.

The increase in percent decomposition of the salt with the pressure of nitrogen in the system is easily understood because N_2 pressure would suppress the sublimation of the salt and hence more salt will be available for the decomposition reaction.

Reducing the particle size of the salt has two

important effects on the kinetics of the decomposition. Firstly, in the cubic region the AE equation fits the results with n = 2 from α =0.03 to 0.90 for the "fine" powder, whereas for the "coarse" powder it only fits from =0.03 to 0.30, the rest being fitted by the UWD law (Section 3.12). Secondly, the discontinuity in the Arrhenius plot (Fig. 4) at the temperature of the phase transition (240°C) is less for the "fine" powder than for the "coarse" one. Both of these observations can be easily explained by the fact that there is no difference in the results for the two particle sizes below 240°C (when there is no phase change). The phase transition will probably result in extensive cracking up of the crystal. The effect of this would be greater, the larger the particle size and hence in the cubic region the coruse powder would mainly decompose as isolated blocks and the UWD law will hold for most of the reaction which is found to be so. For "fine" powder the phase transition would result in less strain and less damage to the crystal and hence the (AE equation with n = 2) holds throughout. Similarly, the discontinuity in the Arrhenius plot is smaller for the "fine" powder than that for the "coarse" one.

4.2 THERMAL DECOMPOSITION OF Cu_2O:NH_4ClO_4 MIXTURES.

4.21 Chemistry of the reaction. The variation in the composition of Cu_2O:NH_4ClO_4 mixture shows that the decomposition reaction is complex. Firstly, by an examination of pressure-time curves in Fig.4, three stages of the reaction may be distinguished. There is an initial reaction associated with a pressure rise roughly linear with time. This is undoubtedly the catalysed decomposition of NH_4ClO_4 caused by contact with Cu_2O. The reaction, which requires no induction period, does not propagate far into the salt particles and soon ceases. An exactly similar situation has been found in the decomposition of NH_4ClO_4 catalysed by MnO_2(19). As expected from this hypothesis, the amount of reaction increases with the amount of catalyst, and is hardly apparent at low catalyst concentration. As this reaction does not lead to the ignition of the salt and the extent is hardly amalysable mathematically, it has not been considered further in this discussion. Subsequently, after an induction period of the order of a few minutes, NH_4ClO_4 commences slow decomposition and the oxygen resulting from this and from the initial interface reaction, oxidises the Cu_2O to CuO. This oxidation is highly exothermic and if sufficient catalyst is present, the self-heating resulting raises the temperature of the pellet above that of the reaction vessel. The decomposition of NH_4ClO_4 consequently accelerates and the self-heating resulting from further oxidation and from the exothermicity of the perchlorate decomposition may result in ignition. This occurs,

for example, at 270°C for Cu_2O concentrations of greater than 2% (Fig.5.).

For lower catalyst concentrations, the self-heating initiated by the oxidation of Cu_2O does not lead to explosion (at 270°C) but may result in an accelerator reaction which then ceases without getting fairly under way. This is shown by the p-t plot 17.76% Cu_2O in Fig.4, the fall in pressure between 230 and 300 sec being due to oxidation of Cu_2O. At higher temperatures or for higher masses, the decomposition rate of NH_4ClO_4 would be just that much higher to enable the heat derived from the oxidation of catalyst to generate a rapidly accelerating process. This results in an explosion, at this concentration, at 279°C. This reaction and its mechanism are termed as "first reaction" and "first mechanism" respectively.

If this "first reaction", assisted by oxidation of Cu_2O, fails to lead to ignition, another reaction sets in after a few minutes. (This is termed as "second reaction" and its mechanism as "second mechanism"). This

reaction is most probably the decomposition of NH_4ClO_4 catalysed by CuO. Since the initial process was halted by loss of contact between Cu_2O and perchlorate, the oxidation reaction must result in some rearrangement of the two phases in the loosely compacted pellet. Some mobility of the oxide phase as a result of either fracture or sintering on oxidation to the di-valent oxide seems probable. The larger the molar fraction of oxide in the original pellet the more oxygen is required to effect oxidation and renewal of contact and the longer the induction period to the "second reaction". Thus the increase in τ with catalyst concentration up to 8.5% Cu_2O (Fig. 5) is consistent with this hypothesis. The ability of CuO to act as a catalyst was demonstrated by the following experiment. Four pellets were made containing, respectively, the same molar concentration of Cu_2O as received, lightly oxidised Cu_2O, highly oxidised Cu_2O and CuO. These four pellets were respectively pink, pink, violet and black. The induction periods for the "second reaction", were in the order $4 = 3 < 2 < 1$ (Fig. 28).

Once this second reaction is initiated, self-heating from the exothermic decomposition of NH_4ClO_4 causes acceleration of the reaction which within suitable ranges of temperature, mass and catalyst concentration, leads to ignition. Explosions could be induced down to

0.5% catalyst with the suitable choice of other parameters.

Fig. 6 shows a cross-section of critical mass-temperature-composition surface at 257°C. As shall be discussed later the fact that a given sample will explode depends on the rate of heat generation due to reaction and the rate of heat loss due to temperature difference between the pellet and its surroundings. Fig. 6 has been introduced here only to elucidate, further, the sharp difference between the two types of mechanisms and that at certain compositions (e.g. 31% Cu_2O) ignition may take place at the same temperature by either mechanism depending upon the mass of the sample. The m* - composition curve for "second reaction" (Fig. 6) shows a minima at about 4.56% Cu_2O composition. This further confirms the hypothesis that the "second reaction" is the catalysed decomposition of NH_4ClO_4 by CuO, because at low concentration (below 4.5%) a little increase in the amount of catalyst will cause a considerable increase in the reaction rate but not much in the heat loss conditions (i.e. colour and conductivity of the pellet), and hence the critical mass will decrease sharply. Whereas, at higher catalyst concentrations (above 4.5% Cu_2O) the increase in reaction rate due to more catalyst will be balanced by the opposing factor that more NH_4ClO_4 is being used for the oxidation reaction so that the heat generation factor (i.e. reaction

rate) will not change very much but the heat loss factors are increasing causing an increase in the critical mass.

4.22 Thermal ignition of 45.39% mixture: The ignition of this mixture occurs only by the "first mechanism" because if the oxidation of Cu_2O does not result in enough self-heating to ignite the sample the amount of ammonium perchlorate left is insufficient to cause ignition by the "second reaction". The induction period for ignition increases linearly with increasing mass of sample and the slope of this straight line is independent of temperature (Fig. 7). This is probably due to an increase in heat up time of the sample. The effect of doing a run in air in place of dry nitrogen was also studied. The induction period in air was much lower (126 sec as compared with 170 sec) than that in dry nitrogen. This again shows that it is the oxidation of Cu_2O which starts the ignition reaction for this composition.

The pre-ignition kinetics could not be studied as the pressure rise before ignition was very small. However, a value of 33.4 kcal/mole for the activation energy associated with this process was obtained from a plot of log $(\gamma_m - \gamma_o)$ against 1/T (Fig. 9) where γ_m is

the induction period for ignition (mean of three values) and is the heat-up time (45 sec). This value of activation energy implies that although the ignition reaction consists of two chemical processes (i.e. oxidation of Cu_2O and decomposition of NH_4ClO_4) only one of them is rate determining. As the value of activation energy obtained is very close to that for the thermal decomposition of "pure" NH_4ClO_4, it seems that it is the rate-determining factor.

4.23 Thermal ignition of 4.56% mixture: As the amount of catalyst is low in this mixture, the thermal ignition occurs only by "second mechenism" up to temperatures as high as 333.8°C. The pre-explosion reaction is fitted by the exponential law. As it is shown later (section 4.3) that the thermal ignition is undoubtedly due to the self-heating of the sample, the fit of the exponential law is reasonable. The rise in temperature due to self-heating will result in faster decomposition rate which will cause a further increase in rate of heat-generation. The interdependence of reaction rate and rise in temperature causes the pressure to rise exponentially with time. This aspect will be discussed quantitatively in Section 4.3. It is noteworthy that the decomposition goes faster than would correspond to the exponential law, just prior to

explosion (Fig. 13b) and falls away from the exponential law in those runs which do not explode (Fig. 15b) showing that the fit of the exponential law is entirely dependent on the rate of self-heating. Under the critical conditions the exponential law holds all the way (Fig. 13b). Although, the temperature of the sample is varying yet the exponential law rate constants give a reasonable value for the activation energy. Fig. 15 is an Arrhenius plot of these rate constants and an activation energy of 29.0 kcal/mole for the reaction is obtained from this plot. This value is in good agreement with the value for "pure" salt and the values (28.1 kcal/mole) obtained from the plot of log $(\tau-\tau_o)$, where τ is the induction period to ignition and τ_o the heat-up time found to be 30 sec (Fig. 16). These values (and others quoted in section 4.3) show that again the rate determining step is the decomposition of NH_4ClO_4 the mechanism for which has been proposed as that of electron transfer (3, 4) CuO catalyses this reaction by facilitating this process as now the electron transfer from ClO_4^- to NH_4^+ can take place via Cu^{++}.

4.3 SELF-HEATING IN THERMAL IGNITION OF Cu_2O:NH_4ClO_4 MIXTURES.

4.31 General: The results described in section 3.6 show that the thermal ignition of Cu_2O:NH_4ClO_4 mixtures is caused by the self-heating of the sample. The ΔT-t plots for 17.8% Cu_2O mixture (Fig. 24) again confirm the fact that the explosion of Cu_2O:NH_4ClO_4 mixtures can occur by two different mechanisms (Section 4.21). The "second" mechanism described in Section 4.21 is further confirmed by the ΔT-t plots for mixtures containing Cu_2O, lightly oxidised Cu_2O, highly oxidised Cu_2O and pure CuO (Fig. 28). The induction period decreases in the order Cu_2O > lightly oxidised Cu_2O > highly oxidised Cu_2O = CuO, showing that the decomposition is catalysed by CuO. The degree of self-heating also decreases in the same order indicating that heat is lost more quickly in mixtures containing CuO (black) than in those containing Cu_2O (pink). Therefore, although CuO is a better catalyst for the initiation of the reaction it is not such an efficient catalyst for ignition.

4.32 Theory of self-heating: The mechanism for the ignition reaction can be based on self-heating. Qualitatively the reaction rate for the decomposition of NH_4ClO_4 is increased by the catalytic effect of Cu_2O (Pure NH_4ClO_4 shows

practically no self-heating in this temperature range Fig. 20). Due to this increased rate of decomposition the heat is generated at a faster rate than it can be lost; consequently, the temperature of the sample rises leading to faster rates of decomposition and ignition. Quantitatively, the heat balance equation with the assumption of uniform temperature can be written as:

$$C_p m \frac{dT}{dt} = -\chi S (T - T_o) + Q m_o \frac{d\alpha}{dt} \qquad (22)$$

where Cp is the specific heat (cal g^{-1} deg^{-1}); dT/dt the rate of temperature rise (deg sec^{-1}); m, the mass of the sample at any instant; χ , the coefficient of heat transfer (cal cm^{-2} sec^{-1} deg^{-1}); S , the surface area (cm^2); T the temperature of the sample at any instant (deg K); T_o, the temperature of the surroundings; Q , the heat of reaction (cal g^{-1}); m_o the initial mass of the sample (g); and $d\alpha/dt$ is the rate of fractional decomposition. As described in section 4.23 the pre-exponential reaction for 4.56% Cu_2O mixture can be fitted by an exponential law. Empirically:

$$\phi = C e^{kt} \qquad (23)$$

where ϕ is the deflection of the gauge, k the rate constant and t the time. This can be written in terms of α as:

$$\alpha = \frac{m_o - m}{m_o} = \frac{k\phi}{\phi_\infty} = (C/a m_o) e^{kt} \qquad (24)$$

where $\alpha = b$ is the fraction decomposed when the decomposition ceases (note that for NH_4ClO_4 only about 25% of the total mass decomposes during the low-temperature decomposition and consequently b = 0.25), ϕ_∞ is the deflection corresponding to complete decomposition and is equal to a b m_o where a is an apparatus constant relating the mass decomposed to deflection on the gauge (for Apparatus C a = 1.0 cm deflection/mg NH_4ClO_4; and for Apparatus B, a = 1.2 cm deflection/mg NH_4ClO_4) Equation (24) can be written as:

$$\alpha = \alpha_o e^{kt} \qquad (25)$$

where $\alpha_o = (c/a\ m_o)$.

It may be noted here that k is not the true rate constant (which is varying as the temperature of the sample varies) but an effective rate constant which is constant at a particular value of T_o even though the temperature of the sample is varying. As k is not the true rate constant it also varies with the mass of the sample (Fig. 11a) and comparisons can only be made if the mass is kept constant.

From equation (25), $d\alpha/dt = k\alpha$. Therefore, equation (22) can be written as:

$$(C_p m)\, dT/dt = -(\chi S)(T-T_o) + Q m_o k\alpha \qquad (26)$$

Let $\theta = E(T-T_o)/RT_o^2$, then equation (26) becomes

$$(C_p m R T_o^2/E)\, d\theta/dt = -(\chi S R T_o^2/E)\theta + Q m_o k\alpha$$

Rearranging and putting $m_o/m = 1/(1-\alpha)$ from equation (24)

$$d\theta/dt = -(\chi S/C_p m)\theta + (QEk/C_p RT_o^2)(\alpha/1-\alpha) \qquad (27)$$

Equation (27) can be integrated by assuming that self-cooling term $(\chi S/C_p m)\theta$ is negligible compared with the self-heating term. This we term the zero-order approximation; it is in fact the usual adiabatic approximation. With this approximation equation (27) can be written as:

$$d\theta = \frac{1}{\tau_\infty}\left(\frac{\alpha\, dt}{1-\alpha}\right)$$

where $\tau_\infty = (C_p R T_o^2/QEk)$. Replacing $\alpha\, dt$ by $d\alpha/k$ from equation (25):

$$d\theta = \frac{1}{k\tau_\infty}\left(\frac{d\alpha}{1-\alpha}\right)$$

Integrating between the limits 0 to and 0 to

$$\theta = -\frac{1}{k\tau_\infty}\ln(1-\alpha) \simeq \frac{1}{k\tau_\infty}\alpha = \frac{1}{k\tau_\infty}\alpha_o e^{kt} \qquad (28)$$

The approximation in the logarithmic term is good for $\alpha < 0.1$; experimentally, it was possible to judge from the values of ϕ at which explosion occurred that α never exceeded 0.1

If explosion occurs at a particular value of $= n$, the time for explosion $\tau^{(o)} = t_n^{(o)}$, where $t_n^{(o)}$ can be calculated from equation (28) by putting $\theta = n$, i.e.:

$$n k \tau_\infty = \alpha_o e^{k t_n^{(o)}}$$

or

$$(1/k)\ln(n k \tau_\infty/\alpha_o) = t_n^{(o)} = \tau^{(o)} \qquad (29)$$

For the first order approximation, θ in the self-cooling term of equation (27) is replaced by the value found from the zero-order approximation equation ( ), so that (27) becomes:

$$d\theta/dt = -(\chi S/C_p m)(1/k\tau_\infty)\alpha_o e^{kt} + (1/k\tau_\infty)(\alpha/1-\alpha) \qquad (30)$$

As $m = m_o(1-\alpha)$ and $\alpha_o e^{kt} = \alpha$ equation (30) can be written as:

$$\tau_\infty \, d\theta = \left\{ 1 - \frac{\chi S}{C_p m_o k} \right\} \frac{\alpha \, dt}{1-\alpha} \qquad (31)$$

Replacing $\alpha \, dt$ by $d\alpha/k$

$$d\theta = (\beta/k\tau_\infty)(d\alpha/1-\alpha) \qquad (32)$$

where $\beta = 1 - (\chi S/C_p m_o k)$.

From equation (32) expressions for θ and τ can be obtained on integration as in zero-order approximation.

These are:

$$\theta = (\beta/k\tau_\infty)\alpha_o e^{kt} \qquad (33)$$

and $$\tau^{(1)} = t_n^{(1)} = (1/k) \ln (nk\tau_\infty/\beta\alpha_o) \qquad (34)$$

4.33 Explosion limits: From equation (34) a critical condition for explosion can be predicted because as $\beta \to 0$, $t_n \to \infty$. Therefore, the critical condition is $\beta = 0$

or $$(\chi S/C_p m^* k) = 1 \qquad (35)$$

where m^* is the critical mass. Writing $k = Ae^{-E/RT_o}$

$$m^* = (\chi S/C_p A) e^{E/RT_o} \qquad (36)$$

The limits for 4.56%, 23.9% and 45.39% compositions have been determined and described in section 3.33, 3.43 and 3.51. Equation (36) was tested for these limits and plots of log m^* against 1/T are shown in Figs. 29, 30 and 31. The boundaries dividing explosion and no-explosion regions are straight lines showing that an equation of the form (36)

holds. The activation energies determined from these plots are 22.4 kcal/mole for 4.56% mixture, 33.8 kcal/mole and 59.00 kcal/mole for 23.9% mixture and 61.7 kcal/mole, for 45.39% mixture. If the heat loss is mainly due to radiation from the surface these values should correspond to 3E as $S \propto m^{2/3}$. But the heat loss term is made up of several terms, i.e. conduction through thermocouple which is independent of mass of the sample, conduction through the glass walls of the reaction vessel which is complete function of mass as the samples were irregular in shape and the contact area between the reaction vessel and the sample consequently depended more on the shape than the mass of the reactant. Finally some heat is also lost with product gases which leave the sample while they are still hot. Therefore, it is not unreasonable to assume that χS term is roughly independent of mass. The activation energies thus obtained are in fair agreement with (although somewhat lower than) the values obtained from the log γ plots (28.1 kcal/mole for 4.56% and 37.9 kcal/mole for 17.8% composition). In contrast the activation energies associated with the "first" mechanism (i.e. 59.0 and 61.7 kcal/mole obtained from limits) are vastly different from the value obtained previously from log γ plots for 45.39% Cu_2O mixture (33.4 kcal/mole). The reason for this deviation is not fully understood but

as the reaction involved is complex (i.e. decomposition of NH_4ClO_4 with simultaneous oxidation of Cu_2O), this inconsistency in the values of activation energies is perhaps not too surprising. The lower values of activation energy obtained from limits can be readily explained by considering equation (36) more closely. As mentioned before (section 3.41) the effective rate constant k' is not only a function of temperature but also of mass (Fig.11a). In determining the limits, mass is varied considerably and hence the values of k' are no longer directly comparable. For lower masses k' is lower than that interpolated from the Arrhenius plot (determined with 30 mg sample) and hence m^* predicted by equation (36) is lower than the experimental value, this making the activation energy apparently lower than its real value.

4.34 Calculations of induction periods The time taken for explosion can be calculated from equations (25) and (34). The values used for Q and C_p are 312 cal/g (21) and 0.34 cal/g.deg. (estimated by analogy with NH_4NO_3); k and α_o are obtained from kinetic data! Table 13 gives the values of log α_o for a series of runs from which a mean value of log α_o can be obtained as -7.83 ± 1.1. There is a scatter in these values but the pre-exponential factor is very sensitive

! note that $k = 2.303\,k'$, as k' is determined from log ϕ vs. t plots.

to curves in k. The value for χ_S which is required to calculate β in equation (34) can be found from equation (35). Using the values of k and m^* at 245°C in Apparatus B the value of χ_S is 0.00735 cal min^{-1} deg^{-1}. This value of χ_S gives β = 0.84 at 459°K and as β increases with temperature at higher temperatures it is of the order of unity. Therefore, the values of t_n calculated from the zero and first order approximations are nearly the same. Fig. 32 shows the comparison of theoretical lines of log τ against 1/T (calculated for n = 1, 2 and ∞ from first order approximation) with experimental data for 4.5% mixture. The agreement is excellent and except at high temperatures the experimental points lie between the lines for n = 1 and n = 2. The deviation at high temperatures may be due to increases in the value of χ_S.

4.3% Calculation of $\theta - t$ plots. Equation (33) gives θ as a function of t. Knowing the values of α_o, β and k, θ-t plots can be determined theoretically at various temperatures. This has been done using the data from Apparatus B. When these theoretical curves are compared with the experimental θ-t plots obtained in Apparatus C it is found that the induction periods in Apparatus C are longer than predicted from the theory using the data from

Apparatus B. As k and α_o are constants independent of apparatus these differences must lie in the value of β. This is to be expected as the heat loss coefficient will most certainly vary with the apparatus; it is expected to be higher because of the thermocouple and because the reaction vessel is surrounded by molten woods-metal. The theoretical curves can be displaced along the time axis by changing the value of β. This has been done and Fig. 38 shows the agreement of theoretical curves (with different values of β) and experimental plots for 4.56% Cu_2O mixture. These plots show that the value of k is independent of apparatus as predicted by theory but β is much smaller in Apparatus C than in Apparatus B. This is due to difference in the value of χs. These plots also indicate that χs is not independent of temperature but in fact increases with T. Table 14 gives the value of χs at various temperatures and Fig. 34 shows its variation with temperature. For an inert solid, the heat transfer coefficient should be independent of temperature but for solid that is reacting it is not necessarily so for the product gases also play a part in heat transfer and higher the temperature higher is the reaction rate which adds to the heat loss term thus increasing it.

It may be noted here that in the above discussion

only the assumption of uniform temperature has been made which is quite justifiable (section 1.2) for the system $Cu_2O:NH_4ClO_4$. Taking a reasonable value of λ (0.050 cal cm^{-1} deg^{-1} sec^{-1} for Alumina) and comparing λ/r_o with χ (obtained empirically), it was found that $\chi \ll \lambda/r_o$ and hence the assumption of uniform temperature is justified (15). No other approximations have been necessary because the use of an effective rate constant makes the equation (22) easily integrable.

TABLE 13

VALUES OF PRE-EXPONENTIAL FACTOR, α_o, FOR 4.56% Cu_2O MIXTURE.

a = 1.2 cm/mg for Apparatus B.

Run	Temp°C	log C	log am_o	log α_o
R 156	248.0	-5.42	1.60	-7.02
R 155	252.0	-7.31	1.62	-8.93
R 154	255.2	-6.71	1.58	-8.29
R 151	259.9	-5.95	1.61	-7.56
R 150	264.8	-6.93	1.55	-8.48
R 149	264.8	-5.76	1.57	-7.33
R 130	270.2	-6.93	1.70	-8.09
R 133	270.2	-5.22	1.48	-6.70
R 147	276.0	-6.01	1.52	-7.53
R 148	276.0	-6.50	1.58	-8.08
R 135	282.0	-6.59	1.55	-8.14

TABLE 14

VALUES OF HEAT TRANSFER COEFFICIENT χ_S DETERMINED EMPIRICALLY FOR APPARATUS C.

Temp°C	χ_S,(cal. min^{-1}. deg^{-1})
245.8	0.014
250.4	0.019
253.4	0.011
263.6	0.038
266.8	0.045
271.0	0.047

FIGURE 28

EFFECT OF REPLACING Cu_2O WITH CuO ON SELF-HEATING IN T.D. OF NH_4ClO_4.

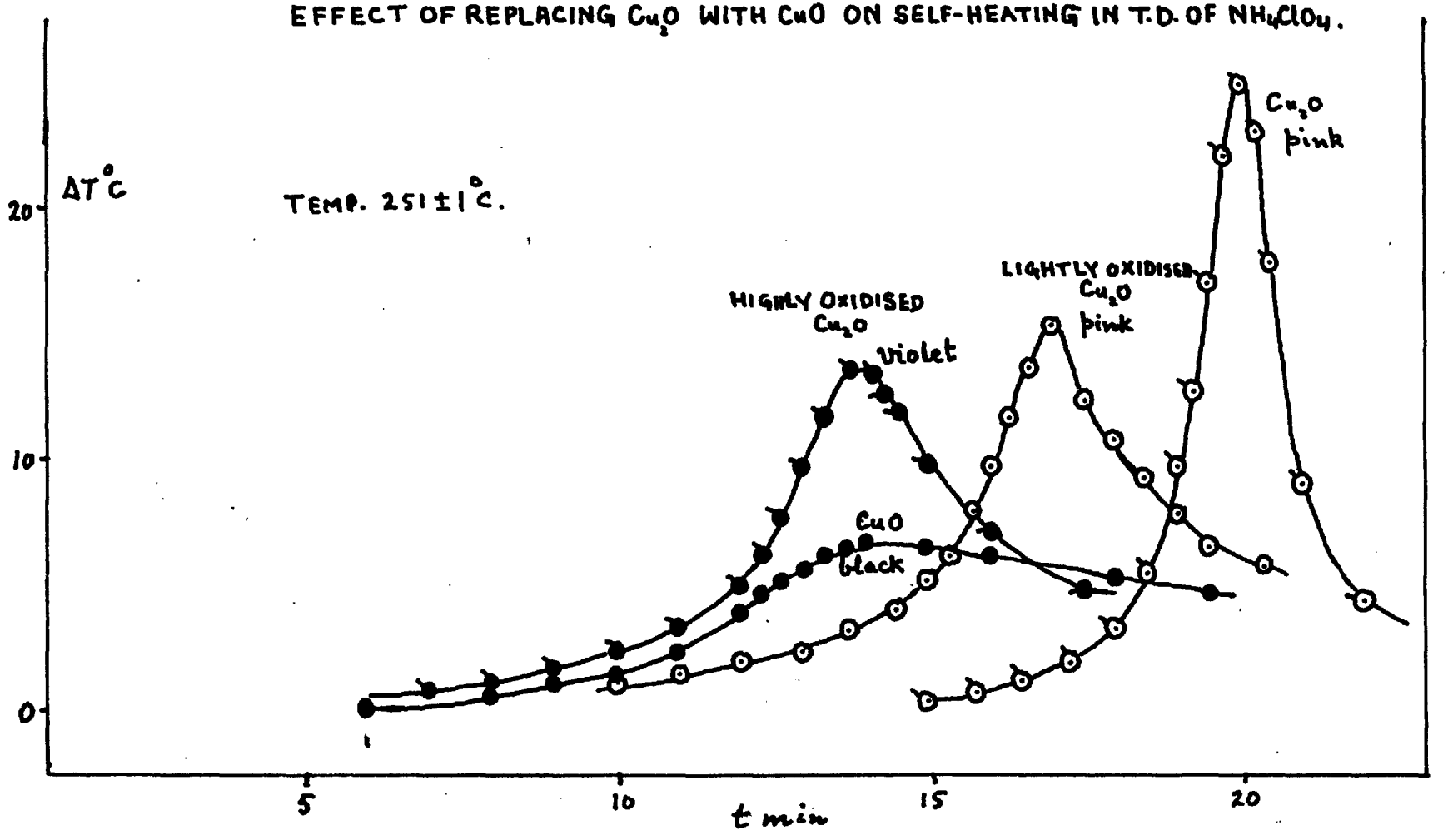

FIGURE 29.

EXPLOSION LIMITS FOR 4.6 % Cu_2O:NH_4ClO_4 MIXTURE. TEST OF SELF-HEATING THEORY.

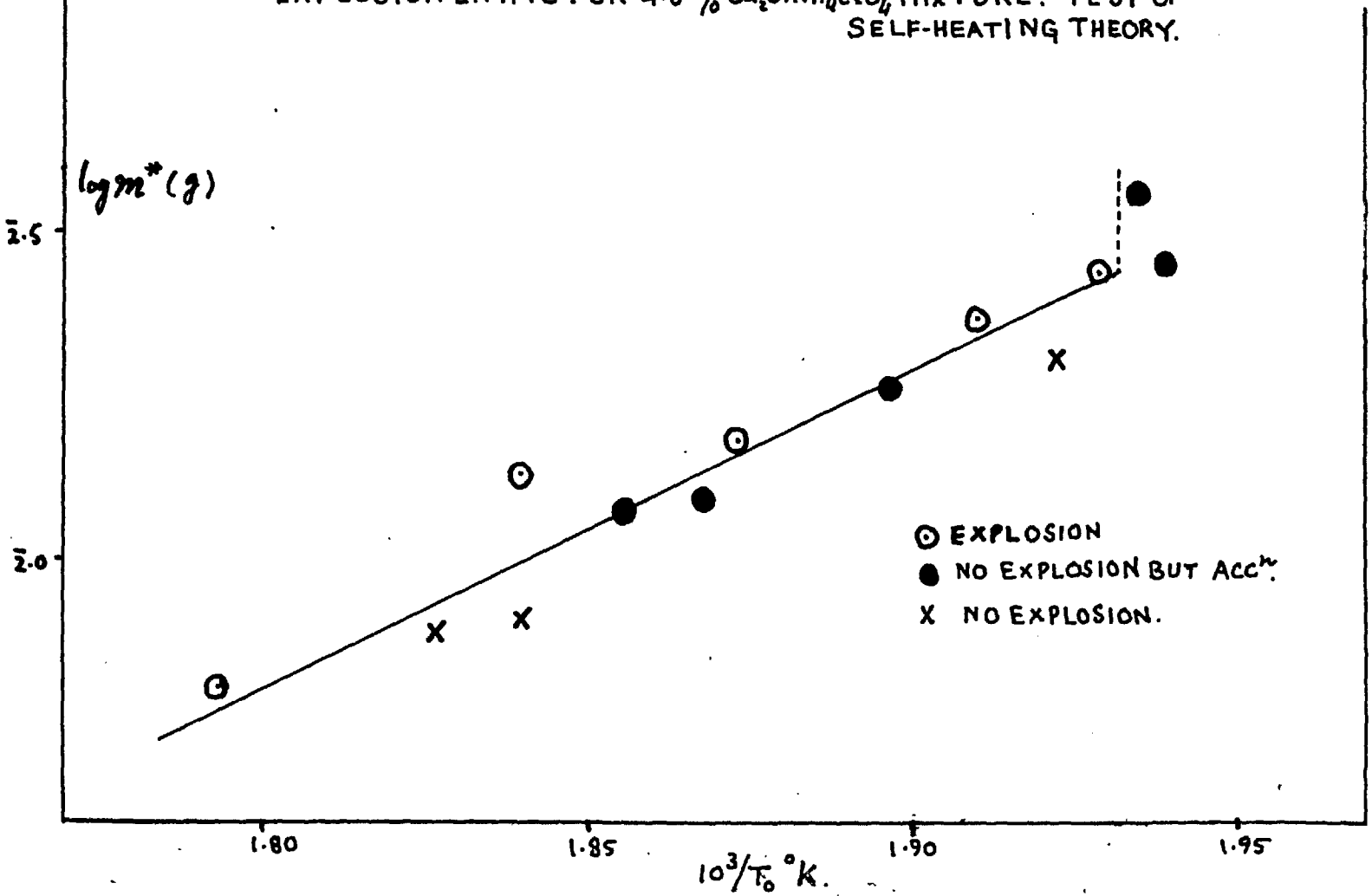

FIGURE 30.

EXPLOSION LIMITS FOR 23.9 % Cu_2O : NH_4ClO_4 MIXTURE. TEST OF SELF-HEATING THEORY.

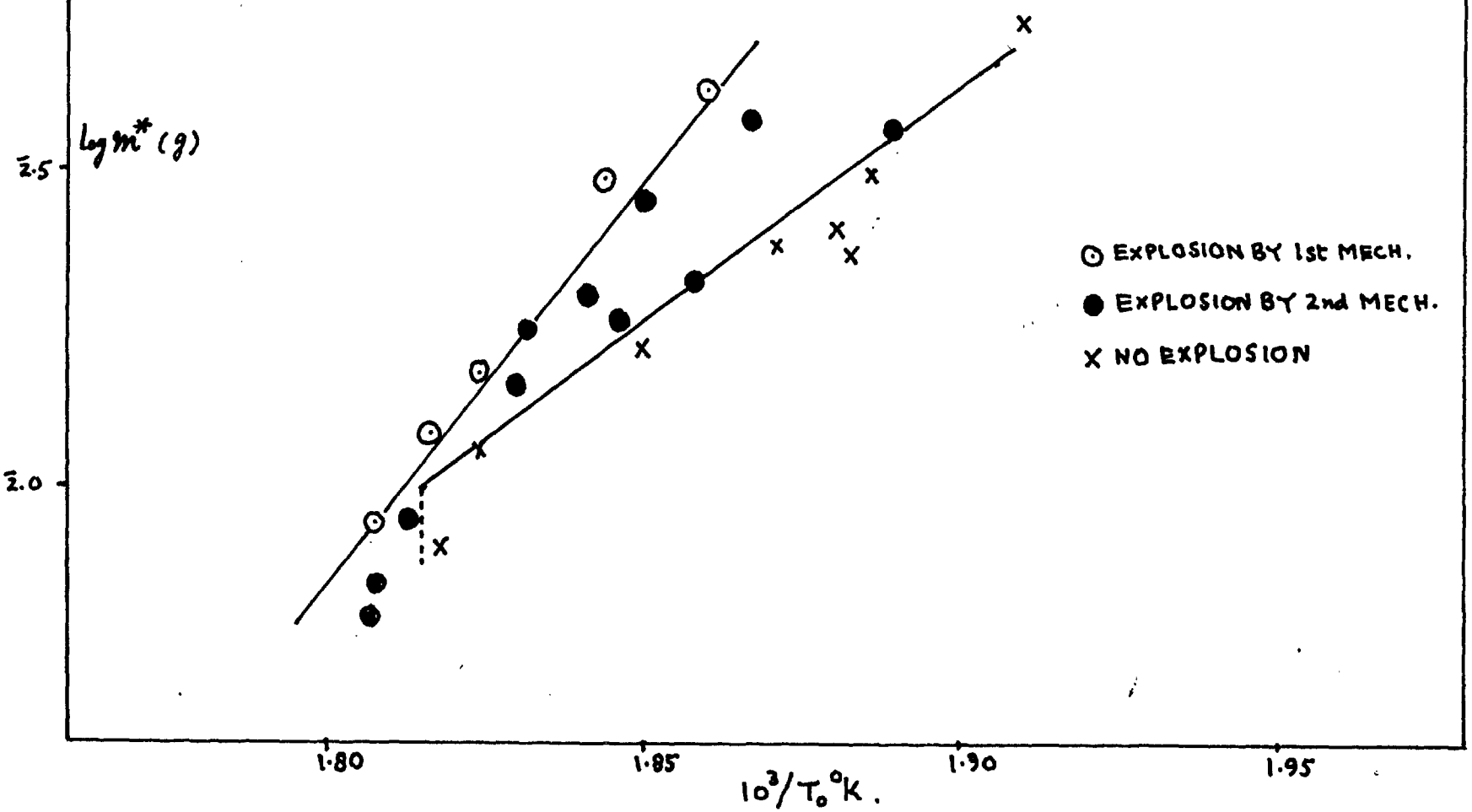

FIGURE 31.

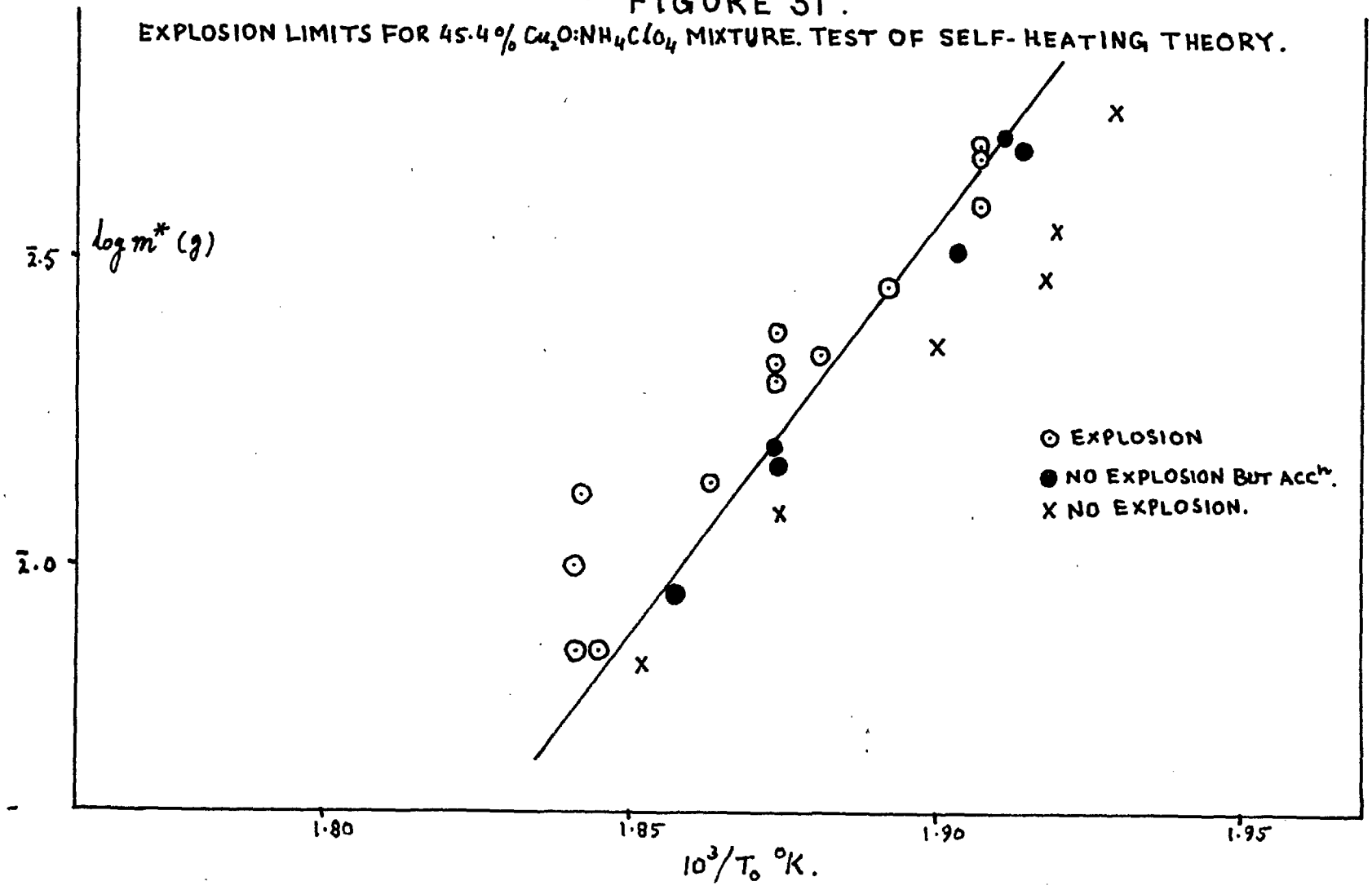
EXPLOSION LIMITS FOR 45.4% Cu_2O:NH_4ClO_4 MIXTURE. TEST OF SELF-HEATING THEORY.
$\log m^*$ (g)
2.5
2.0
1.80
1.85
1.90
1.95
$10^3/T_0$ °K.
EXPLOSION
NO EXPLOSION BUT ACC^{n}.
X NO EXPLOSION.

FIGURE 32.

CALCULATION OF τ FROM 1st ORDER APPROXIMATION. COMPARISON WITH EXPTL. VALUES.

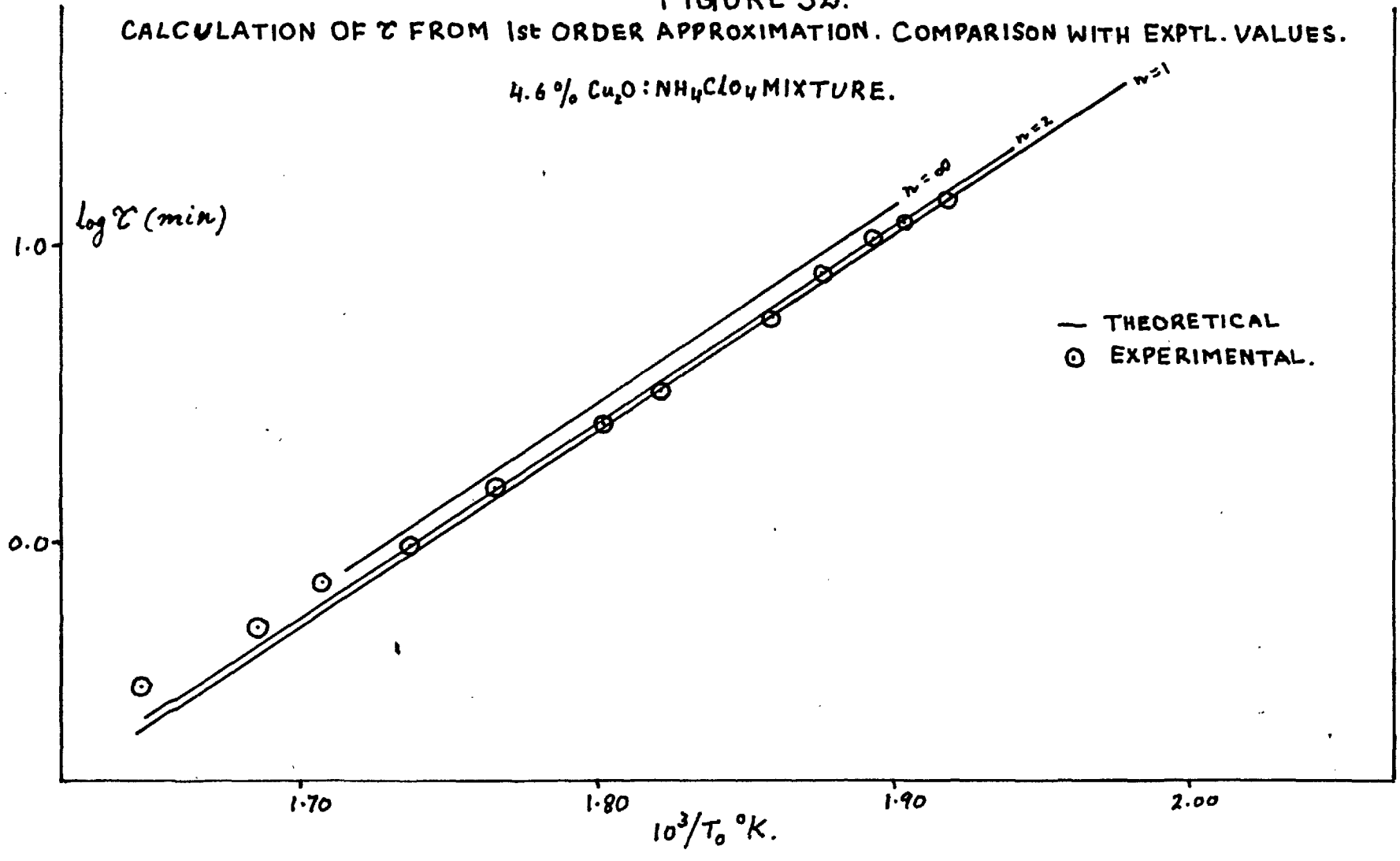

FIGURE 33

CALCULATION OF θ-t PLOTS FROM 1st ORDER APPROXIMATION. COMPARISON WITH EXPTL. PLOTS.
4.6 % Cu_2O : NH_4ClO_4 MIXTURE.

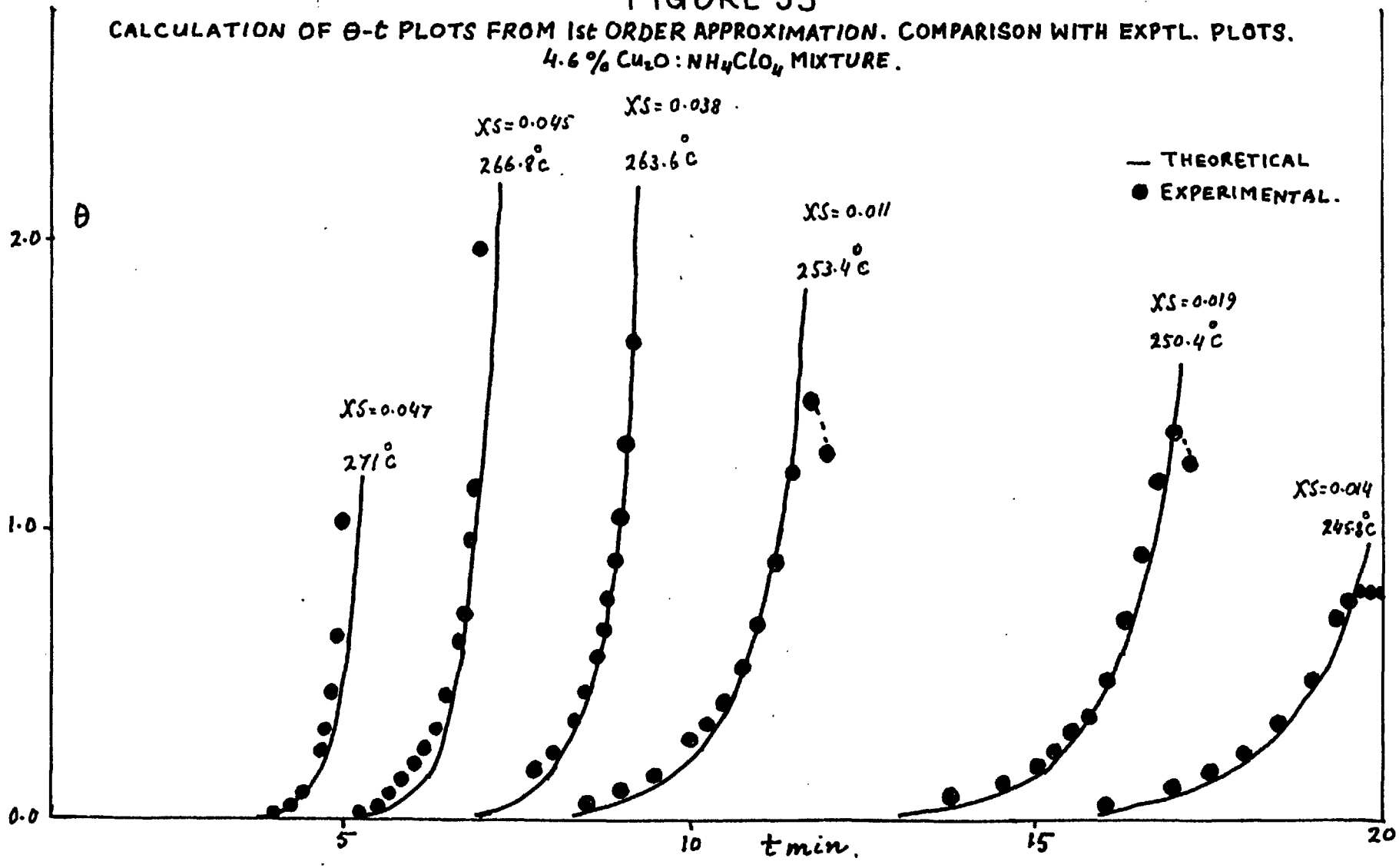

FIGURE 34.

THEORY OF SELF-HEATING. VARIATION OF XS WITH TEMPERATURE.
4.6% Cu_2O:NH_4ClO_4 MIXTURE.

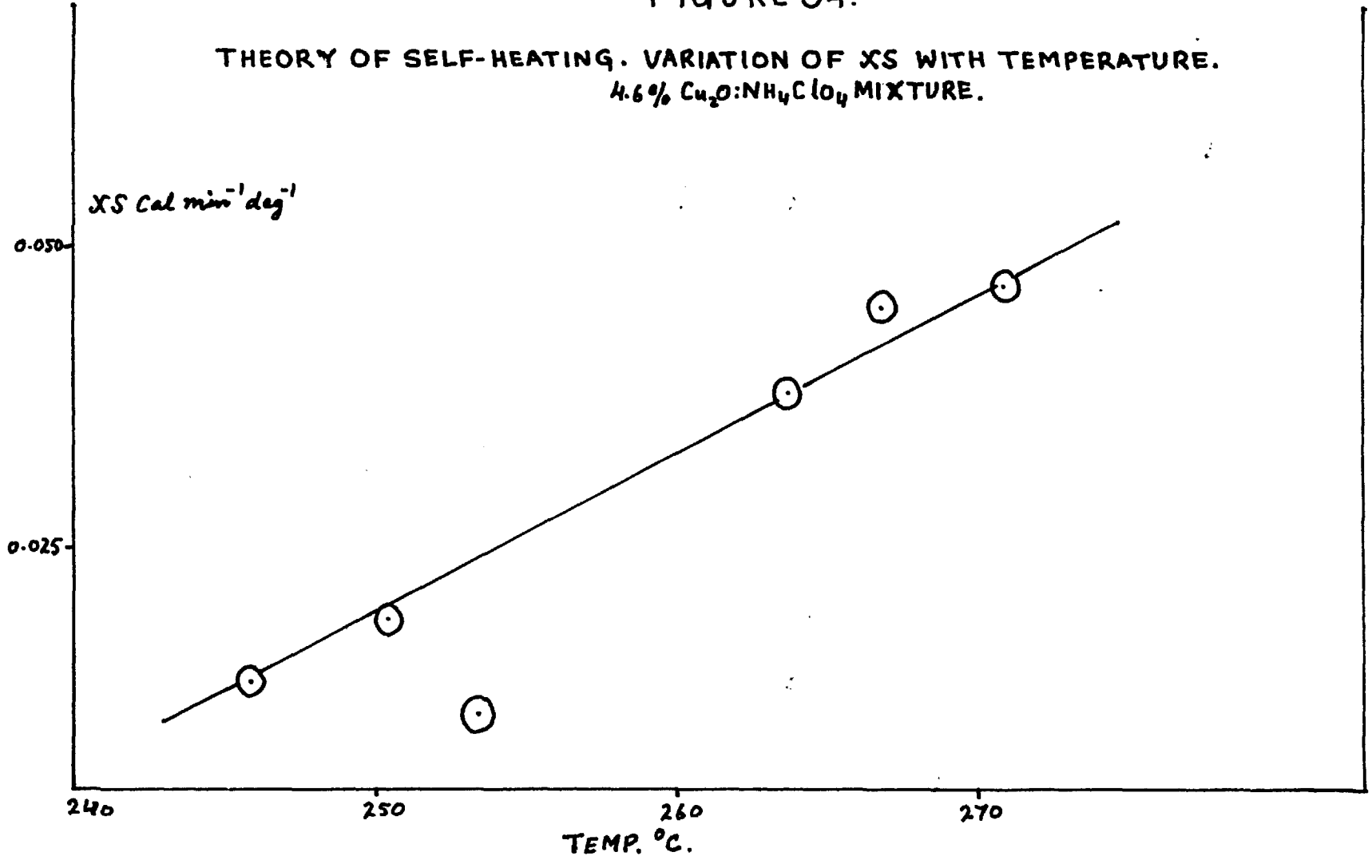

REFERENCES

(1) Naoum and Aufschlager: Z. ges. Schiess-v. Sprengstoffur. (1924). 19. 121.

(2) Dodé: C.R. 200 (1935) 63; Bull. Soc. Chim. (1938) 170.

(3) Bircumshaw and Newman: Proc. Roy. Soc. A.(1954) 227. 115; (1955) 227. 228.

(4) Galway and Jacobs: Proc. Roy. Soc. A (1960) 254. 455.

(5) Galway and Jacobs: J. Chem. Soc. (1959) 837.

(6) Prout and Tompkins: Trans. Farad. Soc. (1944). 40. 488.

(7) Avrami: J. Chem. Phys. (1941) 9. 177.

(8) Erofeyev: C.R. Acad. Sci. U.R.S.S.(1946) 52. 511.

(9) Schultz and Dekker: Sixth Symposium on Combustion (1957). New York: Reinhold.

(10) Galway and Jacobs: Trans. Farad. Soc. (1959) 55. 1165.

(11) Galway and Jacobs: Trans. Farad. Soc. (1960).56. 581.

(12) Semenov: Z. Physik. (1928). 46. 571; Some problems of Chemical Kinetics and Reactivity (Pergamon Press, London, 1959).

(13) Rice, Allen and Campbell: J. Amer. Chem. Soc. (1935). 57. 2212.

(14) Todes: Acta physico chem. (1936). 5. 785.

(15) Gray and Harper: Trans. Farad. Soc. (1959) 55. 581.

(16) Frank-Kamenetskii: Diffusion and Heat Transfer in Chemical Kinetics (Princeton University Press. N.J. 1956).

(17) Thomas: Trans. Farad. Soc. (1958) 54. 60.

(18) Chambre: J. Chem. Phys. (1952) 20. 1795.

(19) Harper: XXXI Congress de Chimie Industrielle (1958, Liege).

(20) Thomas: to be published.

(21) Ubbelohde: Chemistry of the Solid State (Butterworths, 1955). Chap. 11.

(22) Bowden and Yoffe: Initiation and Growth of Explosions in Liquids and Solids (Cambridge Univ. Press. 1952); Fast Reactions in Solids (Butterworths, London 1958).

(23) Garner and Hailes: Proc. Roy. Soc.A (1933) 139. 576.

(24) Vaughan and Philips: J.C.S. (1949). 2736.

(25) Singh: Trans. Farad. Soc. (1956). 52. 1623.

(26) Rideal and Robertson: Proc. Roy. Soc. A. (1948). 195. 135

(27) Evans and Yoffe: Proc. Roy. Soc. A. (1956) 238. 325.

(28) Yoffe: Proc. Roy. Soc. A (1951) 208. 189.

(29) Groocock: Trans. Farad. Soc. (1958) 54. 1526.